

**Doppler Imagery of the Spotted RS CVn Star
HR 1099 (= V711 Tau) from 1981 - 1992¹**

Steven S. Vogt, Artie P. Hatzes², Anthony A. Misch

UCO/Lick Observatory, Board of Studies in Astronomy and Astrophysics

University of California, Santa Cruz, CA 95064

and

M. Kürster

Institut für Astronomie, Universität Wien, Türkenschanzstr. 17, A-1180 Wien, Austria

Received 16 April 1997; accepted

Submitted to: Astrophysical Journal Supplement

¹Based on observations collected at UCO/Lick Observatory, McDonald Observatory, and the European Southern Observatory.

²now at McDonald Observatory, The University of Texas at Austin, Austin, TX 78712

ABSTRACT

Author One, Author Two, Authors ad infinitum (affiliations if desired belong in parentheses, but don't include full snail mail addresses)

We present a set of 23 Doppler images of the spotted RS CVn star HR 1099 (= V711 Tau = HD 22468) obtained from 1981 to 1992. HR 1099 shows a large cool polar spot which has persisted for the 11 years of this study and other low-latitude spots which come and go on relatively short (less than 1-year) timescales, and which can emerge anywhere on the star. The polar spot has variable protuberances which look very similar to the time-variable vertical extensions of the Sun's polar coronal hole. The area of the polar spot and its extensions shows marginal evidence of being periodically variable in time with a period of about 3 yrs. and an amplitude of about 1%, perhaps indicative of a weak cycle, but not yet conclusive.

Comparison of our Doppler images with previously published 'few-spot'-model fits to the light curves shows that such simple spot model solutions are often misleading and nonunique, particularly when the light curve amplitude is small. Moreover, these spot-model fits do not recover the existence of the polar spot. The Doppler images show quite good agreement among multiple images at a given epoch, and between different Doppler imaging research groups using completely independent data sets and imaging software.

Our (cool spots only) Doppler imaging solutions generally do well-reproduce the published light curves, however in one instance the difficulty of fitting light curves suggests that at least one hot spot was present on HR 1099 during one observing season. Variations in the mean brightness of the system, at the observed 0.05 magnitude level, seem to correlate with spot area, particularly the polar spot, indicating that the mean light level is a pretty good proxy of spot

area on HR 1099.

While the polar spot with variable extensions was always present, isolated spots also frequently appeared at both mid and low latitudes. On several occasions, isolated prominent spots emerged and then disappeared on or near the equator.

The ‘migrating photometric wave’ on HR 1099 is due not to a simple longitudinal migration of spots on a differentially rotating star, but rather to changes in the spatial distribution of a few spots (some of which move but most of which are fixed in longitude) that emerge and then disappear. So, at least for HR 1099, the phase drift of this migrating photometric wave minimum contains very little unique information about differential rotation or spot migration.

The tracks of two long-lived spots suggest that some spots which emerge at low or intermediate latitudes migrate up to the pole in a clockwise spiral (slower than the orbit), and then apparently merge with the polar spot. If these dark spots trace magnetic flux, then some of the magnetic flux which emerges at lower latitudes migrates pole-ward and merges with the polar spot flux. It is not yet clear whether this flux is of the same or opposite polarity to the polar spot, and thus whether these northward-migrating low-latitude spots reinforce or cancel the polar spot field. One of the high-latitude spots also appeared to get stretched in longitude as it approached the polar spot, and its overall track is quite reminiscent of the annulus of toroidal field found by Donati et al. (1992b) encircling the polar spot of HR 1099 in 1990.9.

In general, the spots are very tightly locked to the orbital frame of the system, and most disappear before they have had a chance to migrate significantly. Like solar coronal holes, they show very little evidence for shear due to differential rotation. A few selected long-lived features gave longitudinal migration rates

of 1 part in 300 to 1 part in 3600 of the rotation period, in the sense that intermediate and low latitudes rotate slightly slower than the orbital angular velocity, while the pole and highest latitudes appear to be synchronized to the orbit. The implied differential rotation is thus of opposite sign and about a factor of 50 less than for the Sun. The rotation rate versus latitude behavior can be well fit with a variety of formulae including the Maunder formula. One of the best fits is provided by a rotation period vs. latitude that is proportional to the surface strength of a centered axisymmetric magnetic dipole field, with the pole synchronized to the orbit, and lower latitudes rotating more slowly. We believe that these starspots are not measuring photospheric differential rotation. Instead, like solar coronal holes, their lack of shearing and nearly solid-body rotation may be enforced by a multi-kilogauss, axisymmetric, nearly current-free quasi-potential global magnetic field. Our Doppler images also agree very closely with the Zeeman Doppler imagery of Donati et al. (1992b) and support their finding that regions around the edge of the polar spot and within bright spots show largely monopolar fields of at least 300 - 700 G strength.

The large permanent cool polar spots, the very low observable differential rotation of starspots, and the evidence of strong, essentially unipolar magnetic fields associated with them leads us to believe that HR 1099 and other rapidly rotating RS CVn stars harbor quite strong (multi-kilogauss) axisymmetric global magnetic dipole fields. These fields have historically been largely hidden from view by their high degree of rotational symmetry, by being concentrated in the low surface brightness dark spots, and by these stars' high degree of rotational line broadening. We propose that the starspots on HR 1099 and other rapidly rotating RS CVn stars are, by analogy with solar coronal holes, large unipolar magnetic regions tightly frozen into multi-kilogauss axisymmetric

dipole fields in these stars. Since the large cool polar spots, the signature of these dipoles, are not present on more slowly rotating RS CVn stars, we believe that they must be dynamo-induced fields rather than remnant fossil fields.

Subject headings: stars: activity, binaries, imaging, individual (HR 1099, V711 Tau), magnetic fields, rotation, spots

1. Introduction

HR 1099 (= V711 Tau = HD 22468) is one of the brightest and best-studied of the spotted RS CVn stars. It was first discovered by Bopp and Fekel (1976). Many of its fundamental parameters were published by Fekel (1983). It is a binary system consisting of K1IV + G5 V stars. The K1IV star is the more active of the pair, and features prominent spot activity. The G5V companion is also active, showing $H\alpha$ in emission. Because it is one of the brightest members of the RS CVn class, HR 1099 has received considerable attention at all regions of the spectrum over the past 20 years, and the literature on this star is now vast. For brevity, we will refer to many of these references in later sections of the paper rather than trying to summarize them all here. Of greatest interest for the present paper is the history of spot activity on this star, which has been extensively monitored for about three decades by many researchers. These many studies point to a picture of an RS CVn binary system with an extremely active and heavily spotted early-K subgiant component.

The evolution of the large cool spots on the K subgiant give rise to variations in the shape, amplitude, and phase of the light curve of the system. In particular, the phase migration and small period variations of the light curves - quantities easy to measure quite accurately from the photometry - have often been interpreted as evidence of longitudinal migration of spots on a differentially rotating star. By analogy to the solar sunspot ‘butterfly diagram’, some researchers have been led to the conclusion that spots were forming above and below some intermediate latitude of co-rotation. A ‘butterfly diagram’ pattern of spot latitude formation gives rise to light curves which could drift slowly in either phase direction as the spots occupied latitudes which were differentially rotating slightly faster or slower than the co-rotation latitude. Simple models using two or three circular spots have often been used to successfully model the light curves. However, the inherent non-uniqueness of such solutions has always been a worrisome weakness.

The many years of broadband photometric monitoring has been extremely useful for verifying the presence of evolving spots on the surface of HR 1099 and deducing basic spot parameters such as size, temperature, longitude, latitude, etc.. Photometric monitoring has perhaps even detected evidence of stellar differential rotation and longterm spot cycles on some RS CVn stars. But the inferences and conclusions drawn from such studies are always indirect since only the integrated flux from the star is measured, and the integrated flux contains little unambiguous spatial information on the actual spot distribution. For example, the observed migration of the light curve minimum with phase (‘the migrating photometric wave’) could as easily arise from subtle changes in the spot distribution as from actual longitudinal motion of a given spot feature, as is often assumed.

A spatially resolved image of the spot distribution on the star is needed to resolve these ambiguities. Such maps can be obtained using the Doppler imaging technique for stars with sufficient rotation and suitable inclination. Doppler images show unambiguously where spots first emerge, and how they then migrate with time. A many-year set of resolved images of the star can then be examined directly to follow the longitudinal and latitudinal motions of individual spots, and thereby reveal patterns of differential rotation on the star. Such longterm image sets will help in interpreting the large and very valuable body of photometric monitoring data on the class of active late-type spotted stars, many of which are not amenable to Doppler imaging. HR 1099 is well-suited for Doppler imaging by virtue of its intermediate inclination, its intermediate rotation rate (which produces pronounced but not excessive line broadening), and its apparent brightness. It was thus selected as one of our first candidates to follow in detail for many years by Doppler imaging.

The first Doppler image of HR 1099 was presented by Vogt (1983) and by Vogt and Penrod (1983). It showed two large spots on the star in 1981, one roughly circular spot very near the pole with a narrow attached lane descending to intermediate latitude, and a

second, slightly elongated spot, near the equator. An improved version of the 1981 Doppler image along with images for 1984 and 1985 were presented by Vogt 1987a and by Vogt 1987b. In each case, the Doppler image of HR 1099 was dominated by a large cool spot straddling the pole with an attached lane descending to lower latitudes and accompanied by one or two smaller spots near the equator. Vogt and Penrod (1983) were struck by the strong resemblance of this polar spot and attached lane to the X-ray image of CH1 (Coronal Hole No. 1) on the Sun, presented by Timothy, Krieger, and Vaiana (1975). Vogt and Penrod (1983) proposed that starspots are also large unipolar magnetic structures, analogous to solar coronal holes, the only difference being the strength of their magnetic fields. On the Sun, coronal holes are unipolar magnetic regions of only 10-20 Gauss field strength, too low to affect energy transport mechanisms in the photosphere. Thus they show up only very weakly in photospheric images of the Sun. But their fields do significantly effect the low density solar corona, leading to a reduction of both temperature and density in the solar wind outflow above the holes, and producing dramatic ‘dark’ regions (holes) in X-ray images of the hot corona. However, Vogt and Penrod (1983) speculated that the fields in the spots of RS CVn stars are several orders of magnitude stronger, reaching sunspot-umbrae-level strengths of several kilogauss over most of the area of the unipolar magnetic region. Such a field strength is sufficient to dominate convective heat transport mechanisms in the photosphere (as in sunspot umbrae), lowering the surface temperature and thereby giving rise to prominently visible cool photospheric spots. Since the large polar spot appeared to be a permanent feature of HR 1099, Vogt and Penrod (1983) also speculated that the low-latitude isolated spots may migrate poleward to join the polar spot, thereby maintaining its persistence.

Direct observational support for the idea that starspots might be large unipolar magnetic regions of kilogauss field strength came from the spectacular Zeeman Doppler imagery work of Donati et al. (1990), Donati, Semel, and Rees, (1992a), and Donati et

al. (1992b). They first reported the detection of a largely monopolar magnetic region of about 1 kilogauss near quadrature (phase 0.85) on HR 1099 in August, 1989. This magnetic region covered about 18% of the total stellar surface and may have been coincident with a photospheric hot spot. They then found that the magnetic signature from the K1 subgiant component varied with rotational phase, and also that both the intensity and magnetic signatures (Stokes I and V parameters) varied significantly from 1989 to 1990. Their results suggest that large time-variable monopolar regions are present on HR 1099.

The first actual Zeeman-Doppler images (longitudinal field component) of HR 1099 were presented by Donati et al. (1992b) for epochs 1988.9 and 1990.9. There were large polar spots on the star in both years. The 1988.9 image also showed two warm regions (300K hotter than the photosphere) slightly above the equator, one of which seemed to be associated with a region of enhanced magnetic activity from a (incomplete) 1989.6 epoch Zeeman-Doppler image taken 8 months later. The authors suggested that the warm regions of 1988.9 were areas of emerging radial or poloidal magnetic field. Correspondence of the magnetic field structure with the hot and cool spots was dramatically demonstrated in their 1990.9 epoch magnetic and brightness images. Here, their brightness image showed a prominent, roughly circular, cool polar spot with attached proturbence, and a single smaller cool spot near the equator. Their simultaneous Zeeman-Doppler image revealed that the polar spot was surrounded by a (clockwise) ring of -300 Gauss magnetic field, and the smaller equatorial spot was spatially associated with a (counterclockwise) monopolar region of +700 Gauss field. The authors concluded that the fields within the dark spots were not being directly detected due to lack of photons from the dark regions, but were strongly implied from the close association of magnetic signatures with the detailed shape and boundaries of the spots. They also speculated that the toroidal field structure surrounding the polar spot was due to winding of a portion of the dipole field line distribution by differential rotation. We believe that this Zeeman Doppler imaging work provides strong

support for the idea that starspots are large unipolar magnetic regions, similar in structure to solar coronal holes, but possessing magnetic field strengths several orders of magnitude larger.

Over the years, the idea of large cool polar spots on RS CVn stars has had its share of skeptics, no doubt because the spots were not detected by broadband photometric spot modelling, and also perhaps because they had no obvious analog among sunspots. Many mechanisms were proposed - limb brightening, differential rotation, gravity darkening, problems with the line flux profile radiative transfer calculations, chromospheric line-filling, out-of-focus spectrographs, etc. - which might give rise to spurious polar spot features. But, over the past decade, many other Doppler imaging researchers have independently found large polar spots in their images of rapidly rotating RS CVn stars. Furthermore, some more slowly-rotating spotted RS CVn stars have also now been found by Hatzes (1993) which do *not* show these polar spots. Hatzes, Vogt, Ramseyer, and Misch (1996) also recently completed a detailed study of the reality of polar spots using the observed inclination dependence of the mean shape of the line flux profiles from spotted stars. Their modelling simulations argue strongly against gravity darkening, differential rotation, limb brightening, equatorial bright bands, chromospheric line-filling, and unknown effects in line radiative transfer physics as possible causes of spurious polar spots. Rather, the observed inclination dependence of the flattening of the line flux profiles in RS CVn stars is quite naturally and simply explained by the presence of large, cool polar spots.

We have spent the past decade monitoring the spot distributions on several of these stars. In the present paper, we present a set of 23 Doppler images of HR 1099 obtained between 1981 and 1993. In hindsight, HR 1099 has been a rather difficult star to study for Doppler imaging since the spots change on timescales of less than one year, requiring more than one Doppler image per season to obtain a fair sampling of all the changes in their

distribution. Where possible, more than one image per year has been obtained.

We compare theoretically generated light curves from our images with observed light curves and also attempt to tie in many other observations of activity on HR 1099 with our spot maps. It is hoped that researchers studying this star will be able to make use of these images to better interpret their wide variety of optical, radio, ultraviolet, and x-ray observations taken over the same time interval.

2. Observations

Spectral observations for the Doppler imaging represents a combination of data sets taken at three different observatories: Lick, McDonald, and The European Southern Observatory (ESO). During the course of collecting the observations five different spectrographs were used for data acquisition. Tables 1-23 list the journal of observations which include rotation phase, the Julian Day of mid-exposure, the exposure length, the signal-to-noise per pixel, and the observing station. (Lick 80" = 80" coude spectrograph camera, McDonald coude = 2.1m coude spectrograph; ESO = 1.4m CAT + CES; Lick HS is the Hamilton; McDonald SE = 2.1m + Sandiford echelle). In all observations where strong telluric lines were present the observation was divided by an appropriately scaled spectrum of a rapidly rotating hot star.

2.1. Lick observations

The 1981 data were obtained at Lick Observatory using a double-pass echelle and Intensified Dissector Scanner (IDS) system. From 1982 through 1988 observations of the Ca I 8448 Å line were obtained using the coude spectrograph of the Shane 3-m telescope at Lick Observatory and a Texas Instruments 800 × 800 CCD detector. A modified

Bowen-Walraven image slicer was used to reformat the light from a 3 arc-second hole to a 0.67 arc-second slit. The resulting resolving power was 48,000 and typical signal-to-noise was about 200-300 per 15 μm pixel. A resolution element consisted of 3.5 pixels. Since the beginning of 1990, all observations of HR 1099 have been made with the Hamilton Echelle spectrograph (Vogt 1987c) at the coude focus of the Shane 3-m telescope. The Hamilton yielded a resolving power and signal-to-noise roughly equivalent to the conventional coude spectrograph, but with improved throughput and much greater spectral coverage.

2.2. McDonald Observatory Observations

The McDonald data set was obtained using the 2.1-m telescope at McDonald Observatory. From 1988 until early 1992 data was taken using the the coude focus of McDonald Observatory’s 2.1-m telescope. A 1200 gr mm^{-1} grating in second order and a Tektronics 512 \times 512 CCD were used resulting in a dispersion of 0.038 \AA pixel $^{-1}$ and a resolving power of about 65,000. The wavelength coverage was 23 \AA centered on 6430 \AA .

Beginning in late 1992, data at McDonald Observatory were acquired using the Sandiford Cassegrain Echelle Spectrograph, again at the 2.1-m telescope. This instrument is a prism cross-dispersed echelle mounted at the Cassegrain focus of the 2.1-m telescope McCarthy, Sandiford, Boyd, & Booth (1993). It is used with a 1200 \times 400 Reticon CCD and provides a dispersion of about 0.05 \AA pixel $^{-1}$ at 6500 \AA . The instrumental resolution for the observations was 50,000. The spectrograph setup was chosen such that a wavelength coverage of about 5700–6900 \AA was obtained.

2.3. ESO Observations

Spectroscopic observations for four of the images were taken at ESO using the 1.4 m–CAT telescope equipped with the CES spectrograph, the short camera, and an RCA CCD. All spectra were recorded at a dispersion of 3.47 \AA mm^{-1} and centered at 6444 \AA . Since the CCD has 1030 pixels of size 15μ in the dispersion direction, the resulting length of the measured spectrum was $\approx 52.5 \text{ \AA}$. A resolving power of $\lambda/\Delta\lambda = 50,000$, equal to a spectral resolution of 0.129 \AA was used. Data reduction for this data set was performed with the MIDAS software developed by ESO and involved the usual steps of bias subtraction, flatfield division, removal of cosmic ray hits, spectrum extraction (i.e. summation of relevant CCD columns), wavelength calibration, and continuum normalization.

3. Imaging the Photospheric Features

3.1. Stellar Parameters

In order to image a stellar photosphere one needs the stellar inclination, projected rotational velocity ($v \sin i$), rotation period, and the spectral line profile at each location on the stellar surface. For the stellar inclination the value of the orbital inclination, $i = 33 \pm 1^\circ$ determined by Fekel (1983) was adopted. The $v \sin i$ was determined by fitting the mean Ca I 6439 \AA profile with a synthetic profile generated using model atmospheres and a disk integration scheme. The mean profile was calculated by summing individual observations spanning a rotation period. This minimizes the distortions due to spot features and gives a slightly better approximation of the immaculate (i.e. unspotted) line shape than does a single observation. The value we obtained was $v \sin i = 40 \pm 1 \text{ km s}^{-1}$, consistent with the one found by Donati et al. (1992). Synthetic spectral lines were generated using model atmospheres of Bell et al. (1976). Profiles were generated at 20° limb angles to account for

linb darkening. A macroturbulent velocity $\xi_{RT} = 4 \text{ km s}^{-1}$ was also used.

We used the HR 1099 orbital ephemeris of Fekel (1983) for calculating all phases. This formula expresses the heliocentric Julian Day of conjunction (active KIV spotted star in front) as:

$$HJD = 2442766.080 + 2.83774 \pm 0.00001 E$$

Thus Phase 0.0 corresponds to conjunction with the spotted star in front and, on all our Doppler images, the secondary sits fixed at Phase = 0.5. When looking for phase drifts in a highly synchronized orbital system, one must also consider the effects of period errors which accumulate phase errors over time. Fekel (1983) also found the orbital period to be constant over 60 years. Using three times his formal error of the period estimate, we find no more than 0.015 phases (5.4°) of longitude error (with respect to the orbit) over the entire 11.1 year span of the datasets analyzed in this paper. Thus the adoption of this constant period is more than adequate to compare longitudes of all features on HR 1099 over those 11.1 years.

3.2. Reconstruction Technique

The spot distribution was derived from a time series of spectral line profiles using the maximum entropy method (MEM), the details of which can be found in Vogt, Penrod, & Hatzes (1987). Because the problem of deriving a surface distribution from spectral line profiles is non-invertible (i.e. there are a number of possible solutions), other constraints must be imposed on the image. The maximum entropy method uses the criterion that the image be the smoothest solution (i.e the one with the least amount of spatial information) that still fits the observed data to the level of the noise.

In the Doppler images presented here, the additional constraint was imposed that only

cool spots (i.e. temperatures below the photosphere) be allowed. This was done for two reasons. First, it is well-established that most photometric variations of RS CVn stars can be explained by cool spots. In fact, virtually all spot temperatures that have been derived for RS CVn-type stars have been cooler than the photosphere. Second, and more importantly, simulations indicate that an unconstrained MEM (one that can find hot and cool spots) will find both, even from a data set that was constructed using only cool spots. Thus, unless one has very accurate *simultaneous* photometry to further constrain the temperature of the spots, it is risky to allow the method to find hot spots. Since we generally did not have this simultaneous photometric data, we chose to constrain the method to find only cool spots rather than try to interpret hot features that may well be artifacts.

3.3. Thresholding the Images

3.3.1. Using Spectral Lines

The maximum entropy digital image reconstruction method produces a maximally-smoothed image with a continuous transition from spotted to photospheric regions. This is the case even if the original distribution consists of only two temperatures. This makes it difficult to discern spot boundaries (edges) when comparing different images. To facilitate comparisons between images, as well as to display the more prominent features of the spot distribution, the ‘raw’ MEM images were converted into a two-temperature image in the following manner. First a temperature threshold was selected, below which any image pixel was regarded as being ‘spot’, and above which a pixel was regarded as being unspotted ‘photosphere.’ All ‘spot’ pixels were replaced by a temperature of 1200 K below the photospheric temperature of 4750 K, and all ‘non-spot’ pixels by the nominal photospheric temperature. This “binary” distribution was used to calculate a set of predicted spectral line profiles that were then compared to the observed profiles. The threshold level was

adjusted until a satisfactory match to the observed line profiles was obtained. (Another artifact of MEM is that low-latitude spot features tend to be warmer than high latitude features due to their small projected areas. Consequently the threshold level for these low-latitude features was about 100 K warmer than for high latitude features.)

Although this approach disallows any possibility of imaging penumbrae, such details are probably not warranted by the dataset anyway. The process does capture the essence of the fact that most sunspots, when viewed at low spatial resolution, are probably umbral-dominated structures. These thresholded images will often be referred to as “spectral” images (since they were derived purely from spectral data) and will be shown as a combined two-temperature and grayscale version. The black areas of the Doppler images are regions where spots are highly certain and the presence of darkening is relatively insensitive to the details of thresholding. These regions thus represent the two-temperature distribution that best fits the observed spectral line profiles. Regions of the image that did not survive the thresholding process are shown in their original grayscale level. By showing both the ‘raw’ and the thresholded versions of the Doppler image solution as gray and black respectively, we have sought to focus the viewer’s attention on the most certain features (black), while still preserving other more subtle features (gray), some of which may also be real.

3.3.2. Using Photometry

None of our spectral data were accompanied by simultaneous photometry. Published light curves, when available, are still useful even if not contemporaneous with our spectral data. If the photometry is contemporaneous, then it provides additional constraints to the Doppler image, primarily in fixing spot areas. If the light curve is not contemporaneous with our Doppler image then it may provide us with useful knowledge about spot evolution.

This is particularly important since the time sampling of our images can often be quite poor, so a spot distribution derived from the light curve can fill in gaps between images.

The reconstruction technique, in its current implementation, does not incorporate light curve fitting. However, the derived Doppler image combined with light curve information can be used to produce a photometric spot model in the following manner. The spectral image was used as a starting point for fitting the observed light curve. First, the best fit to the light curve was obtained by increasing or decreasing spot areas (essentially setting a new threshold level) until the predicted light curve best matched the observed. If the fit to the light curve was still poor then individual spot features were removed or added. Additions were generally only made to those regions of the MEM image that indicated the presence of a feature (even if it was at a low level). This way the photometry could bring out low-level features which were not certain in the Doppler image and did not survive the thresholding process, but for which the photometry indicated a feature must be present.

In some instances, the photometric data were acquired significantly far from the time of our spectral data so that spot migrations may be important. In this case, not only were spot areas from the original MEM image allowed to change, but individual spot locations were also allowed to move to obtain a better fit to the light curve. Finally, if the predicted light curve was still a poor fit, additional spots were added at arbitrary locations. The final spot distributions which provided the best fit to the observed light curve will often be referred to as the “photometric” image since the final spot areas and locations were driven more by the light curve than by the spectral data.

3.4. Limitations of Poor Phase Coverage

In trying to discern spot evolution and migration patterns we were often forced to derive images from spectral data with sparse phase coverage. It is worth mentioning here the resulting limitations. For high latitude features sparse phase coverage has minimal effects. The inclination of HR 1099 means that all regions of the star above a latitude of 57° are always in view. Features above this latitude (e.g. polar spot) can be accurately recovered with only a few observations.

The largest effect of sparse phase coverage is on low-latitude features. If a low-latitude spot were to lie in the middle of a large phase gap it would be missed outright by the reconstruction process. If this feature is seen only at one phase, then it may appear in the raw MEM image, but be lost by the thresholding process. For example if, at a given observation, such a spot is near the limb of the star, it will only effect the spectral line profile in the wings where the distortions are more subtle than for features at line center. The reconstruction process would thus put only a weak, low-level feature near the location of the spot. This feature would not survive the thresholding process since there are no additional observations to help us judge whether such a low-level feature is indeed real. On the other hand, if the low-latitude spot is seen at line center in only one observation, it will produce a strong distortion in the line profile, but its latitude will remain completely ambiguous. Thus in the thresholding process a high-latitude feature (e.g. a polar appendage) may be favored at the expense of a low-latitude feature at the same longitude.

Mirroring (i.e. the appearance of ghost images at low-latitudes from high-latitude features) is another subtle effect which may be present at some level even with reasonably good phase coverage. If the star has an inclination of 90° then there is an equal probability that a feature lies in either hemisphere. The spot distribution below the equator will thus be a mirror image of the opposite hemisphere. As the inclination of the star is decreased this

ambiguity is removed and MEM tends to favor placing the spot at the positive latitudes. However, even for low-inclination stars there may still be some residual spot features visible at negative latitudes.

The appearance of ghost or mirror images is also a concern when the phase coverage is sparse. To fit a distortion in a line profile at a given phase, MEM places spots along a constant radial velocity chord. In order for MEM to “choose” whether the feature actually lies at low or high latitude it must have additional information at other phases; the temporal behavior of distortions from low-latitude spots is different from that from high-latitude spots. If the phase coverage is poor, then blurring of features in latitude may cause ghosts to appear at low latitudes.

3.5. Pre-1981 Gleanings

Our first Doppler image of HR 1099 was obtained in 1981. Prior to that, our knowledge of spots was limited to relatively simple (1-spot or 2-spot) models fit to broadband light curves. We begin our discussion of the present 11-year image-set by reviewing the published perception of starspots on HR 1099 from data and modelling done before 1981.

Weiler et. al. (1978) presented coordinated ultraviolet, optical, and radio observations of HR 1099 taken in Sept. 1976. They observed V-band variations as well as variable $H\alpha$, $L\alpha$, and Mg II emission, and strong Ca II H and K emission. Their observations provided strong evidence that significant chromospheric activity was present in this binary system and was associated with the K0IV star.

Dorren and Guinan (1982) modelled a set of light curves collected between 1963 and 1981. As is typical of most spotted RS CVn stars, HR 1099 exhibited large light variations each observing season, with dramatic changes in the light curve’s shape, amplitude, and

phase from season to season. They were able to obtain good fits to the rather complicated changes in the light curves throughout the entire 12-year period with a simple ‘2-spot model’ with cool spots on the K0IV star. The spots were found at latitudes as high as 65° . The complex changes in the light curve were explained by fairly simple systematic changes in the sizes, latitudes, and longitudes of the two spots. They also noted a maximum in spot area which occurred in late 1978, at which time some 20% of the K0IV star was covered with cool spots. They were also able to place a lower limit of 5 years on the length of any spot cycle. They noted a steady increase in the phase of photometric minimum (photometric wave advances with phase), with a migration period of about 9.5 years. Finally, they also noted that observed radio flaring seemed to occur at a time when the spots were changing rapidly in size and position. Kang and Wilson (1989) presented a similar ‘2-spot model’ analysis of essentially the same (1963-1982) light curve set. Their fits to these light curves yielded cool spots on the K0IV star which also produced a photometric ‘migration wave’ which advances with phase with a migration period of about 7.6 years, and came from 2 dominant spots fixed at 45° latitude. The advancing phase of the migrating wave then implied, with their model, that the star is rotating more slowly than the orbital period at 45° latitude.

A large radio outburst observed on February 20, 1978 by Feldman et al. (1978) drew further attention to this star and set off a large number of other observations (many of these are described in the series of papers introduced by Hall (1978)). Feldman et al. (1978) interpreted the observed radio emission as nonthermal gyrosynchrotron radiation from a volume whose characteristic dimension was several times larger than the stellar diameters but comparable with the binary star separation.

Bartolini et al. (1983) presented light curves from 1979-81 and interpreted the remarkable changes in the light curve shapes as due predominantly to latitudinal and

longitudinal migration of two distinct and constant-area spots on a differentially-rotating star whose co-rotating latitude was somewhat away from the equator. They compiled data on the phase of photometric minimum from 1976 to 1981 and concluded that the wave migration rate was neither constant, nor in a single direction. From 1977 to 1979, the migration rate was constant at about 5 years/cycle towards increasing phase, but, as shown by Parthasarathy, Raveendran, and Mekkaden (1981), from 1976 to 1977 the migration rate was much slower and moved toward decreasing phases. This was a key observation since, up to that time, the migration rate had appeared quite uniform and in the same direction for many years. From 1979 to 1980, the migration rate was also towards advancing phases, but slowed considerably from that of 1976 to 1979.

Dorren, Siah, Guinan, and McCook (1981) presented photometry of HR 1099 from 1977-78 and 1979 and derived basic spot parameters from simple ‘2-spot’ model fits to the photometry using cool spots on the chromospherically active K0IV star. They determined the spot temperatures to be about 1800 K cooler than the photosphere, and (circular) spot radii to be about 26° to 32° . Their solutions placed spots as high as 48° in latitude, with spot areas 10-14% of the stellar surface. They noted a significant change in the amplitude, shape, and phase of the light curve from 1978 to 1979. They also reported their strong suspicion that a spot cycle may be in progress on HR 1099, with spot locations migrating from high to low latitudes over a few-year interval. Lodenquai and McTavish (1988) presented a two-component circular spot model which used both penumbral and umbral regions for each spot. They found spots at latitudes as high as 60° . They reached the same basic conclusion as previous modellers of the 1977 to 1981 light curves, that the changes were predominantly due to movement of constant-area spots in longitude and latitude.

Ayres and Linsky, (1982) reported emission features of such high-temperature species as C II and C IV from HR 1099 in 1980.5. These emission features were clearly associated

with the K star and were interpreted as a patchy brightness distribution on and above the K star surface, spread out in velocity by the star’s rapid rotation.

3.6. The 1981 Doppler Image

So, prior to obtaining an actual image of a spotted star, the published perception of the spots on HR 1099 was of a small number of roughly circular cool spots, covering a total combined area of as much as 20% of the stellar surface. These spots were believed to sit at mostly intermediate latitudes, with some spots reaching as high as 65° latitude. These spots were thought to maintain roughly constant area from year to year, and the dramatic changes in the light curves from were ascribed mostly to migration of constant area spots in both longitude and latitude. The ‘migrating photometric wave’ was interpreted as due to motion of spots on a differentially-rotating star whose co-rotating latitude was somewhat away from the equator, though the details were not clear since the migration rate was variable and the direction could also change.

Our first Doppler image (Vogt and Penrod (1983)) of HR 1099 was for the year 1981. It was a rather preliminary and crude version because, at that time, we were approaching the inversion problem by ‘trial and error’ iteration. Nevertheless, it showed something quite unexpected from the previous photometric spot models and from solar analogy; a large spot straddling the pole. This polar spot was always in view in this low-inclination system, and thus contributed little modulation to the light curve. The polar spot had an attached lane which descended to lower latitudes. There was also a second, slightly elongated spot near the equator. Since that preliminary image was made, we have vastly improved the Doppler imaging technique, incorporating principles of maximum entropy digital image reconstruction (Vogt, Penrod, and Hatzes (1987)).

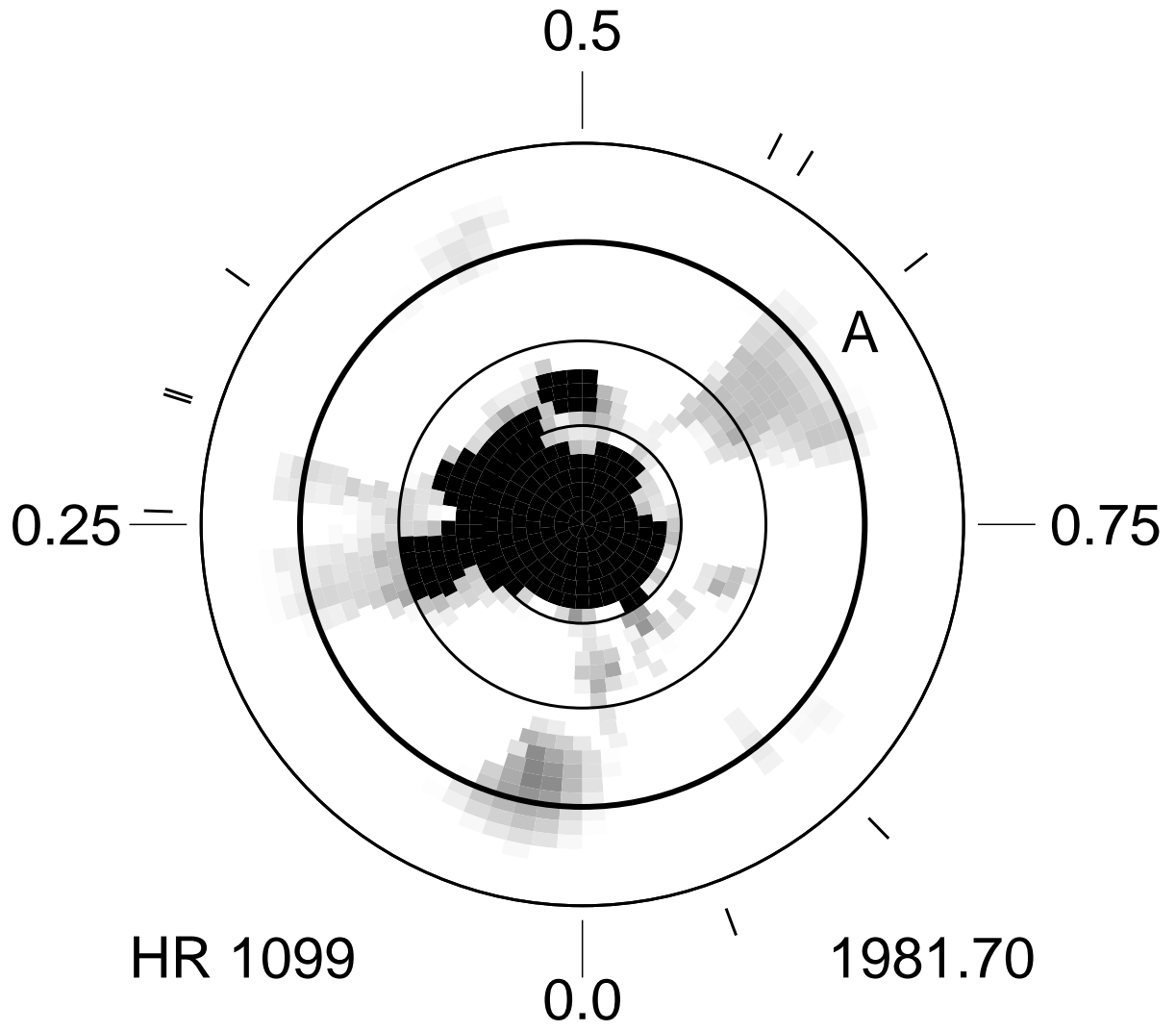


Fig. 1.— HR 1099 raw Doppler image for 1981.7

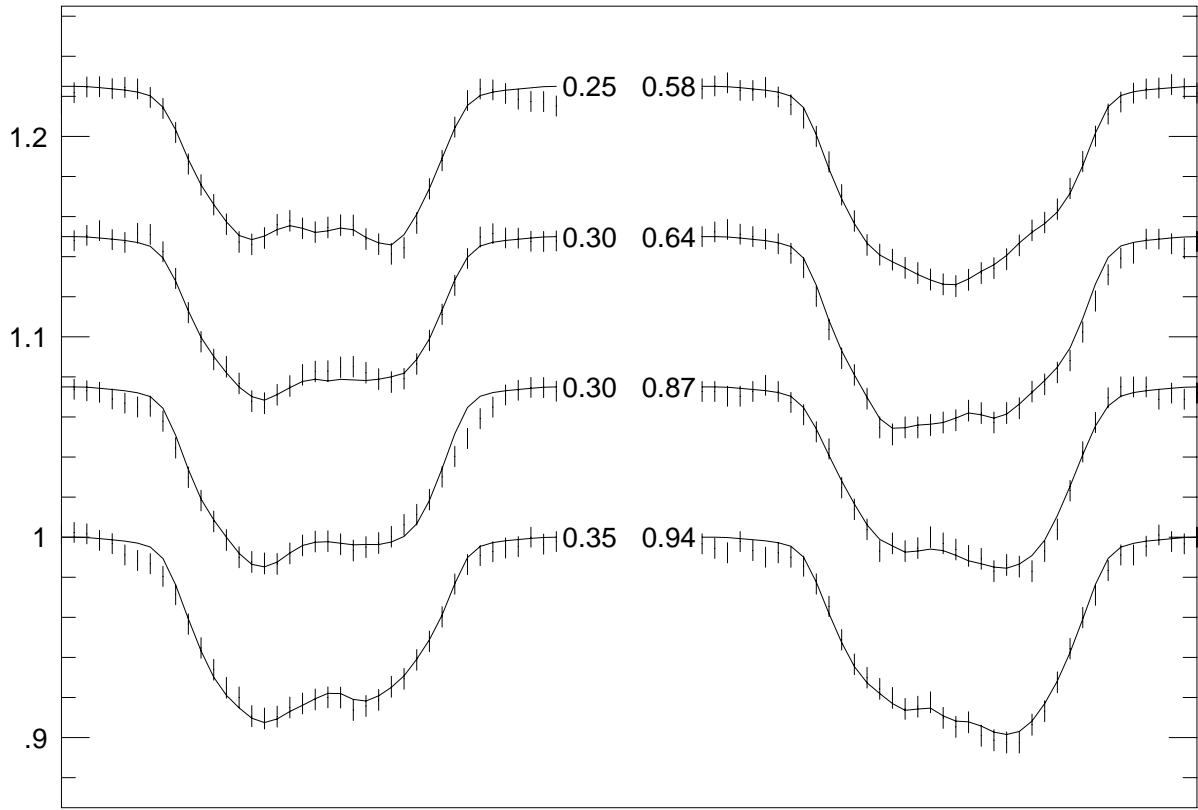


Fig. 2.— Observed spectral line data (vertical bars) and fits (solid lines) for the 1981.7 image

The most recent (raw) version is shown in Figure 1. HR 1099 is actually viewed from an inclination angle of about 33° and, also being spherical, makes representation of the Doppler image of the star difficult, requiring either highly distorted mercator-like projections, or 3-d spherical renderings (globes) at multiple phases. To make intercomparison of images as simple as possible, we have rendered all the Doppler images of this paper as ‘flattened polar’ projections, such that only one minimally-distorted image is required for each epoch, and all areas of the star visible from Earth are shown simultaneously in a single image, including latitudes below the equator, down to the limit of visibility of about -30° . The bold latitude line in Figure 1 represents the stellar equator, with finer lines for latitudes of $+30^\circ$ and $+60^\circ$ also provided. The pole of the star is thus at the center of the figure and the outside edge of the star represents a latitude of about -30° . Phases at which the actual line flux profiles were obtained are denoted as tick marks arranged radially around the star. The spectral line profiles used in the modeling are shown as vertical bars in Figure 2. The length of each bar represents the error in the flux measurement. The MEM fit to the profiles are shown as solid lines.

Figure 1 is called a ‘raw’ image in the sense that it was derived only from the line profile information, with no attempt to fit the broadband lightcurve. It shows a large polar spot of about 55° diameter straddling the pole with an attached protuberance at about phase 0.2 - 0.3. In our original ‘trial and error iteration’ image (Vogt and Penrod (1983)) there was also another large isolated spot at latitude 21° and phase 0.65. However, in our more recent and powerful MEM imagery, this feature essentially disappeared, leaving only a low-level remnant in Figure 1 near latitude 20° and phase 0.65. While neither the line profiles nor the photometry require a feature here, evidence of a similar feature has been reported by others, so in the following discussion we will refer to it hereafter as Feature A.

Rodono et.al. (1986) presented photometry from the 1981-2 observing season (in

conjunction with the 1980 and 1981 IUE observing campaigns, and worked out ‘two-spot’ model fits to the photometry. Their 1981.7-8 light curve data are presented as the points in Figure 3. The theoretical light curve predicted from our raw Doppler image of Figure 1 is shown as the dotted line. Clearly its amplitude is too low, and is not an acceptable fit to the observations. However, the fit from the thresholded image (2-temperature distribution) does provide an adequate fit to the data.

The best fit to the photometry with a thresholded image was obtained *without* the low latitude phase 0.65 spot (Feature A). This spot is actually at a fairly low level in the MEM image and the line profile fits of the thresholded image are totally consistent with not having a spot there at all. Our best and final Doppler image, obtained after further thresholding to improve the light curve fit and still fit all the line profiles is shown in Figure 4. Its predicted light curve is shown as the solid line in Figure 3. The polar spot was pretty much unchanged by the additional constraints of light curve fitting, but Feature A completely disappeared.

Figure 5 shows the Rodono et.al. (1986) spot model superimposed on a grayscale version of the MEM image (without thresholding) from 1981. Clearly their spot at high latitude corresponds to our polar spot protuberance near phase 0.3 in Figure 4. This feature has smaller diameter and does not straddle the pole as does the corresponding feature in the Doppler image primarily because the photometry is not sensitive to spot regions very near and symmetrical about the rotation pole. Their spot 2 was of diameter 30° in 1981.7 and situated at $+10^\circ$ latitude and at their phase 0.57. This phase corresponds to phase 0.59 in our image and is somewhat near Feature A in our original and raw Doppler images. Their Spot 2 was also growing in diameter and shifting toward earlier phases, reaching a diameter of about 48° by the time it reached phase 0.49 at epoch 1981.9. It would be natural to then use such a result, longitude migration of a single spot, to derive the differential rotation of

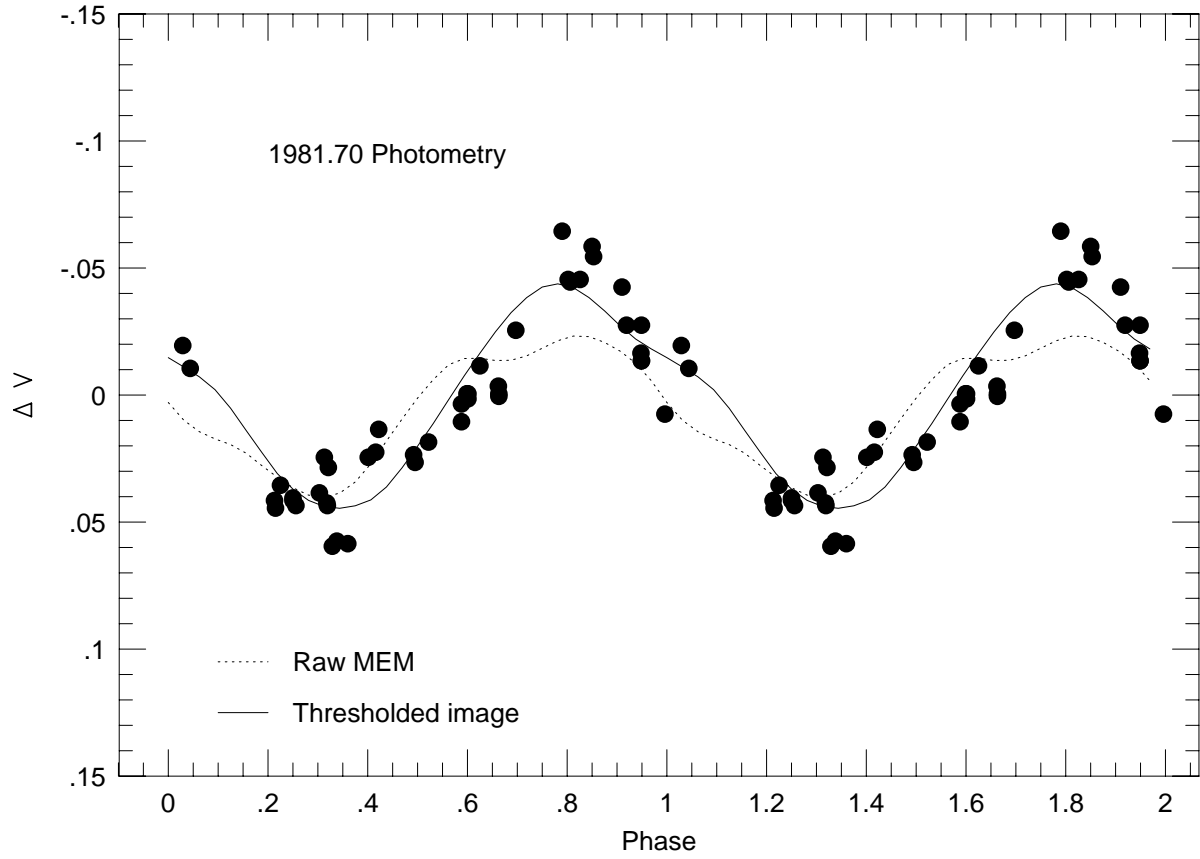


Fig. 3.— HR 1099 light curve for 1981.70 - 1981.80

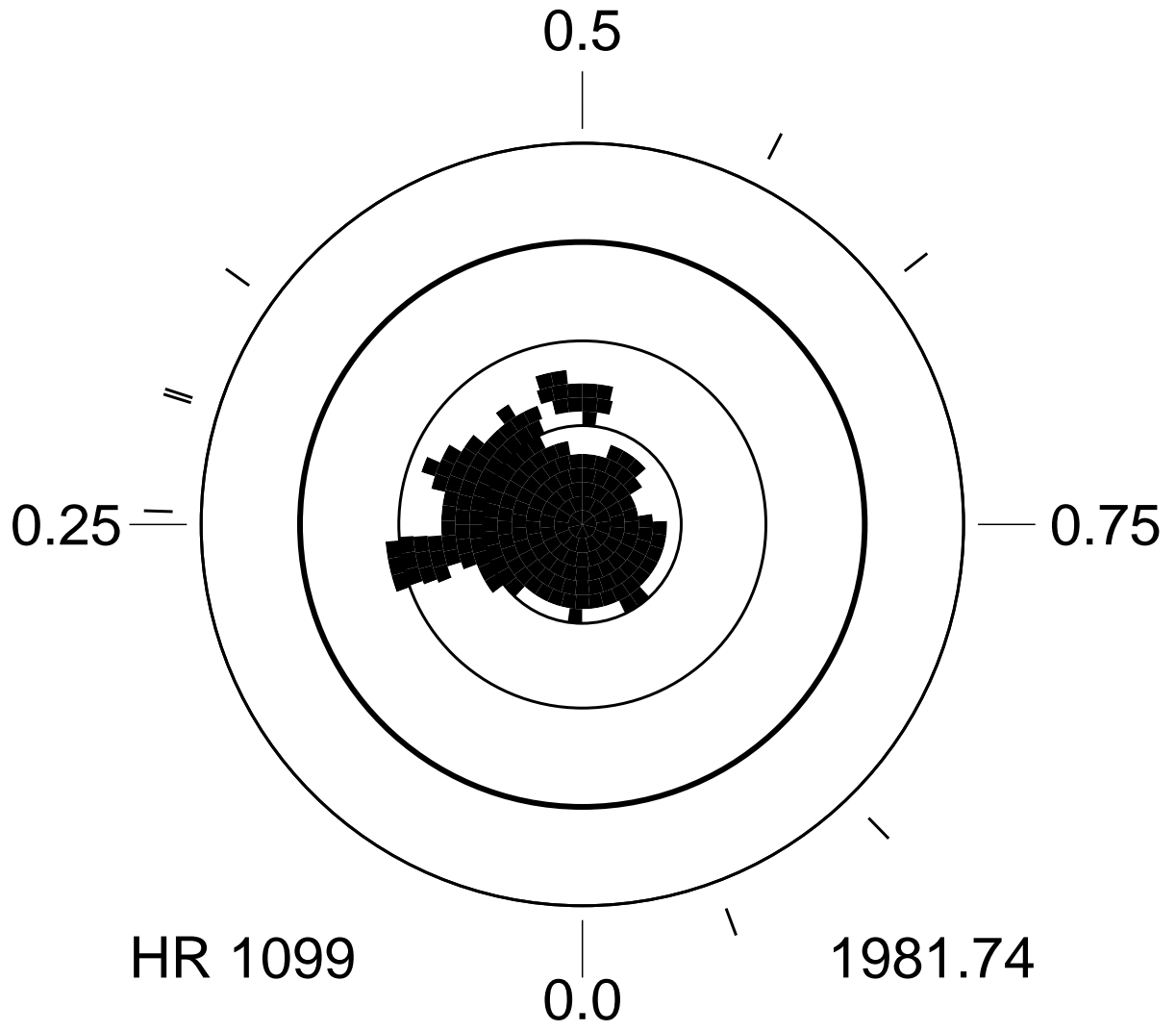


Fig. 4.— HR 1099 thresholded Doppler image for 1981.7

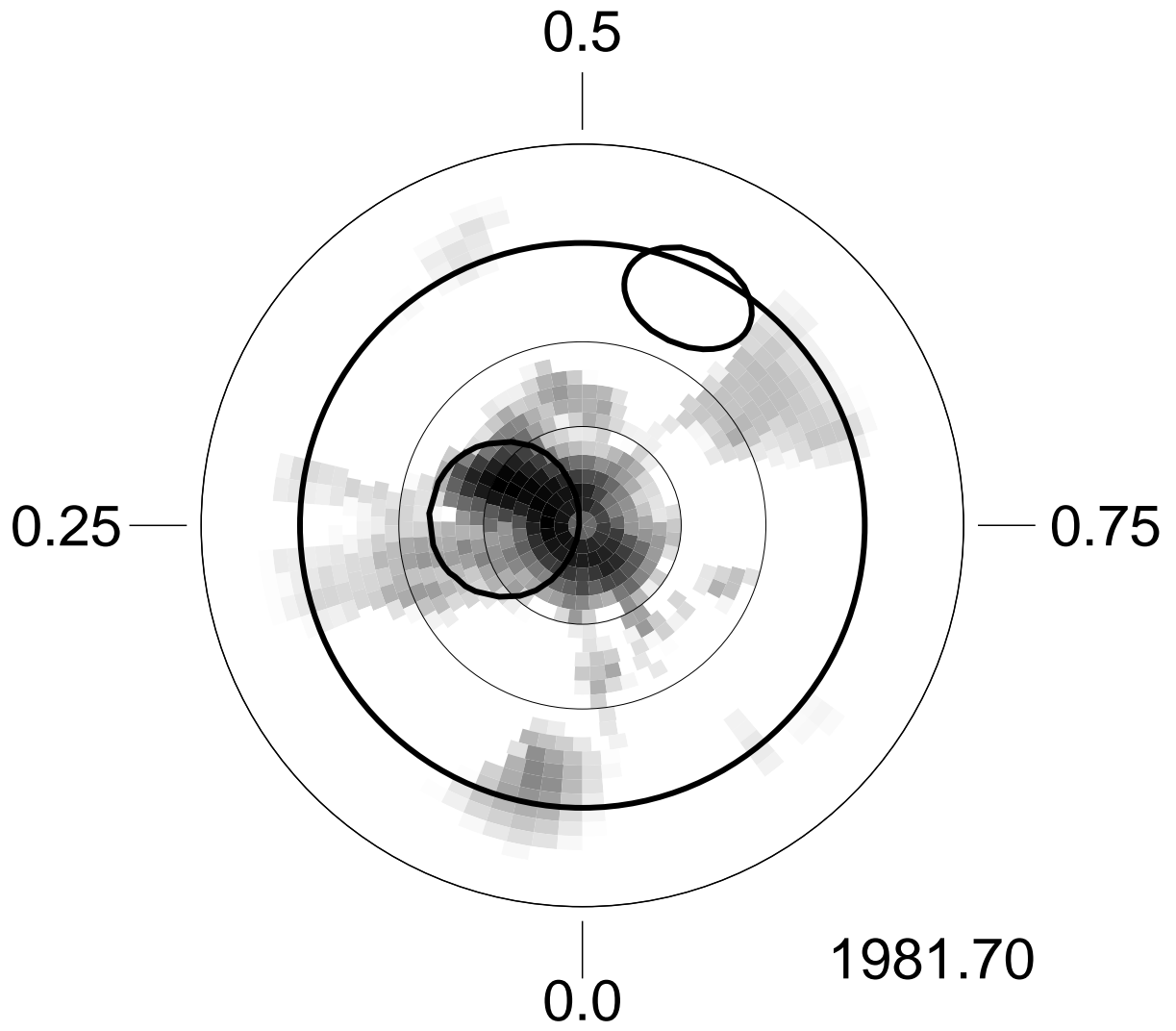


Fig. 5.— The 2-circular-spot photometric model of Rodono et al. superimposed on the raw MEM Doppler image

the star. However doing so in this case would have been quite misleading since Feature A probably does not exist.

Rodono et.al. (1986) may have been guided by our original published HR 1099 image from Vogt and Penrod (1983) (which *did* show a prominent Feature A) in their choice of a spot solution which fit their photometry. Thus the initial agreement between their 2-spot solution and our original Doppler image looked promising. However, since Feature A did not survive our more modern MEM imaging technique and our further constraints of thresholding to fit the photometry, its existence is quite suspect. We cannot, however, absolutely rule out the existence of Feature A, and could tolerate some spot at that general location on the star and still be consistent with all the line profile and photometric data. Unfortunately, the 0.02 magnitude scatter in the photometry does not allow us to be more definitive since the reality of features such as Feature A hinge crucially on fitting inflections in the light curve at these levels. But, to within the S/N of the data, Feature A is certainly *not* required by either the line profile fits or the photometry. Our Doppler imaging method, by design, yields the simplest image (i.e the one with the least amount of information content) consistent with all the data. It is thus an ‘Occam’s razor’ approach to a highly non-unique inversion problem. Thus there may be image structure present on the star beyond what is revealed in the maximum entropy image, but the data cannot unambiguously support such structure. By the same token, the minimal information content nature of our Doppler images assures that any structure present in the image is fully demanded by the dataset. Since the much simpler final image we present, without any Feature A, is fully consistent with both the photometry and all the line profiles, we must conclude that Feature A probably does not exist. The end result is that, overall, the agreement between our final thresholded Doppler image, and the 2-circular-spot solution of Rodono et.al. (1986) is not very good.

Lodenquai and McTavish (1988) also presented a ‘2-spot’ model solution to the 1981 light curve data of Rodono et.al. (1986). Their solution provided a basically adequate fit to a single light curve, but their fit was clearly not as good as the fits to multiple light curves by Rodono et.al. (1986). Not surprisingly, Lodenquai and McTavish (1988) derived a quite different characterization of the spots, further indicating how far off the mark the ‘2-spot’ approach can stray. They found two spots of diameter 58° and 42° respectively, separated by 110° in longitude, and both situated at 23° latitude. They did not include a phase zero point in their solution, so their only longitude information was the relative longitude separation of the spots.

Another 2-spot model fit to the light curve for this epoch is provided by the results of Kang and Wilson (1989). Their solution is shown as the circles in Figure 6. Again however, they fit only a single epoch curve for 1981.9; this curve had only 8 observed points. Their ‘2-spot’ fit to the 1981.9 light curve of Rucinski (1983) yielded two spots, both at 35° latitude. Their first spot was at their longitude 345° (our phase 0.458) and was 42° in diameter, while their second spot was at their longitude 244° (our phase 0.178) and had a diameter of 47° . Again, while they did achieve a respectable fit to the light curve, that light curve did not contain enough constraints for a meaningful spot solution (6 spot parameters were derived from a light curve with only 8 observed points). Their 2-spot solution is a clearly not an accurate representation of the spot distribution. Their conclusions about spot longitude migration and spot cycles drawn from these solutions must be judged accordingly.

So we see three different attempts at deriving the spot distribution at epoch 1981.7 via ‘2-circular-spot’ model fits to light curves. All three yielded respectable light curve fits but gave quite different spot solutions. None of the three agreed well with our Doppler image. Our Doppler image is certainly not to be regarded as an absolute standard against which other solutions should be judged. Doppler images also have some degree of nonuniqueness,

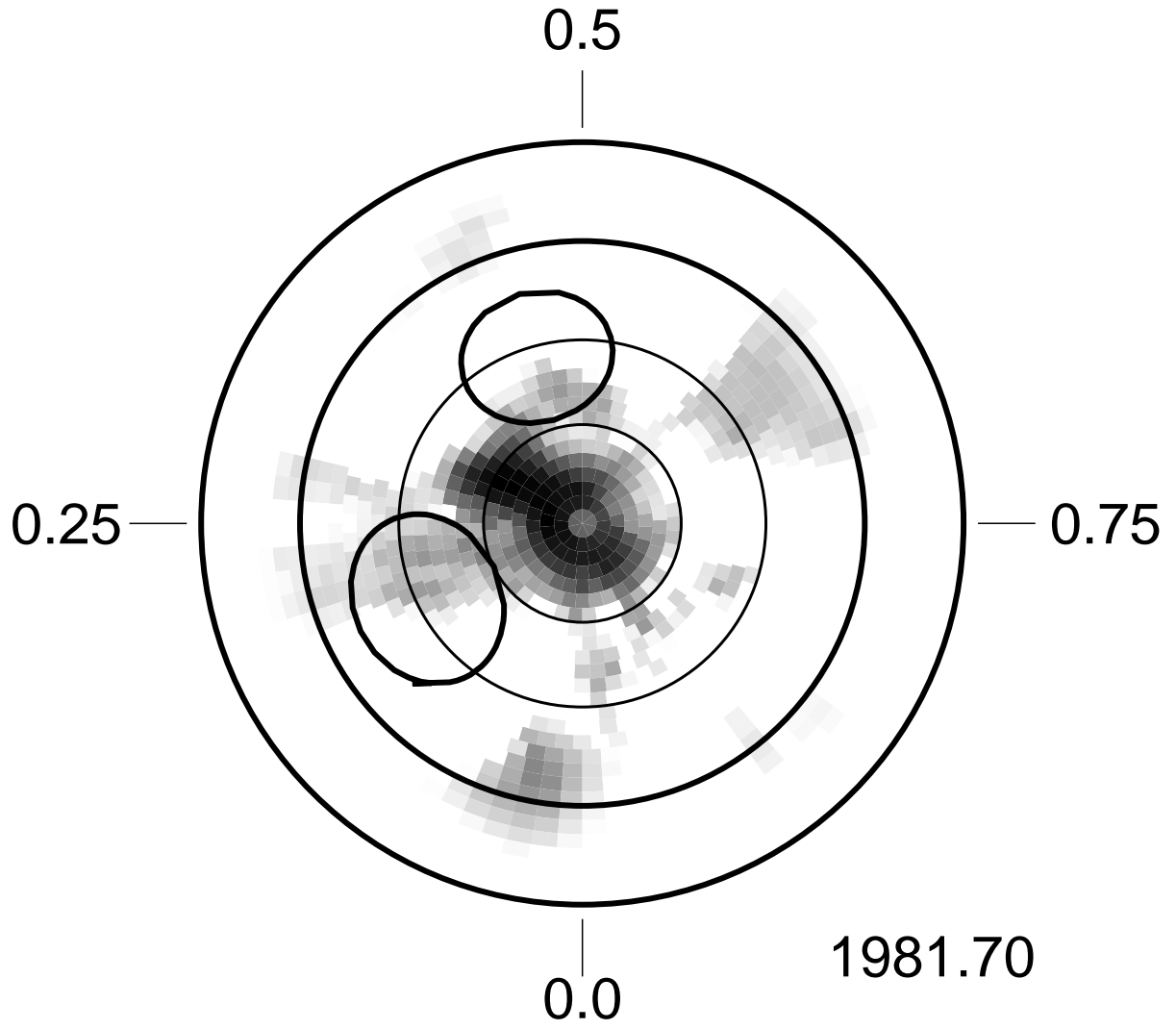


Fig. 6.— The 2-spot 1981.9 photometric model of Kang & Wilson superimposed on the raw MEM Doppler image of 1981.7

but the images are much more highly constrained (by a large set of intensity measurements at many different velocities) than are the photometric solutions. Also, the ‘maximum entropy’ criterion of the images guarantees that every feature shown in the image is actually required by the data, and that there is no more image information than is minimally necessary to reproduce all the data. We thus believe that the Doppler images are likely to be a much more highly constrained and accurate representation of the spot distribution.

The lesson to be learned here is that ‘2-spot’ modeling of light curves is, at best, a non-unique process, largely because it uses so few constraints for the image solution, that - as demonstrated above - multiple solutions can be found, each of which fits the light curve equally well. At the very least, the technique requires very accurate fitting of the subtle inflections in high quality photometry. A relaxed light curve fit and/or noise in the data can easily mask the true details of the spot distribution, yielding highly non-unique solutions. A reduced light curve amplitude also can contribute to non-uniqueness. 2-spot and 3-spot solutions must always be viewed in that light. In particular, drawing conclusions about spot locations, spot migration, or differential rotation from such modelling can be quite misleading.

There were some other observations of HR 1099 reported during this epoch. Rodono et al. (1987) presented IUE emission line flux observations obtained during October, 1981. They found stellar line fluxes to be hundreds of times larger than solar values and found a close spatial correlation between the cool spots and the plage-like features giving rise to the line emission. This was interpreted as an indication of large spot areas down in the photosphere with overlying magnetic loops, which then give rise to plages higher in the atmosphere. Byrne et al. (1987) combined ground-based optical and IUE satellite-ultraviolet observations of HR 1099 in 1981 to show that solar-like densities are present in the outer atmosphere of the star, and that total radiative losses were at least

two orders of magnitude larger than on the Sun. Linsky et al. (1989) published a detailed study of a well-observed flare of Oct. 3, 1981 on HR 1099. They concluded that they had observed a region of turbulent infall on the K1IV star near phase 0.2. That might place it over the protuberance of the polar spot in Figure 4. Nations and Ramsey (1986) reported some H-alpha line emission observations taken in the late 1981 which showed that 86% of the emission was coming from the K1IV star.

3.7. The 1982 Doppler Image

Our next Doppler image was obtained almost exactly one year later at epoch 1982.74. Unfortunately, we did not have a contemporaneous light curve for this exact epoch. Andrews et al. (1988) presented light curve data for the interval 1982.78 through 1983.17, but most of these data are an uncomfortable 2-3 months later than our image epoch, and we were concerned about the light curve varying over this long interval.

As usual, we first derived a Doppler image from the line profile information alone, and this is shown in Figure 7. Figure 8 shows the spectral line profiles and fits. In the image one sees the same basic polar spot straddling the pole, but now substantially larger in area, and with more protuberances. It is not clear that any of these protuberances can be identified with the one from the previous year (and thereby used to measure the relative rotation rate of the polar spot) since the polar spot now looks quite different.

The 1982.93 light curve data of Andrews et al. (1988) is shown in Figure 9. Our raw image produced a light curve (dotted line) which fit these data marginally well, even with the light curve taken nearly 2-3 months after the image solution centroid. Only a slight bit of thresholding was needed to produce the final predicted light curve (solid line) which fit quite well. The resultant final thresholded image is shown in Figure 10 and is essentially

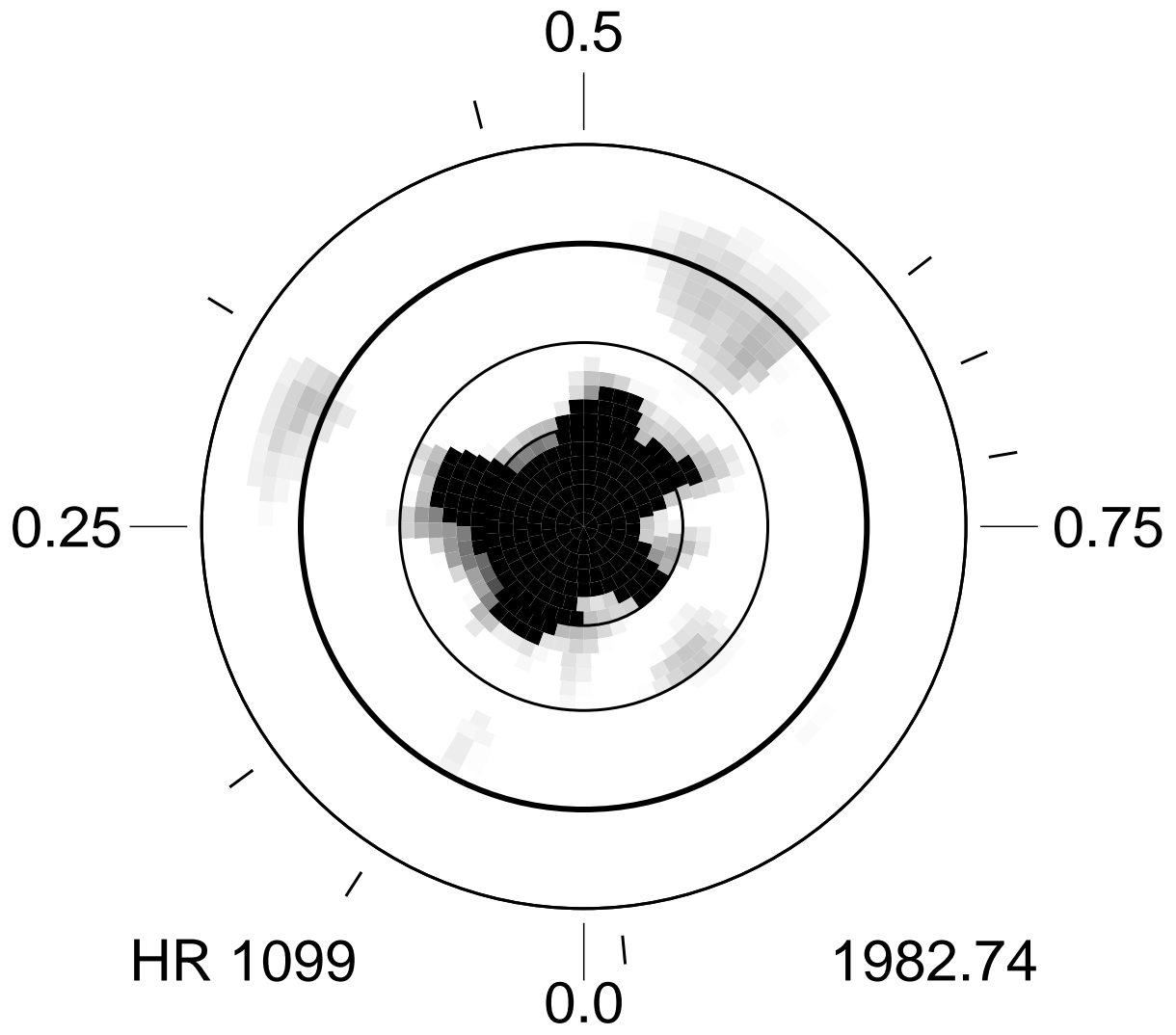


Fig. 7.— HR 1099 raw (unthreshholded) Doppler image for 1982.74

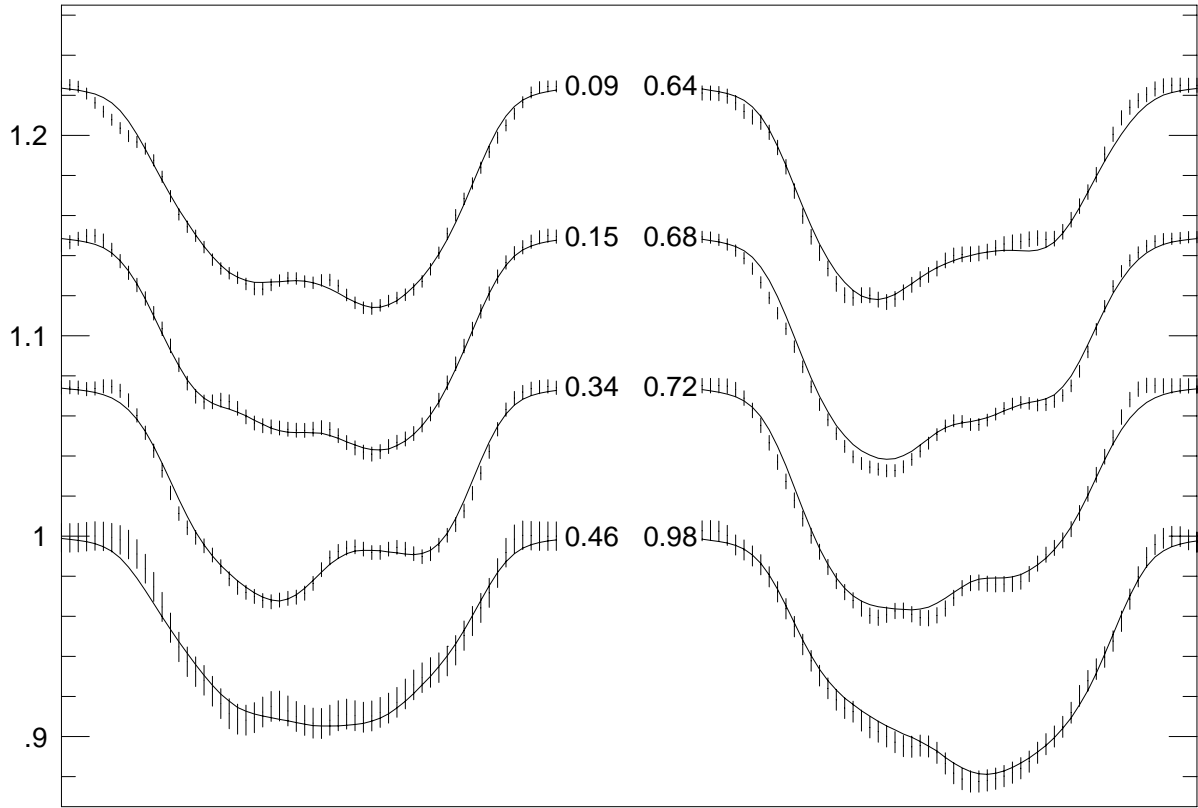


Fig. 8.— The spectral line profiles and line fits for the 1982.74 image

identical to the original unthreshholded image. Again, the low-latitude spot near last year’s Feature A, as well as all the other low-latitude spots, did not survive the threshholding constraint.

Andrews et al. (1988) also presented a 2-spot solution from fits to their photometry. This is shown in Figure 11 along with a grayscale version of the raw Doppler image. Their Spot 1 was of diameter 36° at latitude 60° and phase 0.15. Their Spot 2 was of diameter 40° at latitude 5° and phase 0.5. While their Spot 1 does reflect some sense of the protuberance on our polar spot near phase 0.2, we see no evidence of their Spot 2. Overall, their 2-spot solution is not a good representation of the spot distribution from our Doppler imagery.

Lestrade et.al. (1984), using a five station VLBI, detected a sub-milliarcsecond radio component from HR 1099 at epoch 1983.2, during a strong radio outburst at orbital phase 0.226, when the polar spot’s protuberance was facing the earth. Their data suggested gyrosynchrotron emission from a power-law energy distribution of electrons in a magnetic field of strength about 30 gauss and from an area 75% of the diameter of the K-subgiant.

3.8. The 1984 Doppler Image

Unfortunately, due to bad weather, we were unable to obtain a Doppler image for the 1983 season. The image set resumes with a Doppler image for 1984.81. Our raw version, unthreshholded by any light curve constraints, is shown in Figure 12. The spectral line profiles and fits are shown in Figure 13. Light curves for the 1984-5 observing season were published by Strassmeier et al. (1989) and by Mohin and Raveendran (1993). The amplitude was about 0.12 magnitudes and the shape rather similar to that of the previous and following years. We were unable to find any spot model fits to these light curves for this epoch. Our fits to the 1984.94 light curve of Strassmeier et al. (1989) are presented

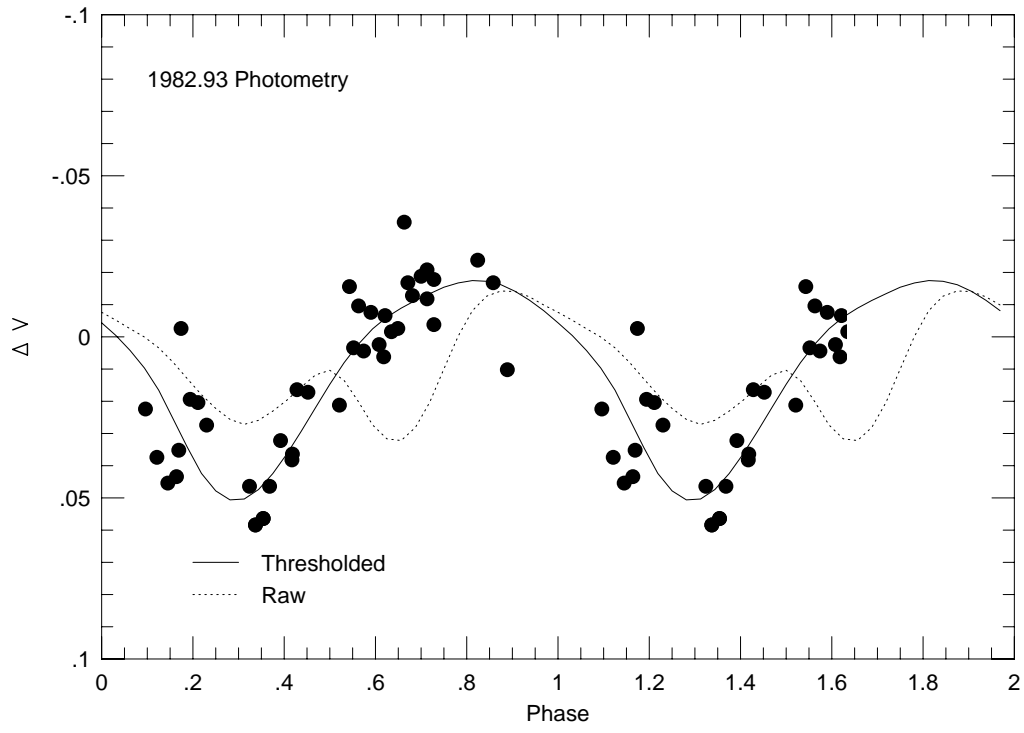


Fig. 9.— 1982.93 light curve of HR 1099 used for the 1982.74 image

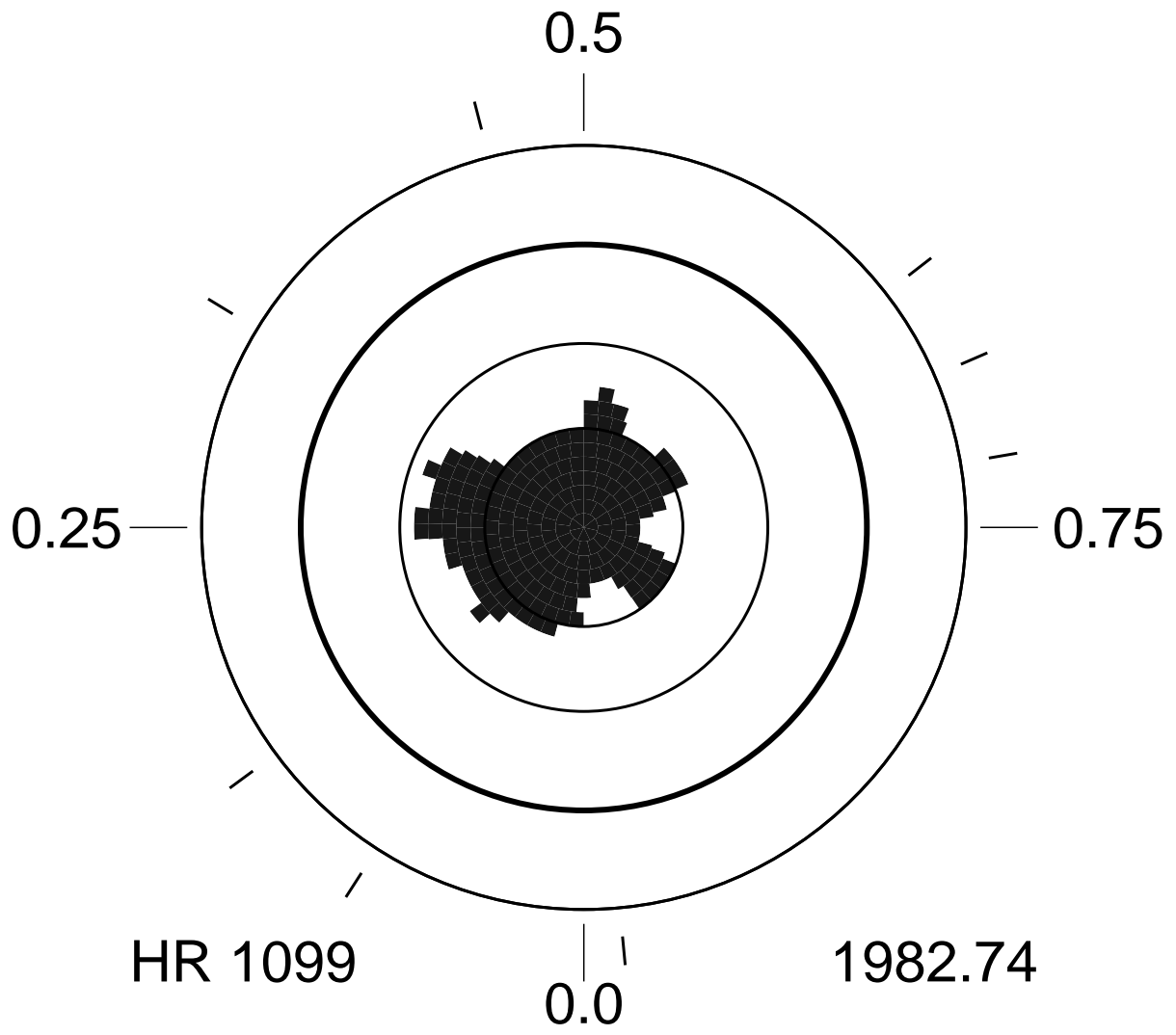


Fig. 10.— HR 1099 thresholded Doppler image for 1982.74

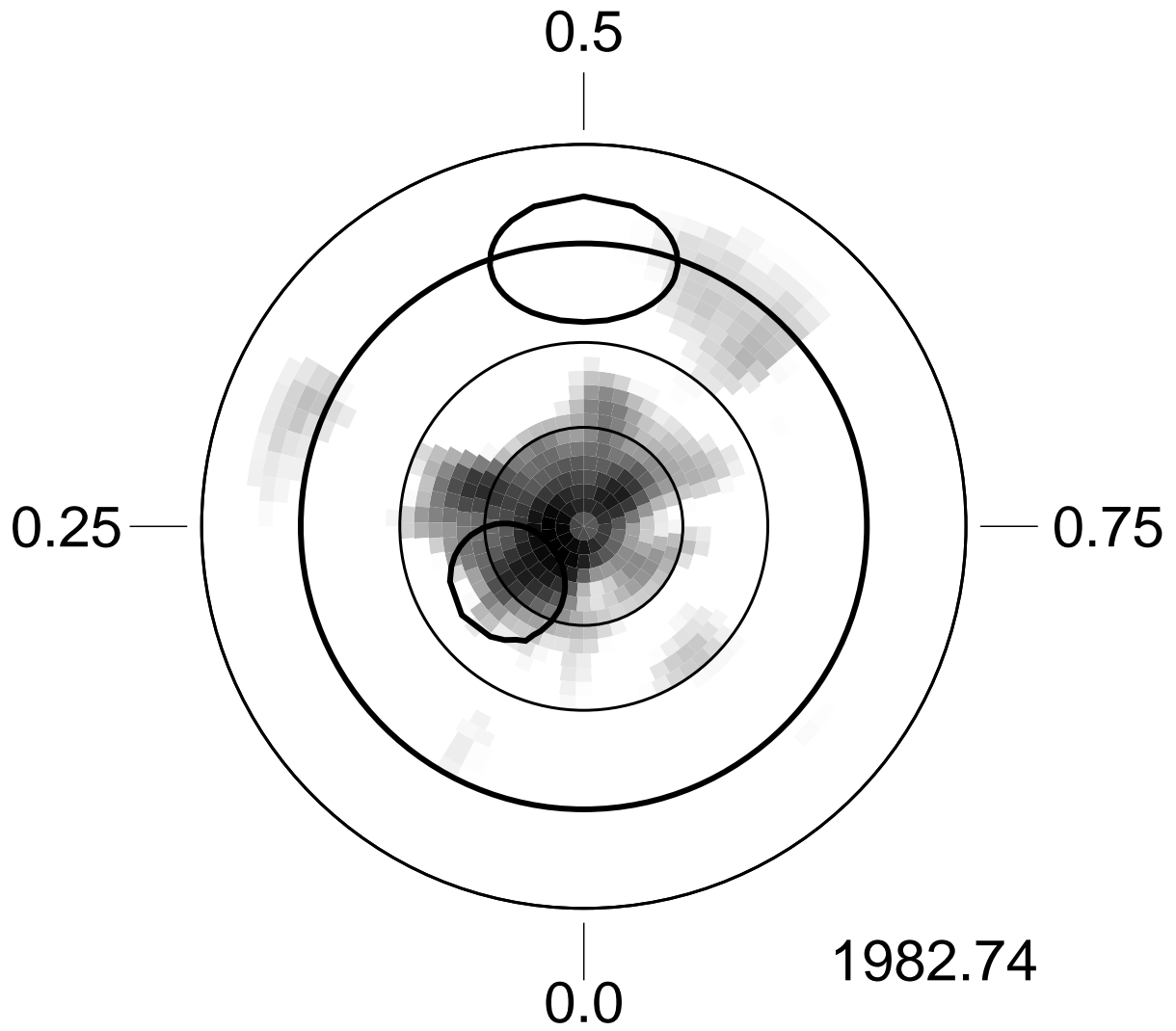


Fig. 11.— The 2-spot photometric model of Andrews et.al (1988) superimposed on the raw 1982.74 Doppler image

in Figure 14. The predicted light curve (dotted line) from the raw MEM image again fit the measured light curve reasonably well but was slightly too low in amplitude. A slight thresholding adjustment yielded the final image of Figure 15, and brought the light curve amplitude (solid line in Figure 14) up to the observed level. As can be seen, there is no significant difference (other than spot area scaling) between the raw and the photometrically-thresholded images. In this case, the light curve was taken some 1-2 months later, but the close agreement between image solutions, with and without the light curve constraints, indicates that the spot distribution was quite stable over this season’s entire observing interval.

The polar spot is still present and still straddling the pole, but with ever-changing shape as protuberances come and go, or perhaps shift in phase. The polar spot changes shape to such an extent that again we cannot find a simple rotation that uniquely matches previous polar spots and that would allow us to derive relative rotation (if, indeed, the true evolution is really that simple). The true situation may be a mixture of both spot rotation and evolving protuberances. The polar spot has a prominent, nearby, almost-attached spot at phase 0.32 and latitude 41° . We shall refer to this spot as ‘Feature B1’. This feature is truly resolved from the polar spot. There is also now a small and isolated spot near phase 0.85 and latitude 37° . Again, it is not known whether this isolated spot is at all related to any of the features in the 1982.74 image. It also seems unlikely to be a phase ghost since, at a latitude of 37° it is seen in the line profiles at about 5 phases.

3.9. The 1985 Doppler Image

The raw Doppler image for 1985.86 is shown in Figure 16 and the spectral line profiles and fits in Figure 17. Light curves for this season were published by Strassmeier et al. (1989), by Mohin and Raveendran (1993), and by Cutispoto (1990). Figure 18 shows the

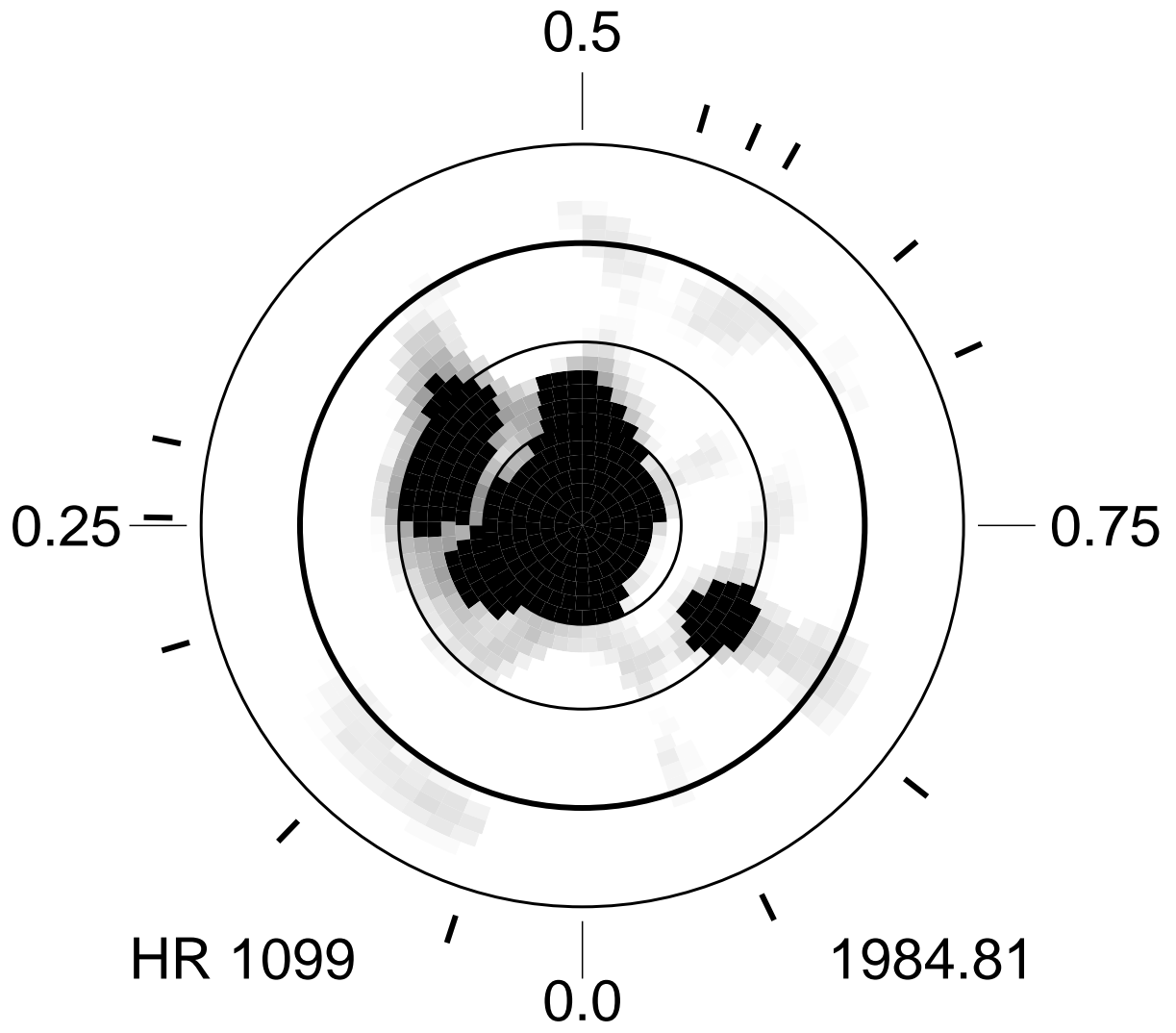


Fig. 12.— HR 1099 raw (unthressholded) Doppler image for 1984.81

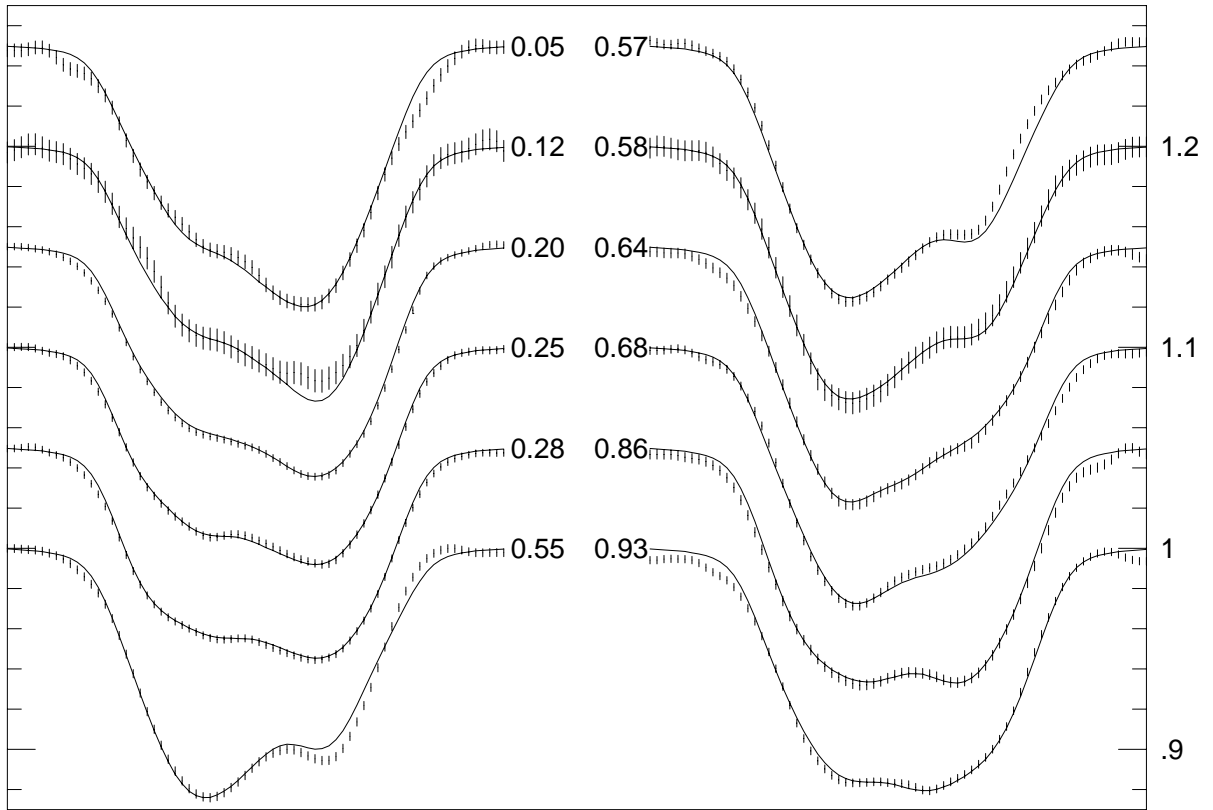


Fig. 13.— The spectral line profiles and fits for the 1984.81 image

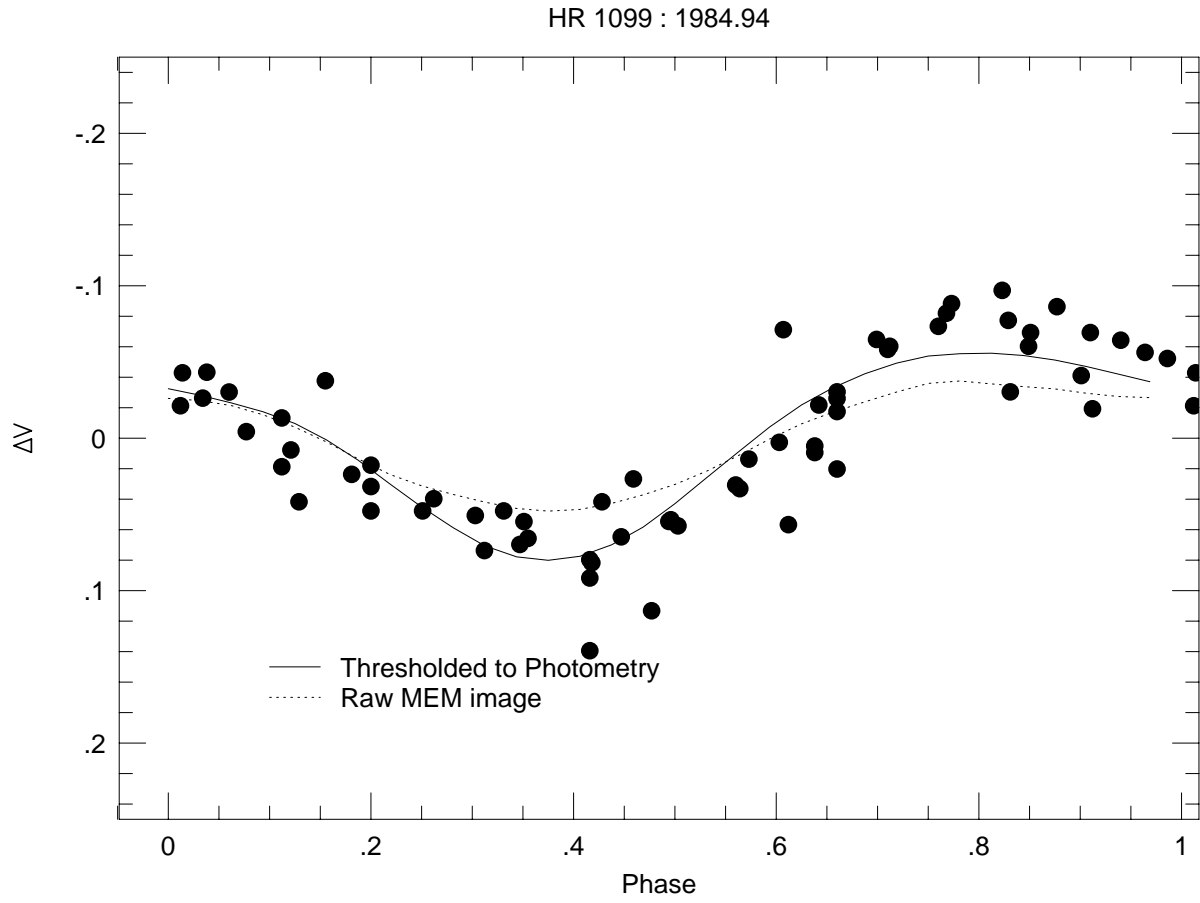


Fig. 14.— 1984.94 light curve used for the 1984.81 HR 1099 image

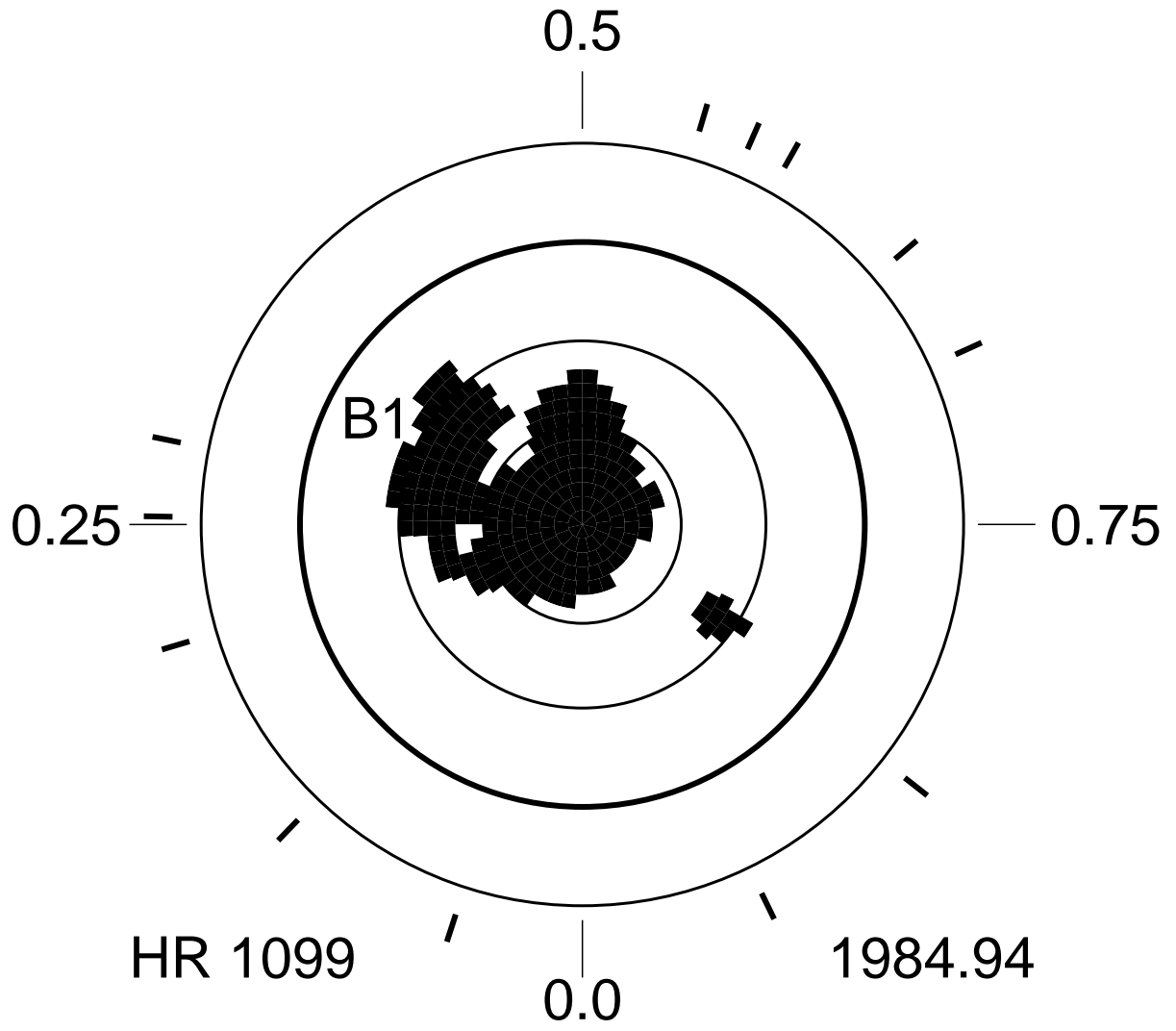


Fig. 15.— HR 1099 thresholded Doppler image for 1984.94

1985.75 photometry of Strassmeier et al. (1989) (points) along with our predicted light curves from the unthresholded (dotted line) and thresholded (solid line) Doppler image solutions. Again the predicted light curve from the raw MEM image fits the observed photometry quite well. Thresholding the image improved the fit only slightly, and again produced no significant change in the image. The final thresholded image is shown in Figure 19.

At this epoch, there were no isolated low-latitude spots, only the omnipresent polar spot with a large protuberance again near phase 0.35. We note a similarity in both shape and area of this protuberance to Feature B1 from 1984.81. It looks as though Feature B1, first seen at latitude 41° and phase 0.32 in 1984.81, simply moved poleward to 50° latitude and clockwise to phase 0.35 in 1985.86, with little change in either its shape or area. Feature B1 thus seems to be slowly circling the pole in a clockwise direction, and may even be merging with the polar spot as it approaches from lower latitudes. If correct, the migration rate implied from Feature B1 (with respect to the co-rotating frame of the orbit) is about $9^\circ - 17^\circ$ per year at latitudes of roughly $37^\circ - 50^\circ$. This corresponds to about $1/3600$ of the orbital period and in the sense that high latitudes are rotating slightly more slowly than the orbit. Note that a 3-sigma error on the orbital period determined by Fekel (1983) amounts to a longitude error due to period uncertainty of only 0.5° . Of course, with a time sequence of only two images, many other interpretations are possible. In particular, it is not clear what if any role the other time variable protuberances on the polar spot may have played. But the similarity of the shape of the phase 0.3 protuberance in 1985.86 with Feature B1 of 1984.81 leads us to suspect that we are seeing Feature B1 circle clockwise around the pole.

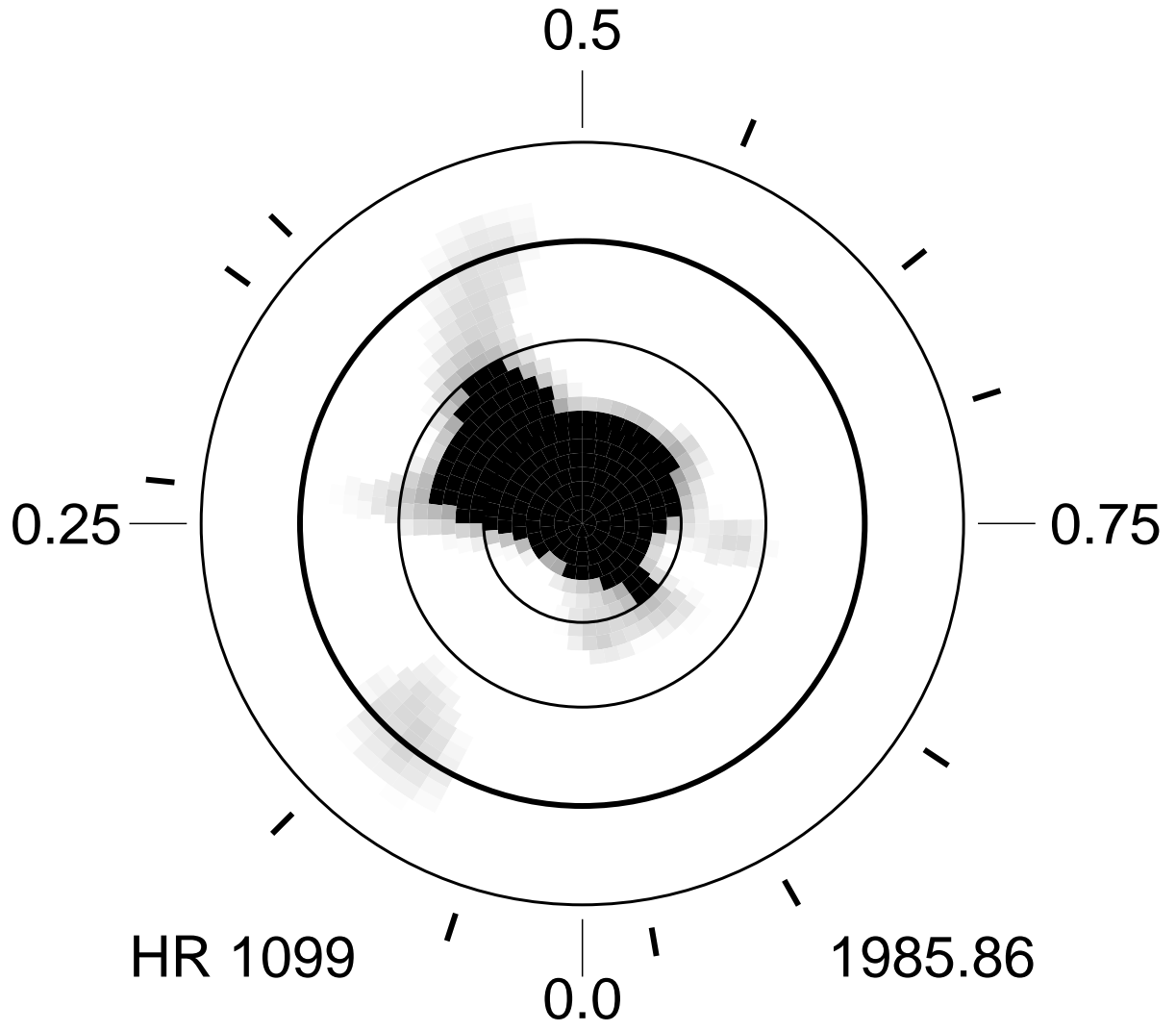


Fig. 16.— HR 1099 raw (unthresholded) Doppler image for 1985.86

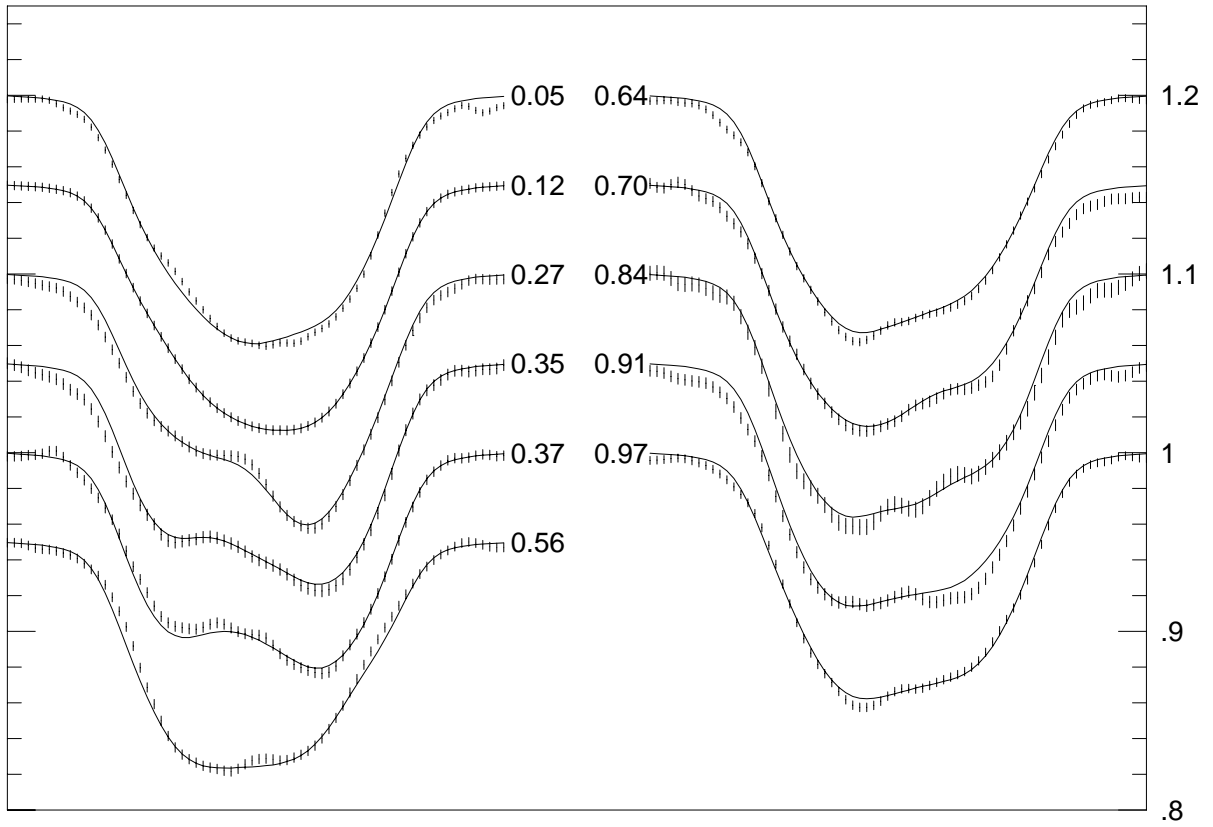


Fig. 17.— The spectral line profiles and fits for the 1985.86 image

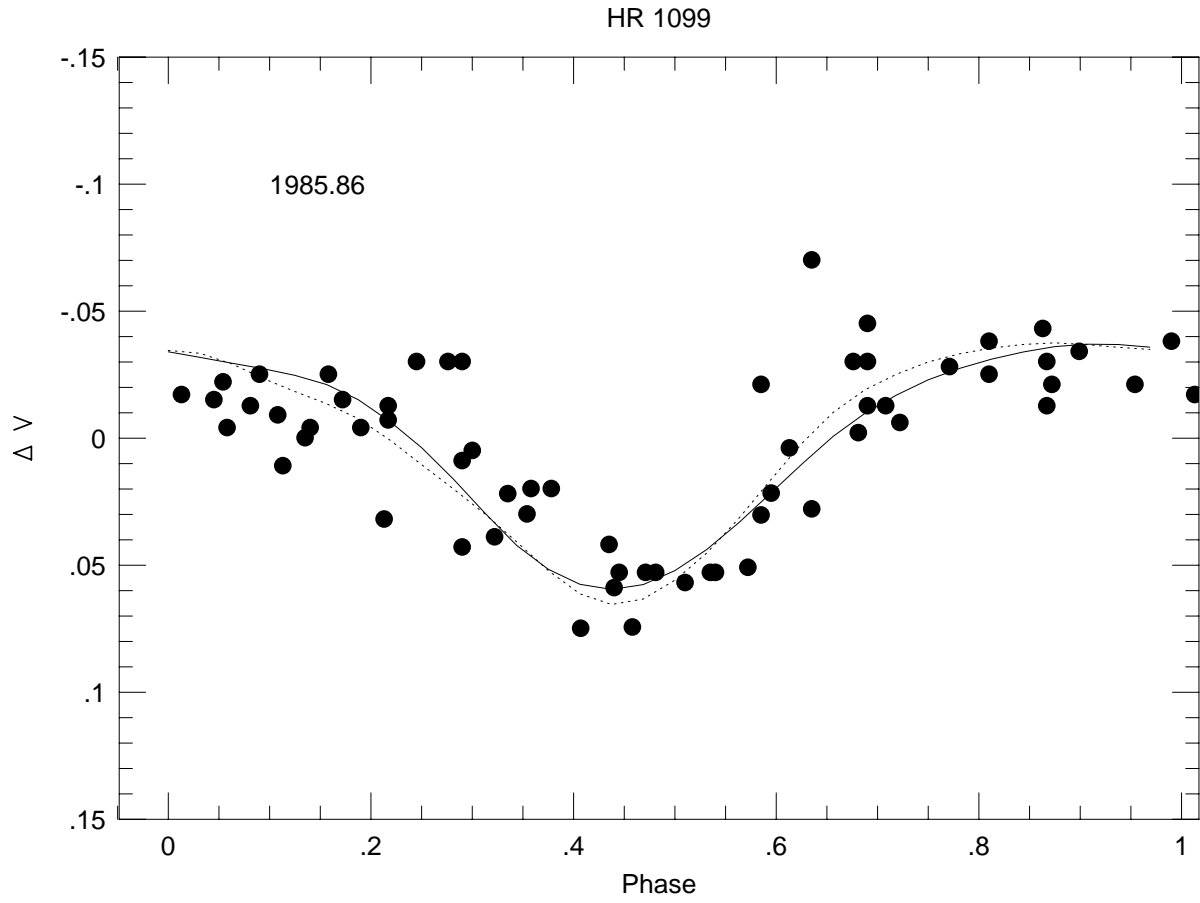


Fig. 18.— HR 1099 1985.75 light curve used for the 1985.86 image

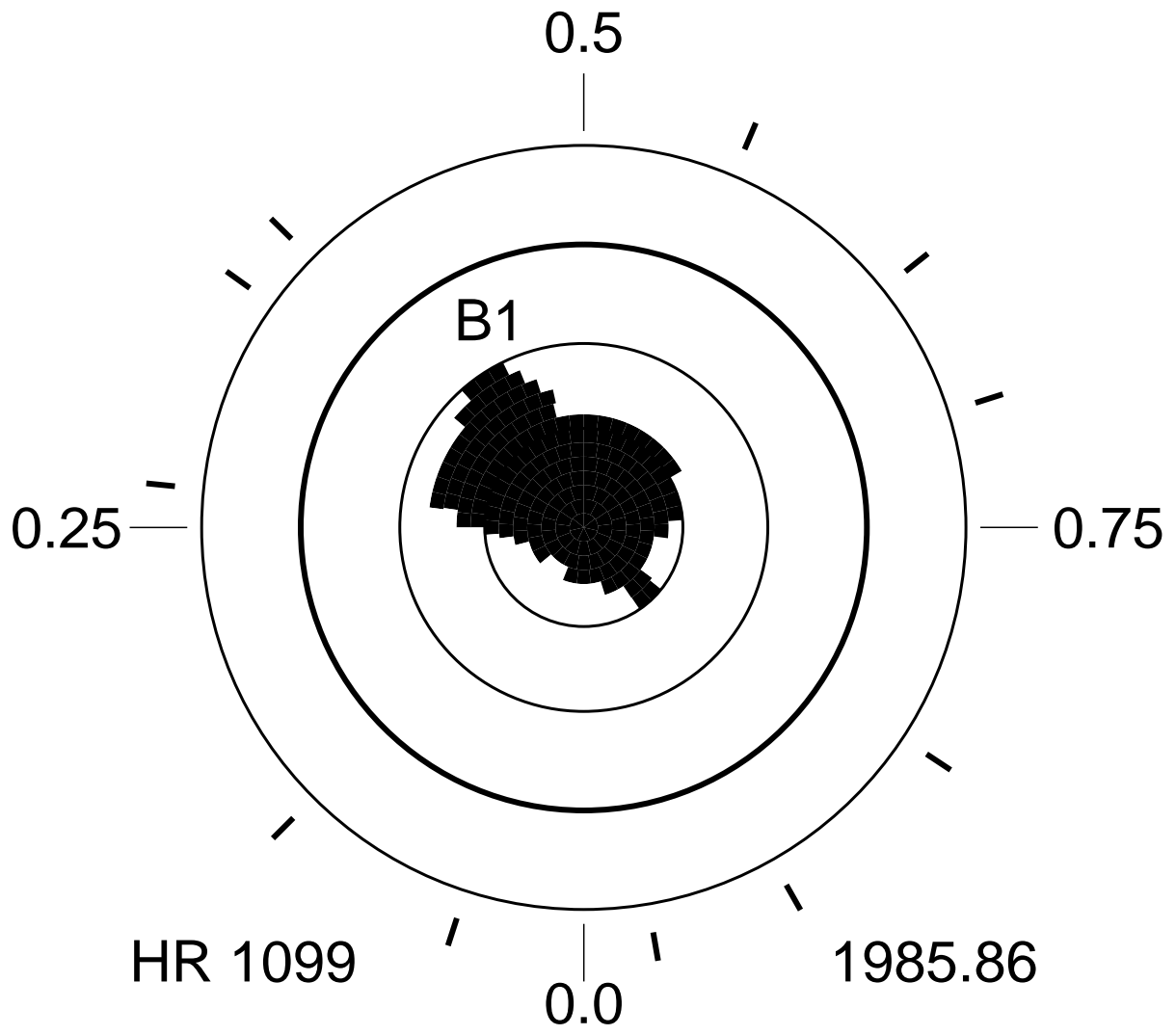


Fig. 19.— HR 1099 thresholded Doppler image for 1985.86

3.10. The 1986 Season Doppler Images

The 1986 season was the first for which we managed to obtain two images, separated by only 5 months rather than the usual 12-month gap. Our unthreshholded raw image for 1986.63 is shown in Figure 20 and the spectral data and fits in Figure 21. Light curves for 1986-7 were published by Strassmeier et al. (1989), Cutispoto (1990), Mohin and Raveendran (1993), and by Mekkaden (1987). Figure 22 shows the 1986.83 light curve of Mekkaden (1987) (points) along with our predicted light curve (dotted line) from the raw Doppler image. The light curve amplitude is modest because the low latitude spots and polar appendages are roughly evenly distributed in longitude. In fact, there is probably little hope of recovering much about the complex spot geometry of this epoch from 2-spot or 3-spot fits to this low amplitude light curve, and, indeed, no spot models were found in the literature for comparison with this season’s Doppler images.

The predicted light curve from our 1986.63 raw MEM image clearly did not fit the 1986.83 photometry adequately. (This is not entirely surprising since the light curve was taken some 2.4 months later, and furthermore, large phase gaps in our data may have caused the imaging process to miss some low-latitude spots). We then attempted to fit the light curve with a slightly modified version of the Doppler image. The image that gave the best fit to the photometry is shown in Figure 23; the resulting photometric fit is shown as the solid line in Figure 22. The photometrically revised image (Figure 22) has a slightly larger area for the mid-latitude spot at phase 0.38 (this spot is in the middle of our phase gap and therefore not well-constrained by the line profiles) as well as a slightly larger polar appendage at phase 0.88. This latter change may be due to changes in the polar spot between the time of the photometry and Doppler imagery, but we cannot say for sure. Also the narrow protuberance on the polar spot near phase 0.75 in the original Doppler images became a detached spot in the photometrically-constrained image.

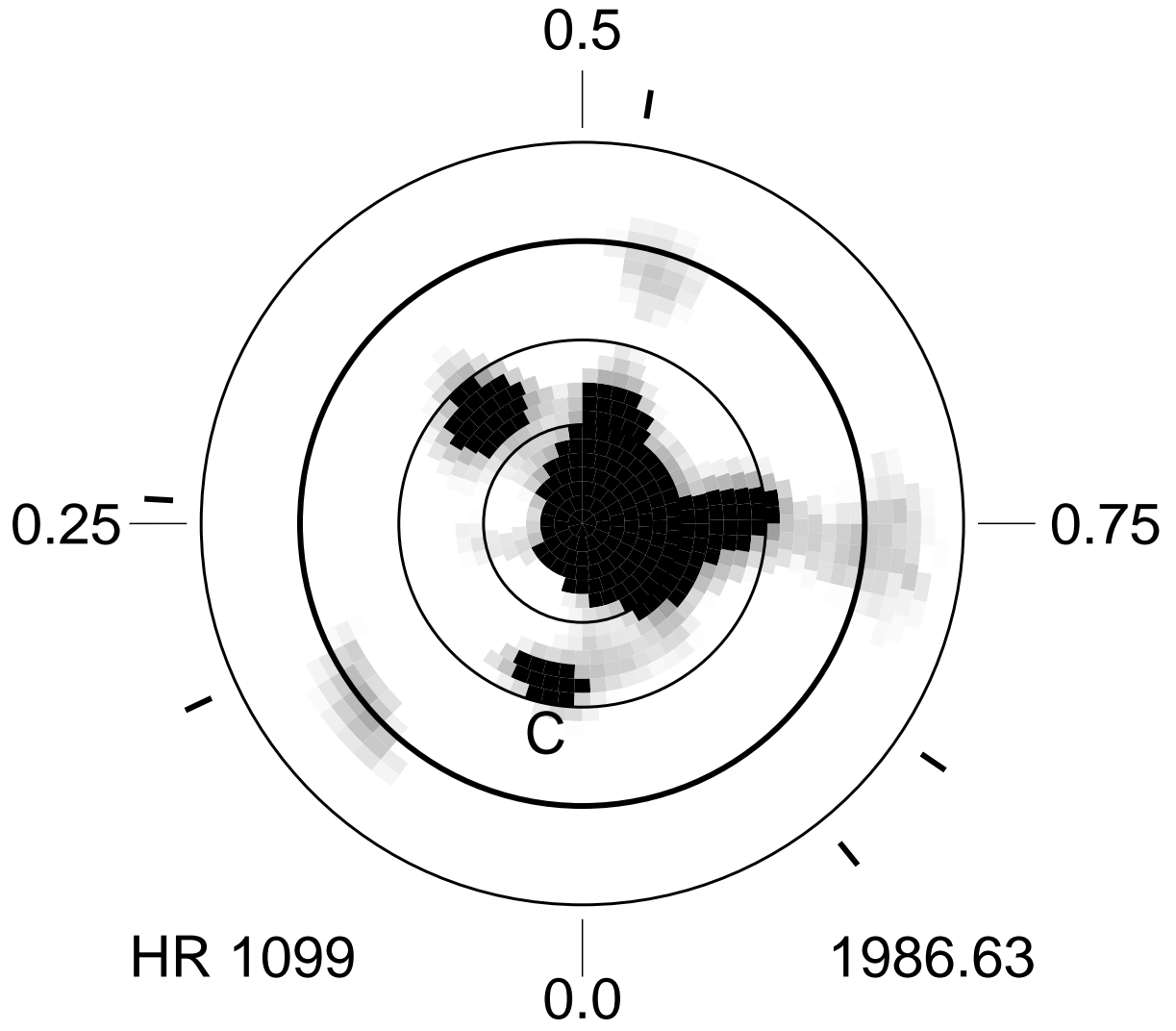


Fig. 20.— HR 1099 raw (unthreshholded) Doppler image for 1986.63

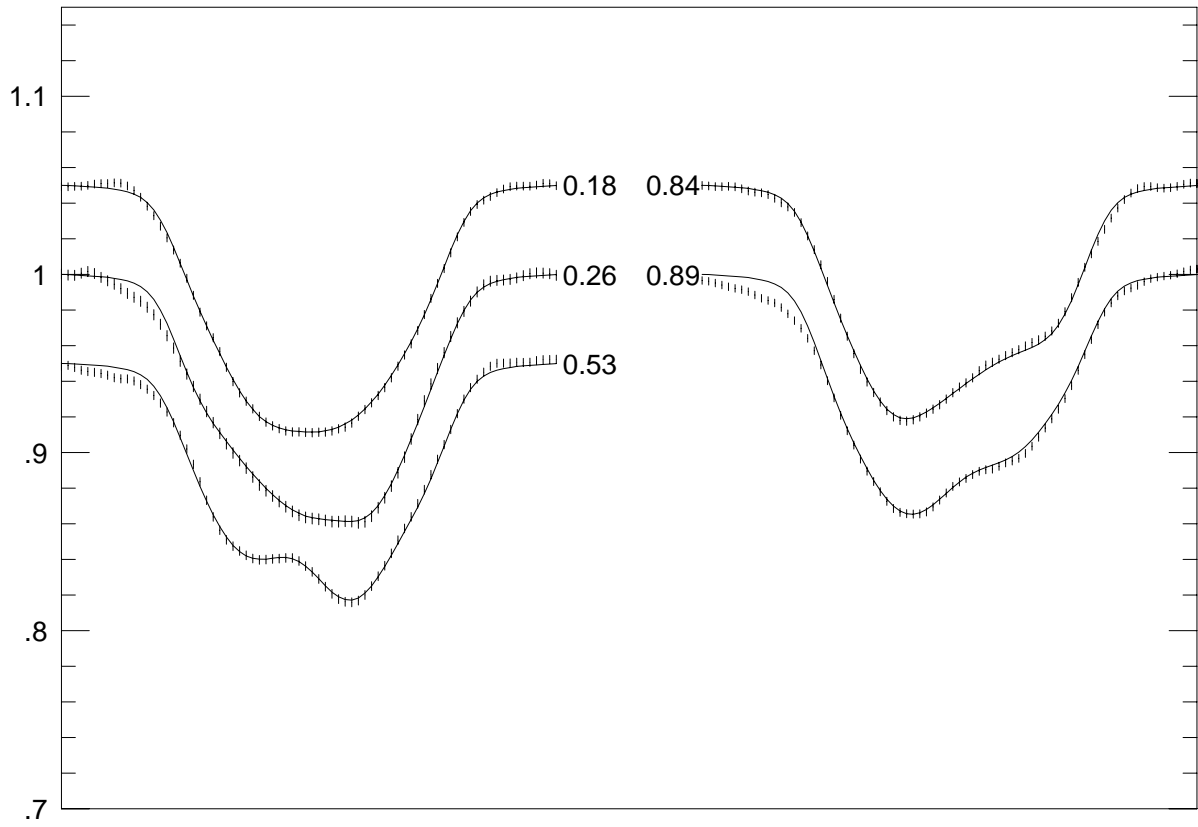


Fig. 21.— The spectral line profiles and fits for the 1986.63 image

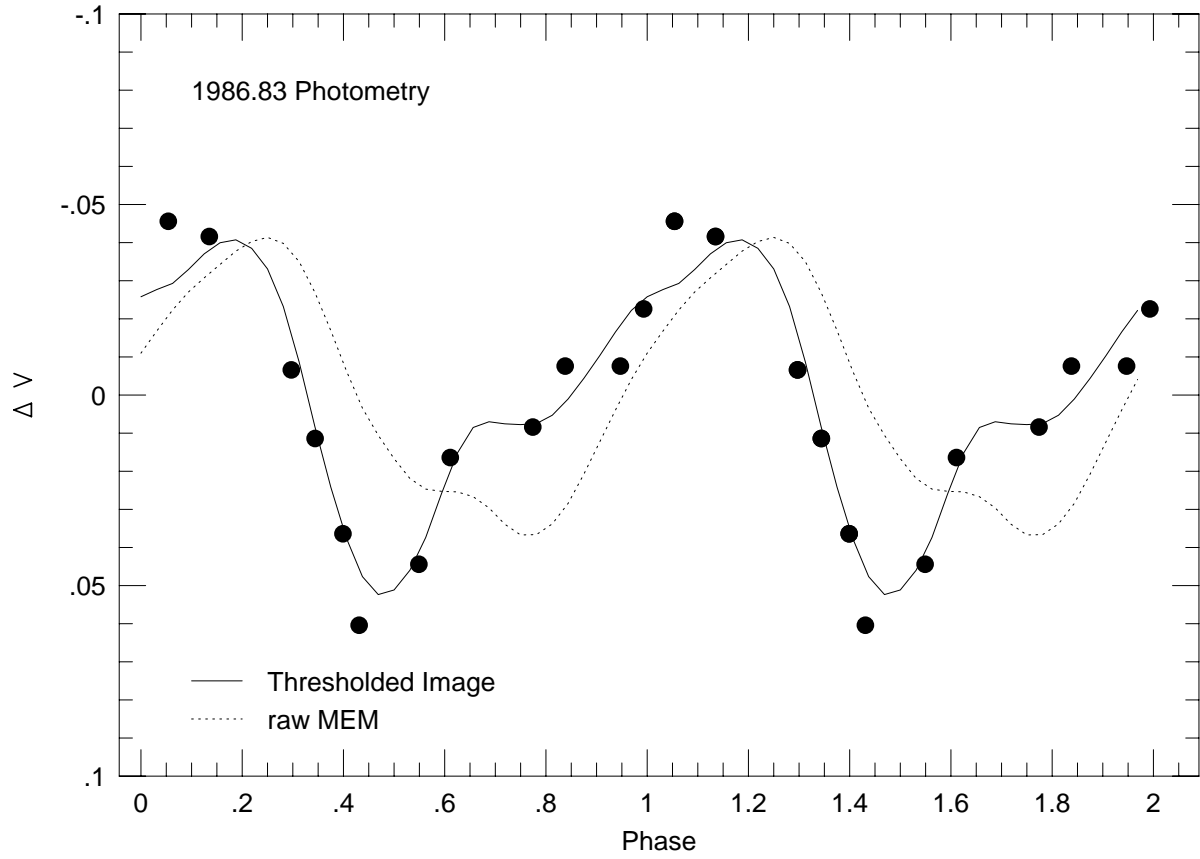


Fig. 22.— 1986.83 light curve used for the 1986.63 HR 1099 image

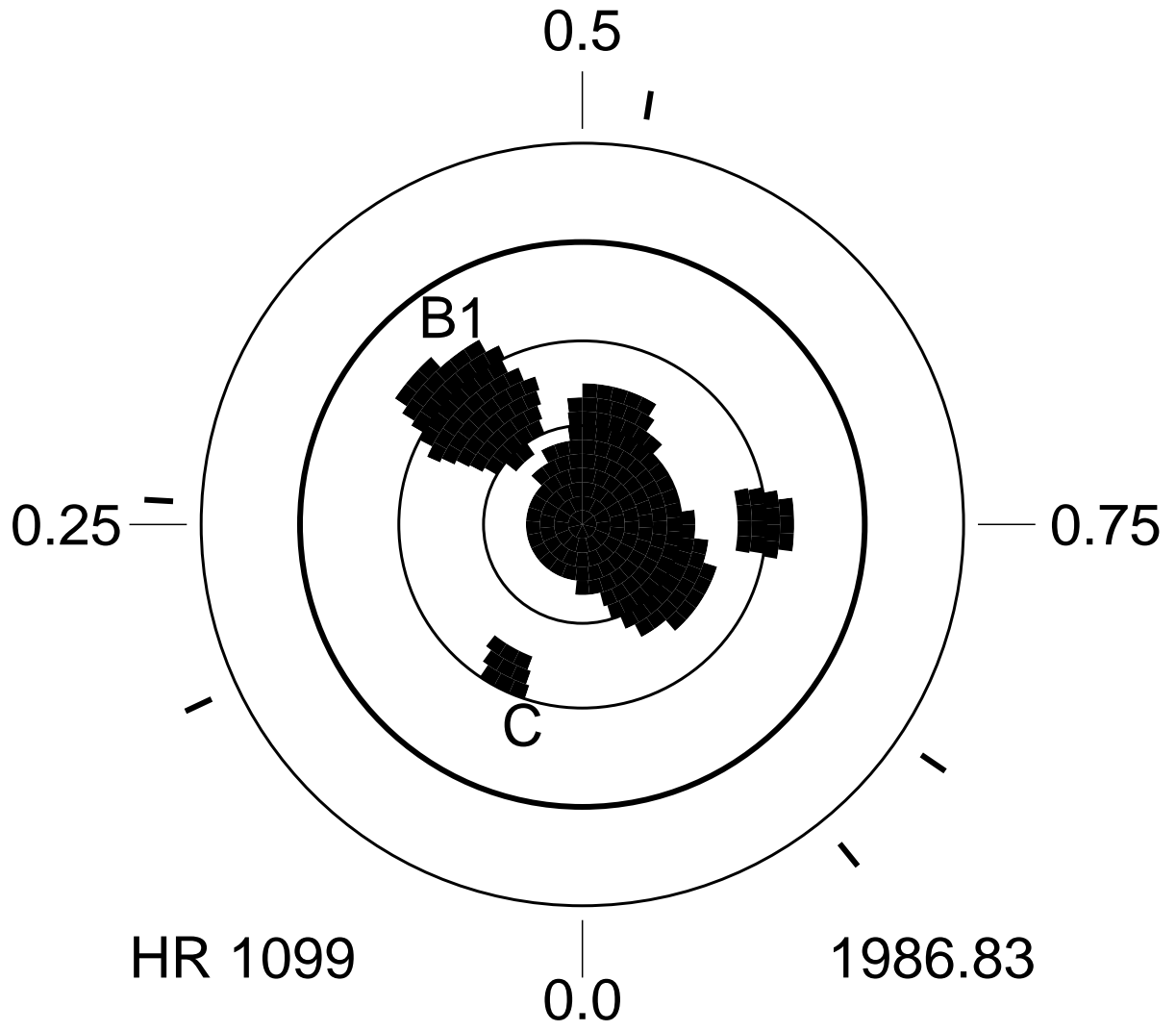


Fig. 23.— HR 1099 thresholded Doppler image for 1986.83

There is an isolated mid-latitude spot (hereafter referred to as Feature C) seen near phase 0.03 and latitude 38° in the 1986.63 raw image, and at phase 0.11 and latitude 45° in the 1987.05 image (see below). The best fit to the 1986.83 light curve required moving Feature C from phase 0.03 in the 1986.63 raw image to slightly higher phases (about 0.08) in the photometric image. We did this by assuming that the feature was migrating at a constant rate in longitude, and simply used the migration rate of this spot derived from the 1986.63 and 1987.05 images to interpolate its position for the 1986.83 photometrically-constrained image. This yielded a predicted light curve (solid line in Figure 22) which then agreed quite well with the 1986.83 photometry. There is a slight indication that Feature C was also moving northward since its latitude in the 1987.05 image is about 45° , whereas it was 38° in 1986.63. Perhaps, like Feature B1/B2, it is following a northward clockwise spiral path toward eventual merger with the polar spot.

For the 1987.05 epoch, the raw spectral image is shown in Figure 24. Note the spurious low-latitude ‘mirroring’ of the high-latitude spot appendage at phase 0.38. The spectral line profiles in Figure 25. The predicted light curve from this image as fit to the 1987.08 photometry of Mohin and Raveendran (1993) is shown as the dotted line in Figure 26. The fit of the predicted light curve for the 1987.05 raw MEM image was again clearly inadequate.

Figure 27 shows the photometrically-constrained image that best fits the observed light curve. It is identical to the original Doppler image derived from the spectral line profiles except for the large equatorial spot at phase 0.915 that seems to be required by the photometry. We hereafter refer to this spot as Feature D. The predicted light curve for this image is shown as the solid line in Figure 26. Clearly, the 1986.83 light curve shows significant differences to the one in 1987.08. The latter light curve developed a pronounced dip near phase 0.9 signifying the rapid appearance of Feature D sometime after January

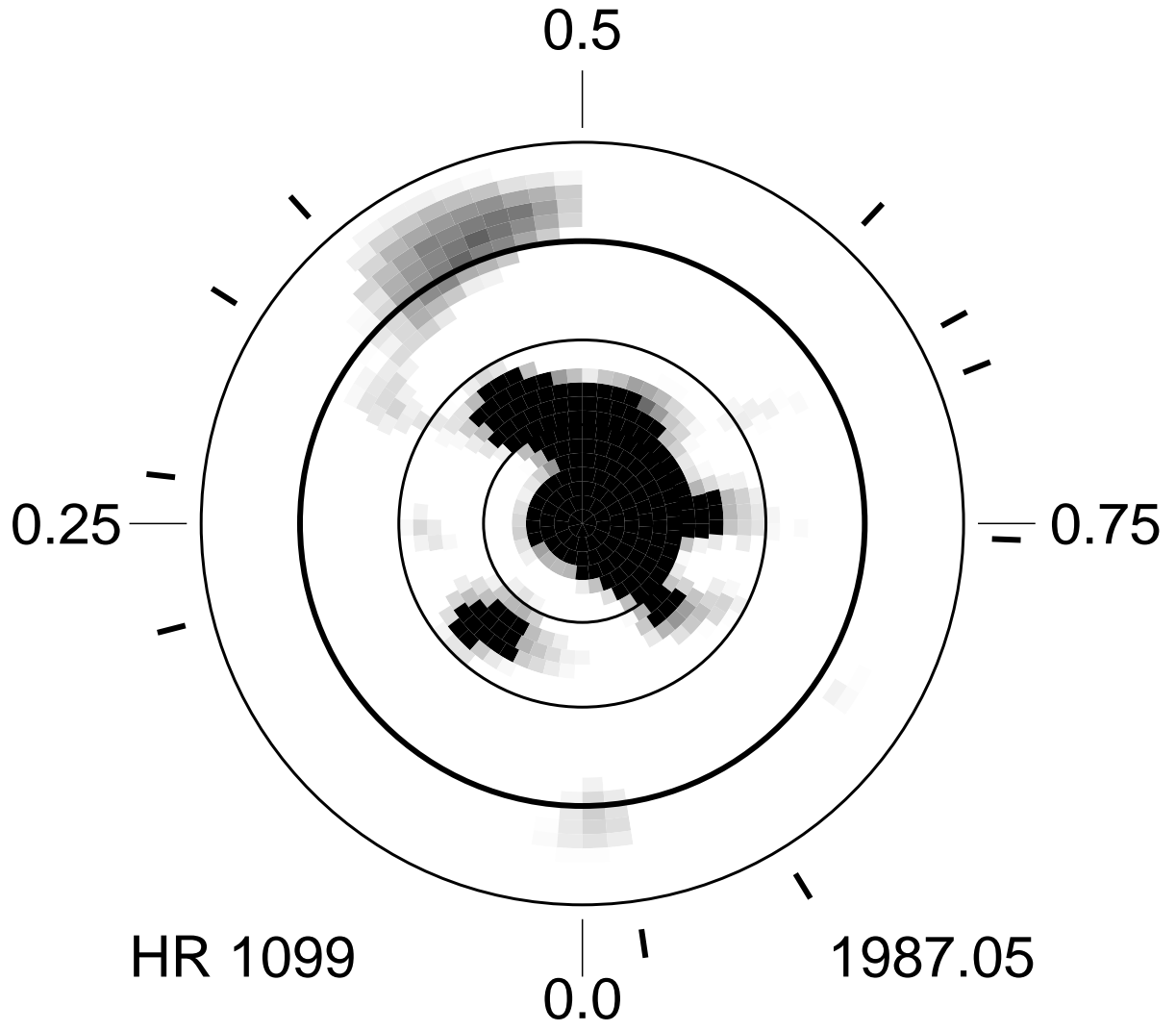


Fig. 24.— HR 1099 raw (unthressholded) Doppler image for 1987.05

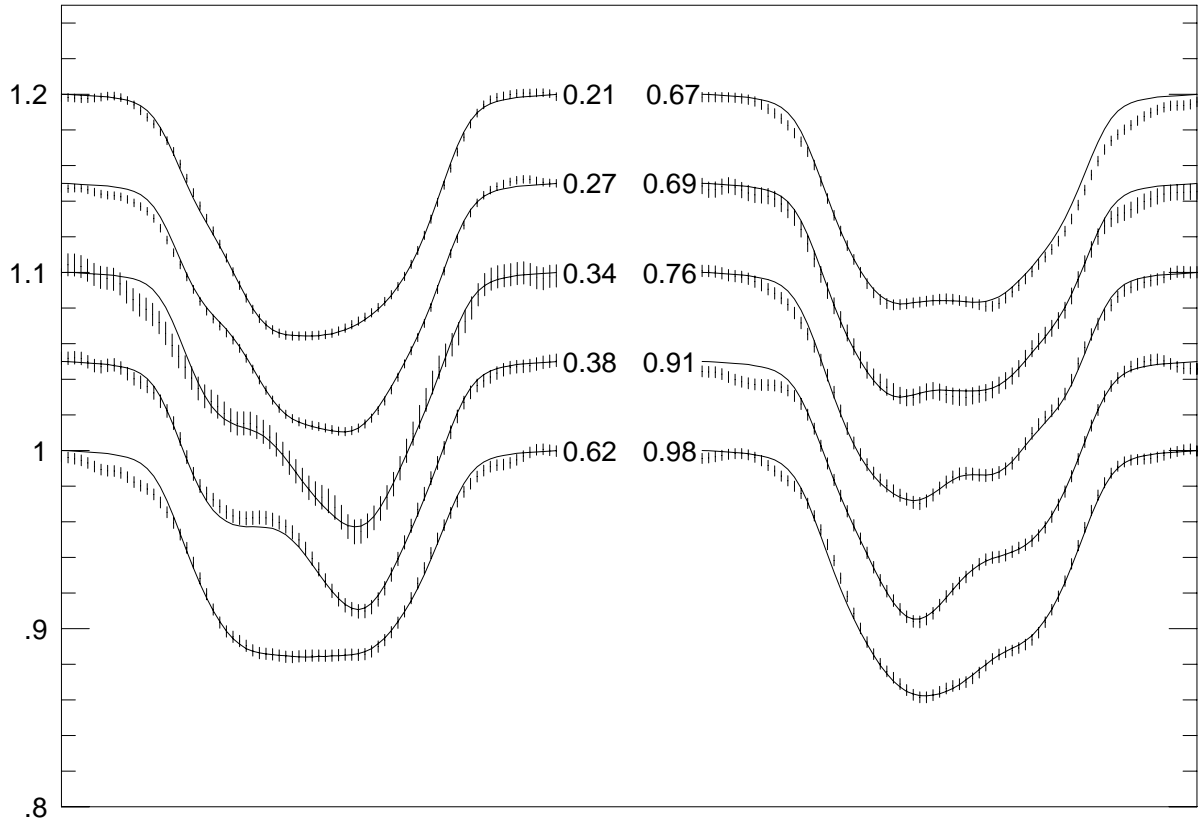


Fig. 25.— The spectral line profiles and fits for the 1987.05 image

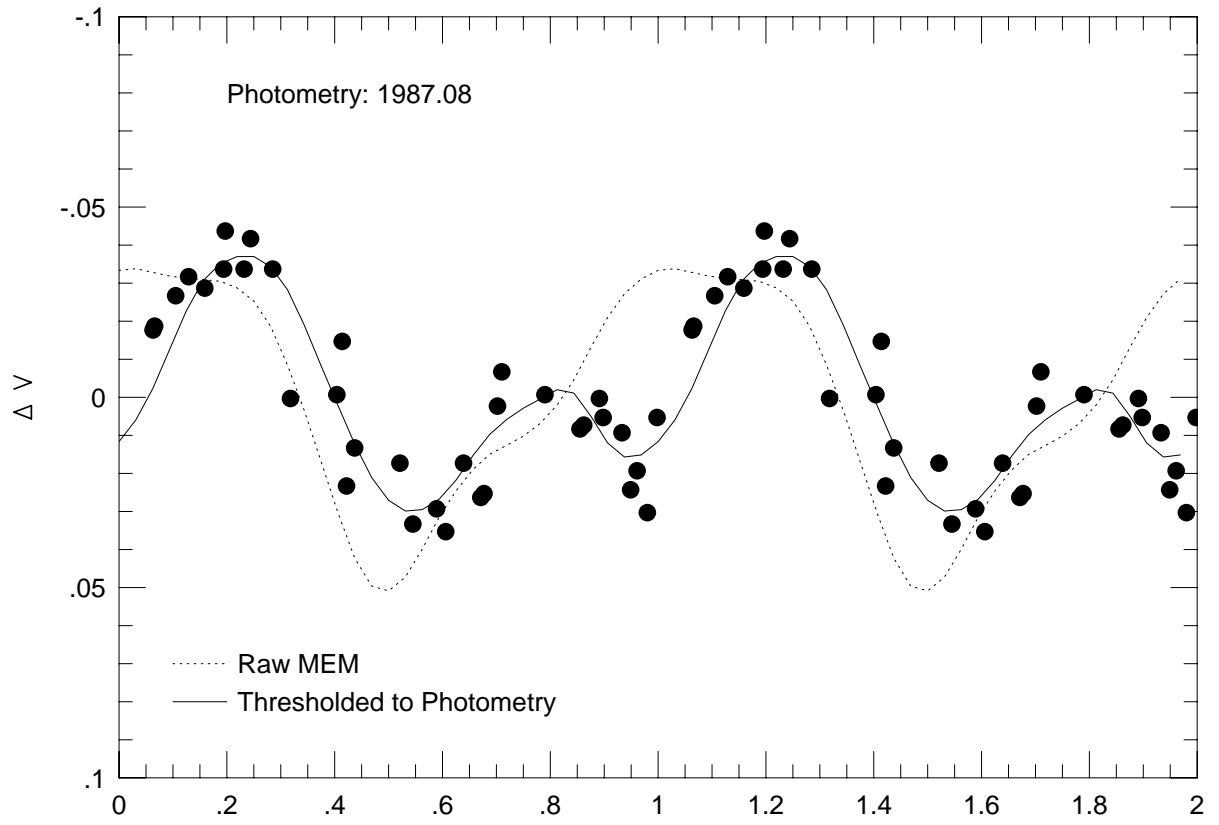


Fig. 26.— 1987.08 light curve used for the 1987.05 HR 1099 image

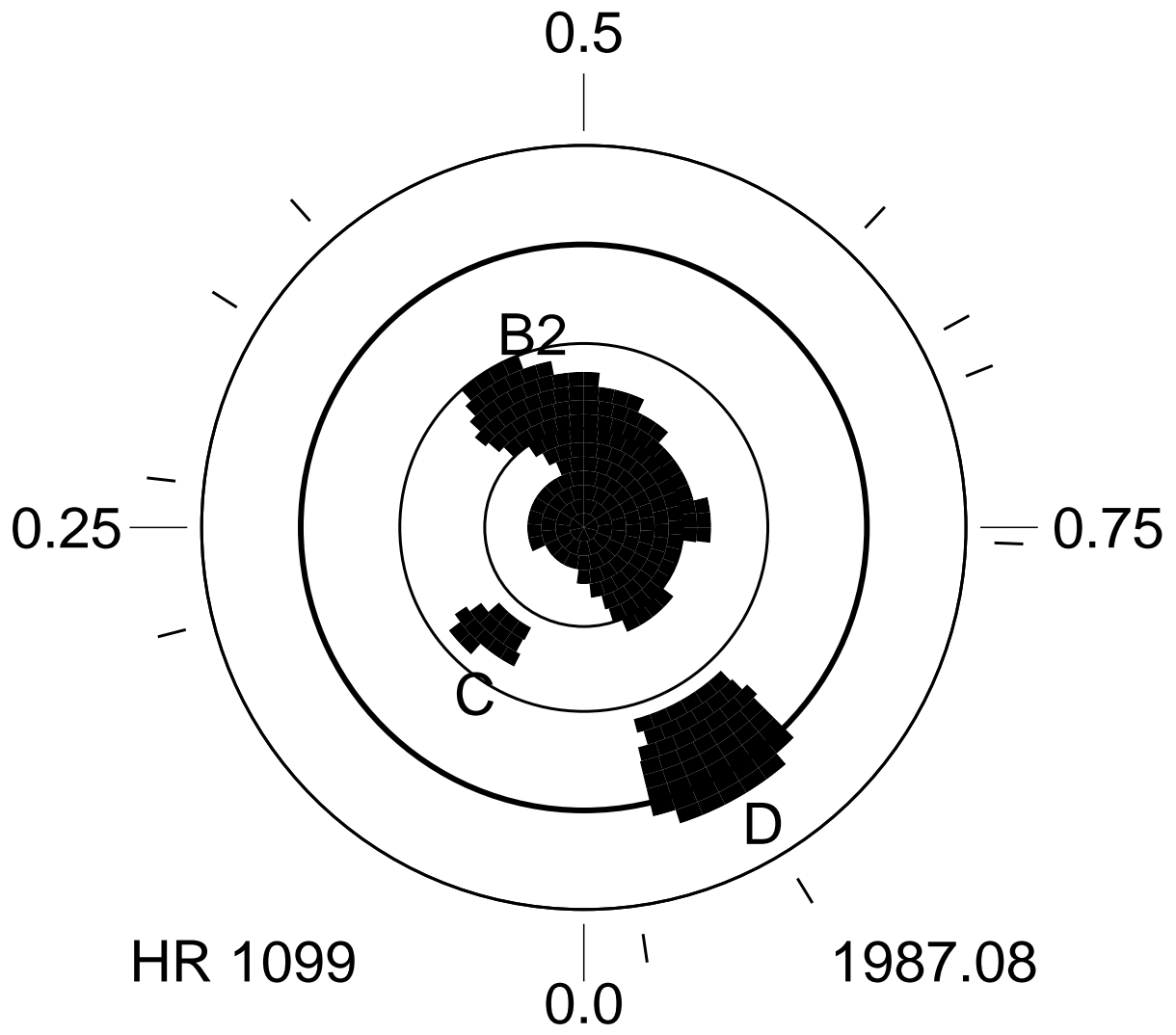


Fig. 27.— HR 1099 thresholded Doppler image for 1987.08

1987. The Mohin and Raveendran (1993) light curve was made between 5 Jan – 8 Mar 1987, with the bulk of the measurements taken after 21 Jan. This is somewhat after our Doppler image (which was derived from data covering 12-19 Jan 1987). Feature D was therefore probably missed in the Doppler image due to limited phase coverage and lack of time resolution.

Here, we were able to use photometry taken at a slightly different time to fill in the time gaps in our images and glean information about spot evolution. The combination of the photometry, together with the line profiles, tells us that there is rapid spot evolution occurring that is not being adequately reproduced by our infrequent images. We have tried here to weave the photometry and line profile constraints together as best we can, but it is clear that, in this regard, we are working near the sampling limits of our data set.

We believe, from combining both the imagery and light curve fitting, that Feature C is real and was migrating clockwise as discussed above. It was also well-isolated from other spots, and had similar size, shape, and latitude in all images. Furthermore, the time span of these images being only 5 months, this assumption has a reasonable chance of being correct. If we are indeed tracking the same spot, then Feature C, like Feature B1, is also migrating clockwise. A least squares fit to the phases for Feature C of 0.03, 0.08, and 0.11 in 1986.63, 1986.83, and 1987.05 respectively gives a longitudinal migration rate of $64^\circ \pm 13^\circ \text{ yr}^{-1}$ at latitude 40° , or about 1 part in 723 of the orbital period. Again, the implication is that the spot longitude migration rate (differential rotation?) is much smaller (2-3 orders of magnitude) than the Sun and again in the sense that intermediate latitudes of HR 1099 are rotating more slowly than the orbital rate.

Assuming a constant longitudinal migration rate for Feature C of 64° yr^{-1} , places Feature C at about phase 0.89 in the 1985.86 image (Figure 19), interestingly close to, but perhaps just coincidentally at the phase of the small projection and low-level feature at

phase 0.88 on the polar spot in 1985.86. Extrapolation of Feature C to 1984.81 puts it at phase 0.71, well away from the low-latitude spot seen there at phase 0.85, and not near any other obvious mid-latitude feature. Extrapolation of Feature C to the 1987.75 image puts it at phase 0.23 in Figure 31, slightly past but quite near the narrow projection on the polar spot at phase 0.21 and latitude 45° - 70° in the 1987.75 image, as will be discussed in the next section.

The polar spot is again present in both images this observing season, with several large protuberances and intermediate-latitude spots. A study of TiO absorption detected in January 1987 by Huenemoerder (1987) indicated a polar spot area of 10%. Our Doppler image also yields an area of 10% for the polar spots in both of the 1986-7 images, in excellent agreement with Huenemoerder (1987).

In both the 1986.83 and 1987.08 images, a persistent feature remains at or near the location of Feature B1 from 1984.81 and 1985.86. Some spot activity has thus been present on this particular area of the star (phase 0.3-0.4 and latitude 30° to 60°) for at least 2 years. It is difficult to say with certainty what is happening with Feature B1. It seemed to have merged with the polar spot by 1985.86 but perhaps it was only that our phase coverage was not sufficient to have resolved it from the polar spot. Clearly it looks detached again in 1986.83, and then a bridge forms and it becomes reconnected in 1987.08. At this point, it seems to have changed its basic shape, so we now change its name to Feature B2 to reflect the fact that it may still be associated with the original Feature B1, but is now being tracked as a possibly different feature. Whatever the case, Features B1/B2 seem to show little or no longitudinal migration with respect to the orbit. This is yet another indication that the high latitude spots of HR 1099 seem to be rotating precisely at, or only slightly slower than the orbital angular velocity. Feature B2 may even be discernable for several more years in the image set as it follows a slow clockwise drift around the polar spot.

3.11. The 1987 Doppler Image

We obtained only a single Doppler image of HR 1099 in the 1987-88 observing season at epoch 1987.75. The raw unthreshhoulded image solution is shown in Figure 28. The spectral line profiles and fits for the Doppler image are shown in Figure 29. Light curves for epochs 1987.17 and 1988.07 were presented by Mohin and Raveendran (1993), and a curve for 1988.16 was presented by Rodono and Cutispoto (1992). The light curve amplitude was only about 0.05 magnitudes at this time and would have resulted in fairly ambiguous 2-spot or 3-spot model solutions. In any case, no spot model solutions were found in the literature to compare with our Doppler image of this year.

Our raw image shows a polar spot with a large protuberance near phase 0.5 which looks quite similar to the polar spot protuberance named Feature B2 of the 1987.08 image, as though this is still Feature B on its slow clockwise migration around the pole. There is also a pronounced equatorial spot at phase 0.96 which probably corresponds to Feature D from the previous (1987.08) image but advanced in phase by about 0.045.

Figure 30 shows the light curve for epoch 1988.07 (points) from Mohin and Raveendran (1993) along with our predicted light curve (dotted line) from the unthreshhoulded 1987.75 Doppler image of Figure 28. Here, the predicted light curve from the raw MEM image was a quite poor fit to the photometry. In fact, the predicted photometry is 180° out of phase with the actual photometry! Again this is no great surprise since the Doppler image and photometry were taken an uncomfortable 4 months apart.

Once again an attempt was made to fit the photometry using a modified version of the 1987.75 raw Doppler image with the results shown in Figure 31. The epoch of this image is labeled as 1988.07 to reflect the mid-time of the photometric observations. The light curve from this distribution is shown as the solid line in Figure 30. The polar spot of the original Doppler image retained its shape. Only the sizes of some of the appendages

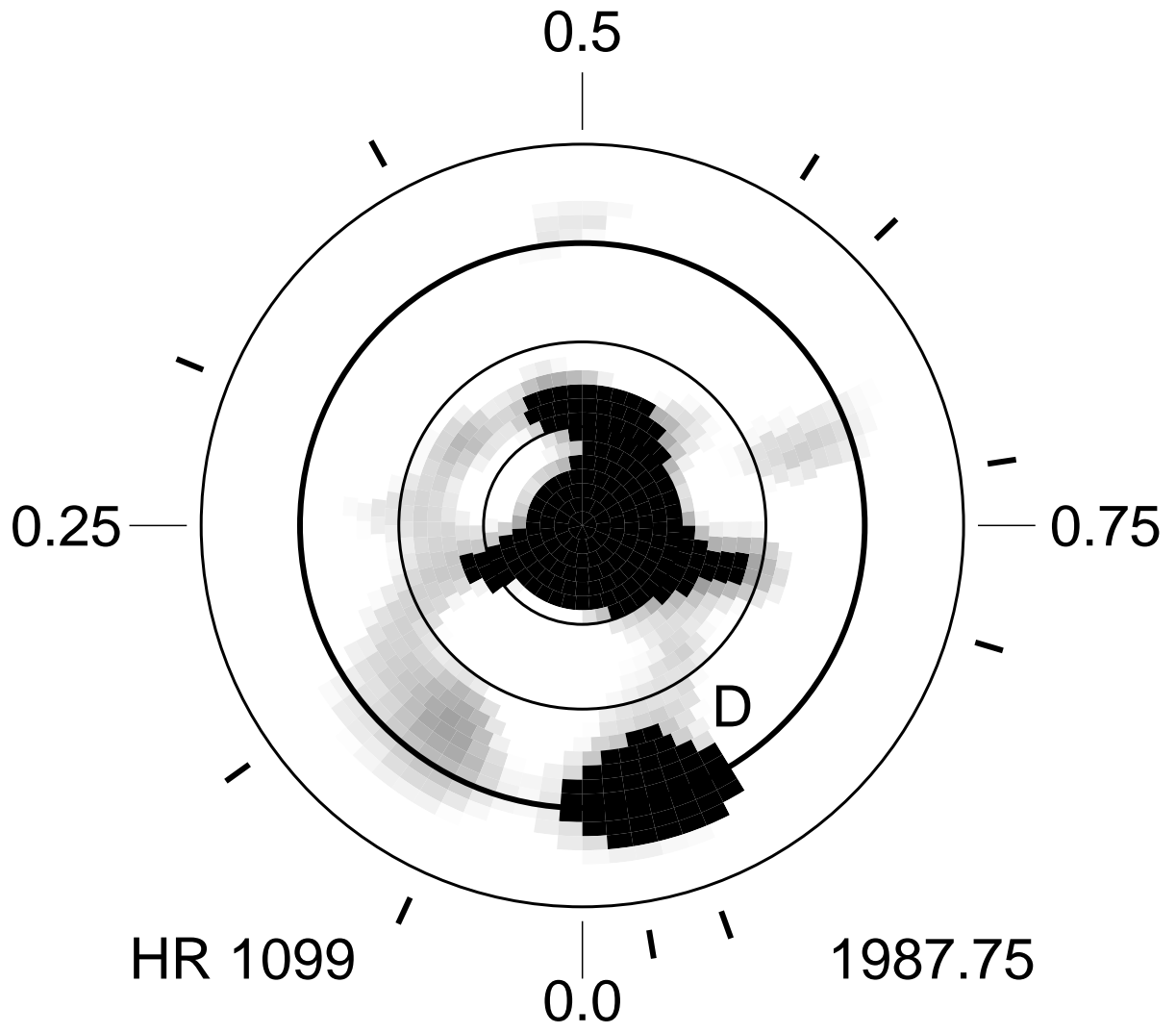


Fig. 28.— HR 1099 raw (unthresholded) Doppler image for 1987.75

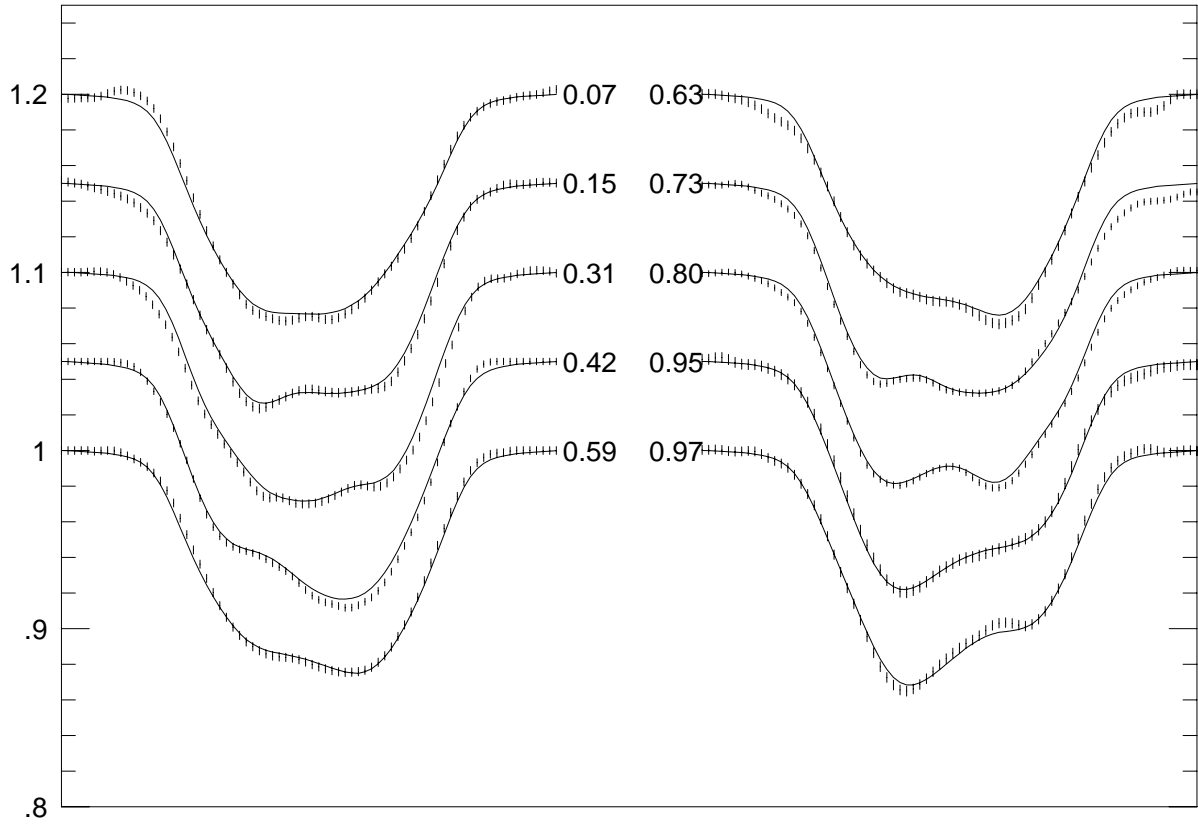


Fig. 29.— The spectral line profiles and fits for the 1987.75 image

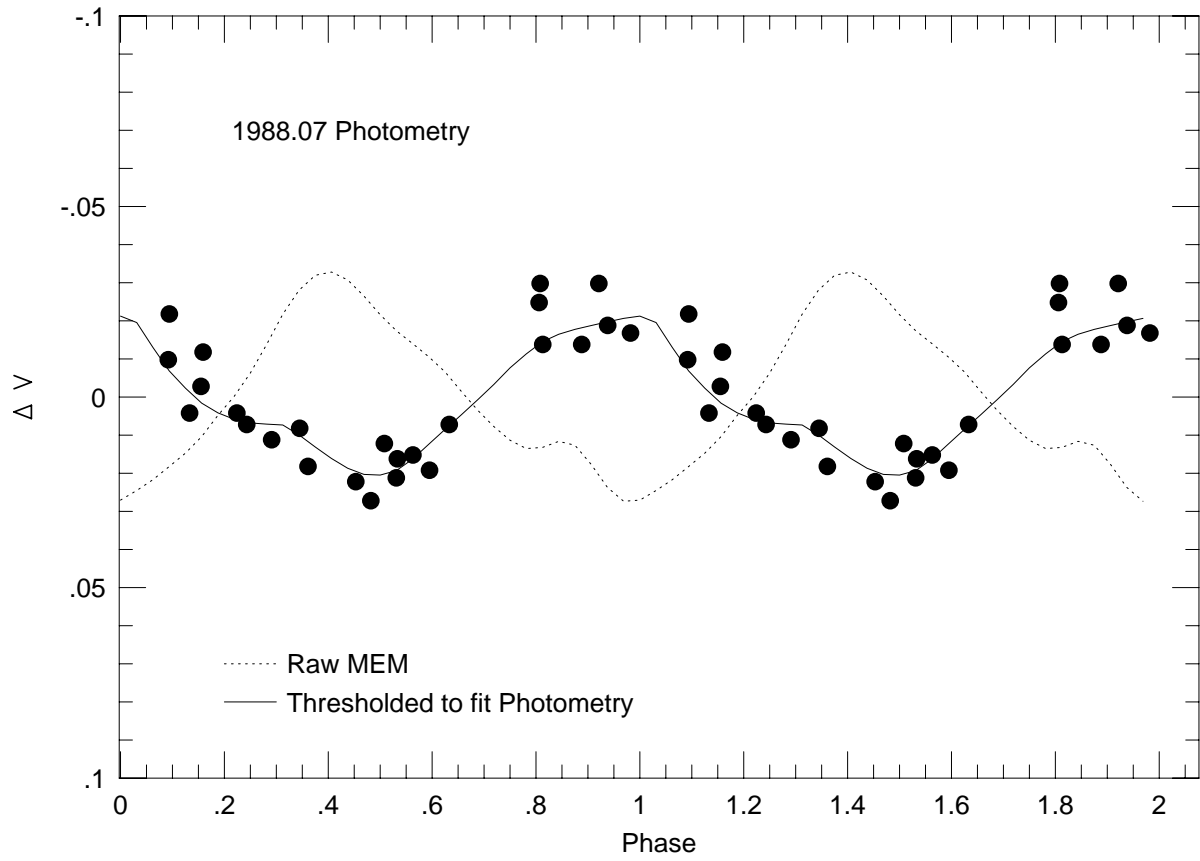


Fig. 30.— 1988.07 light curve used for the 1987.75 HR 1099 image

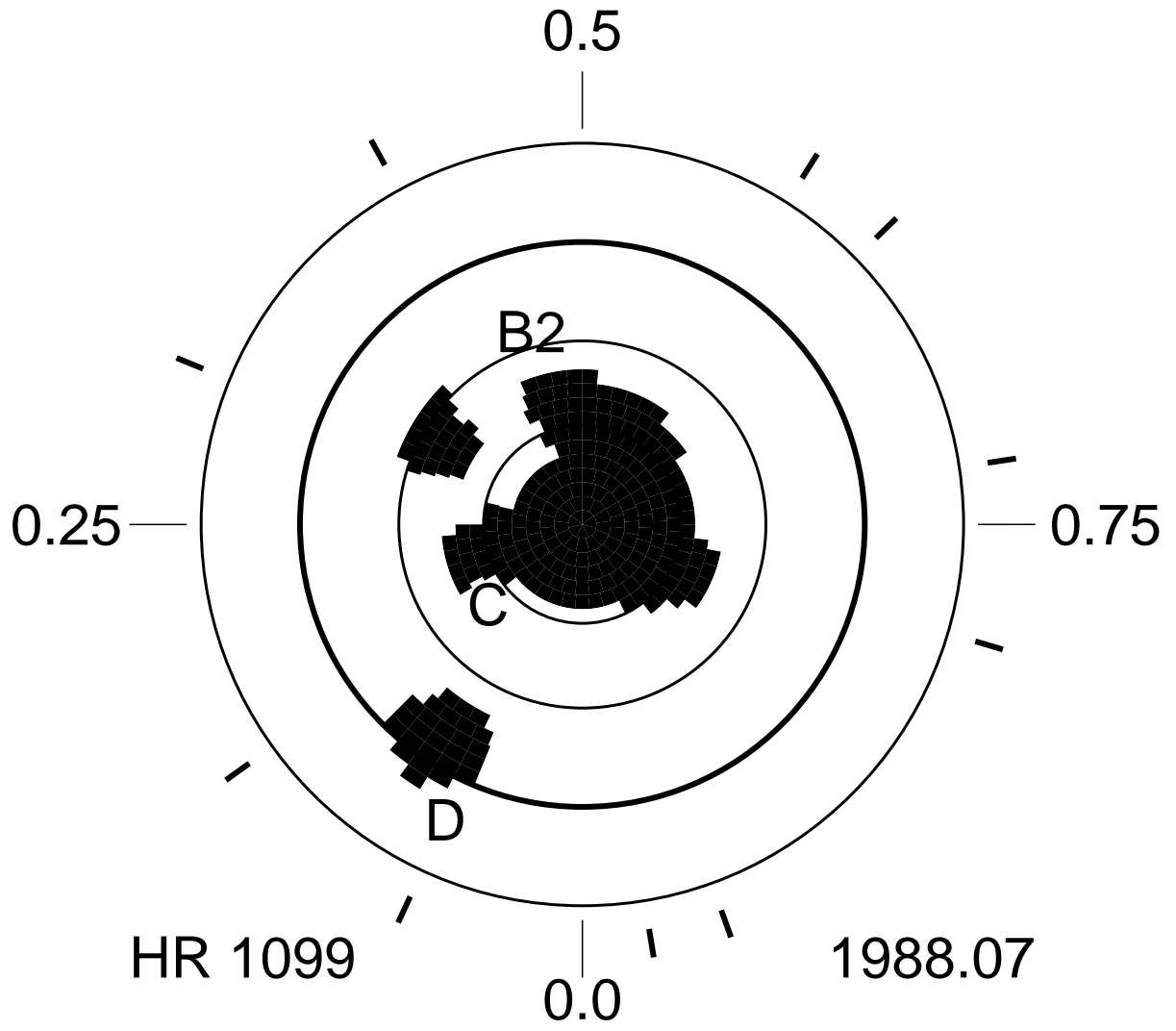


Fig. 31.— 1987.75 Doppler image of HR 1099 thresholded by the 1988.07 photometry

increased slightly. An additional mid-latitude spot was added at phase 0.3 at the location of a low-level spot in the raw Doppler image. The main discrepancy between the raw (Figure 28) and photometrically-constrained (Figure 31) images is the requirement that the low-latitude spot (Feature D) seen at phase 0.96 in the former, be shrunk somewhat and moved to phase 0.095 in the latter.

There are a number of hypotheses which can account for the discrepancy in location of this low-latitude feature between the two images. Could Feature D from the photometrically-constrained image actually have been present at the time the spectral data were acquired? There is a low-level spot in the spectral image that coincides with this location in the photometric image, but it is not as strong as the low-latitude feature at phase 0.96. The phase coverage of the spectral data is such that any information about low-latitude spots centered on phase 0.09 must come from the two observations centered on phase 0.06 and 0.15, respectively. Possibly the spot feature in the spectral image appears so weak because it had recently emerged and was present at the time of the observation at phase 0.15, but not at phase 0.06. Because spectral distortions resulting from this spot appear only at one phase, MEM, in trying to fit both profiles puts weak spot features at this location. If true then this implies a rapid emergence time for magnetic flux since the time difference for the two observations is only one day! There is some evidence to support this. Placing a very cool ($\Delta T = 1200$ K) spot at the location required by the photometric image results in an excellent fit to the observed spectral line profile at phase 0.15, but a rather poor one at phase 0.06, suggesting the presence of a spot only at the time of the later phase.

Another explanation, and the one we favor on grounds of pure simplicity, is that the low-level equatorial feature at phase 0.095 in the raw image is not actually a real spot. Rather, the appearance of a spot at this location in the photometrically-constrained image

is simply due to the fact that 4 months later - at the time the light curve was observed - Feature D seen at phase 0.96 in the 1987.75 raw Doppler image had migrated to phase 0.095.

Finally, it may well be that the low-latitude spot that appears in the photometric image represents a different spot feature entirely. Unfortunately, with so few Doppler images to guide our interpretation we can never be sure which scenario is correct.

Assuming we are tracking the migration of Feature D, we can derive a longitudinal migration rate for this isolated spot. It moved from phase 0.915 in 1987.05 to phase 0.96 in the 1987.75 raw image, and then on to phase 0.095 in the 1988.07 photometrically-constrained image. These three positions are not consistent with a strictly constant drift rate, but a least squares solution gives 57° yr^{-1} clockwise. As we shall see though, it is likely that the spot sat fixed for a while before moving off. In this case, taking only the last two positions would give a better estimate of the terminal migration rate and yields $152^\circ \text{ yr}^{-1}$ at latitude 7° for Feature D. We also found that this maximum migration rate was consistent with the longitude extents of all the Feature D spots. All Feature D spots were at least as large as the expected phase smearing due to such migration in each image.

Feature B2, and/or some remnant thereof, seems to persist near phase 0.3 and latitude 37° , and a piece which may have calved off seems to continue its slow clockwise arc around the pole, showing up as a large protuberance projecting from the polar spot between phases 0.4-0.7. The detailed shape of this phase 0.4-0.7 protuberance (Feature B2) on the polar spot in the 1988.07 photometric image is very similar to the same Feature B2 protuberance in the 1987.08 spectral image, but advanced by about $16^\circ \pm 4^\circ$ in longitude between the 1987.08 image and the 1987.75 image (whose epoch by the light curve constraints is actually 1988.07), leading us to suspect that we are seeing slow clockwise migration of this edge of the polar spot. Again, if we assume that this is the same feature, making a slow clockwise

circle around the pole, we get a migration rate of about $16^\circ \pm 3^\circ \text{ yr}^{-1}$ at this latitude, quite similar to what we previously derived for Feature B1 (which may in fact be the same feature). It is difficult to say what latitude this feature corresponds to as it also appears to be moving northward as it proceeds clockwise. Also, above 70° it merges with, and becomes indistinguishable from, the permanent polar spot, so much of its area may be northward of 70° . We'll use its mean latitude of about 55° from the 1988.07 epoch with the caveat that it appears to be a rather rigid structure and may be part of a single, totally rigid polar spot, in which case its effective latitude is probably much higher. There is a definite sense between the 1987.08 and 1987.75 images that Feature B2 is spiraling northward and clockwise towards a merger with the polar spot.

This same sense of a northward, clockwise spiraling migration towards the polar spot is suggested by Feature C. As mentioned in the previous section, extrapolation of the (assumed constant) 64° yr^{-1} clockwise longitudinal migration of Feature C from the 1986.63 image to the 1987.75 image puts it at phase 0.23 in Figure 31, slightly past but quite near the narrow projection on the polar spot at phase 0.21 and latitude $45^\circ - 70^\circ$ in the 1987.75 image. Now, between the 1986.63 and 1987.05 images, Feature C also moved 7.5° northward in 0.42 years or about 18° yr^{-1} . This northward rate would then place it near latitude 58° in our 1987.75 image, right at the latitude of the phase 0.21 protuberance on the polar spot in the 1987.75 image. Furthermore, though the assumed constant migration rate of 64° yr^{-1} places it 0.02 in phase beyond this protuberance, it is likely that the migration rate decreases with increasing latitude, and we should probably be taking a slightly smaller migration rate appropriately averaged over latitude. In any event, the correspondence between the expected position of Feature C (extrapolated from its migration trajectory) and the phase 0.21 protuberance on the polar spot in the 1987.75 image is quite good, and may be further indication that there is a systematic clockwise northward spiraling flow of some intermediate-latitude spots up to eventual merger with the polar spot.

3.12. The 1988 Season Doppler Images

We obtained two images this observing season at epochs 1988.79 and 1989.11. Light curves for 1988.80, 1988.87, and 1988.97 were presented by Rodono and Cutispoto (1992), though no accompanying spot models were given. Mohin and Raveendran (1993) presented a light curve for 1989.11 and Cutispoto (1992) also presented a light curve for the 1989.09 epoch. The light curve was quite complex, but relatively low in amplitude. For most all of our other images which had contemporaneous or near-contemporaneous light curves, we were able to find satisfactory fits to both the line profiles and the light curve simply by properly thresholding the Doppler image, or by slight modifications of the spot distribution to reflect spot evolution. However, for both images this season, we were quite unable to reproduce the light curve from any reasonably adjusted version of the raw MEM image.

The spectral image for 1988.79 is shown in Figure 32 and the spectral line fits in Figure 33. The predicted light curve from this image is shown in Figure 34 as the dotted line along with the 1988.80 light curve (points) of Rodono and Cutispoto (1992). As can be seen, the predicted curve is much too low in amplitude and does not fit well.

It quickly became apparent that thresholding and/or adding cool spots alone could not fit the observed light curve; the Doppler image would have to be modified to such an extent that it would no longer fit the observed spectral line profiles. Clearly, some feature was required to significantly raise the brightness level near phase 0.80. This was accomplished by placing a hot spot with a temperature 400 K above the photosphere at the equator at phase 0.71. All other cool spot features remained essentially the same as in the raw Doppler image. This photometrically-constrained 1988.80 image is shown in Figure 35, and the light curve from this image is shown as the solid line in Figure 34.

We encountered similar difficulty in deriving the 1989.11 image solution in that no simple combination of dark spots was found which could adequately fit both the line

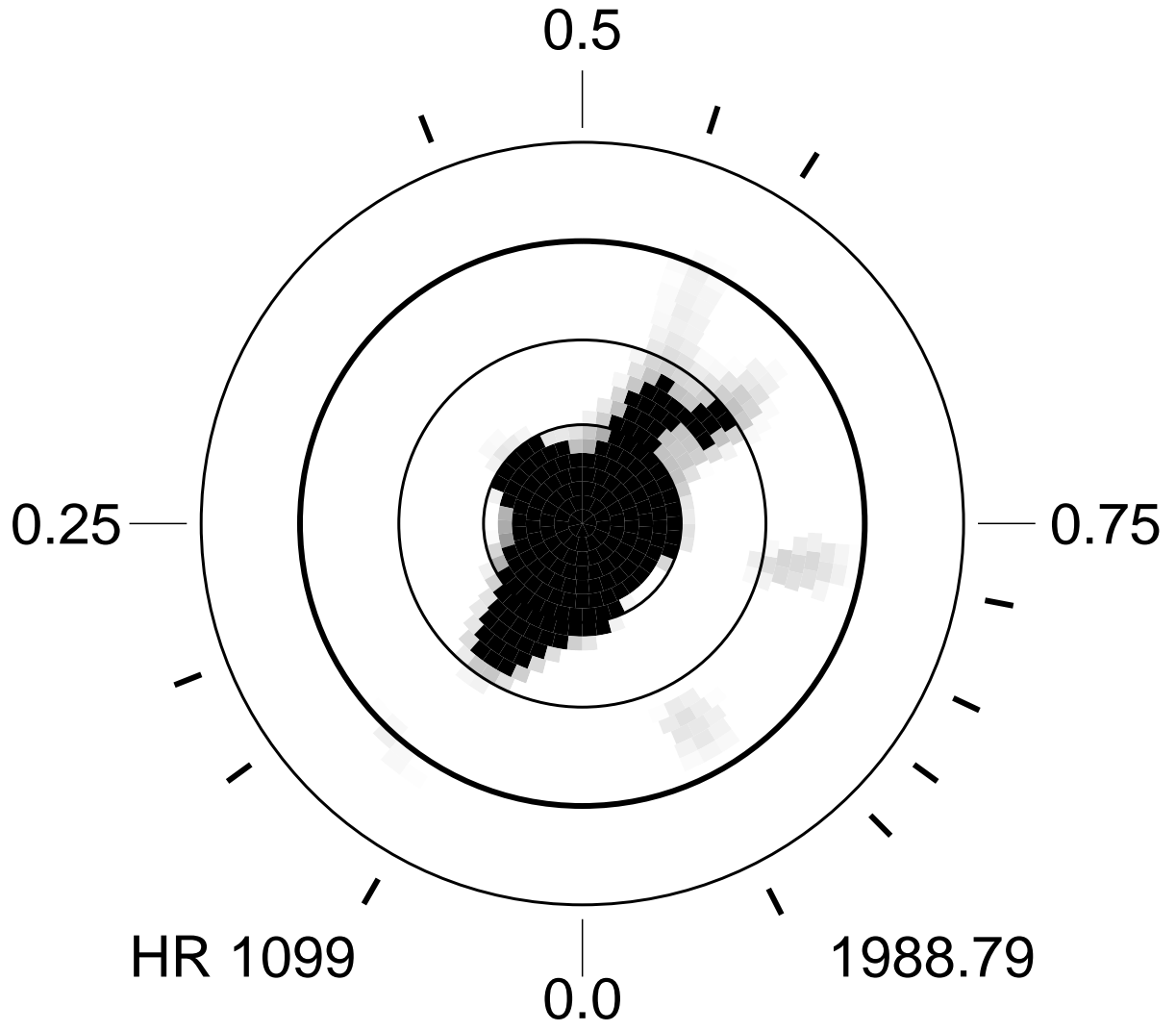


Fig. 32.— HR 1099 raw (unthresholded) Doppler image for 1988.79

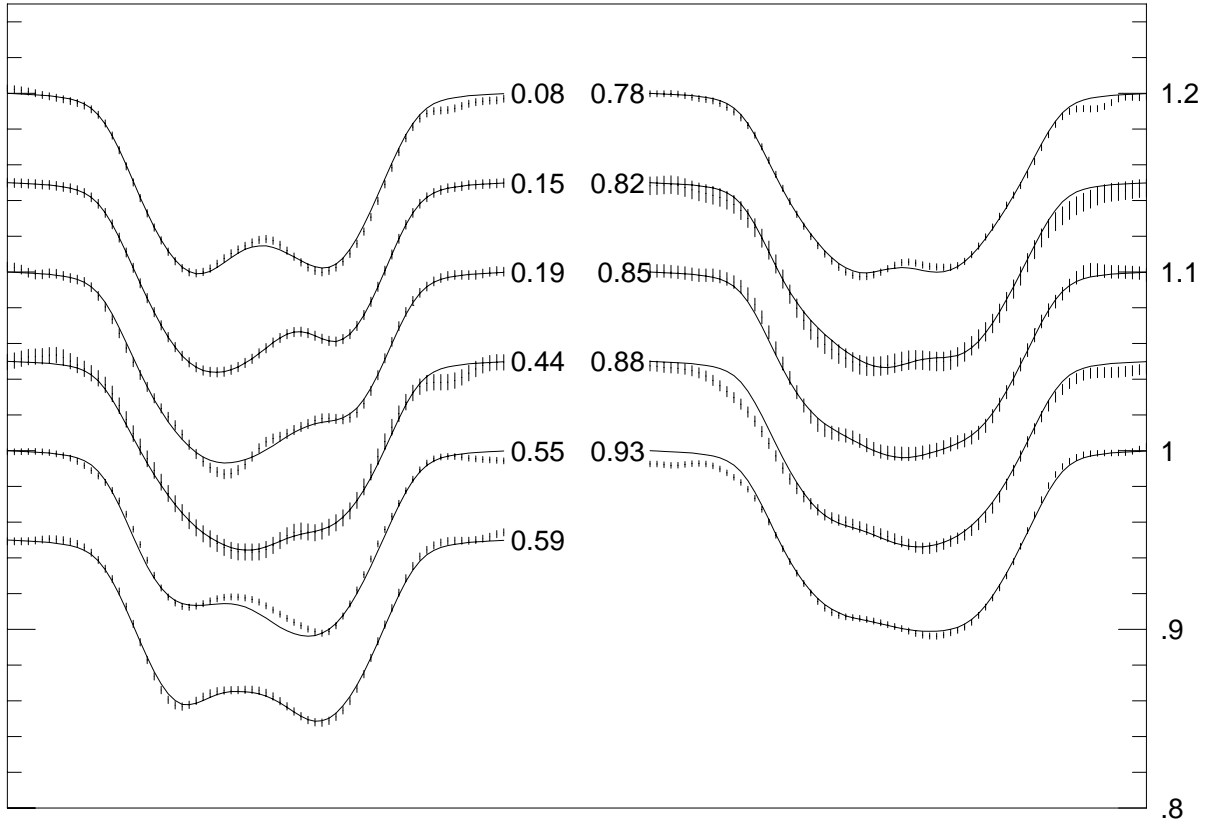


Fig. 33.— The spectral line profiles and fits for the 1988.79 image

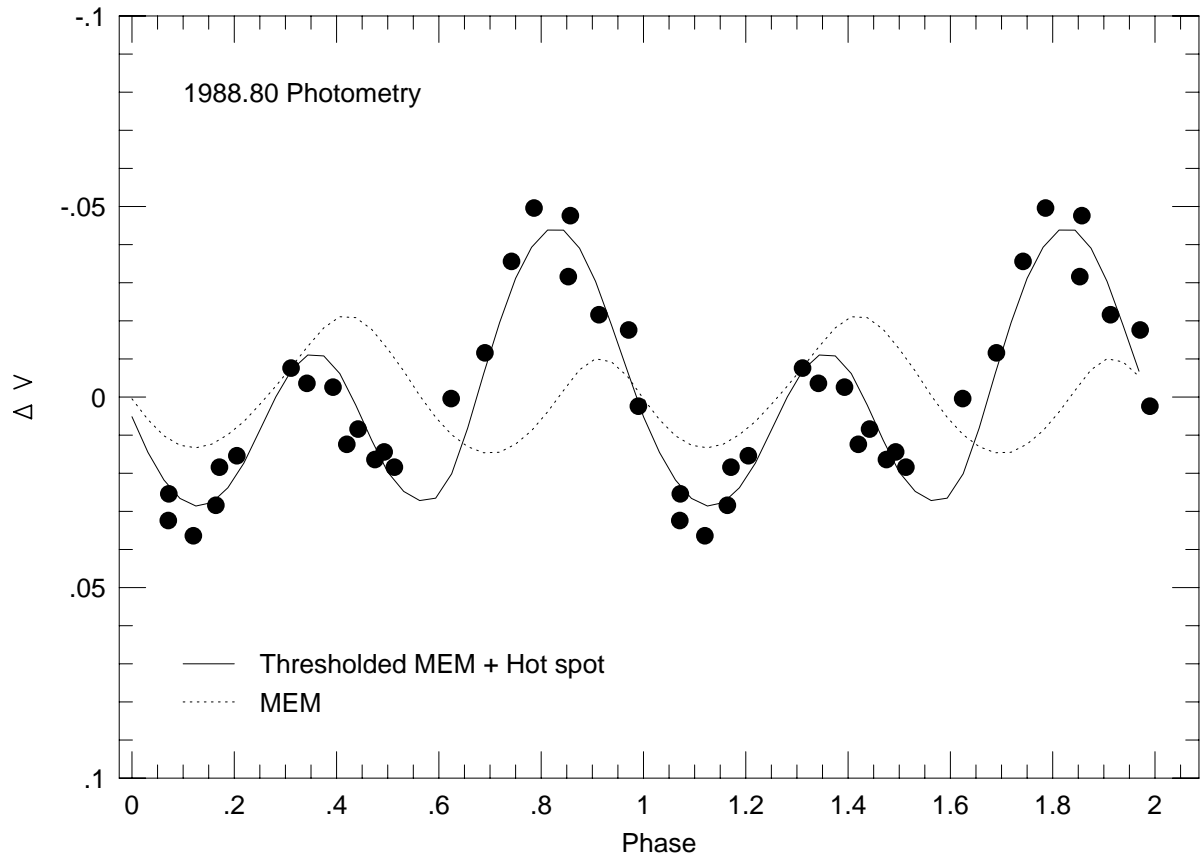


Fig. 34.— HR 1099 light curve for 1988.80

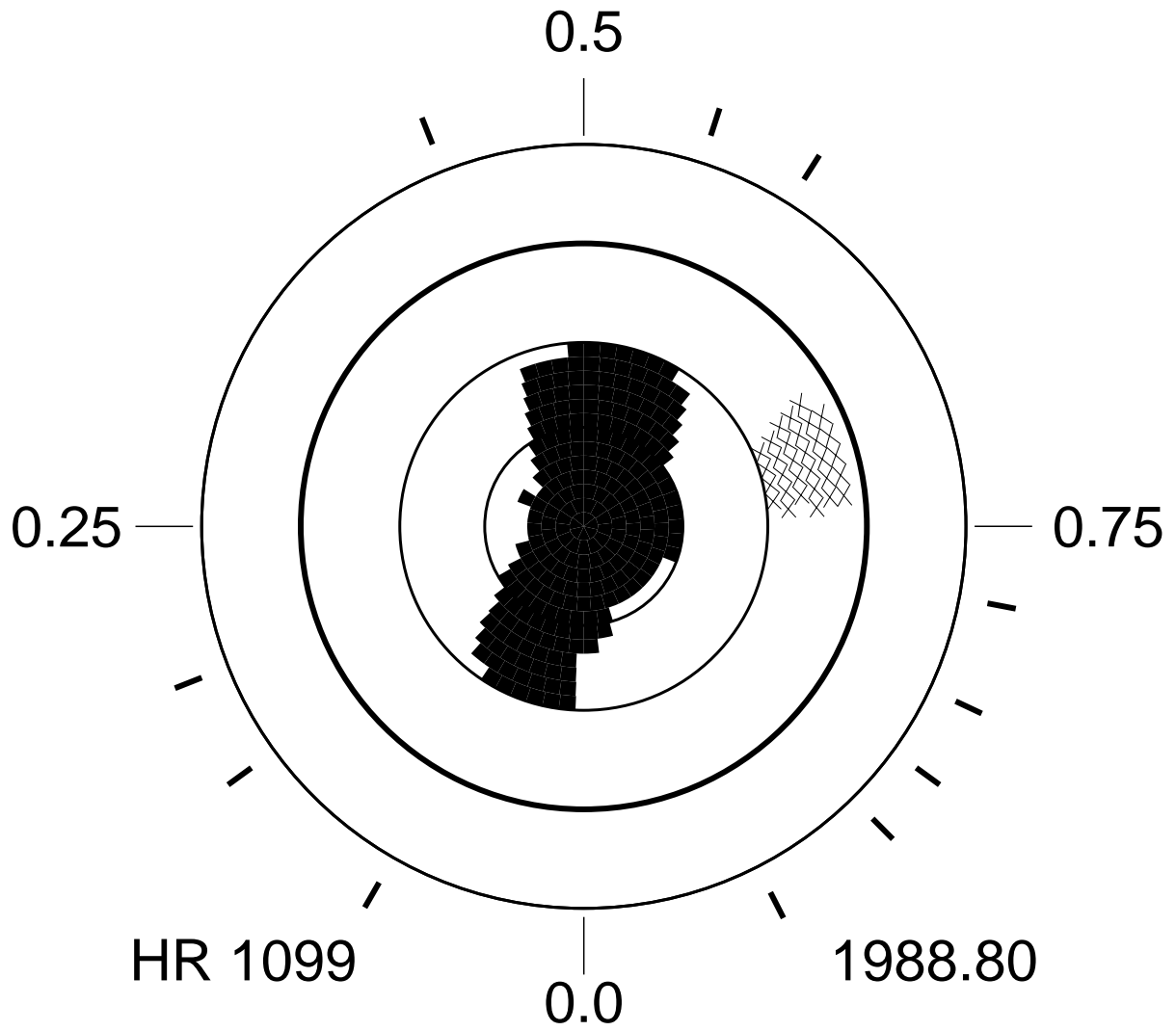


Fig. 35.— HR 1099 photometrically-constrained Doppler image for 1988.80. The cross-hatched region represents a hot spot 400 K warmer than the photosphere.

profiles and photometry simultaneously. Figure 36 is our raw unthreshhoulded MEM image for 1989.11. The spectral line profile and fits are shown in Figure 37. The predicted light curve from the raw image is shown by the dotted line in Figure 38 along with the 1989.11 photometry (points) of Rodono and Cutispoto (1992) which have been re-phased to the Fekel (1983) ephemeris.

Again, this raw MEM image gave a very poor fit to the photometry. We were, however, able to get a decent fit by including a hot spot with a temperature of 400-500 K above the photosphere placed near the equator at phase 0.74 (a spot at a similar location was also required to fit the photometry accompanying the 1988.79 image) and by increasing the area of one of the polar appendages.

The photometrically-constrained image, which fits adequately both the line profiles and the light curve is shown in Figure 39 and its predicted light curve is shown as the solid line in Figure 38. The basic shape of the polar spot was largely unchanged in the process, although its area increased somewhat. The most striking change again was the apparent need to have a low-latitude hot spot near phase 0.74.

We were quite uneasy with including hot spots in our solutions since we deliberately constrained the MEM method to only image features *cooler* than some quiescent photospheric temperature. In most other cases, this has been adequate and has produced good fits to both line profiles and, with a little threshholding, to light curves as well, even when the light curves were added after the fact. But it was quite clear in this year’s images that we simply could *not* achieve a satisfactory fit with only dark spots. Our result certainly does not confirm the presence of optically-visible hot spots on RS CVn stars, but it is perhaps corroborated by Donati et al. (1992b) who also found evidence for a hot spot in their 1988.9 image at the same latitude and near phase 0.78, as will be further discussed below.

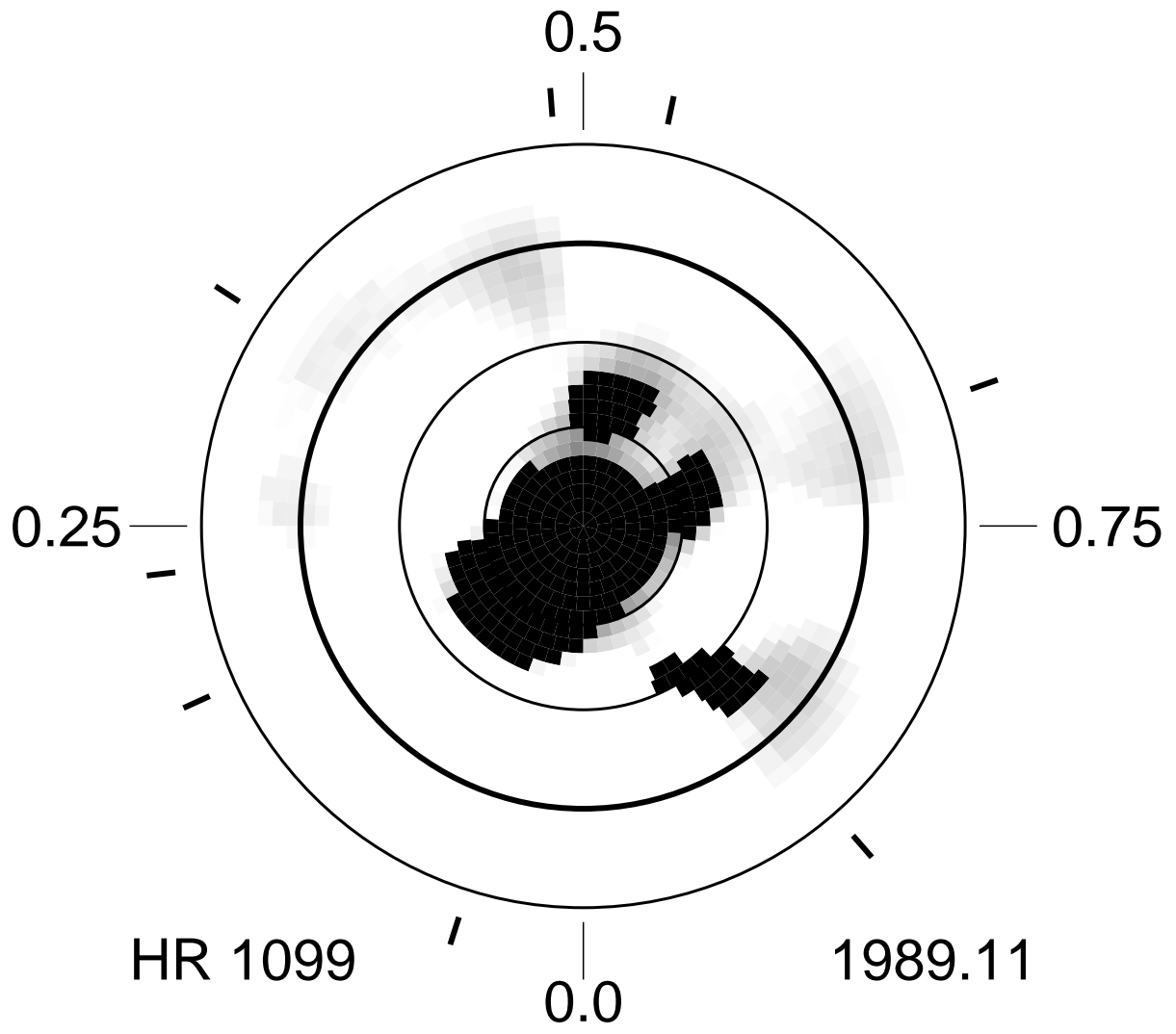


Fig. 36.— HR 1099 raw (unthresholded) Doppler image for 1989.11

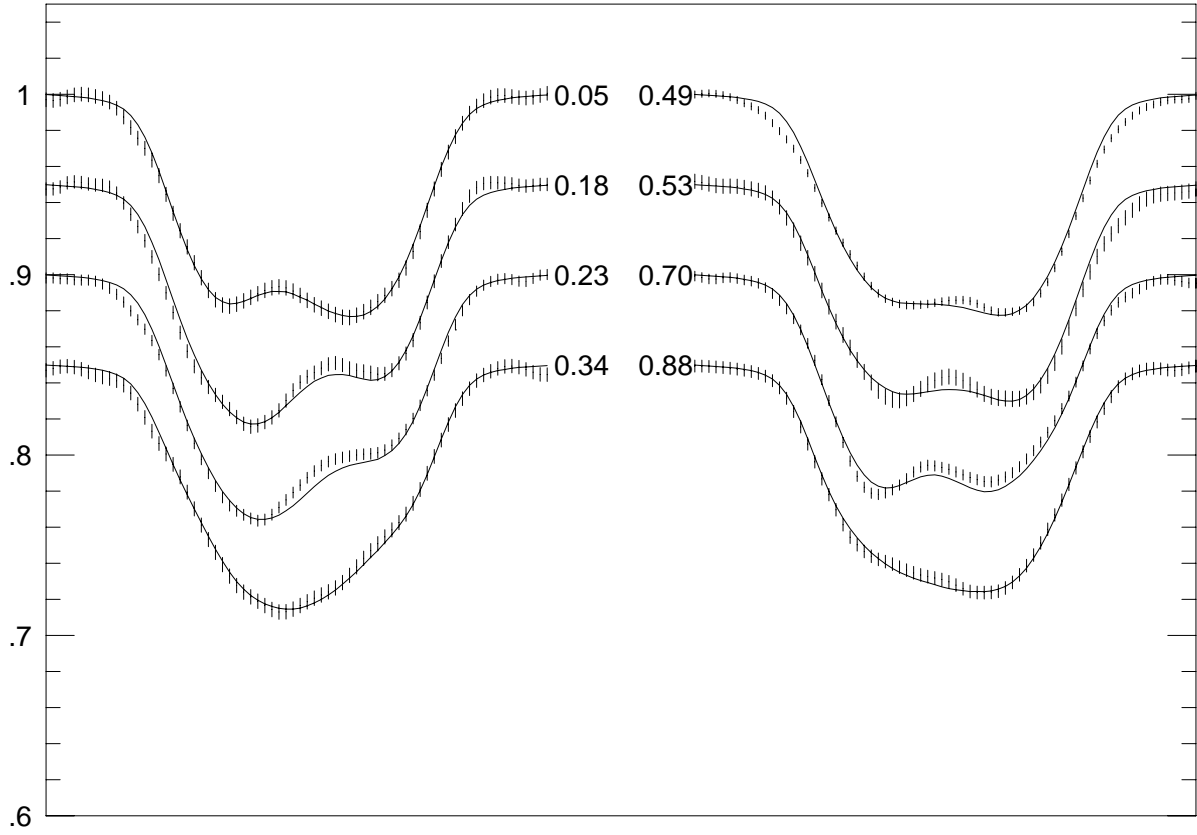


Fig. 37.— The spectral line profiles and fits for the 1989.11 image

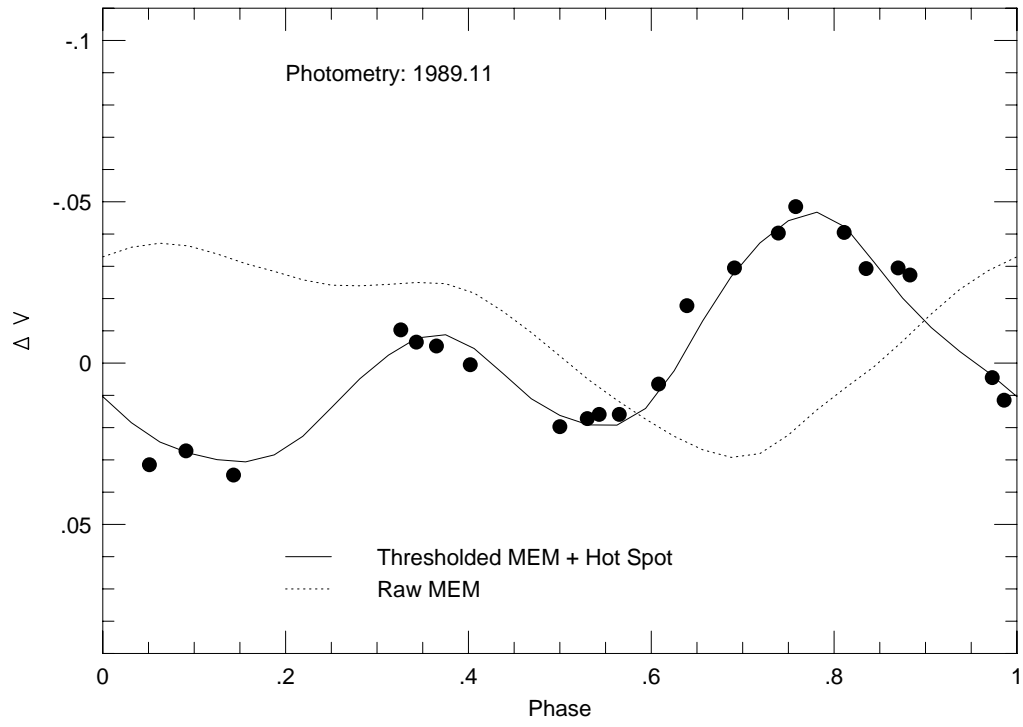


Fig. 38.— HR 1099 light curve for 1989.11

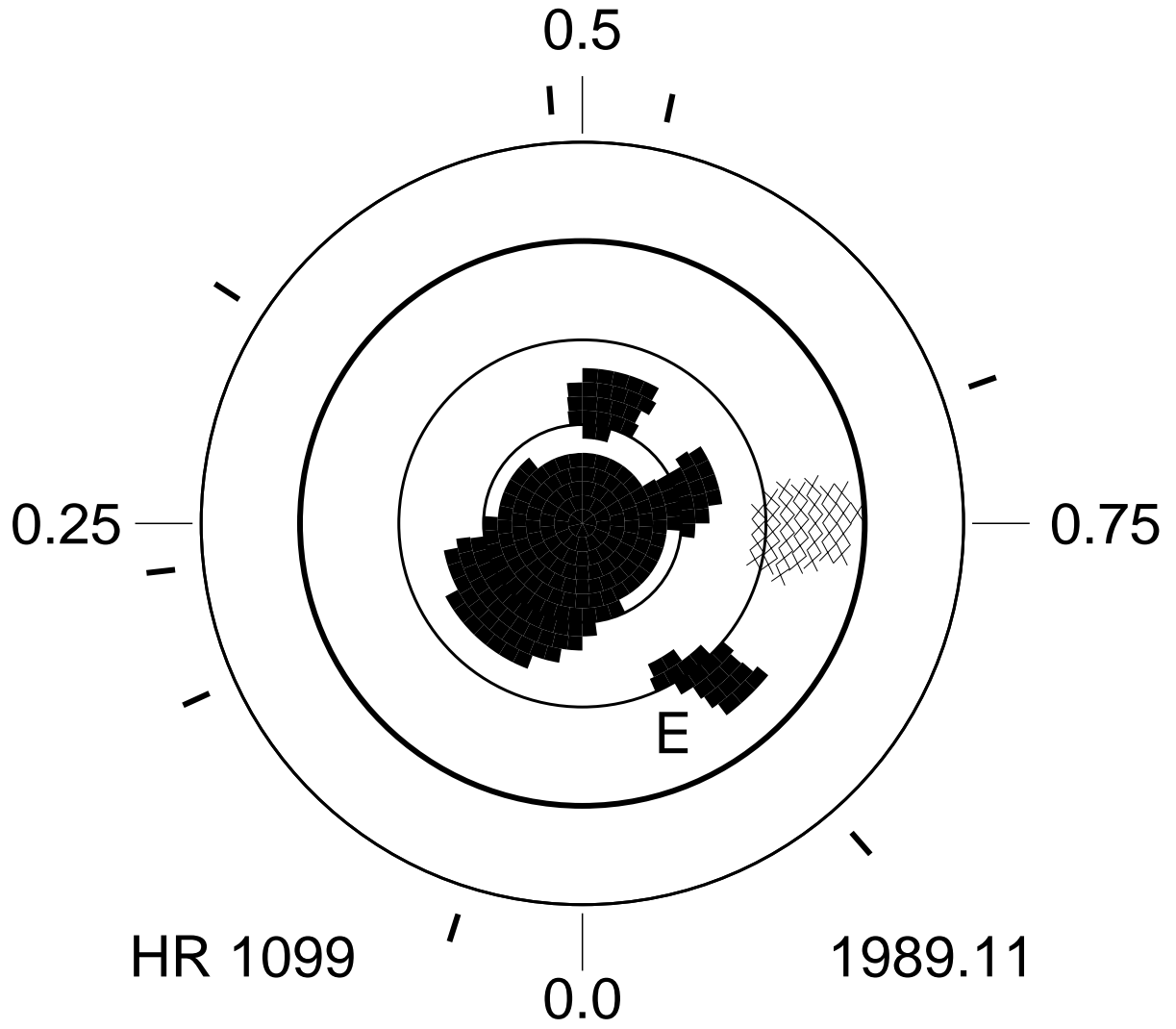


Fig. 39.— HR 1099 photometrically-constrained Doppler image for 1989.11. The cross-hatched region is a hot spot at a temperature of 400-500 K above the photosphere.

If prominent, optically-visible hot spots do exist on HR 1099, then they must not be very common. In our 11 years of Doppler imaging with 23 independent images, there was evidence for hot spots in only two images and they were both from this 1988-89 observing season. While one may well criticize our constraint of imaging only cool spots, in most cases our Doppler imaging shows that it is a good assumption, and that indications of prominent hot spots are quite apparent from the solution fitting. Furthermore, adding these hot spots does not seem to alter the gross features of the dark spot component of the image. It is clear that it would be preferable to implement a version of Doppler imaging which allows both hot and cool spots, but in the absence of very accurate simultaneous photometry, one runs the considerable risk of introducing spurious hot spots. It would be crucial to have excellent simultaneous multi-color photometry to be sure of hot spots.

The prominent feature near the polar spot at about phase 0.53 in the final photometrically-constrained 1989.11 image (Figure 39) may be the persistent signature of Feature B2, though it's difficult to calculate a migration rate since the structure of that feature has now changed considerably. There is now no sign of Feature D but there is a very large protuberance on the polar spot at phase 0.09 whose origin is difficult to connect with any previous feature due to gross changes in the spots. Its longitude is consistent with the phase 0.095 of Feature D in the 1987.75 image, but is not consistent with Feature D's position if it simply continued its $152^\circ \text{ yr}^{-1}$ migration rate observed previously. So, if Feature D were related to this major protuberance, it would have had to have come to a sudden stop in longitude migration between 1987.75 and 1989.11.

In other work, Buzasi, Heunemoerder, and Ramsey (1991) reported a dramatic reduction of 'extraphotospheric' emission on the primary star at about epoch 1988.71 which they ascribed to the disappearance of a prominence on the K star. They also reported seeing evidence for mass transfer in this binary system. A 'Doppler snapshot' of HR 1099

computed by Dempsey et al. (1992) for the Oct. 1988 - Sept. 1989 interval suggested the presence of a large polar spot (from the flattening in the cores of the spectral line profiles), but no actual image was presented.

Donati et al. (1992b) presented a detailed Doppler image of HR 1099 at epoch 1988.9, very close in time to our image of 1988.80 in Figure 35. Comparing our Doppler images with their image (Figure 4 of their paper) shows quite good agreement between these two completely independent Doppler imaging solutions, both for the shape and size of the polar spot, even for two low-level features near latitude 15° and phases 0.78 and 0.92 in our raw image (Figure 32). While most of the Donati et al. (1992b) data were obtained over a 3-month interval from Oct. 11 through Dec. 22, one of their crucial phases (phase 0.855) for Stokes V observations was obtained 4 months later, on March 24, 1989. At that time, they detected quite a large monopolar circular polarization signal near phase 0.855, indicative of a 1 kG monopolar region near the equator. They also found indications that the region was bright, and, though dark regions may also have been associated with that region, the polarization signature would have been dominated by any associated bright region. They also remarked that their largest fitting residuals occurred for the phase 0.855 line profile core.

It seems likely that this region corresponds with the emergence of Feature E in our 1989.11 image (Figure 39), and that their larger-than-normal fitting residuals were due to time variation of a complex bright and/or dark emerging magnetic region at the position of Feature E. Our Doppler image of 1989.11 (Figure 39) shows that Feature E is indeed changing and, what was only marginally detected as a subtle spot at about phase 0.92 in the 1988.79 raw image (and which did not survive our thresholding process) grew into a prominent dark spot at phase 0.89 by 1989.11. So we may have witnessed the birth of a spot (Feature E) at latitude 25° . This spot first appeared as a weak bright feature, but

then quickly evolved into a prominent dark spot which, as shown below, will then grow in area.

The polar spot also shows complex evolution. The large protuberance at phase 0.54 in 1988.80 evolved into a detached spot at phase 0.53 and latitude 50° , with a new protuberance at phase 0.70. However, since the 1989.11 image did not have many phases observed, and the phases of some of these protuberances coincide with the phases observed, we suspect that some of this structure may be an artifact of the phase sampling which, when lacking sufficient image constraints, tends to favor putting features at the sub-observer longitude. One must resist over-interpreting detailed changes in the image structure when phase sampling gets sparse. We believe that the 1989.11 image does show that there is significant spot presence between latitudes 30° - 60° at phase 0.6, but some of the structural detail in this area in the 1989.11 and 1989.72 (next section) images may be a consequence of insufficient phase sampling. Finally, the large polar spot protuberance near phase 0.09 in 1988.79 does appear to still be present in 1989.11, though much broadened in longitude as though the feature simply grew longitudinally by about 45° in the clockwise direction.

3.13. The 1989 Season Doppler Images

We obtained three separate images in the 1989-90 observing season, at epochs 1989.72, 1989.79, and 1989.83. Four light curves, for epochs 1989.73, 1989.79, 1989.86, and 1989.95 were presented by Rodono and Cutispoto (1992), and a light curve for epoch 1989.98 was presented by Mohin and Raveendran (1993). Multi-color light curves and a ‘3-spot’ model for 1989.98 were also presented by Zhai et al. (1994).

The raw MEM Doppler image for 1989.72 is shown in Figure 40 and the spectral line profiles and fits in Figure 41. The predicted light curve from our raw image is shown as

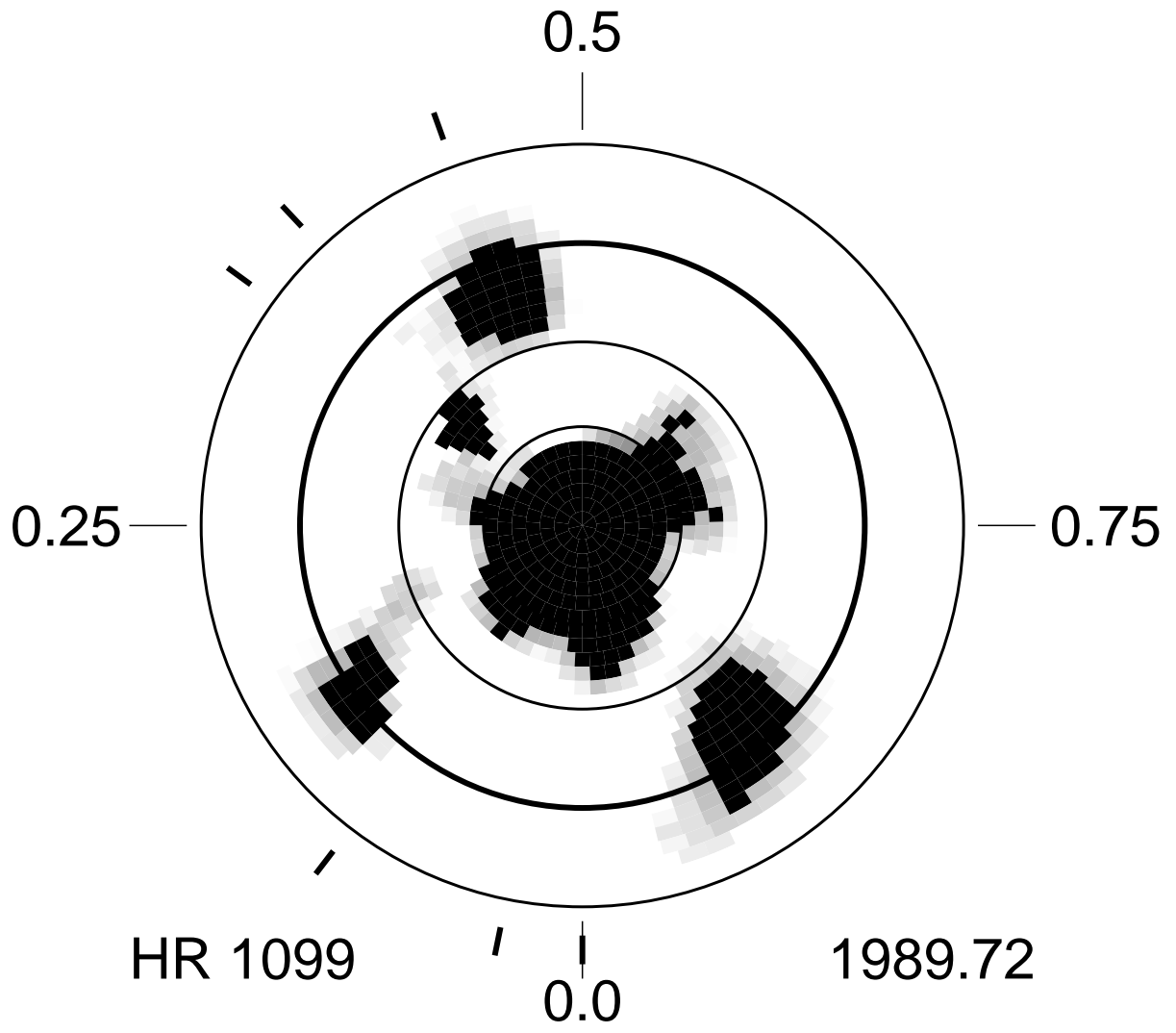


Fig. 40.— HR 1099 raw (unthressholded) Doppler image for 1989.72

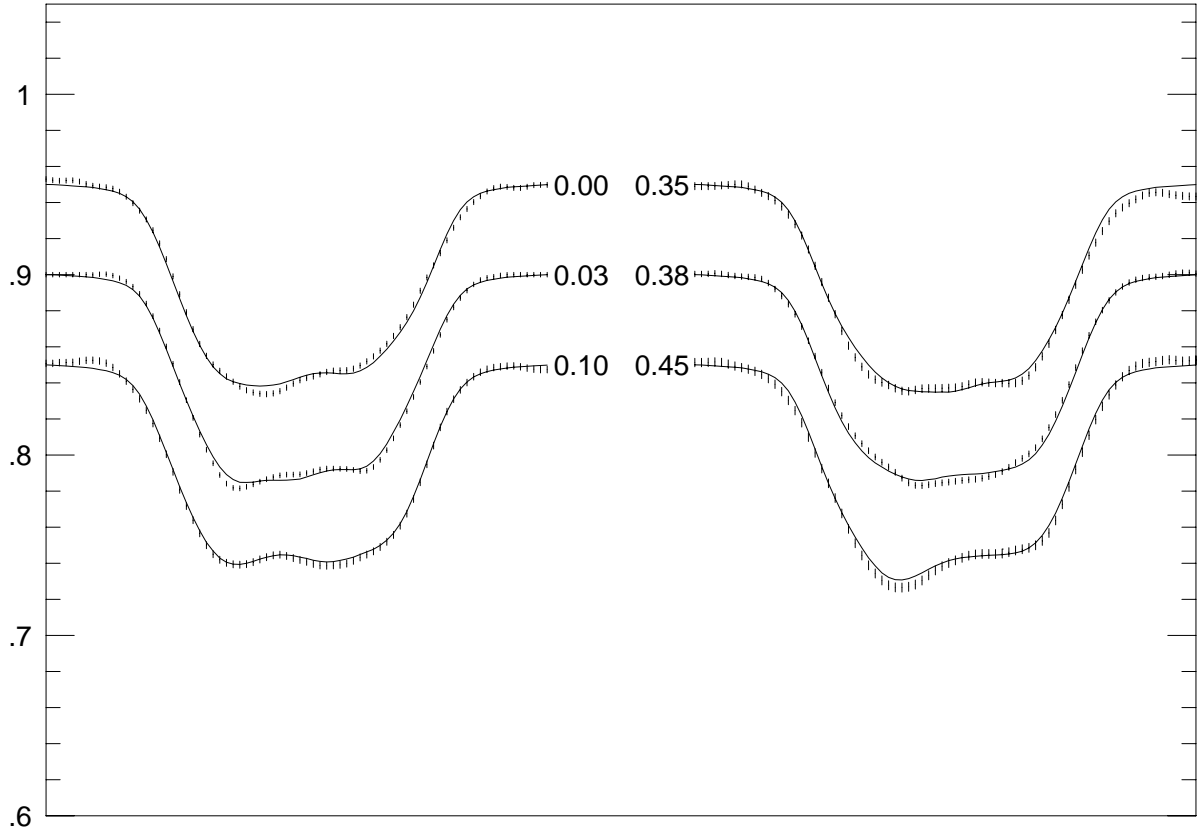


Fig. 41.— Spectral line profiles and fits for 1989.72

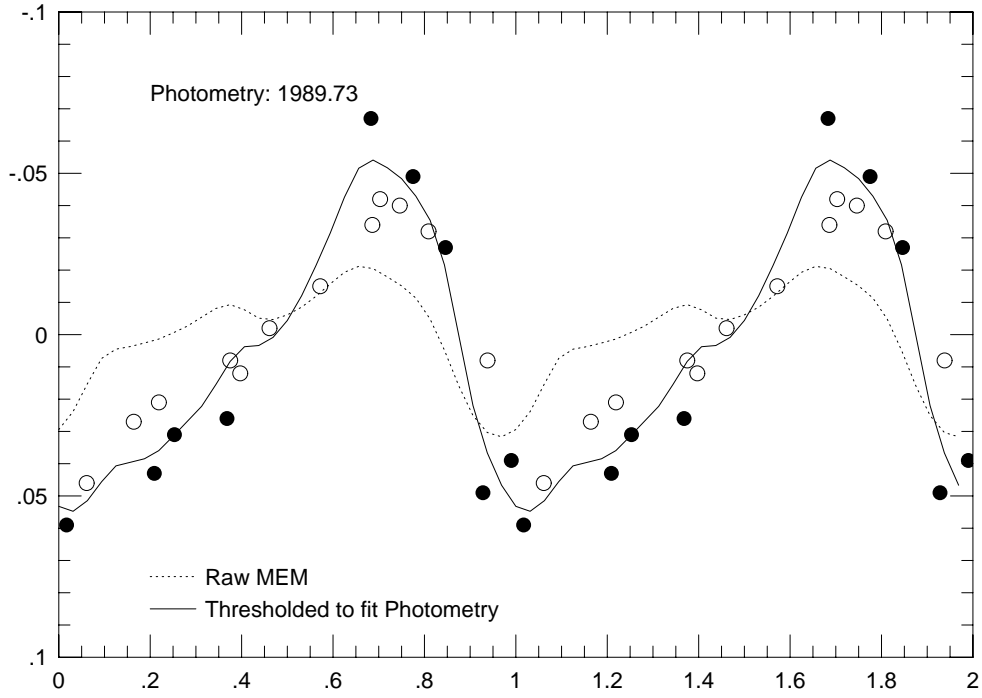


Fig. 42.— HR 1099 light curve for the 1989.73 image. The solid points are from epoch 1989.73. The open circles are from epoch 1989.79.

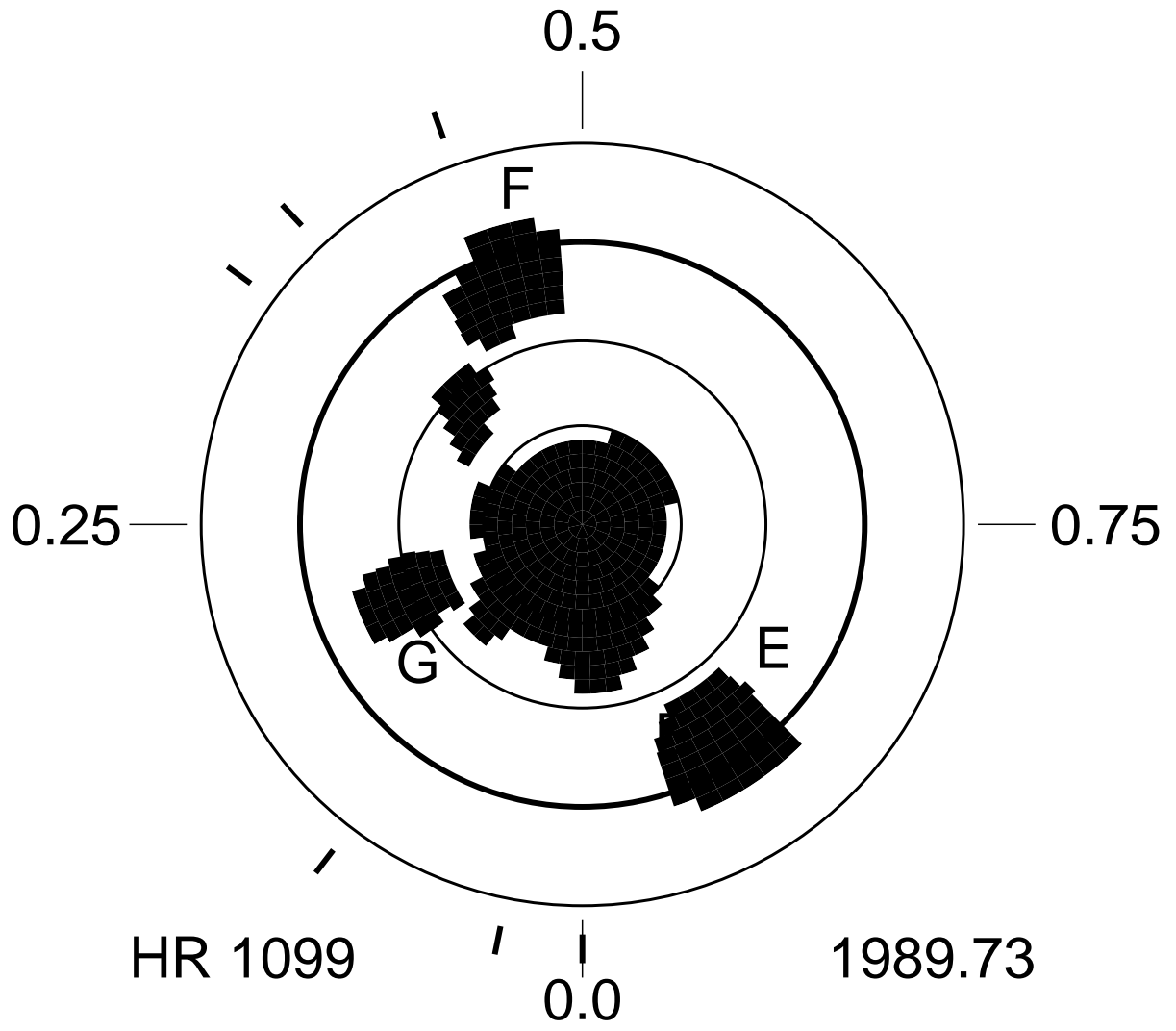


Fig. 43.— HR 1099 thresholded Doppler image for 1989.73

the dotted line along with the 1989.73 (solid points) and 1989.79 (open points) photometry of Rodono and Cutispoto (1992) in Figure 42. Thresholding to better fit the light curve produced little change in the image. The area of the appendages and the low-latitude spot had to be increased somewhat. The final thresholded image, shown in Figure 43, gives a pretty good fit to the observed profiles. The area of the appendages and of all the spots had to be increased somewhat and Feature G is displaced to higher latitude in the final image.

The raw Doppler image for epoch 1989.79 is shown in Figure 44; the spectral line profiles and fits are shown in Figure 45. The predicted light curve from the raw image is shown as the dotted line in Figure 46 along with the photometry (points) of Rodono and Cutispoto (1992). The photometrically-constrained image is shown in Figure 47 and the resulting light curve is shown by the solid line in Figure 46. A slightly better fit was obtained by also removing the mid-latitude spot pair at phase 0.67 in the raw image.

Our raw image for epoch 1989.83 is shown in Figure 48; the spectral line profiles and fits are shown in Figure 49. The predicted light curve is shown as the dotted line in Figure 50 along with the 1989.83 photometry (points) of Rodono and Cutispoto (1992). The strong minimum in the light curve near phase 0.0 in 1989.83 strongly supports the presence of a spot there, consistent with Feature E seen in previous images, but this feature is clearly absent in the raw Doppler image of 1989.83 (Figure 48).

A clue as to this apparent discrepancy can be found by comparing two line profiles taken near the same phase but about a month apart. Figure 52 shows two such profiles of the Ca I 6439 Å line taken one month apart near phase 0.064. The two profiles look significantly different. Note the excess absorption just to the red of center for the profile taken in November (solid line) as compared to the one taken in October (crosses). At this phase, the low-latitude spot should have produced a ‘bump’ just to the red of line center and it is clearly not there. Possibly the spot distribution has changed and the low-latitude

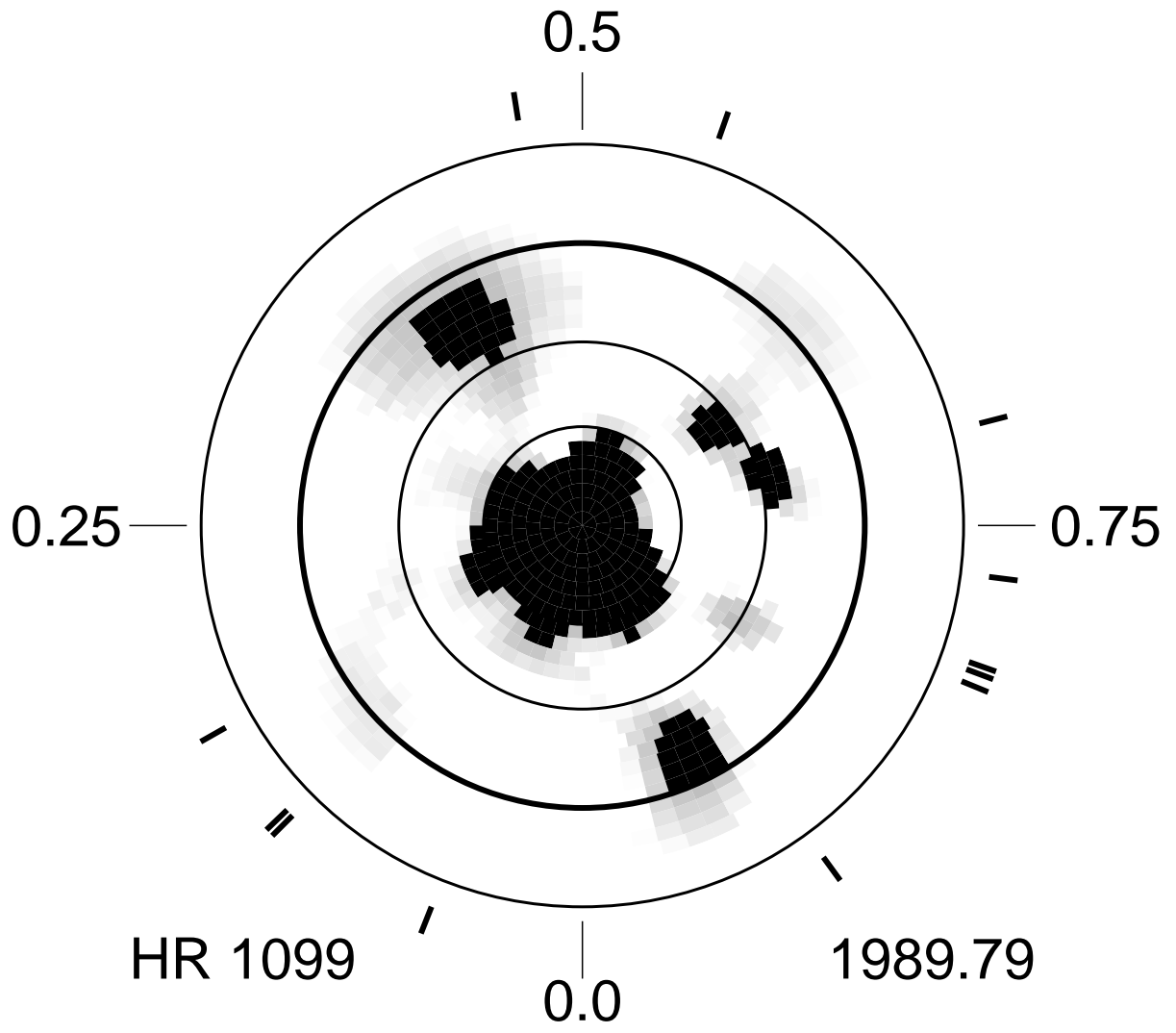


Fig. 44.— HR 1099 raw (unthresholded) Doppler image for 1989.79

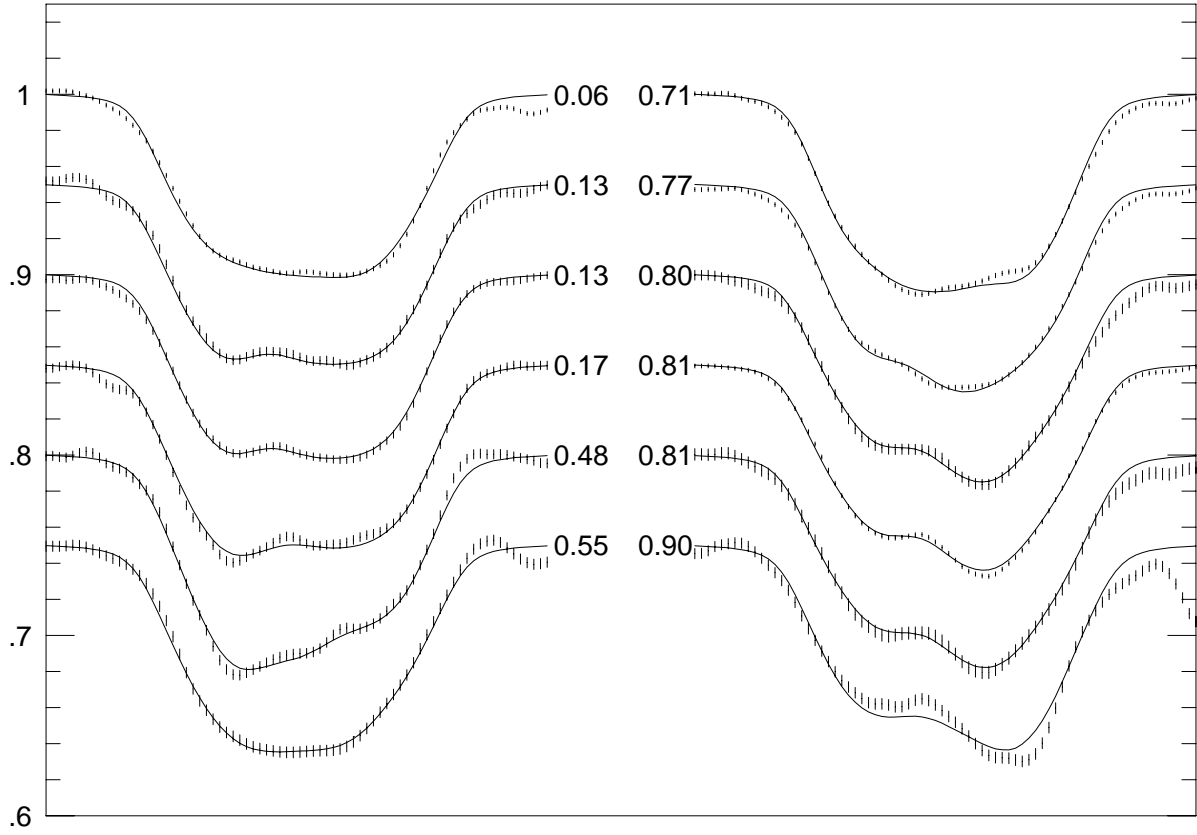


Fig. 45.— Spectral line profiles and fits for 1989.79

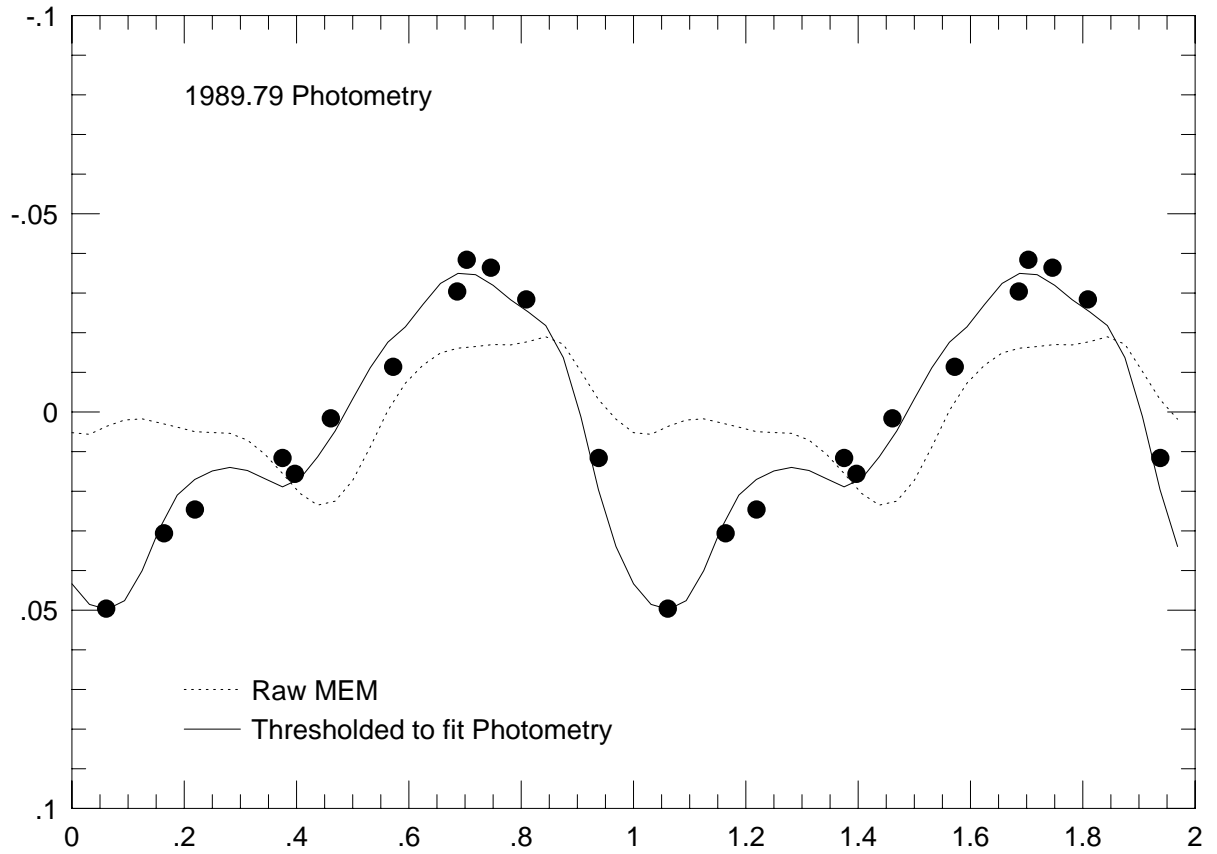


Fig. 46.— HR 1099 light curve for 1989.79

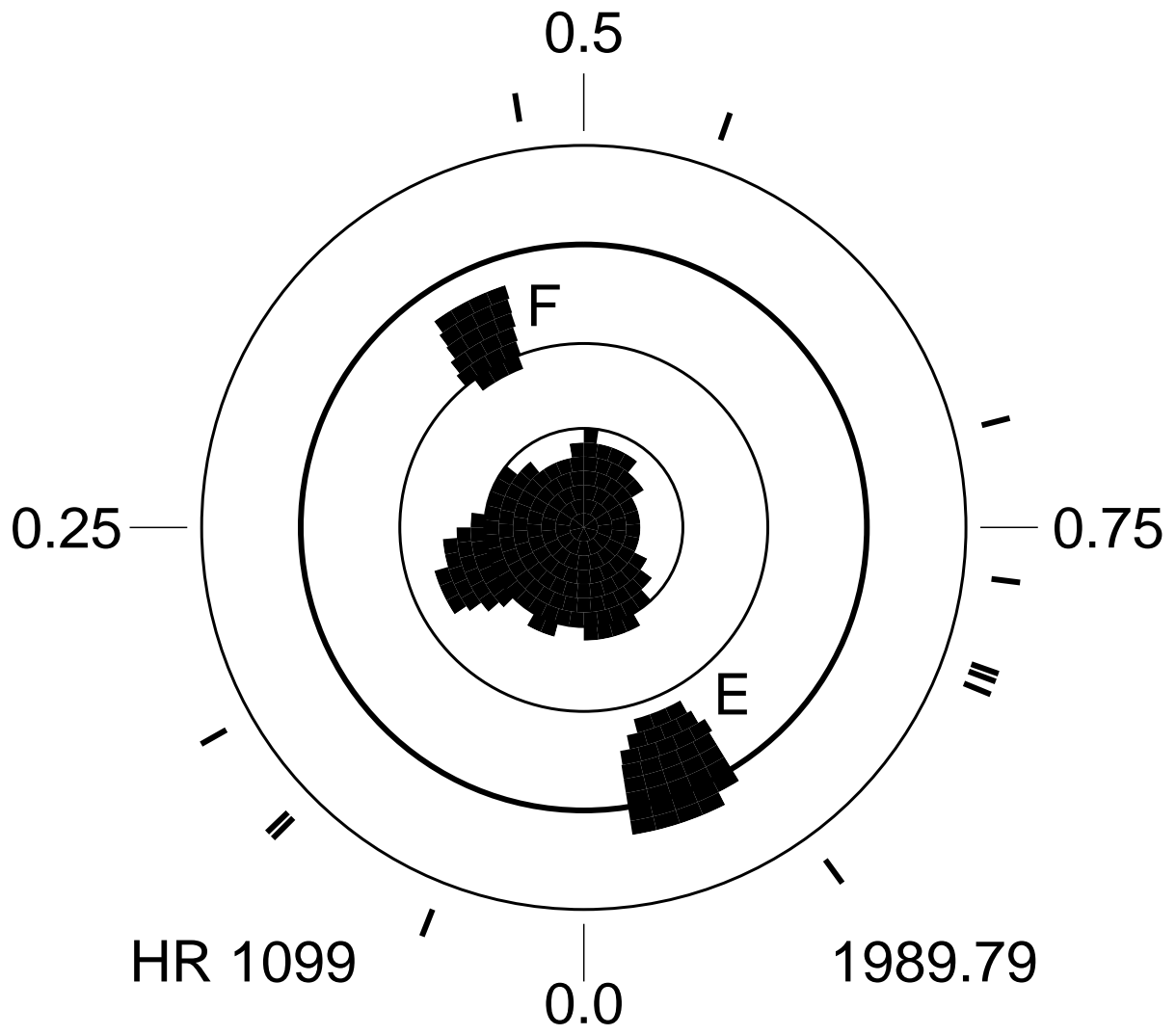


Fig. 47.— HR 1099 thresholded Doppler image for 1989.79

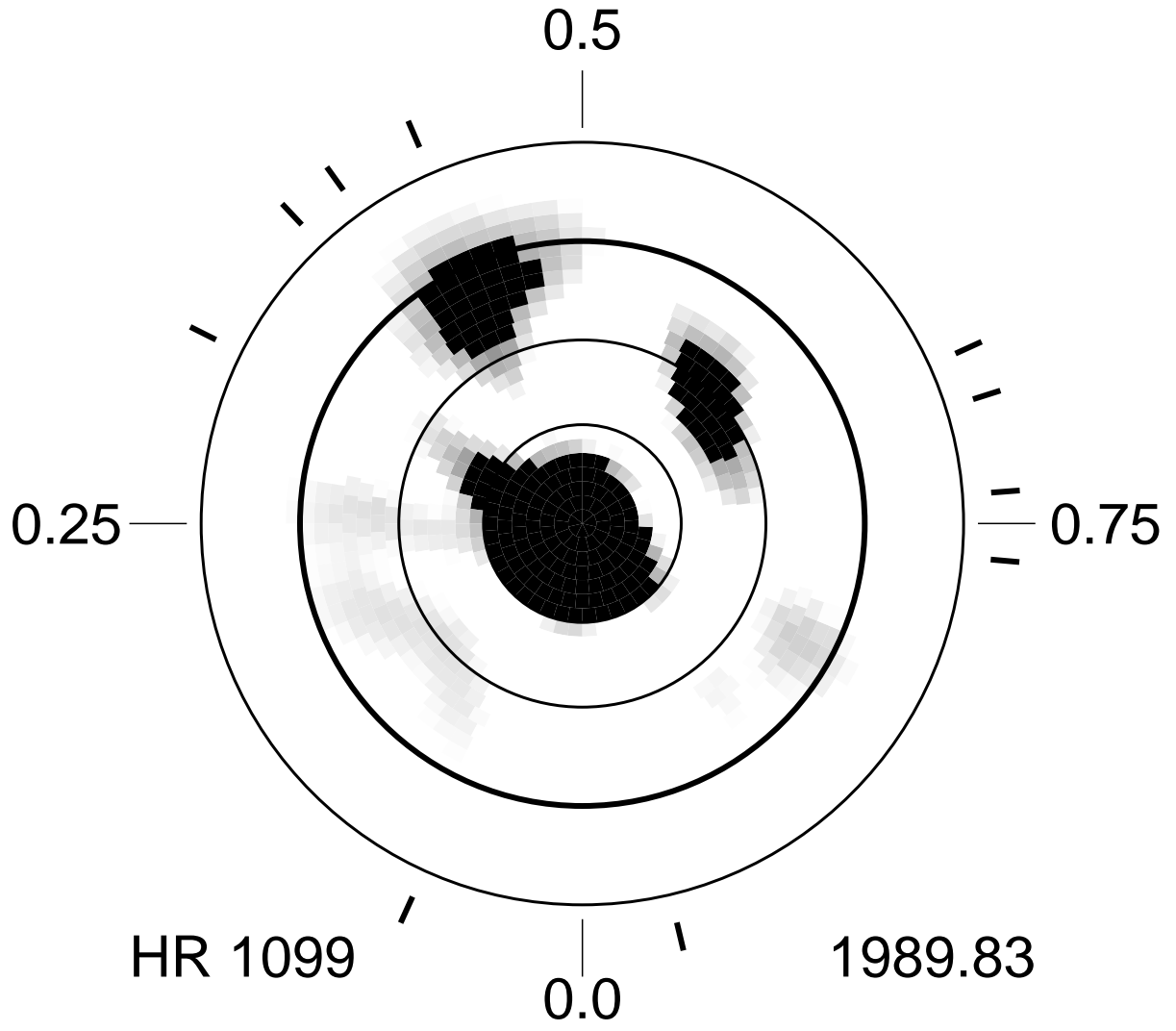


Fig. 48.— HR 1099 raw (unthressholded) Doppler image for 1989.83

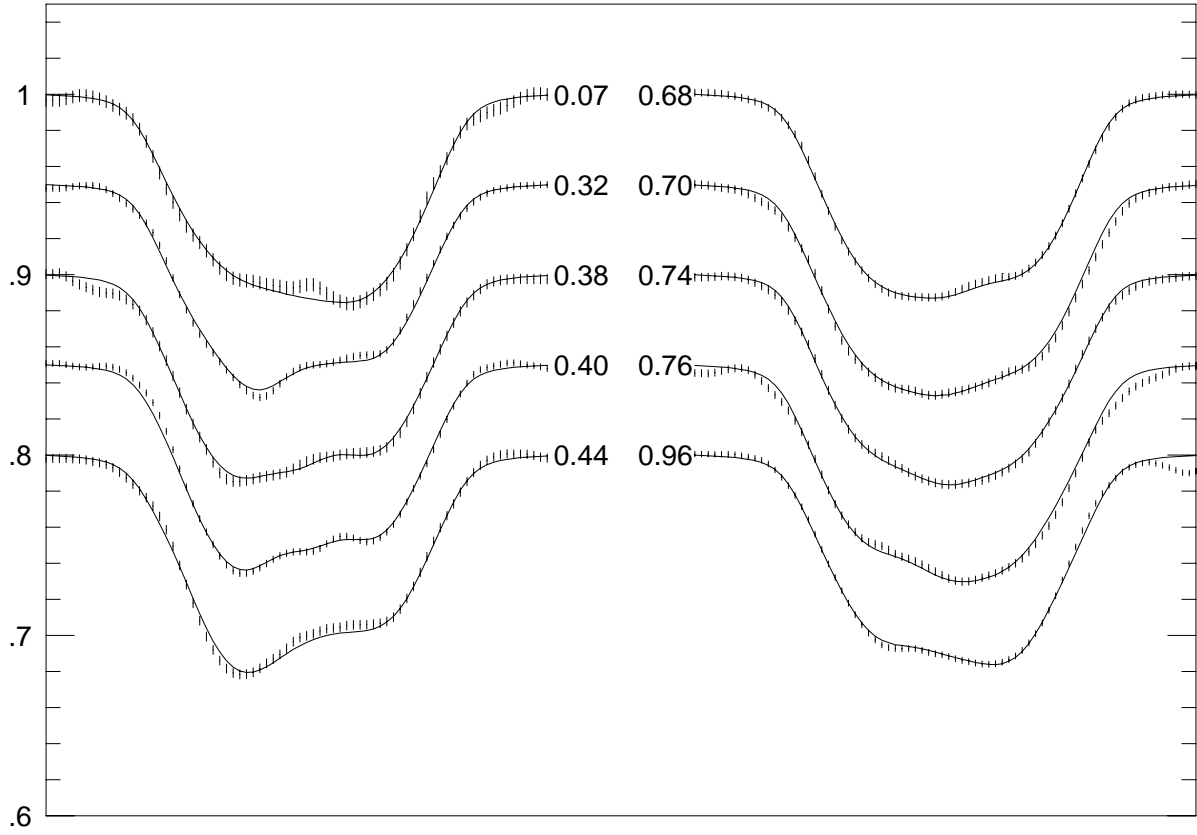


Fig. 49.— Spectral line profiles and fits for 1989.83

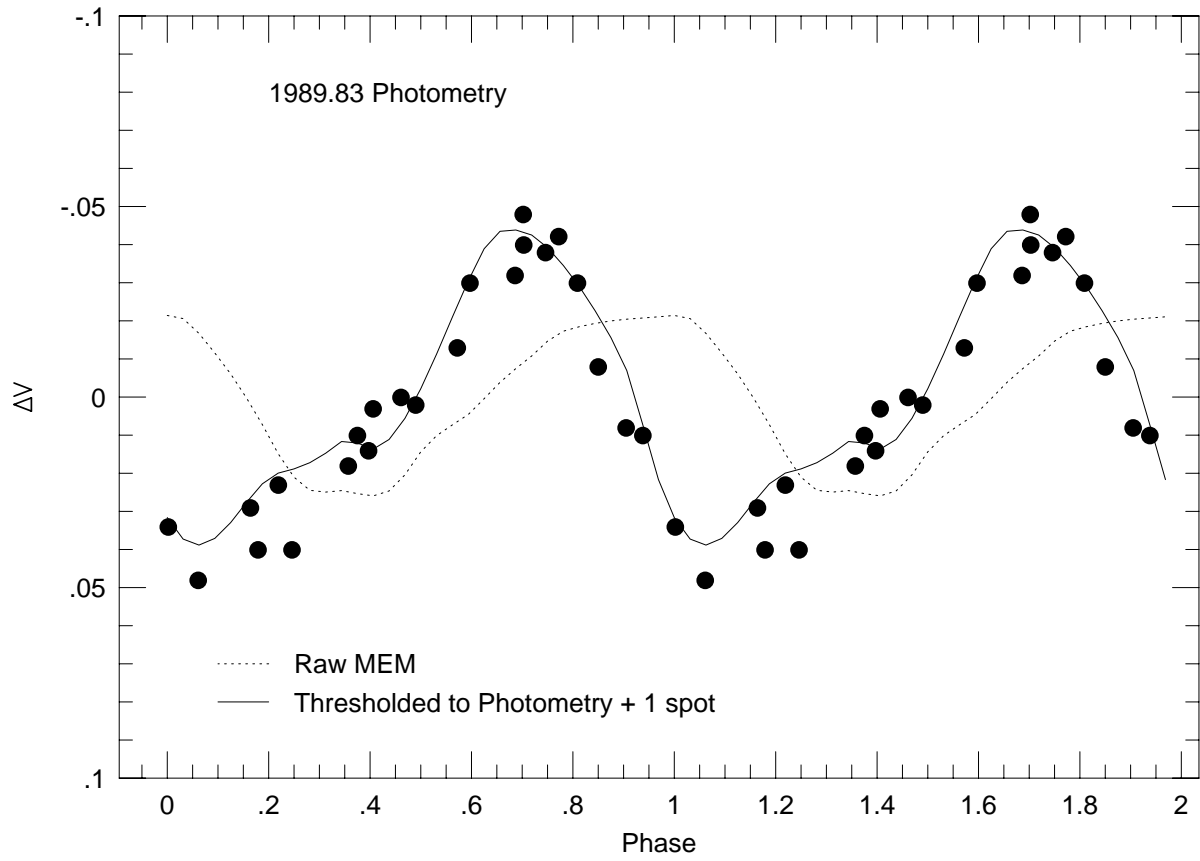


Fig. 50.— HR 1099 light curve for 1989.83

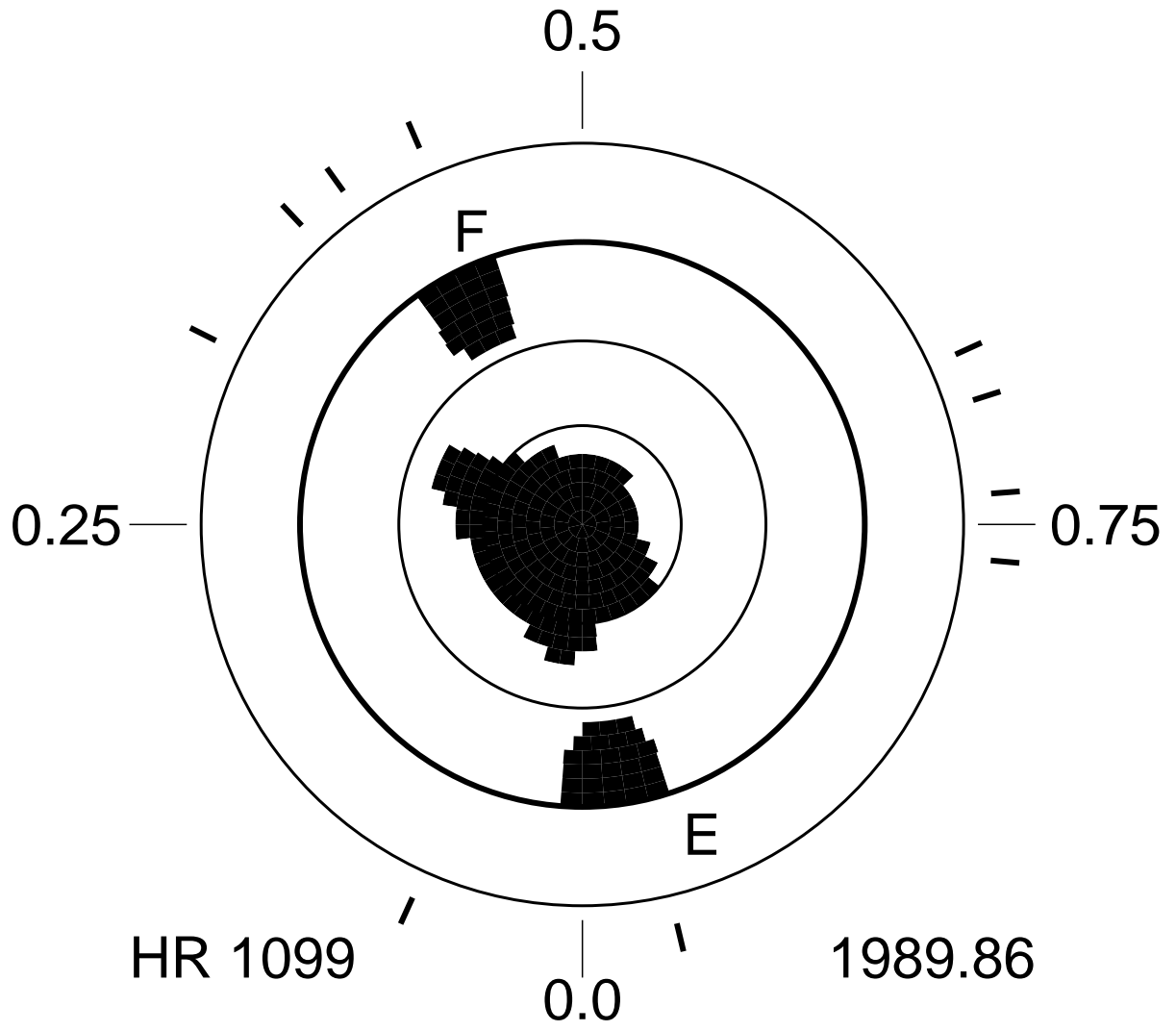


Fig. 51.— HR 1099 thresholded Doppler image for 1989.83

spot no longer exists. This, however, is not supported by the photometry. The other alternative is that there is something else distorting the line profile causing us to miss the low latitude spot. A likely possibility is the presence of a hot spot, possibly even a flare visible in white light. This would cause excess absorption instead of pseudo-emission at that location in the line profile.

Figure 53 shows two line profiles of (Ca I 6439 Å, one (solid line) at $\phi=0.90$ taken on 16 Dec 1989 (this is the last phase used for the 1989.83 image) and the other (crosses) at $\phi=0.96$ taken on 17 Oct 1989. Here, the differences between the two profiles are even more dramatic (the October profile has a lower S/N ratio, but not enough to account for the differences in line shape). Clearly either there are some rapid changes going on in the spot distribution or a hot spot is greatly diminishing the effect of the low-latitude spot on the shape of the spectral line.

Feature E continued to grow from 1989.11 to 1989.73 and there was a pronounced drift in its longitude between the 1989.11, 1989.73, 1989.79, and 1989.86 images. It started at about phase 0.88 in the 1989.11 image, appeared at phase 0.915 in the 1989.73 image, at phase 0.940 in the 1989.79 image, and ended up at phase 0.980 in the 1989.86 image. Whether the present Feature E of this year is related to that first seen in 1988.79 is not clear, but certainly this region of the star has been an active spot-former. This region gave rise to two major spots, Features D and E, which then migrated off to higher phases at constant latitude. Figure 54 illustrates this, showing the phases of Features D and E as a function of year.

This plot shows that the star formed two major spots near phase 0.9, the first (Feature D) in early 1987.0, and the second (Feature E) in early 1989.0. Both features showed a small and about equal drift rate for the first 7 months before then moving off towards higher phases at the same terminal rate of about $152^\circ \text{ yr}^{-1}$. Of course, we have no way of knowing

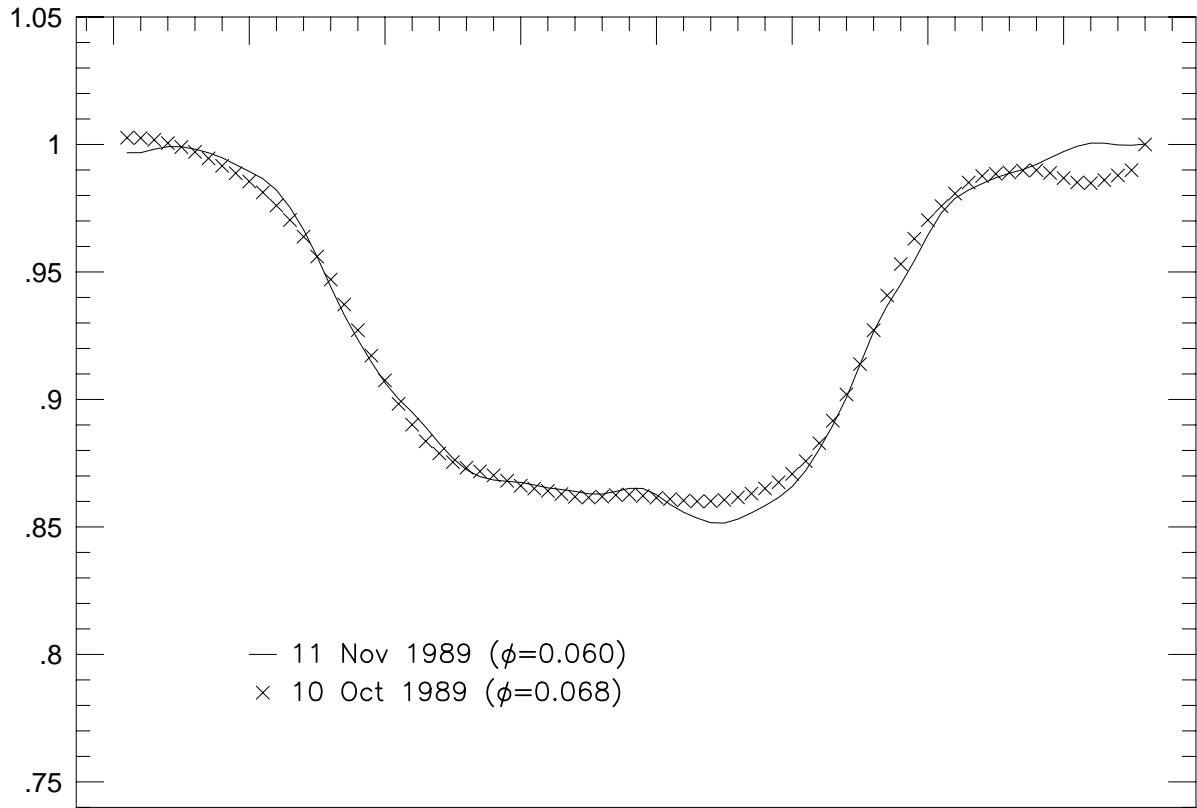


Fig. 52.— HR 1099 Ca I 6439Å line profiles taken one month apart near phase 0.064

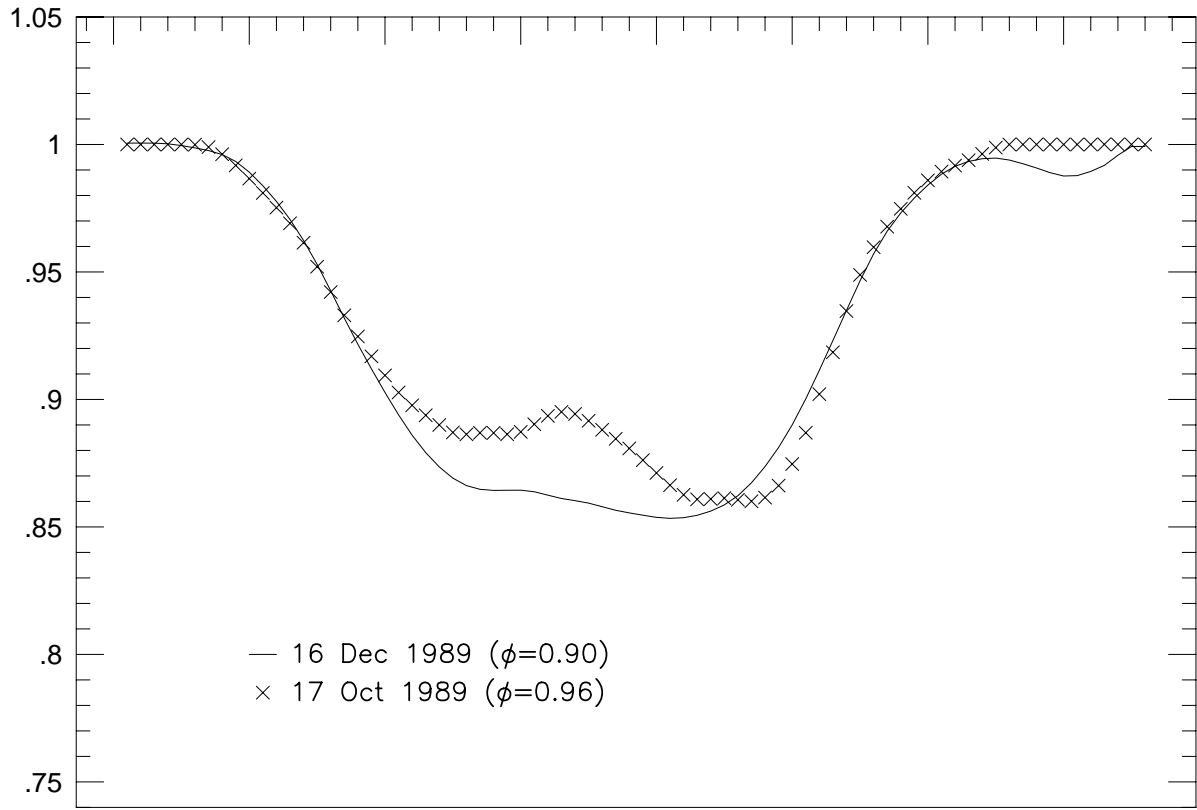


Fig. 53.— HR 1099 Ca I 6439Å line profiles taken two months apart near phase 0.93

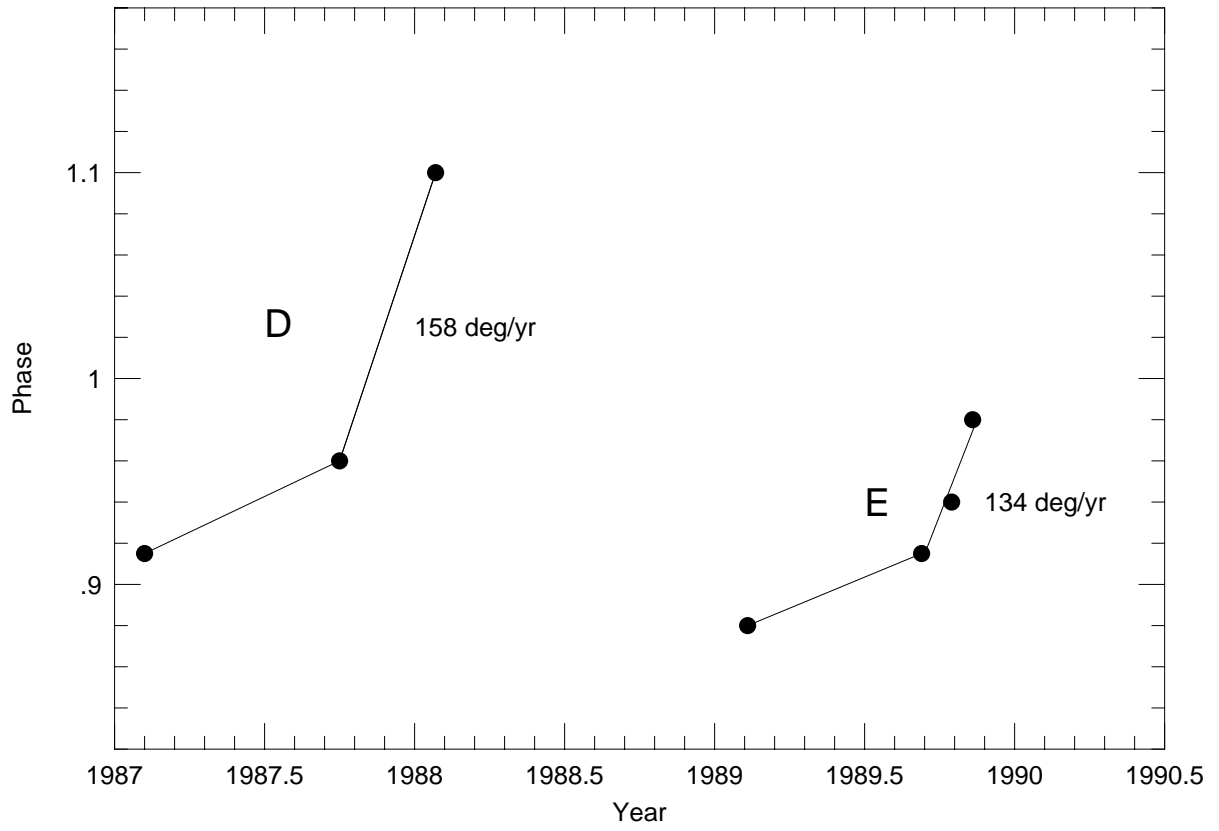


Fig. 54.— Phases of Features D and E as a function of time.

if we are seeing the same spot from month to month, but, at least for the 1989.7 to 1989.83 interval, where we have high time resolution for the imaging, and good contemporaneous light curves, the close agreement between Feature E’s latitude and size, and the smallness and uniformity of longitude advances makes this seem very likely. Feature E did remain at a constant latitude of about 11° , and it also appeared to be steadily shrinking over this time period, perhaps explaining why it was no longer visible by next year’s 1990.69 image. So we can probably use the three closely-spaced images from 1989.73 - 1989.86 to get an accurate estimate of the terminal migration rate for a spot at 11° latitude. A formal least squares fit gives 123 ± 17 degrees yr^{-1} with respect to the orbital frame at 11° latitude, and in the sense that the spot at this latitude is rotating about the star’s axis more slowly than the orbit. While this may seem like an enormous migration rate, it is still only about 1 part in 376 of the star’s rotation period, and thus any implied differential rotation is still quite small.

If Feature E is indeed migrating in longitude at a rate of $123^\circ \text{ yr}^{-1}$, then it might be expected to produce noticeable phase smearing in our images. One simple consistency check is to verify that this migration rate is not inconsistent with the longitudinal extent of each spot over the time required to obtain each image. For the 1989.72 image, Feature E was 25° in longitudinal extent, and the observations required 32 days to obtain. At a migration rate of $123^\circ \text{ yr}^{-1}$, it would then have smeared no more than 11° and is therefore consistent. The 1989.79 Feature E was 22° in longitude extent, and required only 6.2 days to image, implying a smearing of no more than 2° or less than a pixel width on the image and again not inconsistent with the observed migration rate. The 1989.83 Feature E was also 22° in longitude extent, and required 33 days to image, implying a smearing of no more than 11° , and was also consistent with the migration rate. While it is tempting to use the slight elongation differences between spots, coupled with smearing differences, to derive the true (unsmeared) size of Feature E, this is probably over-interpreting the data as their sizes

are also threshold-sensitive.

Donati et al. (1992b) presented a Zeeman Doppler image of the radial component of the surface magnetic field at epoch 1989.6 (their Fig. 10). They observed a very strong longitudinal magnetic signature at phase 0.855. This coincides very well in phase with our Feature E which would have been at phase 0.87 at the time of the 1989.6 magnetic measurements of Donati et al. (1992b). Their magnetic data was quite fragmentary, but their subsequent analysis indicated a large, bright, >1 kG monopolar region at our phase 0.79 and latitude 5° . They cautioned against the risk of interpreting their magnetic solution, and tried to make a case for this magnetic region corresponding to their bright region or plage at phase 0.78, but then wondered why their plage at phase 0.94 had no obvious counterpart in their magnetic image. Unfortunately, their magnetic data and solution were not complete enough to accurately constrain the longitude determination, so one can't say with certainty whether their large monopolar region coincides exactly with our Feature E, or is somewhat earlier in phase. Clearly though, their large monopolar magnetic signature observed at phase 0.855 and the presence of our recently-emerged Feature E near that phase and latitude at that epoch (1989.6) argues that their strong longitudinal magnetic signature was probably associated with our Feature E.

What then happened to Feature E? At a migration rate of 123 ± 17 degrees yr^{-1} , it would have migrated to phase 0.22 - 0.30 by the next image at epoch 1990.69. It doesn't seem to be there. So Feature E is an example of an isolated spot which emerged at low-latitude (about 11°), grew to maximum size in less than a year, migrated toward increasing phase at fixed latitude, and then dissolved in less than a year. At its peak size, it was probably associated with a strong ($\geq 1\text{kG}$) longitudinal magnetic signature. Since Feature E grew to full size in less than one year, and also completely disappeared in less than a year, in images taken 1-year apart, such features as Feature E could appear to come

and go at random, appearing in one image, but not in adjacent yearly images. It is precisely this type of rapid spot evolution which make interpretation of many of our HR 1099 images with time gaps of a year or more so difficult.

The 1989-90 images also show a prominent spot at latitude 14° and phase 0.45 which we hereafter refer to as Feature F. This is another example of a spot which has emerged (or formed) at low-latitude. It was probably not visible in 1989.11, but had fully emerged by 1989.72. It shows some longitude and latitude differences between the 1989.72, 1989.79, and 1989.83 images, but these are suspect for several reasons. First, the time interval spanned by these three images is only about 1.3 months, and one would expect the feature to look very similar in size and shape over such a short time interval, as was indeed the case for Feature E. Rather, Feature F was largest in 1989.72, shrunk significantly in 1989.79, and then grew slightly in 1989.83. Second, the phase coverage in that area of the star in 1989.79 was less than adequate, and can affect both the apparent sizes and locations of features there. Third, Feature F does not move at a uniform rate in longitude, as might be expected of a true migratory motion. Rather, it jumps abruptly between the 1989.72 and 1989.79 images, but then remains fixed in longitude between the 1989.79 and 1989.83 images. Finally, there is another small feature near latitude 39° and phase 0.38 which is complicating the image geometry in this general area of the star. Whether this is a real feature, or an artifact of our phase sampling coupled with ghosting from the true image is unknown. But clearly, the overall spot distribution in this area of the star is complex and variable, and Feature E is not well-isolated from this evolving geometry. Deriving accurate migration rates requires spots which are well-isolated, fixed in shape and size, and moving smoothly at a constant rate in longitude and/or latitude. Feature F fails on all accounts.

There is also a spot which appeared at latitude 28° and phase 0.15 in 1989.73. This spot, hereafter referred to as Feature G, was not present 7 months earlier in the 1989.11

image. Tracing the evolution of the spot geometry in this general area of the star from 1989.73 to 1989.86, it looks very much as if Feature G rapidly moved poleward and merged with the polar spot by 1989.79, and then became the phase 0.31 protuberance on the polar spot by 1989.86. If so, it would be our third case (see previous discussion of Features B, and C) of evidence for poleward and clockwise spot migration, culminating in the merging of the spot with the polar spot. However, this interpretation is admittedly non-unique and verges on over-interpreting the image set. For example, the small feature near latitude 39° and phase 0.38 in the 1989.73 image may instead have become the phase 0.31 protuberance on the polar spot in the 1989.86 image. Other scenarios are also possible. There is also a protuberance at phase 0.98 on the polar spot in the 1989.73 image which may have migrated to phase 0.01 in the 1989.86 image. Again, however, the outline of the polar spot is changing too drastically to draw such a conclusion, or to derive reliable migration rates.

Zhang et al. (1990) reported observing a remarkable optical flare on HR 1099 on Dec. 14/15, 1989. This was followed up with photometry by Henry and Hall (1991) who observed an even larger flare 12 hours later and concluded from the color of the flare that it covered about 8% of the surface of the K1 subgiant. The flare event increased the mean light level of the star by 3% in B, and required 3 months for the star to return to its pre-flare mean light level. The large flare reported by Henry and Hall (1991) occurred at orbital phase 0.62. There is no obvious feature at this phase in our 1989.86 image, which might likely correspond to this flare, but, of course, such an energetic flare could have happened almost anywhere on the observable disk of the star.

HR 1099 was also the focus of an intense MUSICOS coordinated observing campaign in late 1989 as reported by Zhai et al. (1994) and by Foing et al. (1994). Zhai et al. (1994) used a simple ‘3-spot’ model to fit their epoch 1989.96 multi-color light curve observations, and focused on fitting an unusual phase shift of the light minimum among their different

photometric bands. They were able to model the principal features of their 5-color light curves using two cool spots and one hot spot, with two of their spots (one hot and one cool) adjacent to one and other and creating a large temperature gradient in longitude to account for the phase shift in different bands. A comparison of their 3-spot solution with our nearest-in-time Doppler image (1989.86) is instructive. Their 3-spot solution is shown superimposed on a grayscale version of our 1989.83 raw Doppler image in Figure 55.

Their Spot 1 was a hot spot, 17° in diameter located at phase 0.99 and latitude 30° . It agrees quite well in phase and size with our Feature E, and may suggest that Feature E was not simply a dark spot, but rather had associated bright emission. This also makes sense with regard to our discussion earlier in this section concerning Figure 52 where we suspected that emission was filling in the line profile and making Feature E hard to detect from line profile information alone. The longitudes of their Spot 1 and our Feature E agree exactly. The latitude for their Spot 1 was slightly north of our Feature E, but certainly within the latitude accuracy of both methods.

Their Spot 2 was a cool spot 42° in diameter and situated at phase 0.15 and latitude 29° . There is no obvious counterpart to this feature in our images. It may be that this feature is a result of their method’s attempt to parameterize the polar spot with its two large protuberances at phases 0.01 and 0.31 as a single high-latitude circular spot which splits this phase difference.

Their Spot 3 was a cool spot 16° in diameter and located at phase 0.29 and latitude 16° . Again, there is no obvious feature in our images which corresponds precisely with this spot, though it is near the phase 0.31 polar spot protuberance, and may be a reflection of that feature. It might also correspond to our Feature F since it has the same latitude though is fairly far away in longitude. Allowing that distance for correspondence, it could as well correspond to almost any feature on our image. As is usual for spot solutions from

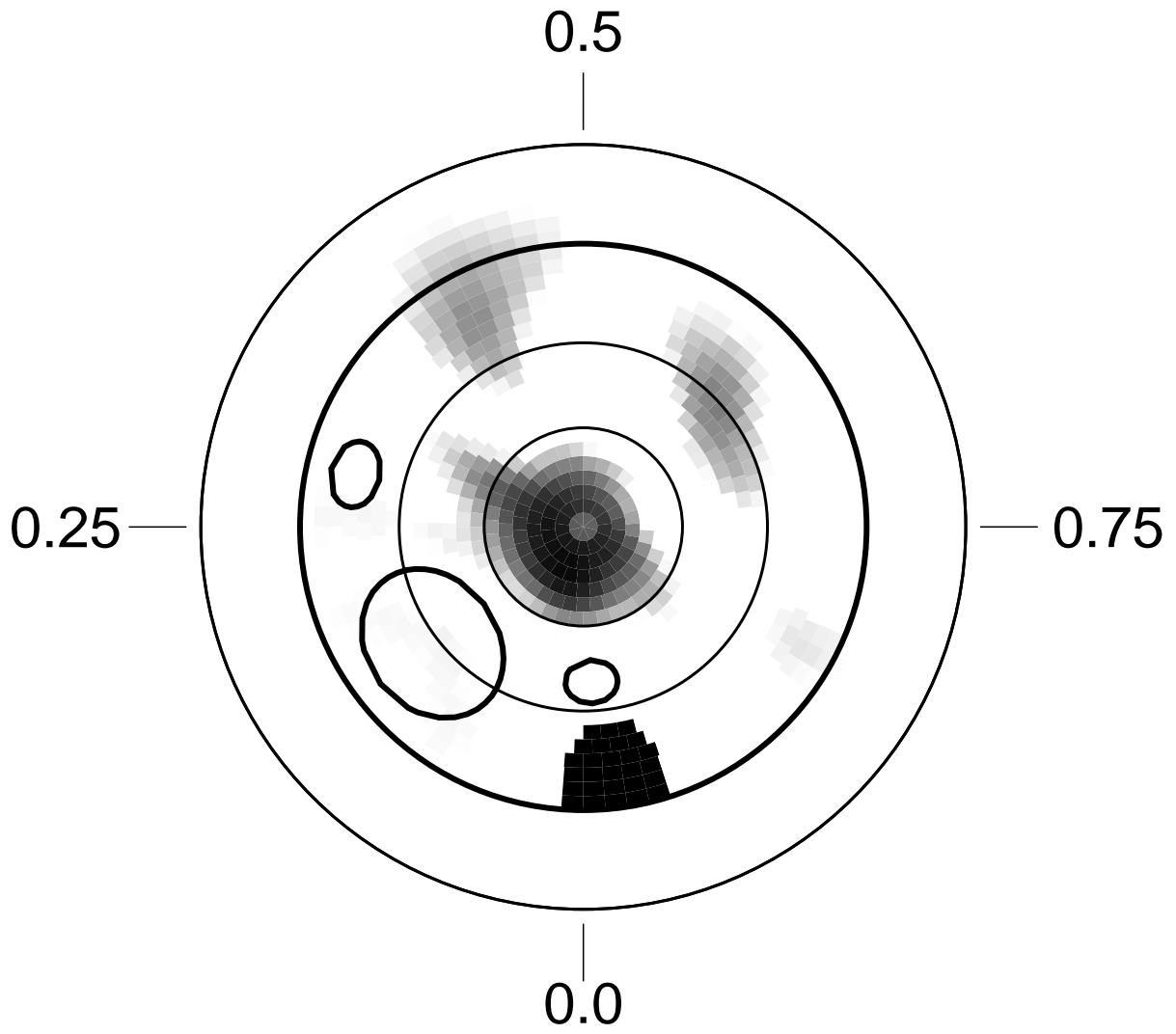


Fig. 55.— Photometric spot model from Zhai et al. (1994) superimposed on the MEM image.

light curve fitting, they did not detect the presence of the polar spot. So except for the possible correspondence of their Spot 1 with our Feature E, the overall agreement between the two solutions is not particularly inspiring.

Foing et al. (1994) reported further on the extensive MUSICOS 1989 campaign on HR 1099, including extensive Doppler imaging spectroscopic observations. Unfortunately, they did not present any Doppler images in that paper. Instead they simply used the spot solution of Zhai et al. (1994) discussed above to interpret their results, so any of their conclusions based on the geometry from this ‘3-spot’ solution should be viewed with due caution.

3.14. The 1990 Season Doppler Images

We obtained 4 separate images in the 1990-91 observing season. Unfortunately, we found only a single light curve for 1991.16, presented by Mohin and Raveendran (1993), with which to threshold and further constrain our imagery.

The Doppler image for epoch 1990.69 is shown in Figure 56 and the spectral line profiles and fits in Figure 57. Since we didn’t have a light curve for this epoch, we cannot present a photometrically-constrained image. It shows a rather simple spot distribution this year, with a fairly featureless polar spot and only a single detached lower latitude feature near phase 0.64. As we have learned from previous thresholded images, this feature is not necessarily detached from the polar spot, and its exact size and latitude may be threshold dependent.

Likewise, the raw unthresholded image for epoch 1990.79 is shown in Figure 58 and the spectral line profiles and fits in Figure 59. There is still some indication of a feature near phase 0.64, but it appears at a rather low level in this unthresholded image. The

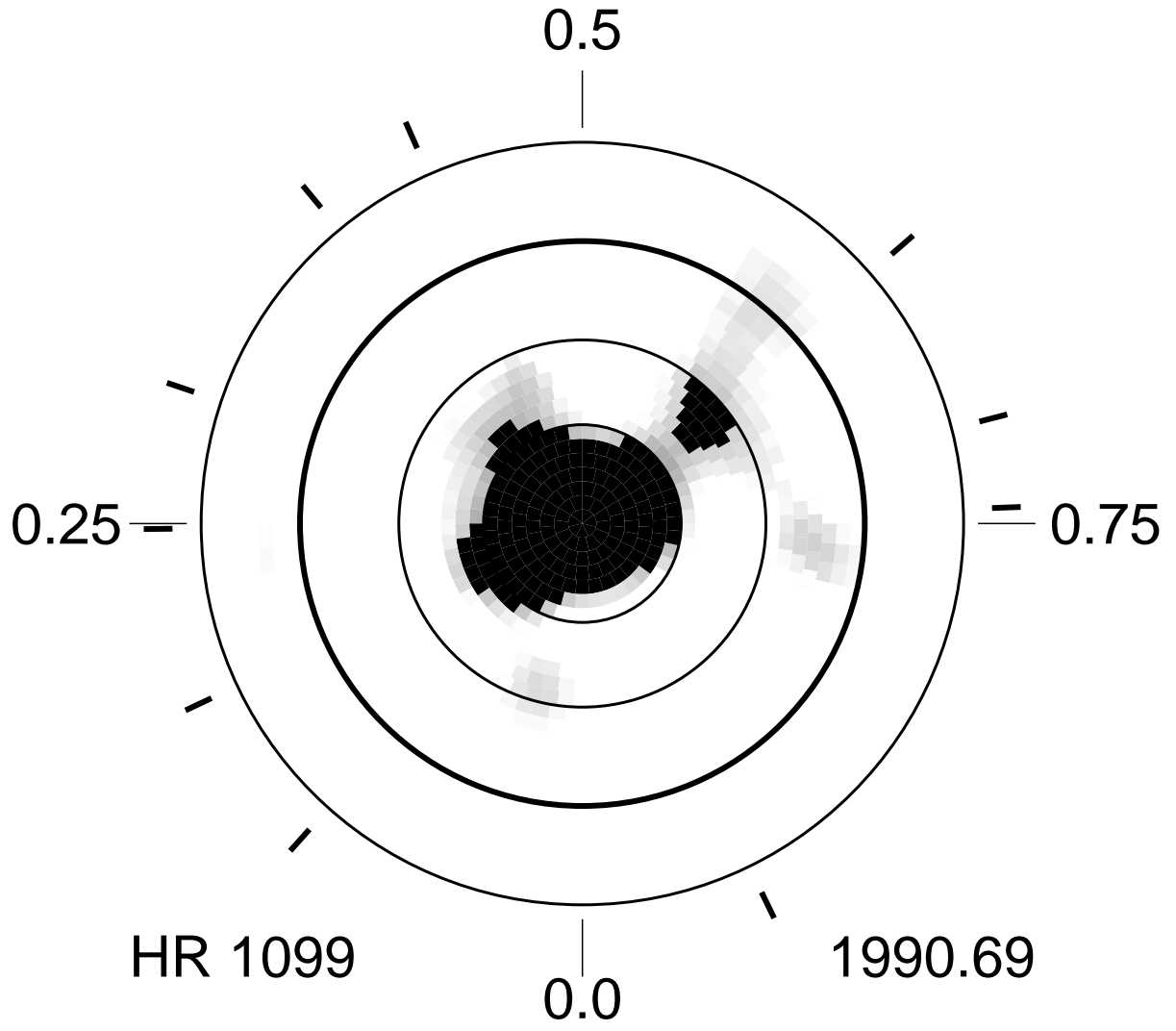


Fig. 56.— HR 1099 raw (unthresholded) Doppler image for 1990.69

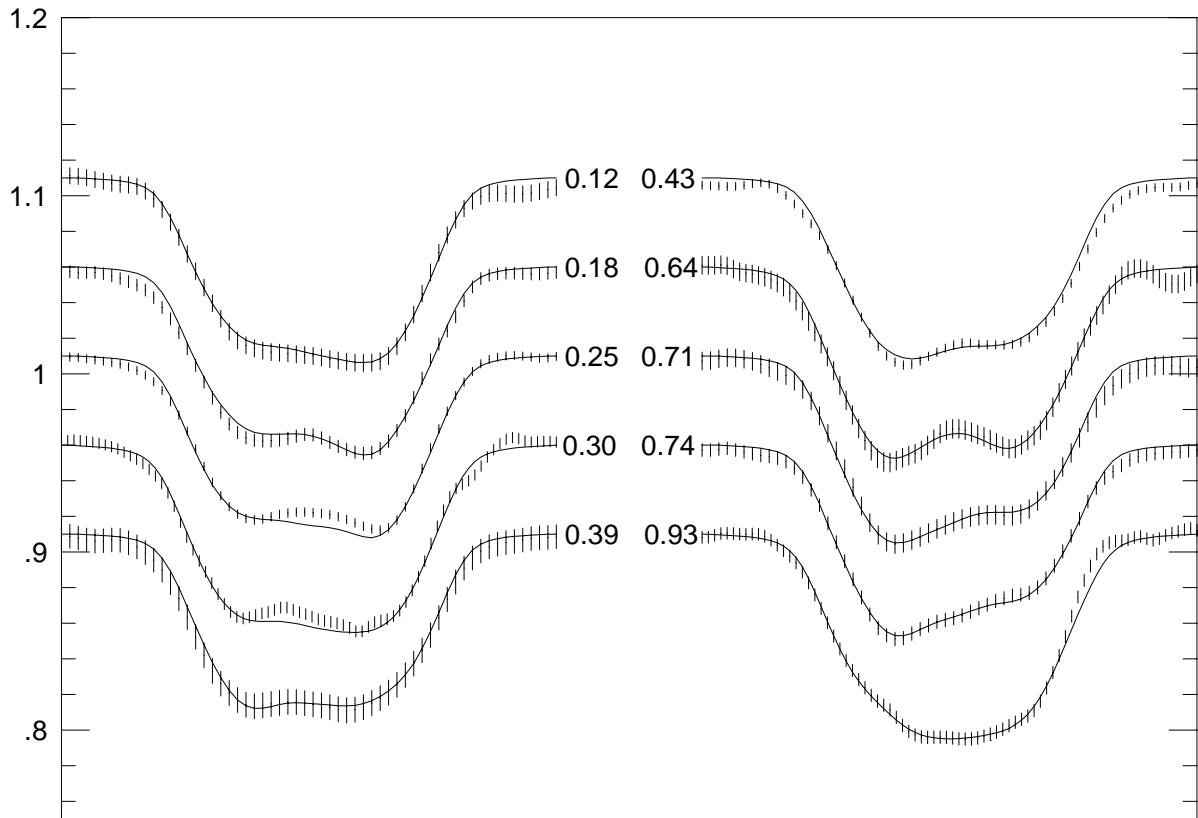


Fig. 57.— Spectral line profiles and fits for 1990.69

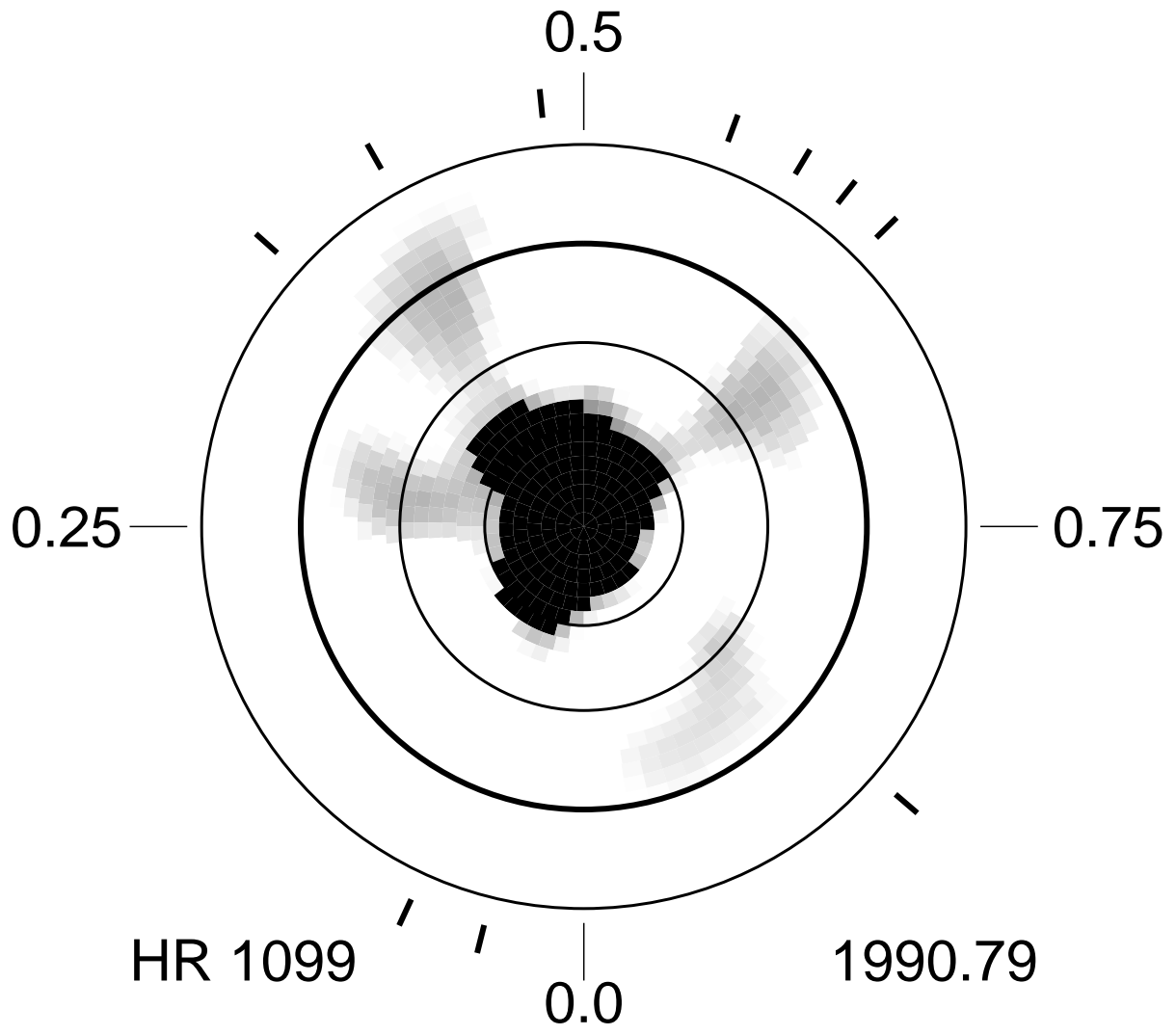


Fig. 58.— HR 1099 raw (unthressholded) Doppler image for 1990.79

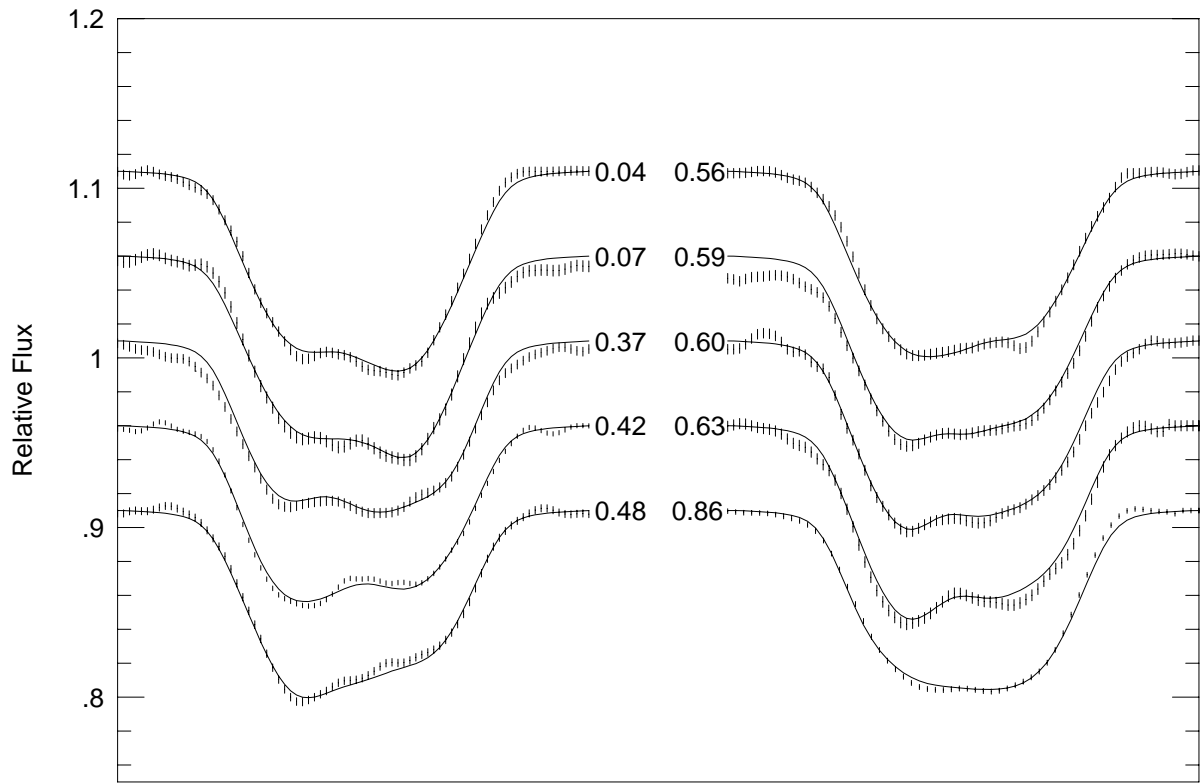


Fig. 59.— Spectral line profiles and fits for 1990.79

polar spot outline has again changed to such a degree that we cannot find any simple rotation which matches the previous image. Also, the polar spot protuberance near phase 0.09 may well be a ‘phase ghost’ of the two observed phases at 0.04 and 0.07 since they are the only two observed phases on that side of the star and are rather isolated. As we’ve seen, poor phase coverage leads to such phase ghosting at isolated phases. Finally, there is also some low-level indication of a feature near the equator near phase 0.4, the location for Feature F from the 1989.83 image, but this cannot be regarded as significant without further thresholding constraints.

The raw unthresholded image for epoch 1990.93 is shown in Figure 60 and the spectral line profiles and fits in Figure 61. Again, differences in the polar spot outline preclude simple rotations to match the previous images and thereby determine the polar spot rotation rate. There does, however, seem to be a persistent suggestion of a stationary protuberance near phase 0.3 - 0.4 in these successive images, and again there is a hint of something near phase 0.64 at a low level. There is also now a hint of significant low-level spot activity near the equator in the phase 0.9 to 0.2 region, almost as though a large annulus of dark spots, some 45° in radius is emerging. But this is all at a quite low-level and cannot be regarded as significant without further constraints from light curves.

For the 1991.02 image, we did have a light curve with which to threshold and further constrain our image, though the thresholding process did not affect the raw image greatly. The raw 1991.02 image is shown in Figure 62 and the spectral line profiles and fits in Figure 63. The predicted light curve from this raw image is shown as the dotted line in Figure 64 along with the 1991.14 photometry (points) of Mohin and Raveendran (1993). The predicted fit from the raw MEM image is good except for a dip around phase 0.82. Applying the threshold cleans this up nicely and an excellent fit is obtained. The photometric image is shown in Figure 65 and its predicted theoretical light curve is shown

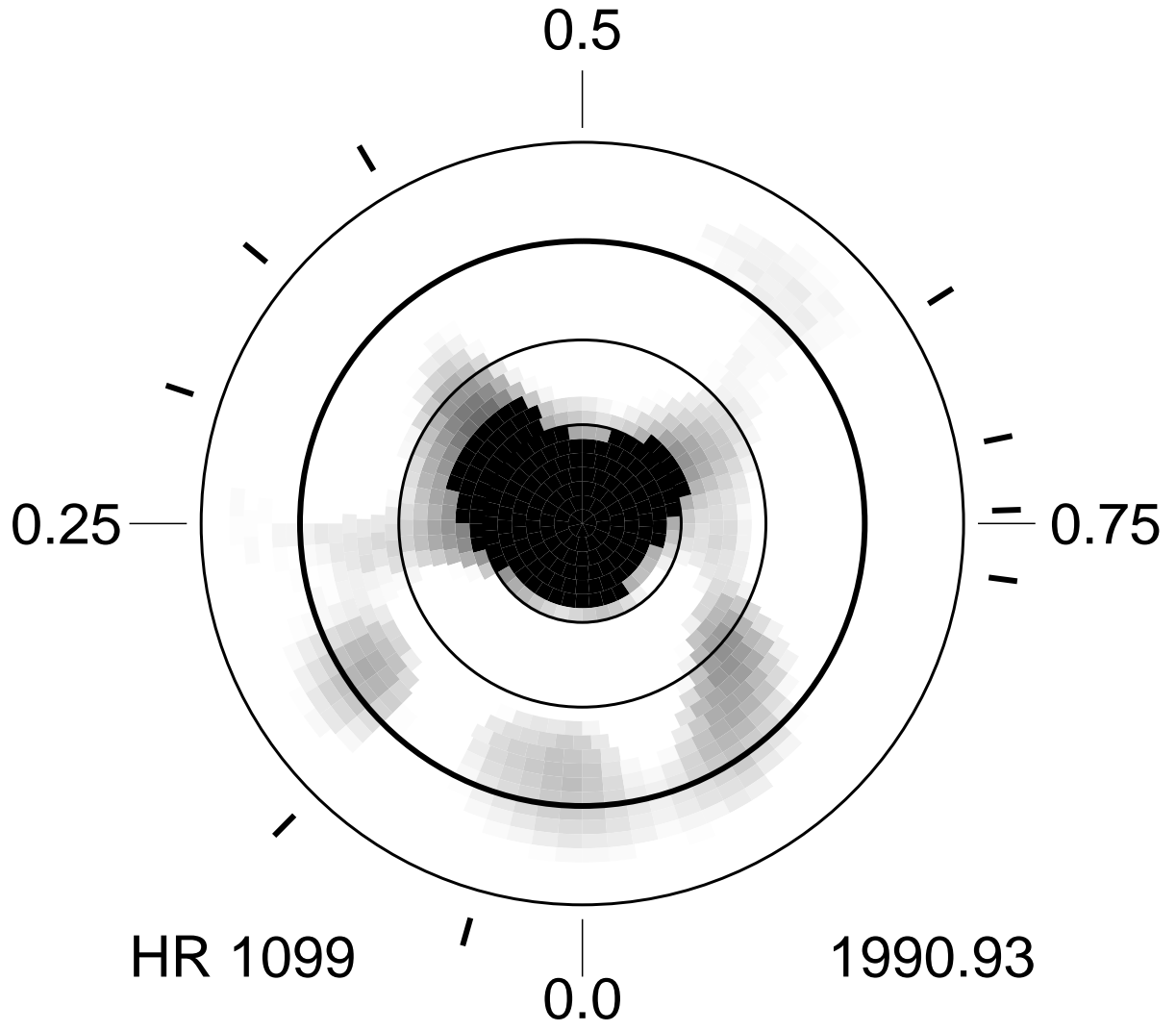


Fig. 60.— HR 1099 raw (unthressholded) Doppler image for 1990.93

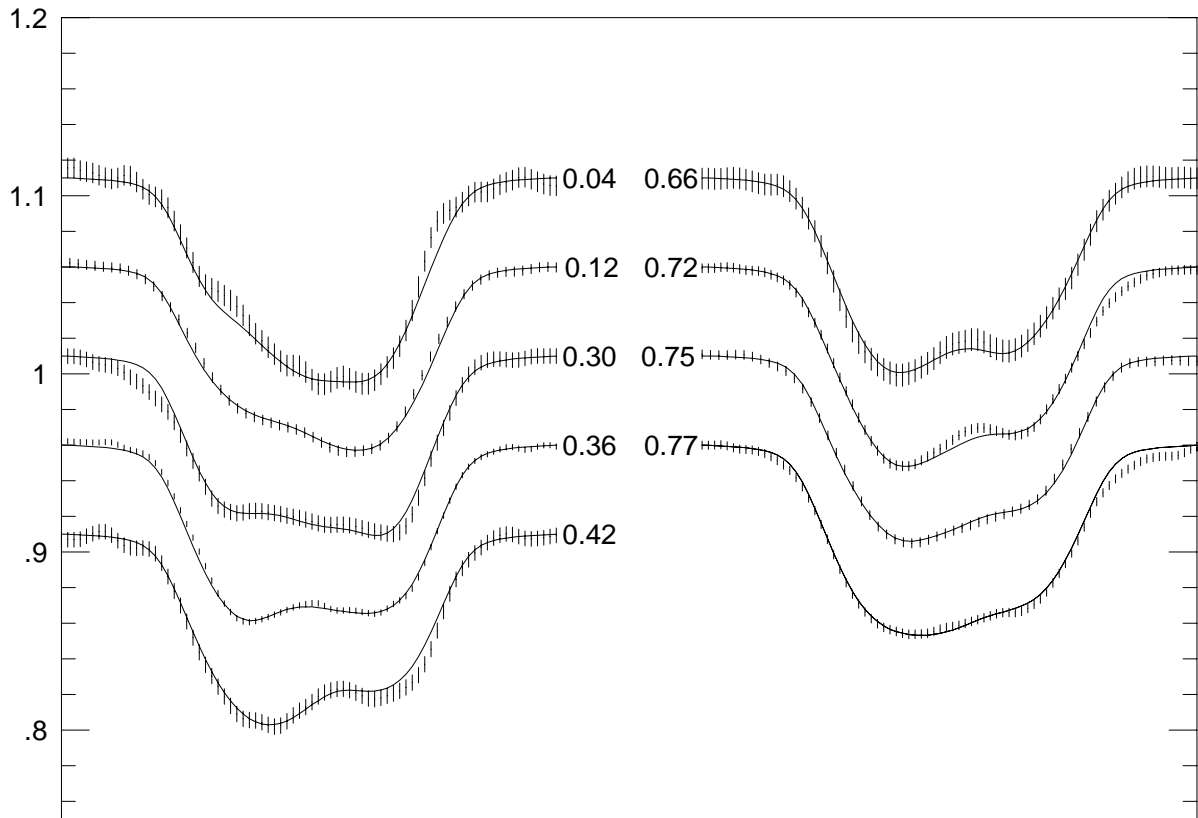


Fig. 61.— Spectra line profiles and fits for 1990.93

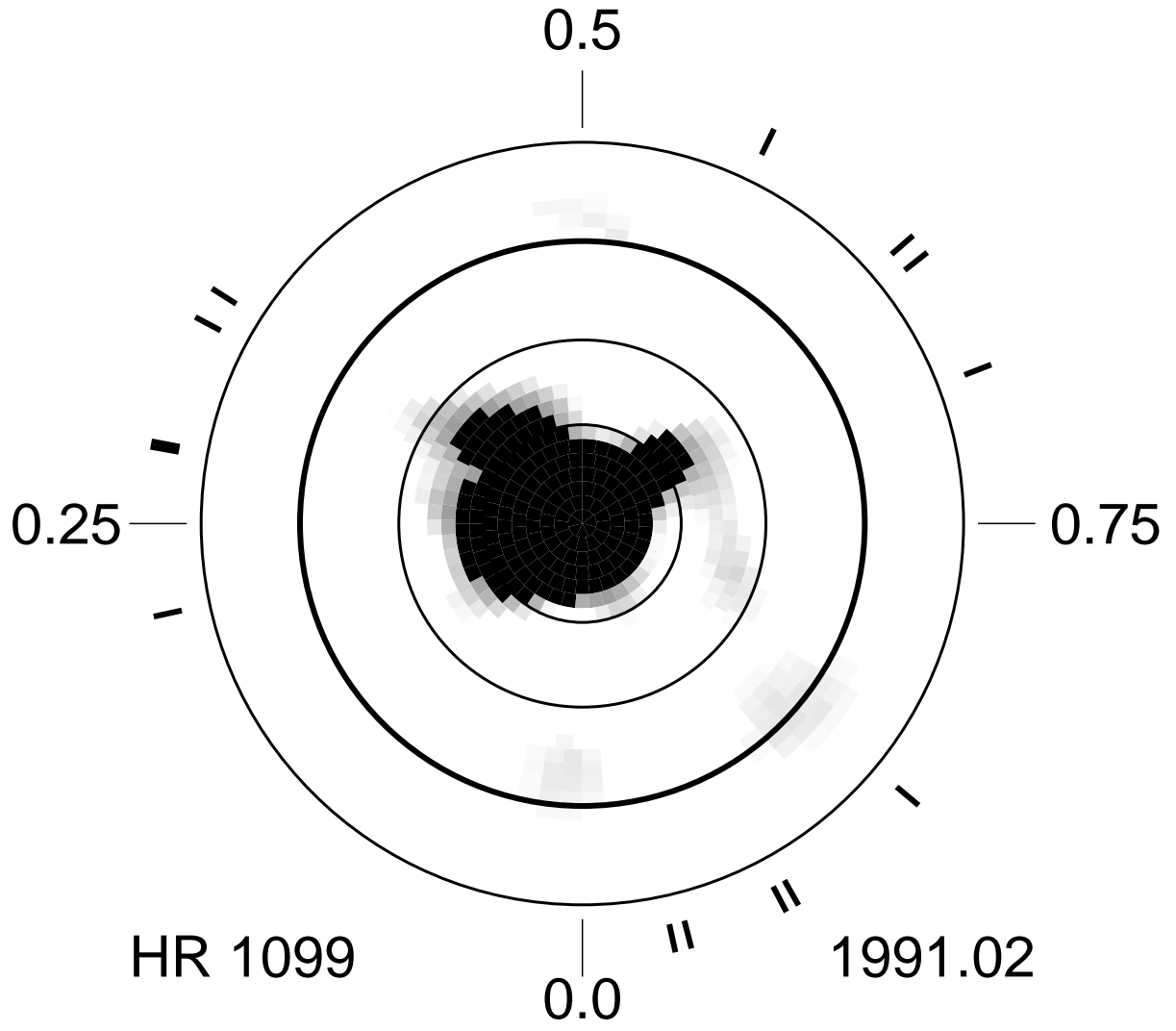


Fig. 62.— HR 1099 raw (unthresholded) Doppler image for 1991.02

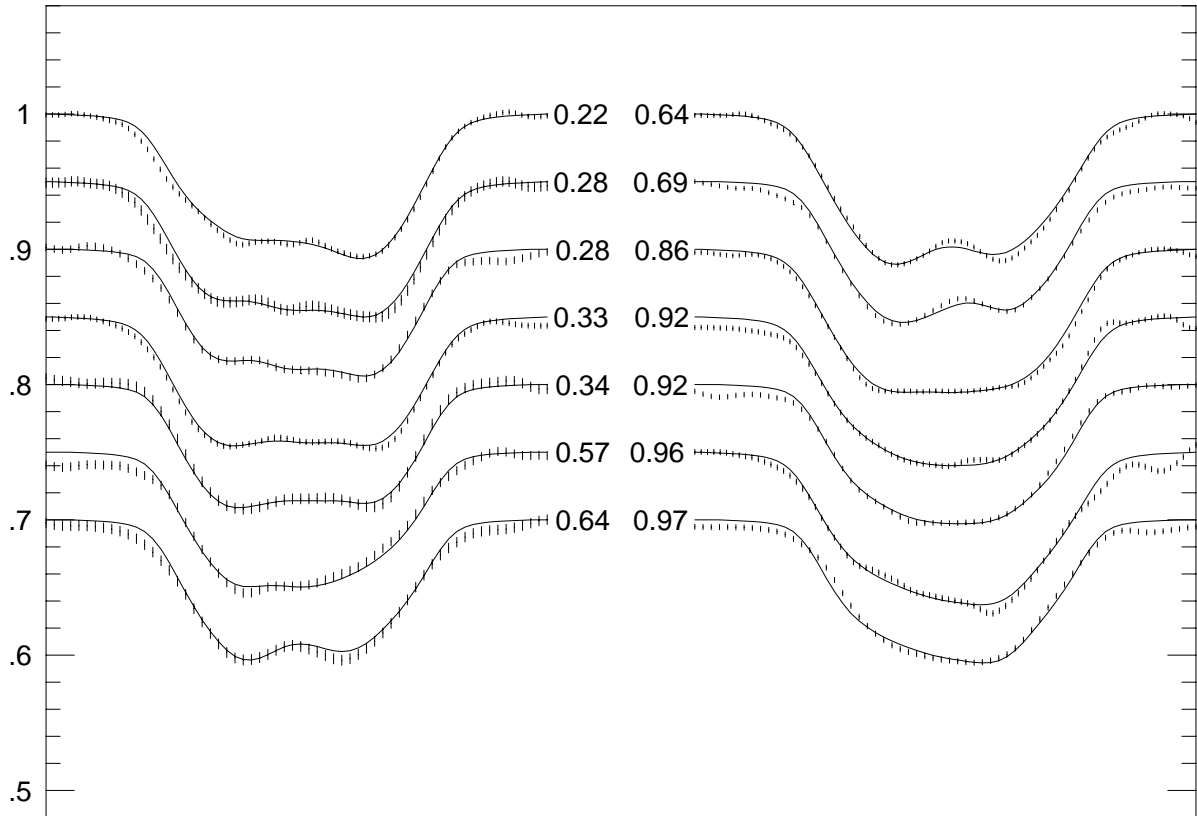


Fig. 63.— Spectral line fits for 1991.02

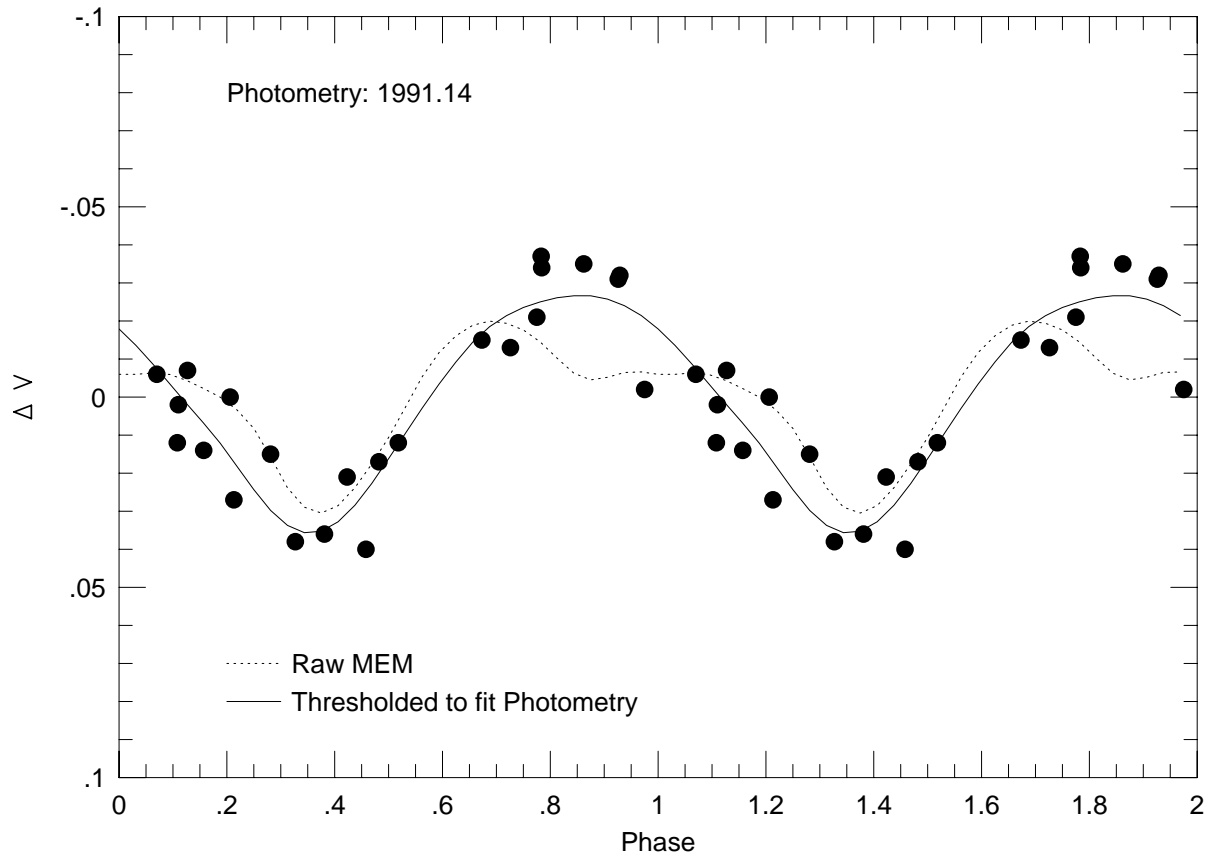


Fig. 64.— 1991.14 light curve used for the 1991.02 HR 1099 image

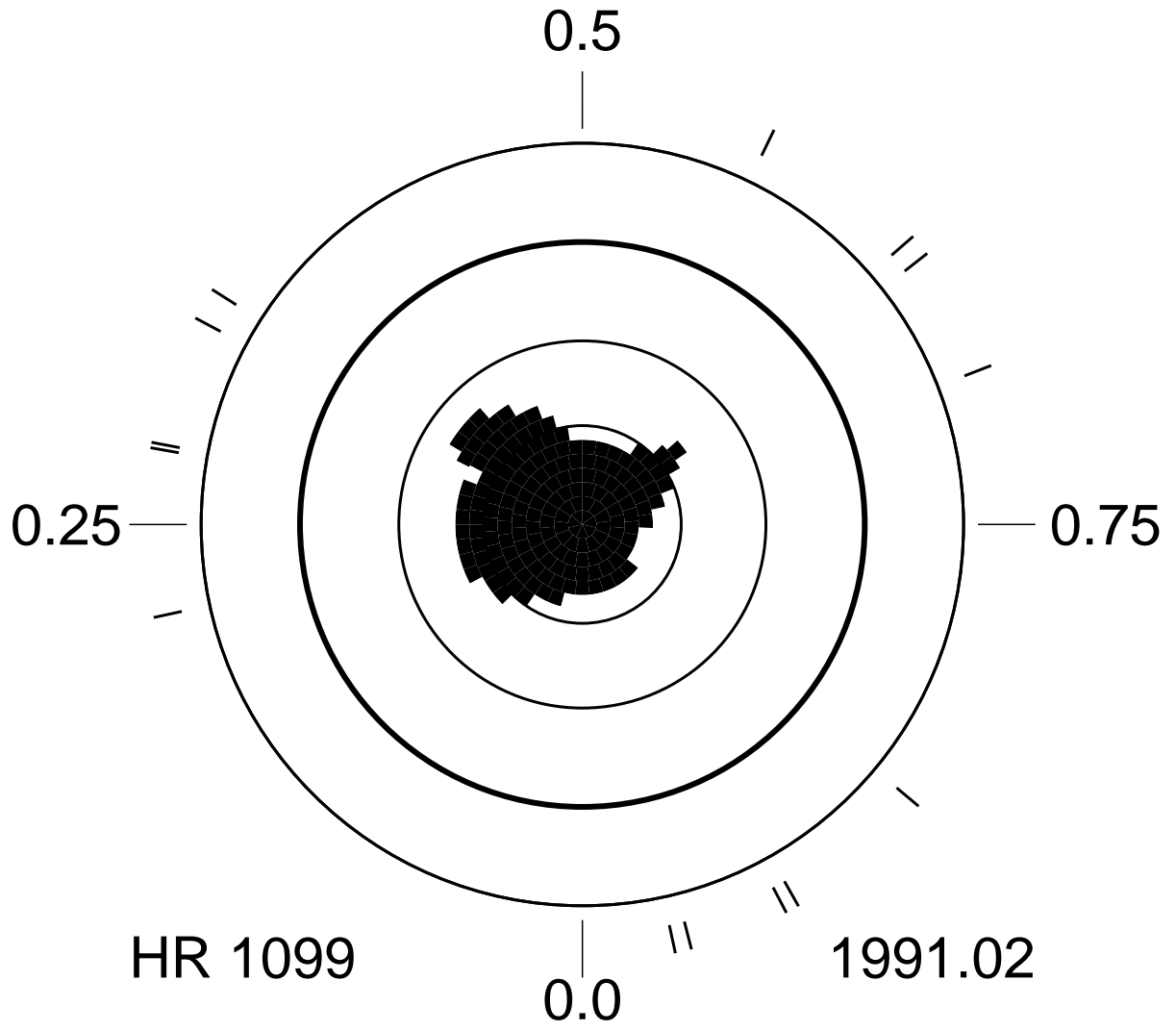


Fig. 65.— HR 1099 thresholded Doppler image for 1991.02

as the solid line in Figure 64. As can be seen, the addition of the light curve data produced almost no change in the image, except to sharpen up the protuberance at phase 0.64 somewhat, and provide strong evidence that it is truly attached to the polar spot. Also, one can get a good feeling here for the level of accuracy required in fitting the light curve to derive accurate spot shapes.

Looking back at all four images for this observing season, one sees that the polar spot was probably totally isolated all this season, with no detached lower-latitude spots. Also, the phase of the 0.64 polar spot protuberance was quite well-fixed in longitude throughout the 4-month interval spanned by these images. If this feature had been migrating at the rate of the low-latitude Feature E ($123^\circ \text{ yr}^{-1}$), it would have moved some 40° or 0.11 in phase, and would have moved from phase 0.64 in 1990.69 to phase 0.75 by 1991.02. This would have been readily apparent and clearly did not occur. In fact, this feature, at a latitude of about 60° and apparently attached to the polar spot, is consistent with little or no relative longitude motion with respect to the orbital reference frame. The obvious inference again is that spots near or at the pole, or otherwise merged with the polar spot, are rotating essentially at the orbital period, and that the polar region of HR 1099 is tightly locked into synchronicity with the orbit. The broad protuberance at phase 0.3-0.4 is also fairly well-reproduced in the 1991.02 image, as though it has remained stationary in phase across these four images. Again, both of these observations suggest that latitudes of 60° and above are quite tightly synchronized to the orbital frame, whereas latitudes near the equator rotate more slowly.

This season, we have another independent, detailed Doppler image with which to do a comparison check of our image. Donati et al. (1992b) presented both a ‘temperature’ Doppler image and a corresponding Zeeman Doppler image for epoch 1990.9. Both of their images were done using the Fe I 5497.520 Å line. Our 1991.02 image is quite close in time

and, being constrained by a light curve, is also the best choice for comparison with their imagery. The agreement between our Doppler image and theirs is again excellent. We both see an isolated polar spot with a narrow protuberance which descends to about latitude 50° near phase 0.64 and has a characteristic triangular shape, coming down to a sharp point at latitude 50° . We also both see a broad protuberance on the polar spot near phase 0.31. Even the detailed shape of this broad protuberance in our 1991.02 Doppler image is well-reproduced in the Donati et al. (1992b) image. They do however see a weak (400 K cooler) spot near phase 0.3 at the equator, whereas this feature does not show up strongly in any of our four images for this season. There might just be a slight hint of it showing up as a low-level extension from the polar spot near phase 0.34 which extends down to about 15° in our raw 1991.02 image, and there was also hint of low-latitude spots near phase 0.35 in our raw 1990.79 image, but they do mention that their line profile at phase 0.34 is substantially noisier and less well-fitted than their other profiles. They also noted minor departures of their fit to the line profile at phase 0.293 where the core of the predicted profile was slightly too low, and cite some difficulties with line blends in the blue wing of this line. So our disagreement on this feature is probably not significant, and all indications are that it is not a strong feature.

Donati et al. (1992b) also presented a Zeeman Doppler image of the toroidal component (i.e. along lines of constant latitude) of the surface magnetic field. The reader is referred to their discussion for a more detailed summary of their B field results. Basically, they found that the polar spot is encircled by a ring of toroidal clockwise-directed field of -300 G strength which lies at about 60° latitude. This ring is not complete, but has a gap which extends about 60° in longitude and is centered near phase 0.65. The ring coincides quite precisely with the edge of the polar spot in both their image and ours, and the gap in the ring sits right at the location of the polar spot protuberance we both see at phase 0.64. They also found a second area of $+700$ G toroidal field component situated at phase 0.27

and latitude 20° , at the position of their low-latitude feature, for which we detected no counterpart as described above.

Donati et al. (1992b) explained the coincidence of the gap in the ring with the polar spot protuberance at phase 0.65 as due to the fact that this dark area of the ring, while probably magnetic, was not detected in the circular polarization measurements because of its low brightness. They further explained that the polar field distribution was a ring (rather than a polar cap) because of the same effect: the polar spot regions are too dark to contribute enough light for field detection in the circular polarization measurements. Our Doppler images agree very closely with their image and strongly support this interpretation of the correspondence between the magnetic and temperature images of the polar spot at this epoch. The polar spot is thus seen as a permanent region of strong surface magnetic field, with field strengths at least as strong - and probably much stronger than - the 300 G fields they detected around the spot periphery.

3.15. The 1991 Season Doppler Images

We obtained three images in the 1991-2 observing season. The raw image for 1991.80 is shown in Figure 66, and its spectral line profiles and fits are shown in Figure 67. The raw image for 1991.90 is shown in Figure 68, and its spectral line profiles and fits are shown in Figure 69. The raw image for 1992.04 is shown in Figure 70, and its spectral line profile fits are shown in Figure 71. A light curve for 1991.16 was presented by Mohin and Raveendran (1993), but was probably too far away in time to be useful.

The images from this season show the appearance and subsequent rapid disappearance of a spot at phase 0.15 and latitude 30° . We hereafter refer to this spot as Feature H. It was not evident in 1991.02, but was strong in 1991.80, and then faded rapidly, without moving,

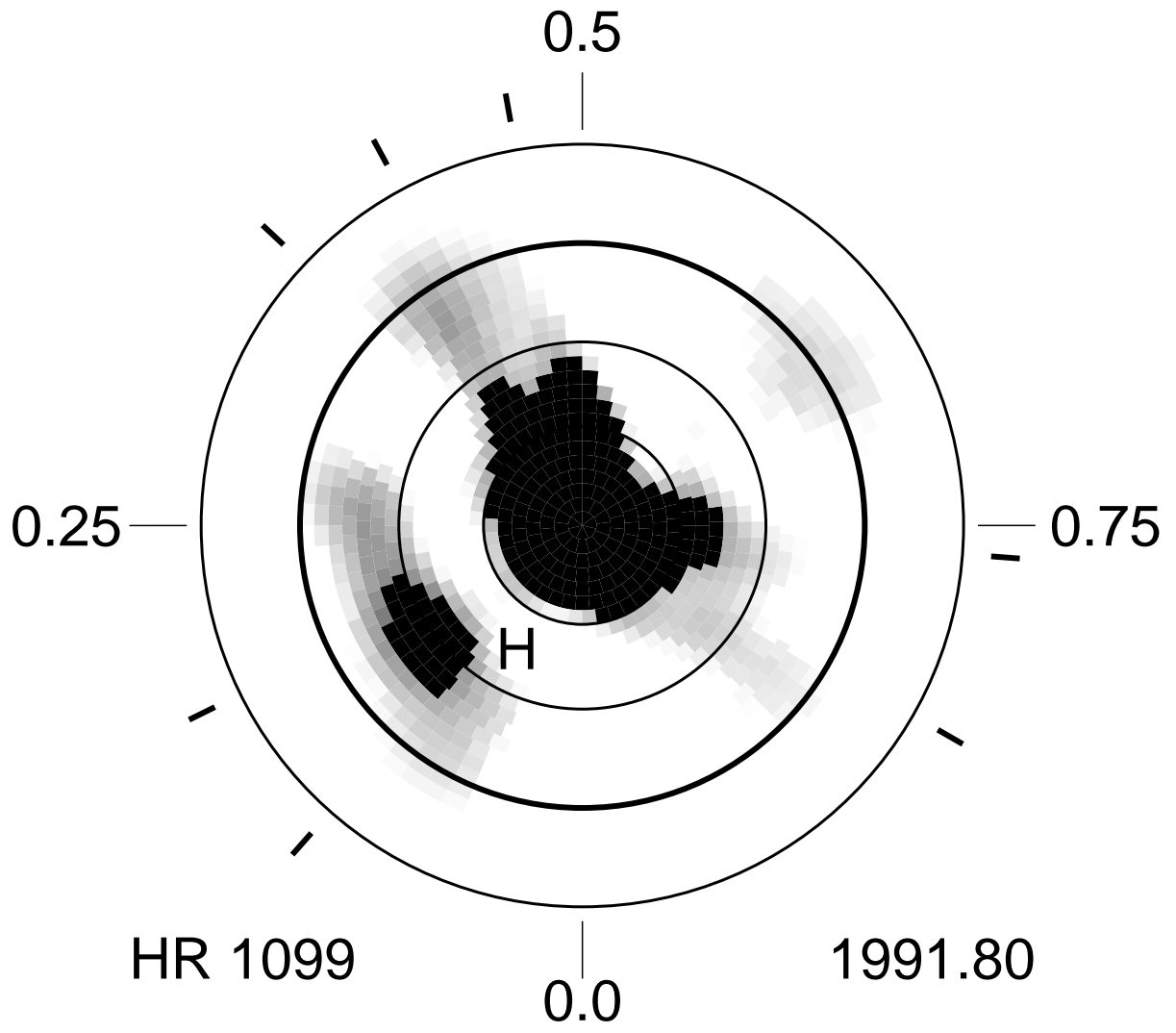


Fig. 66.— HR 1099 raw (unthresholded) Doppler image for 1991.80

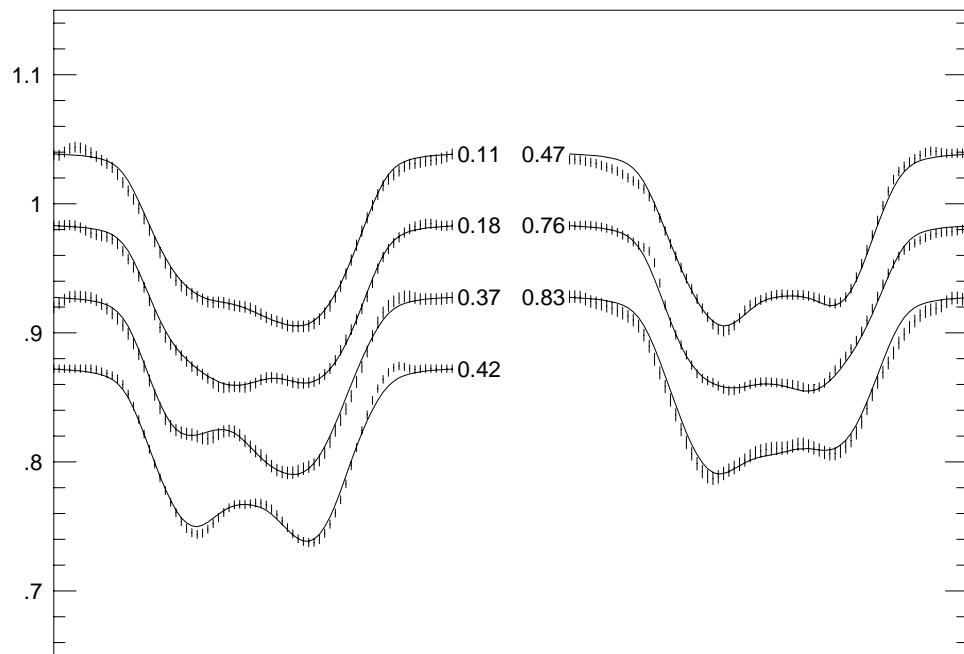


Fig. 67.— Spectral line fits for 1991.80

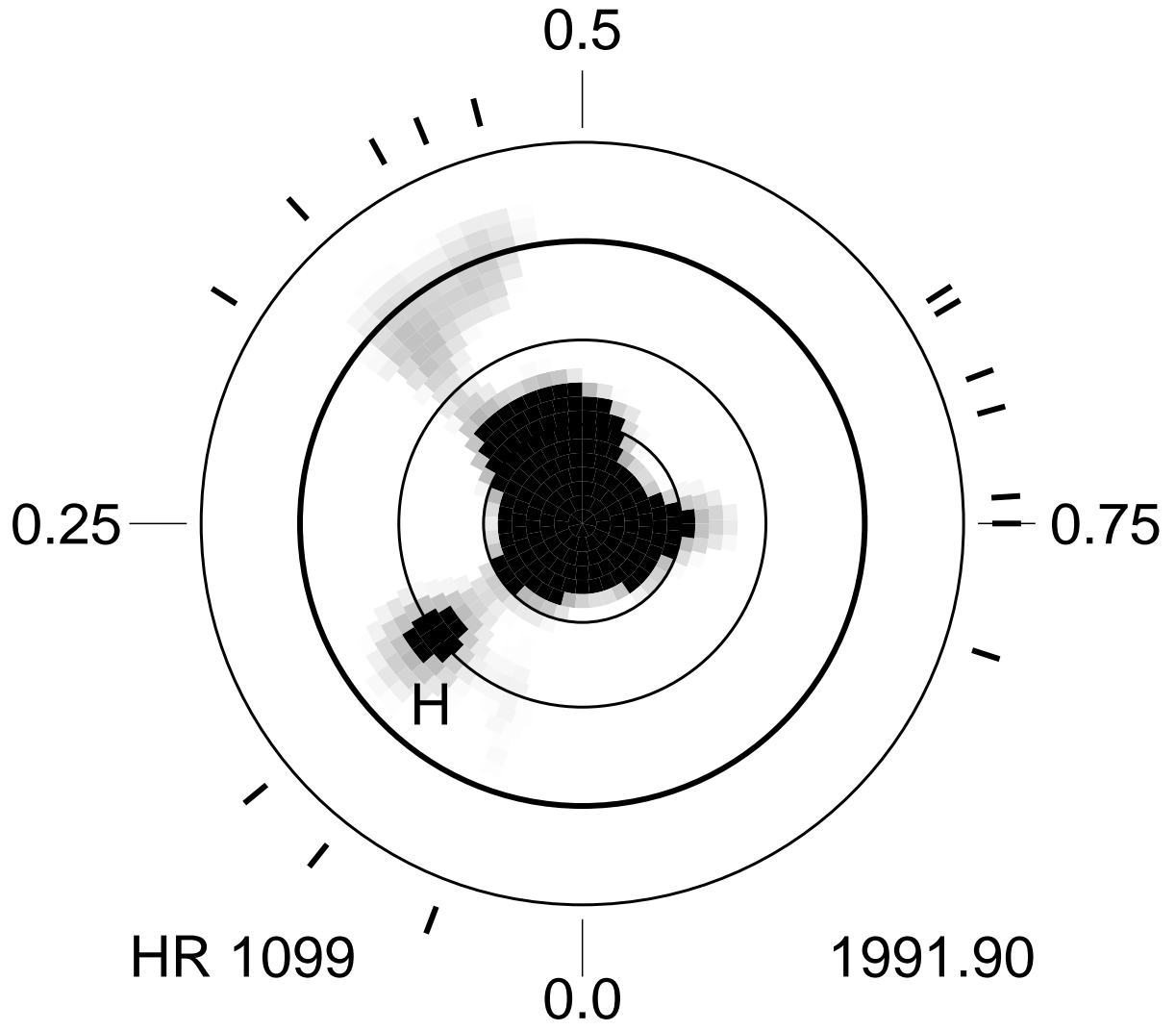


Fig. 68.— HR 1099 raw (unthresholded) Doppler image for 1991.90

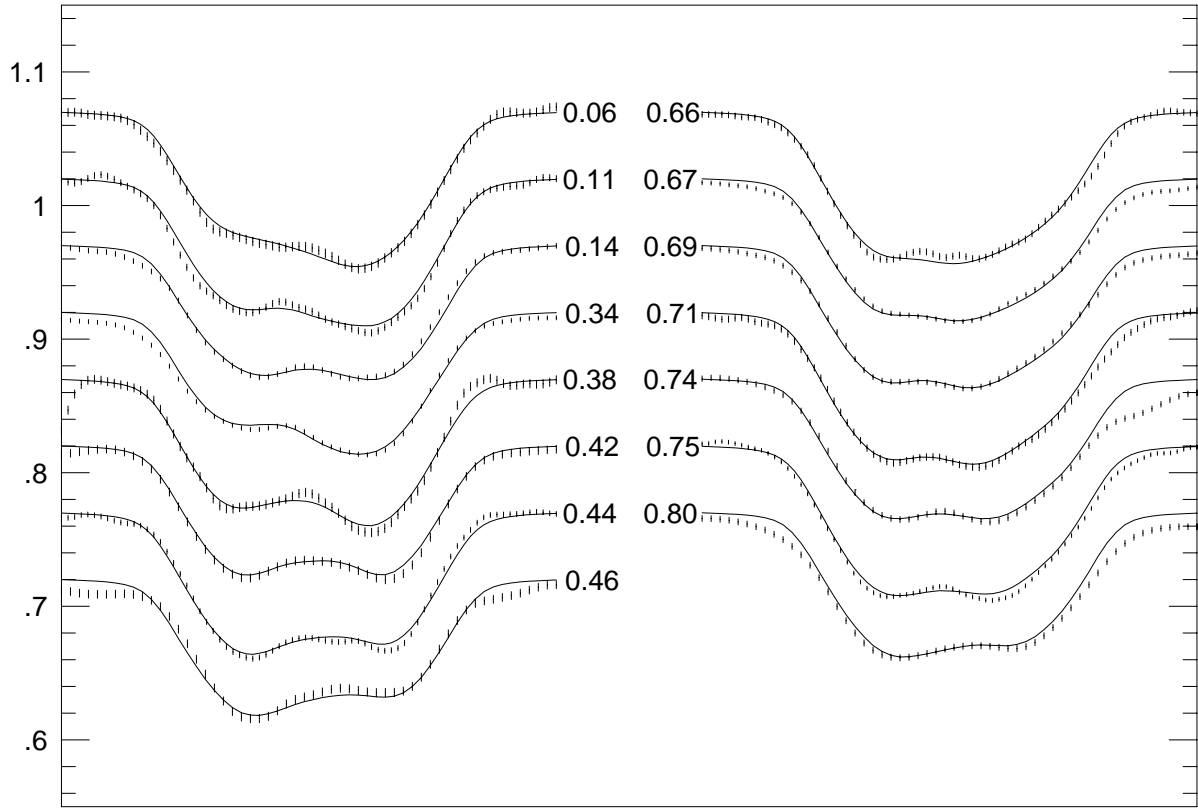


Fig. 69.— Spectral line profiles and fits for 1991.90

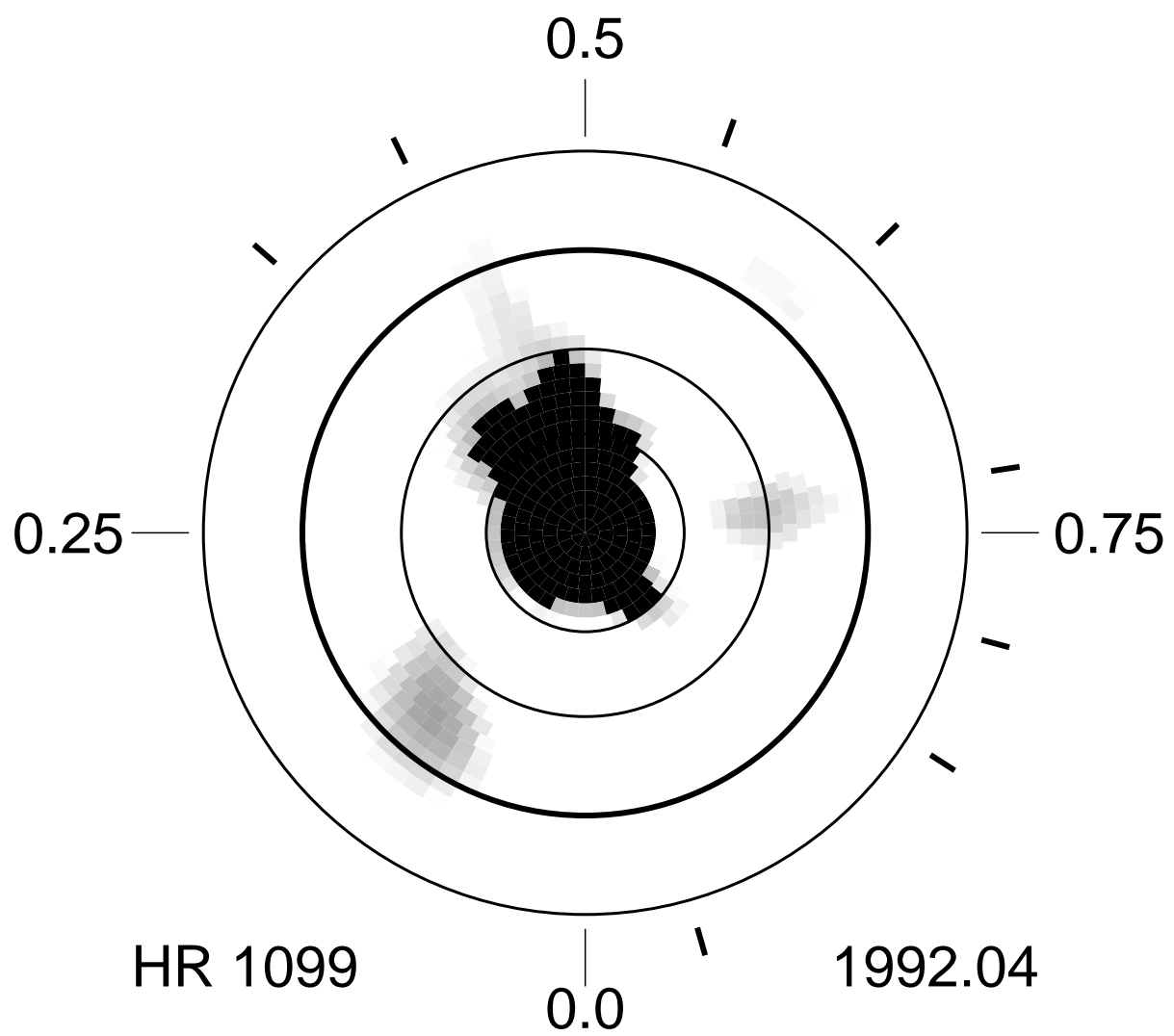


Fig. 70.— HR 1099 raw (unthresholded) Doppler image for 1992.04

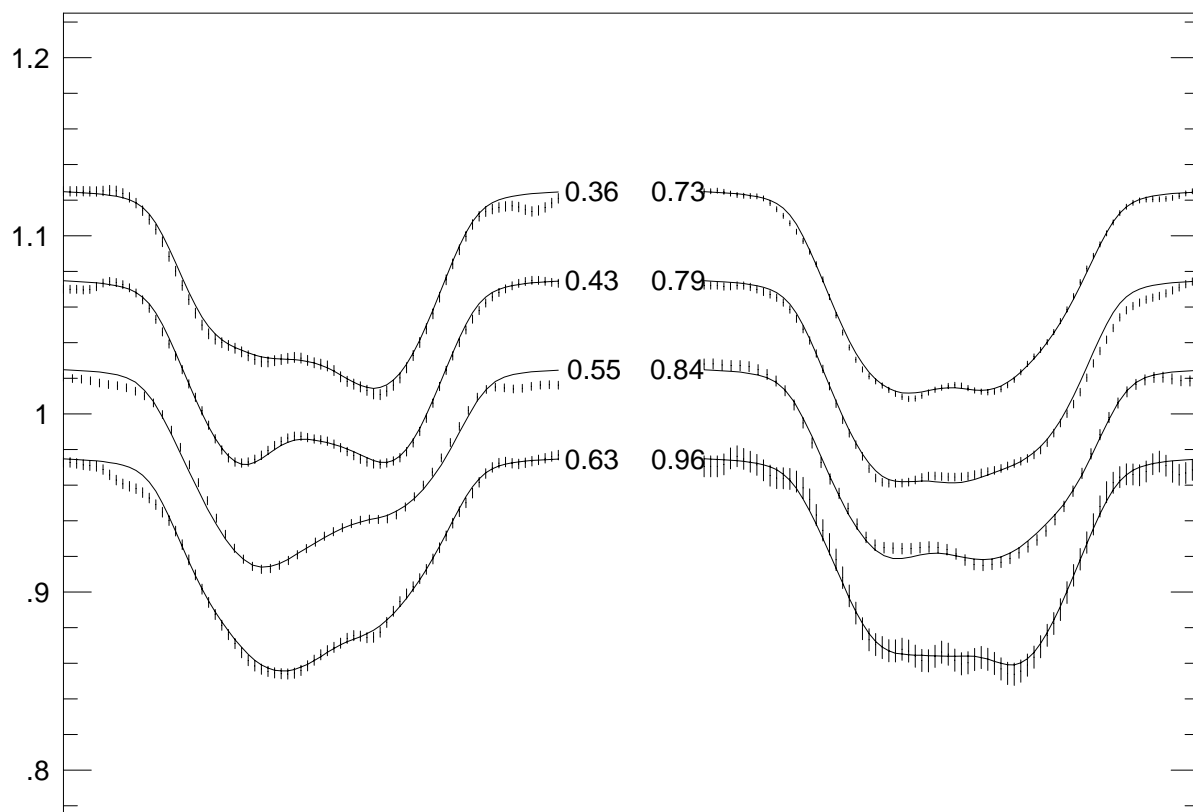


Fig. 71.— Spectral line profiles and fits for 1992.04

to a low-level remnant by 1992.04. There was a broad and fairly stable protuberance on the polar spot at about phase 0.45 which remained quite well-fixed at this phase, again indicating that features at these high latitudes are very closely-synchronized to the orbital frame. Essentially no longitudinal motion of this feature is seen (to within the limits of uncertainty in determining longitudes on a spot whose shape is not absolutely constant) over the 2.9 month interval spanned by the images.

The phase 0.75 polar spot protuberance in the 1991.80 image is probably not the phase 0.64 protuberance of the previous year migrated by 0.11 phases since it does not appear with consistent strength in all of our images for the 1990-91 season. It may be a ‘phase ghost’ in the 1990.80 image, and merely a result of the fact that we observed the star at relatively few phases on that side of the star in 1991.80, one of which was at phase 0.76. Indeed, low-level radial ‘ghosts’ can be seen extending from the polar spot at both of the two observed phases on that side of the star in the 1991.80 image.

3.16. The 1992-93 Season Doppler Images

We obtained four Doppler images at epochs 1992.68, 1992.80, 1992.95, and 1993.15 this observing season. We could only find photometry for 1992.91, presented by Zhang et al. (1993) and 1992.83 from Drake et. al. (1994) so only these two epochs are adequately thresholded to the photometry. The others are presented only as spectral images. Neff, Simon, Pagano, Rodono, and Foing (1993) reported a continuous IUE monitoring of HR 1099 in December, 1992 as part of the MUSICOS 92 campaign. HR 1099 was also the subject of an EUVE study by Drake et. al. (1994). They obtained light curves in the 60-180Å passband in August and October, 1992 and concluded that most of the EUV flux was coming from hot coronal plasma associated with an especially bright coronal structure on the active K subgiant.

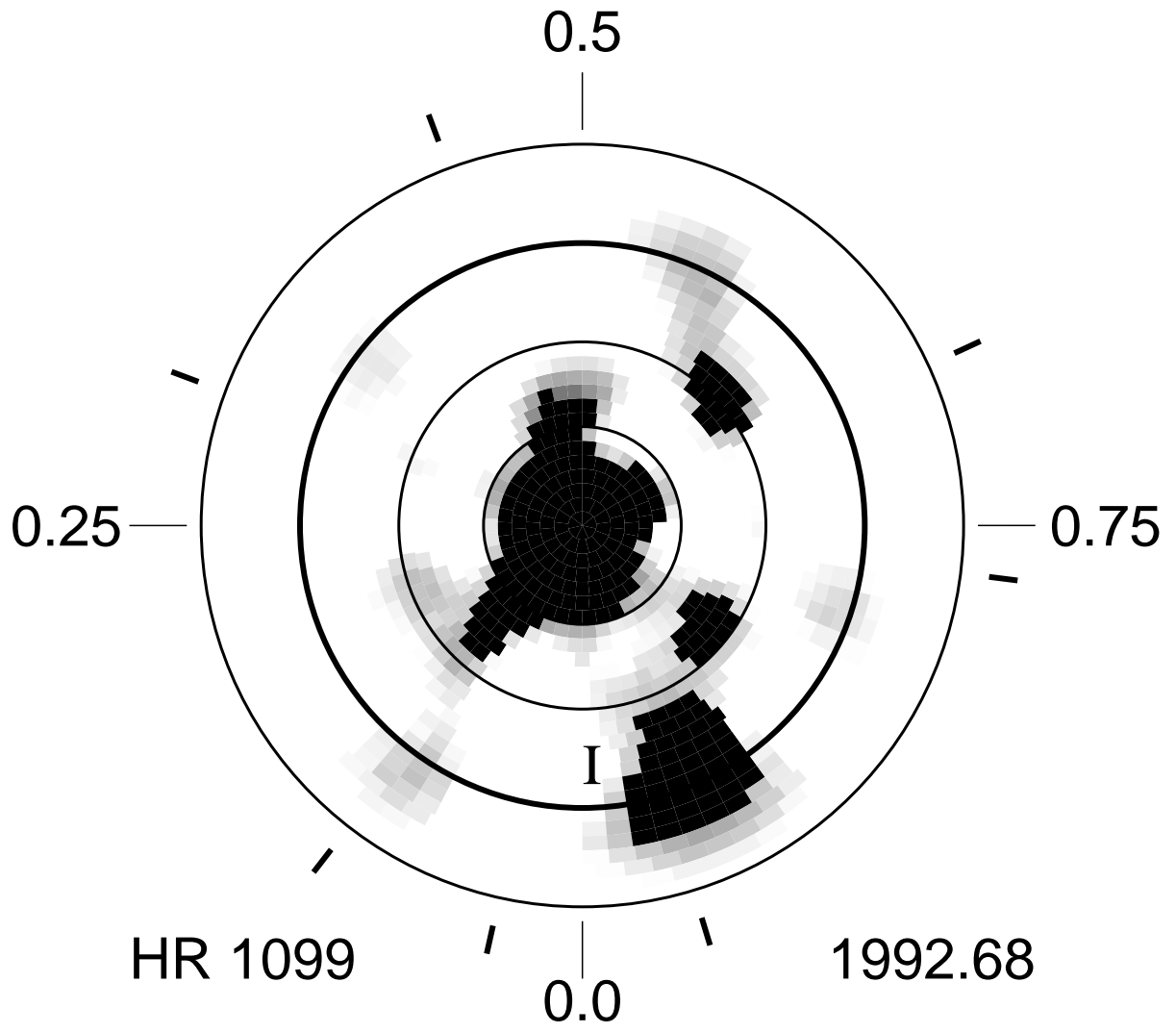


Fig. 72.— HR 1099 raw (unthressholded) Doppler image for 1992.68

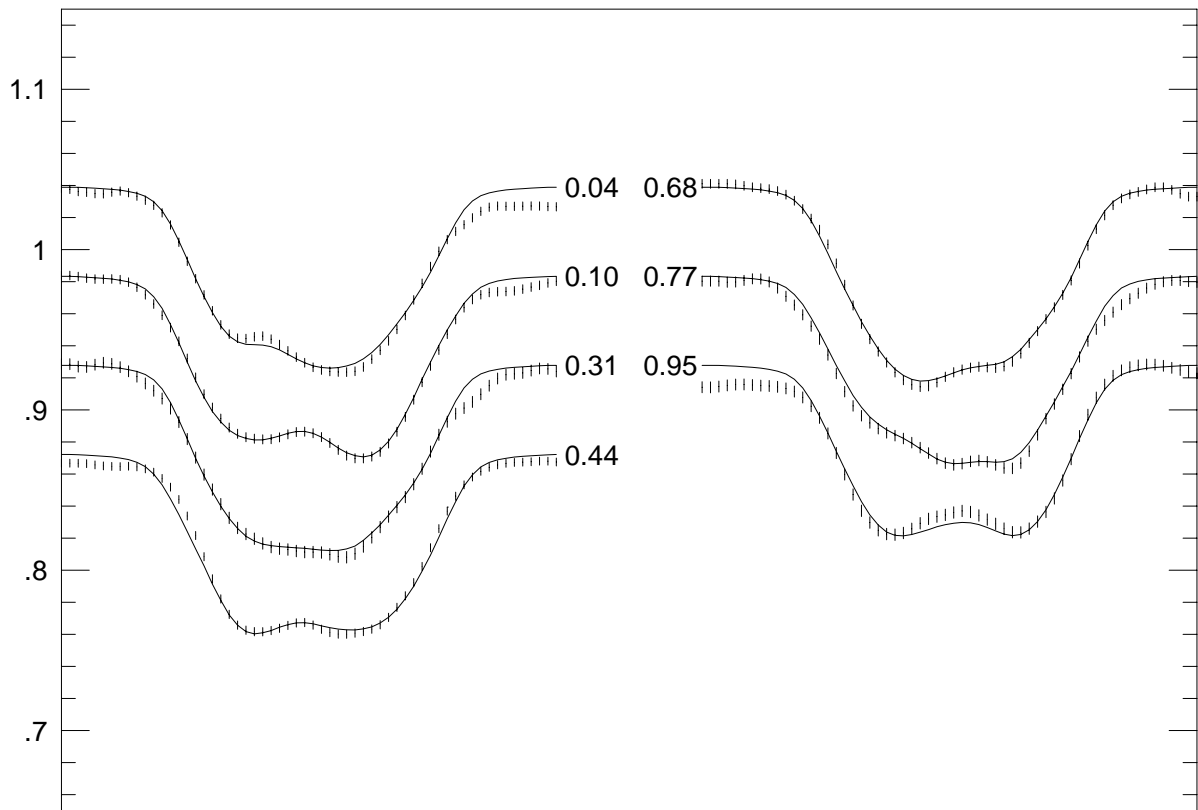


Fig. 73.— Spectral line profiles and fits for 1992.68

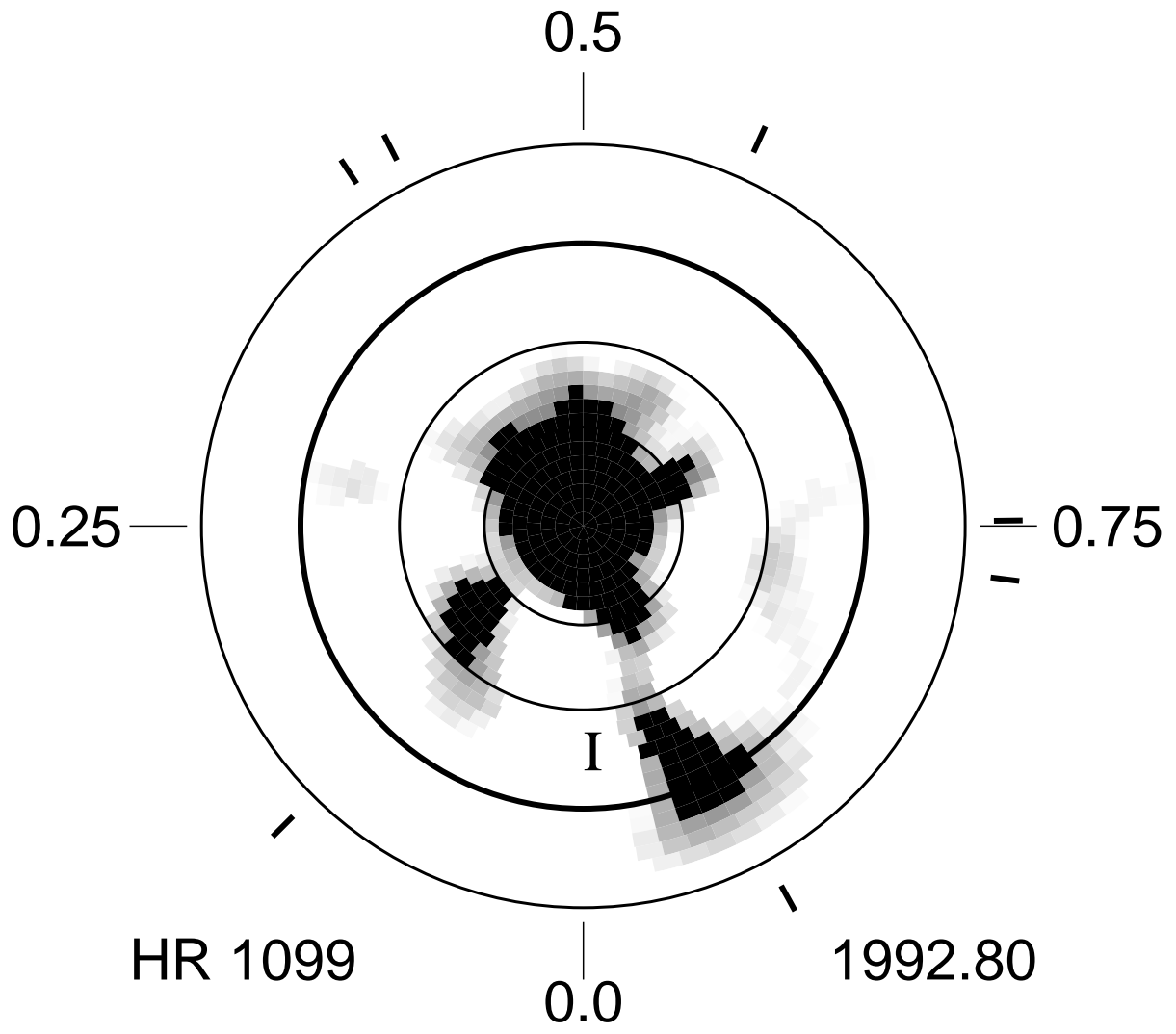


Fig. 74.— HR 1099 raw (unthreshhilded) Doppler image for 1992.80

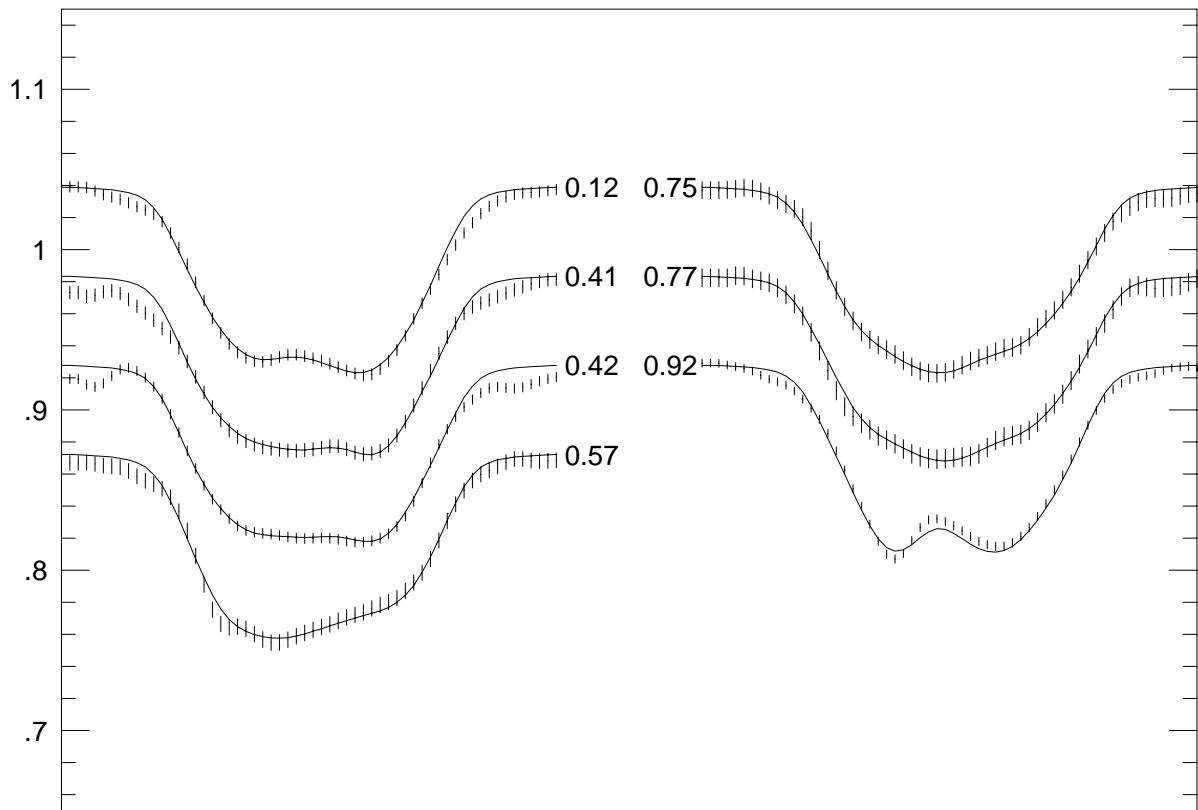


Fig. 75.— Spectral line profiles and fits for 1992.80

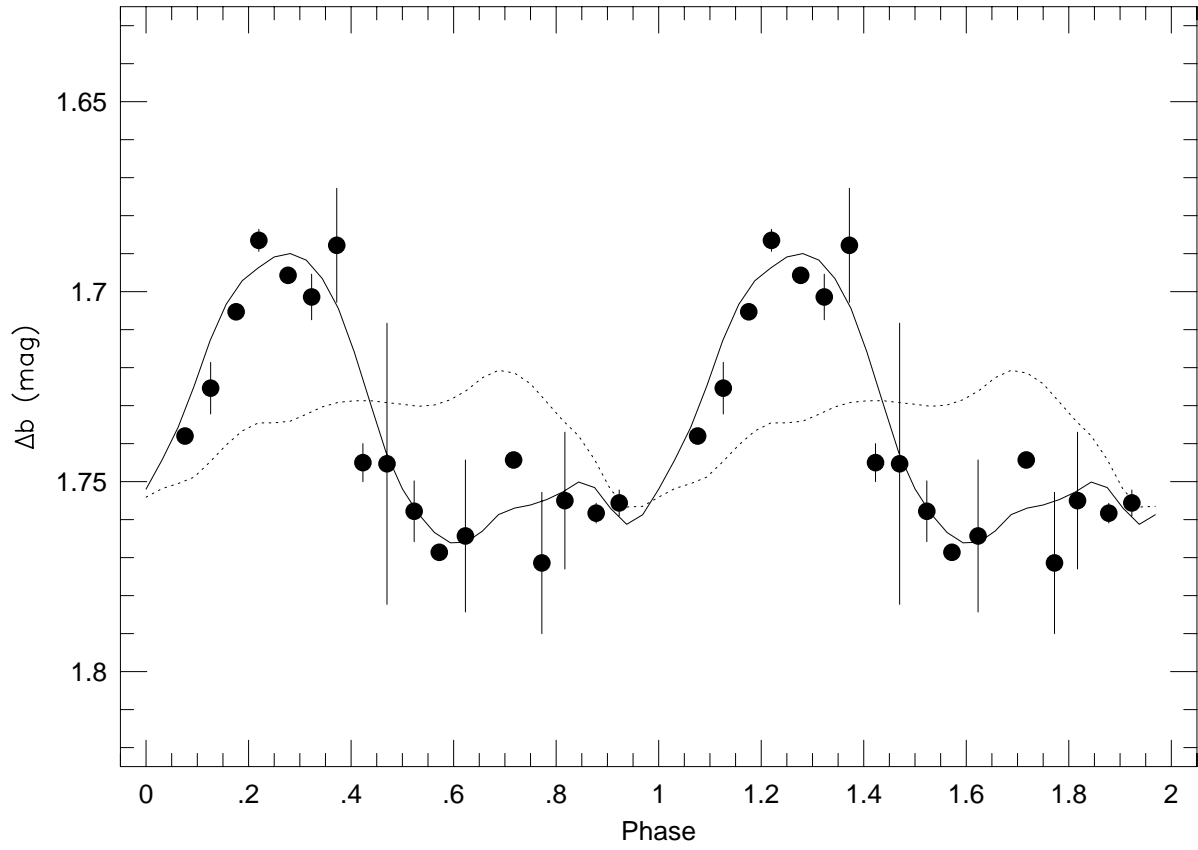


Fig. 76.— b -band photometry for HR 1099 in 1992.83

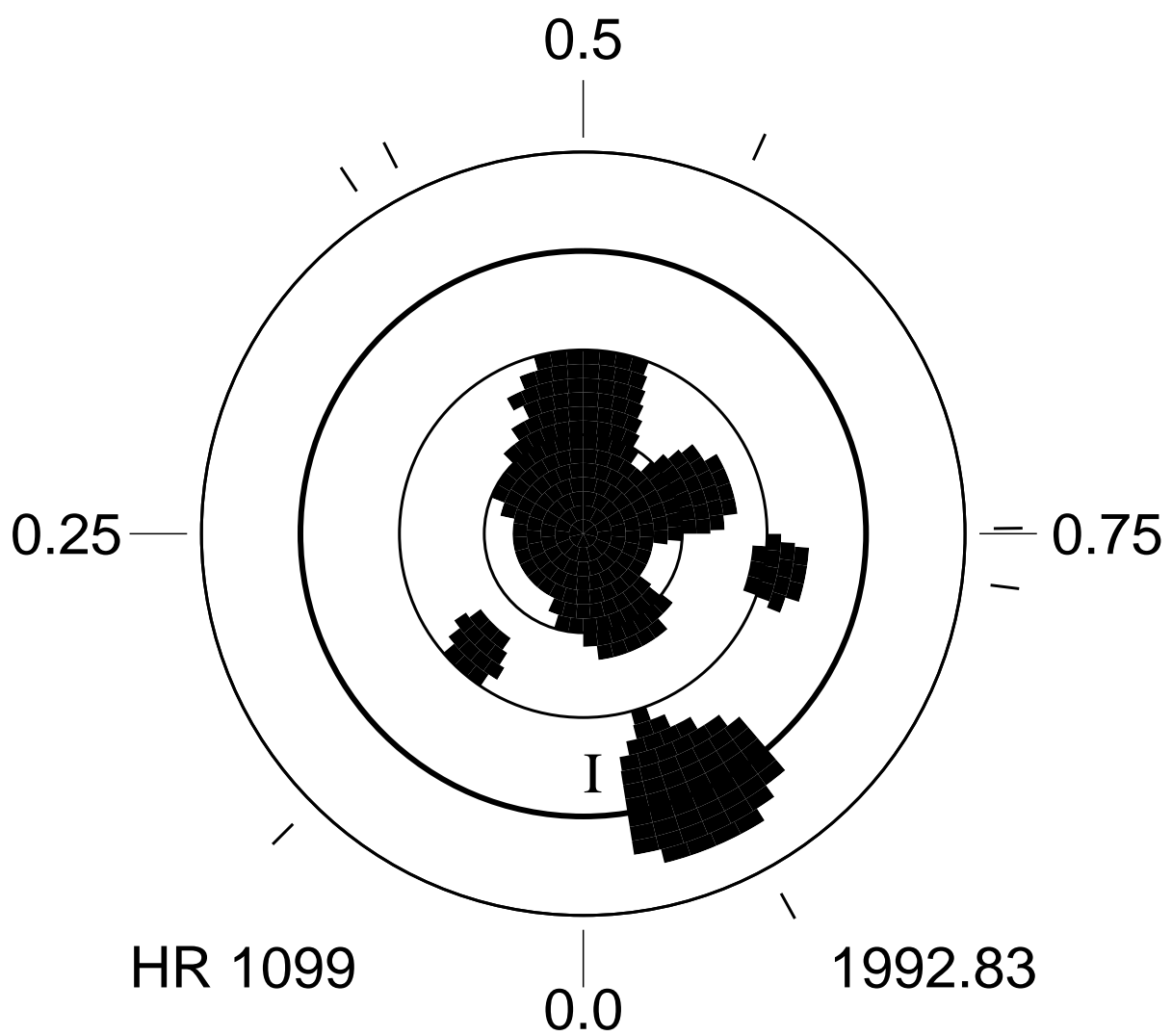


Fig. 77.— HR 1099 thresholded Doppler image for 1992.83

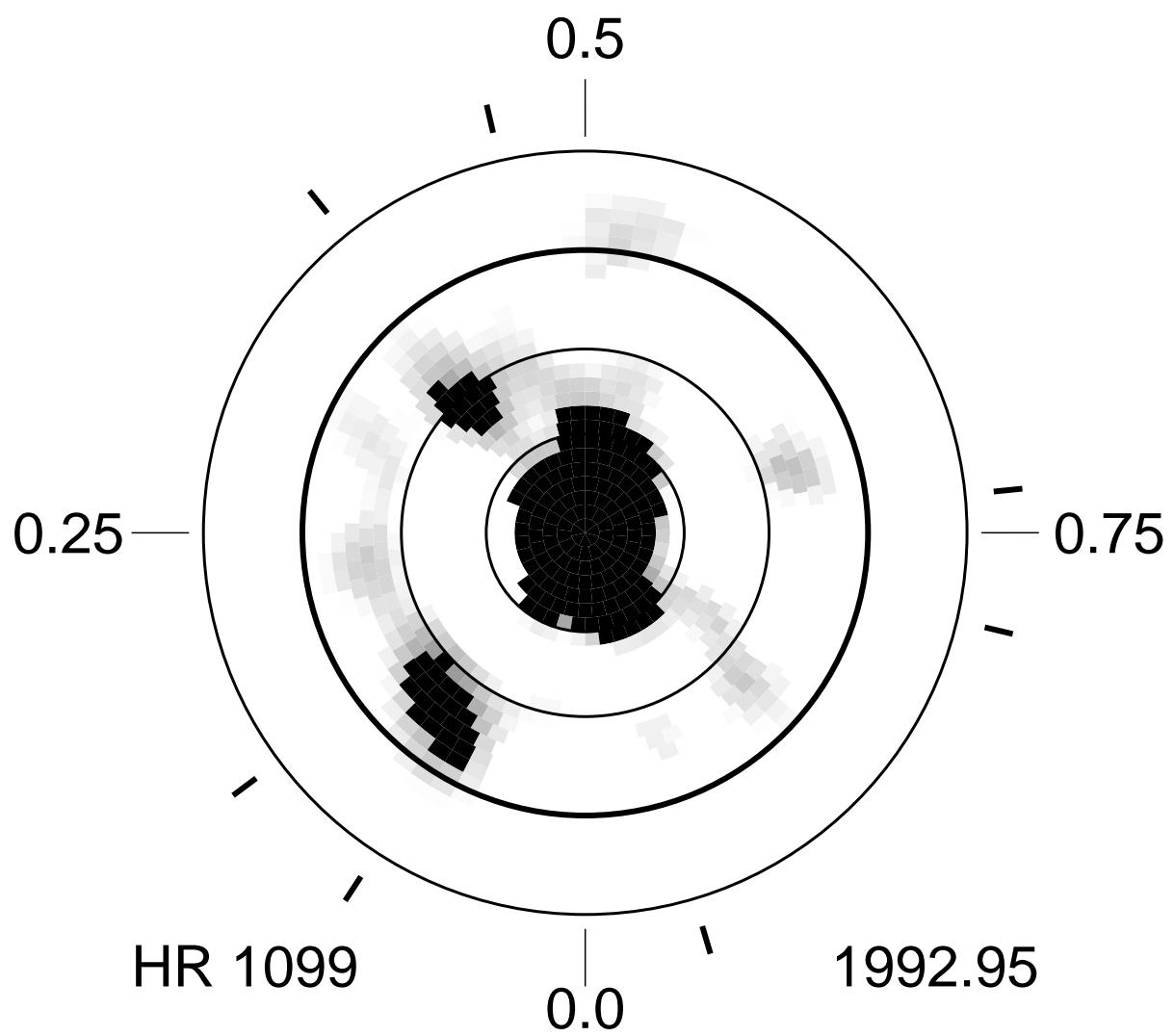


Fig. 78.— HR 1099 raw (unthresholded) Doppler image for 1992.95

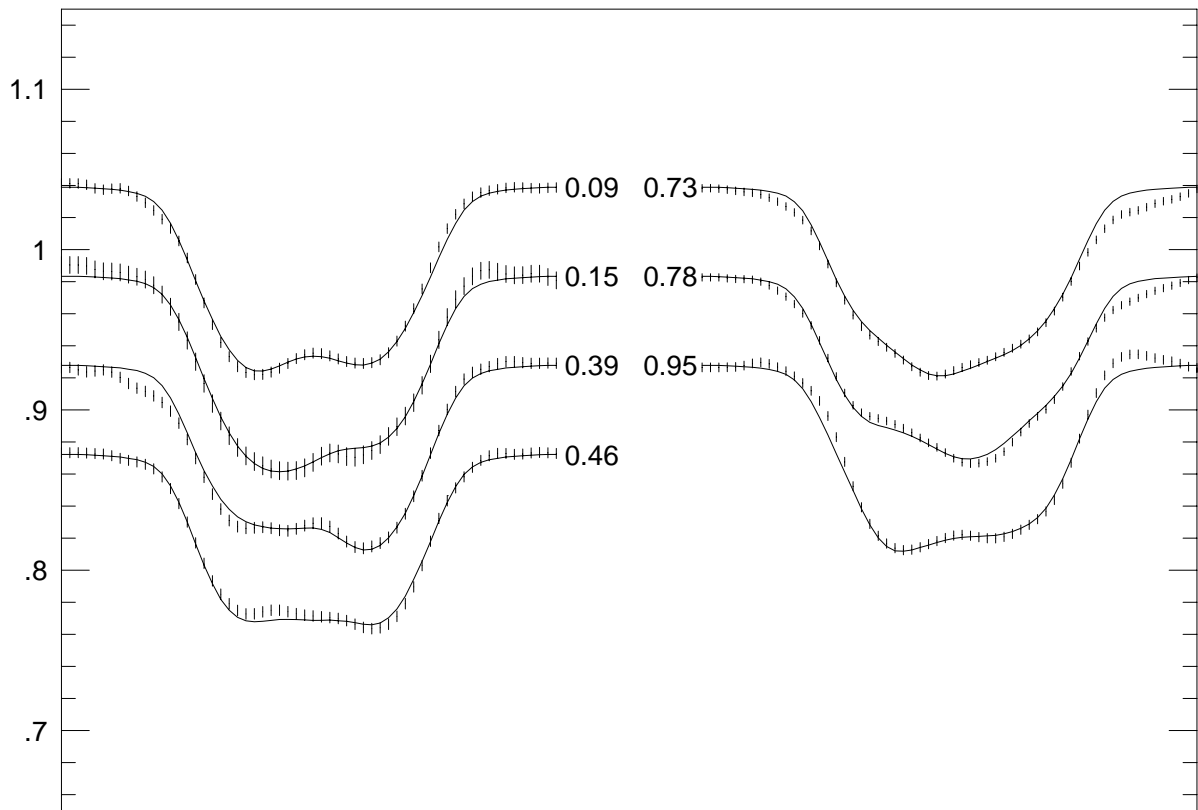


Fig. 79.— Spectral line profiles and fits for 1992.95

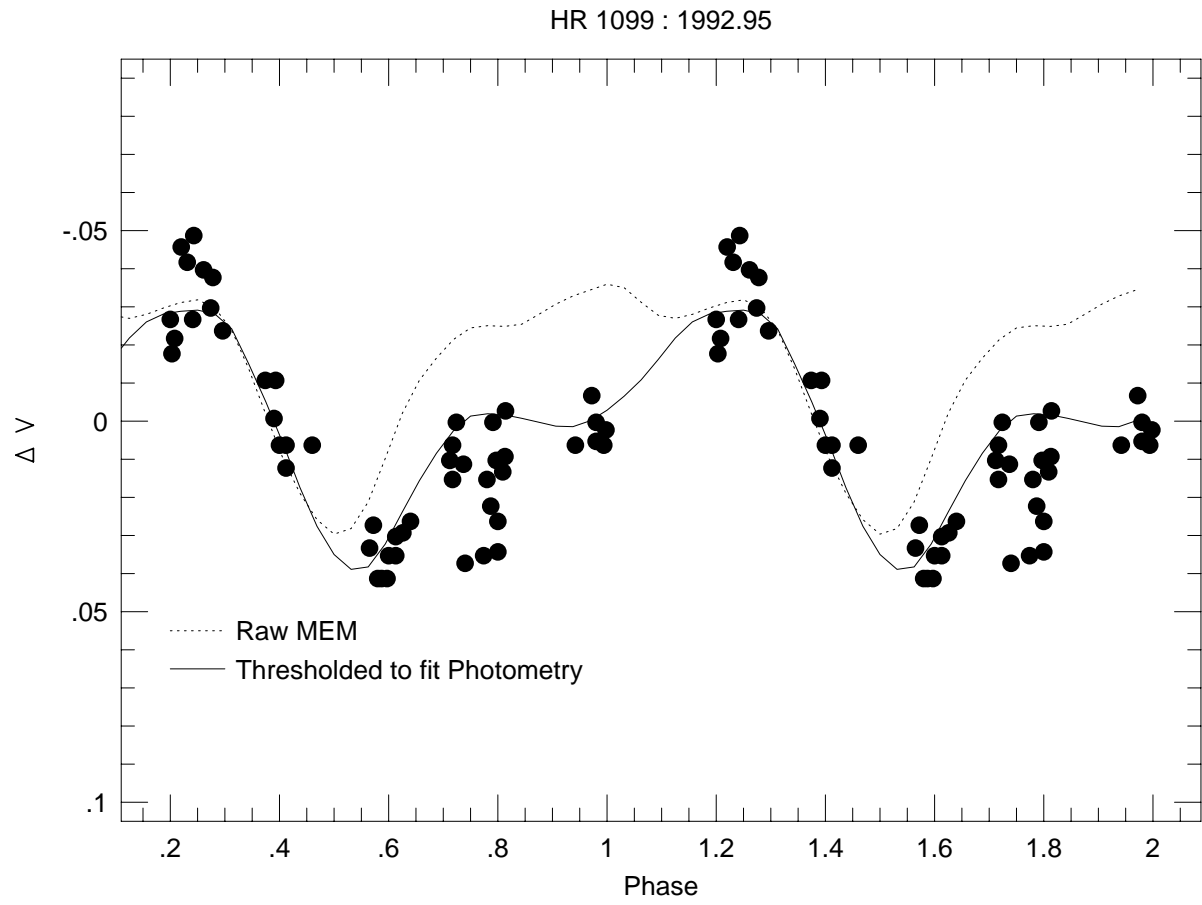


Fig. 80.— HR 1099 light curve for 1992.95

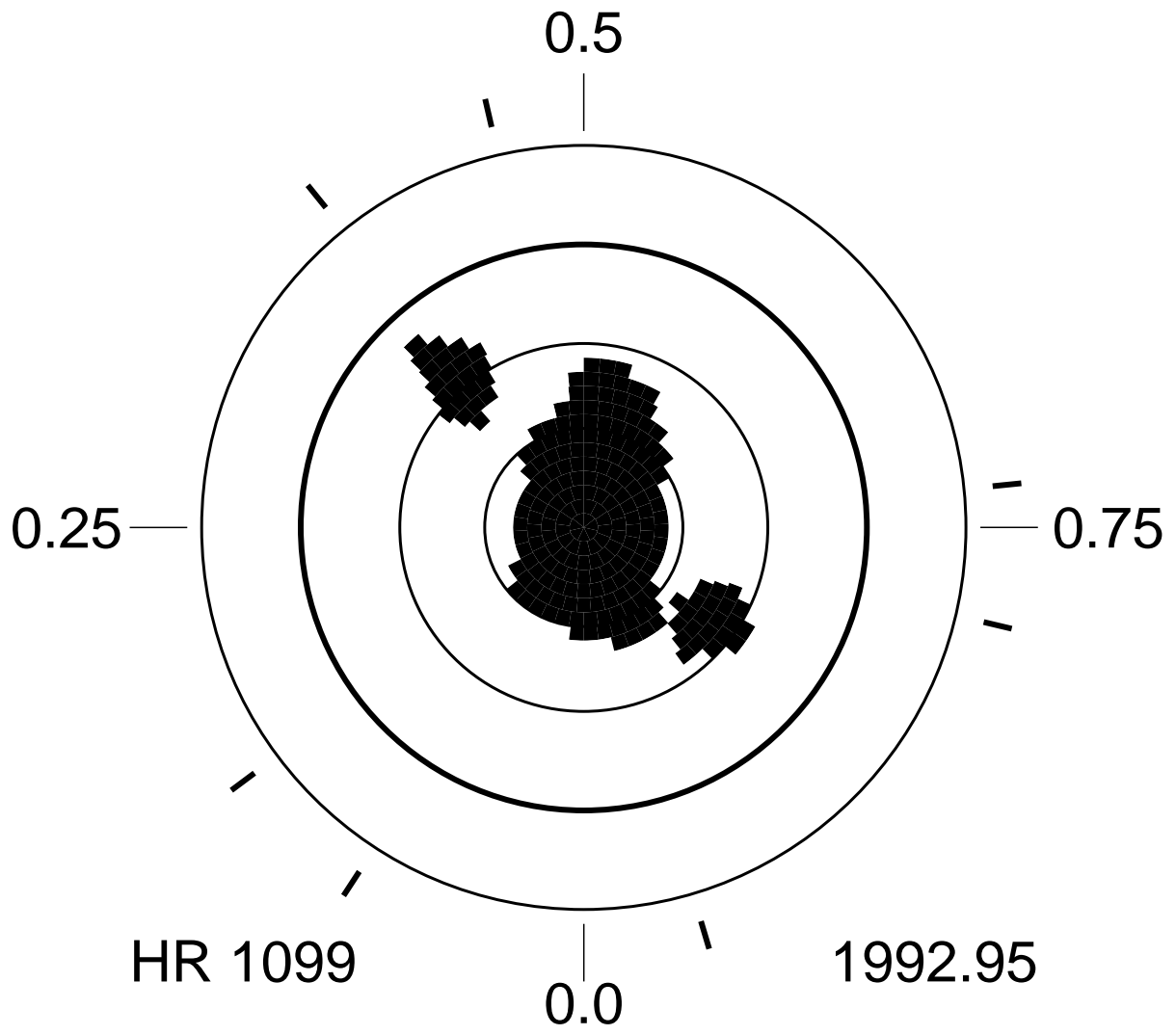


Fig. 81.— HR 1099 thresholded Doppler image for 1992.95

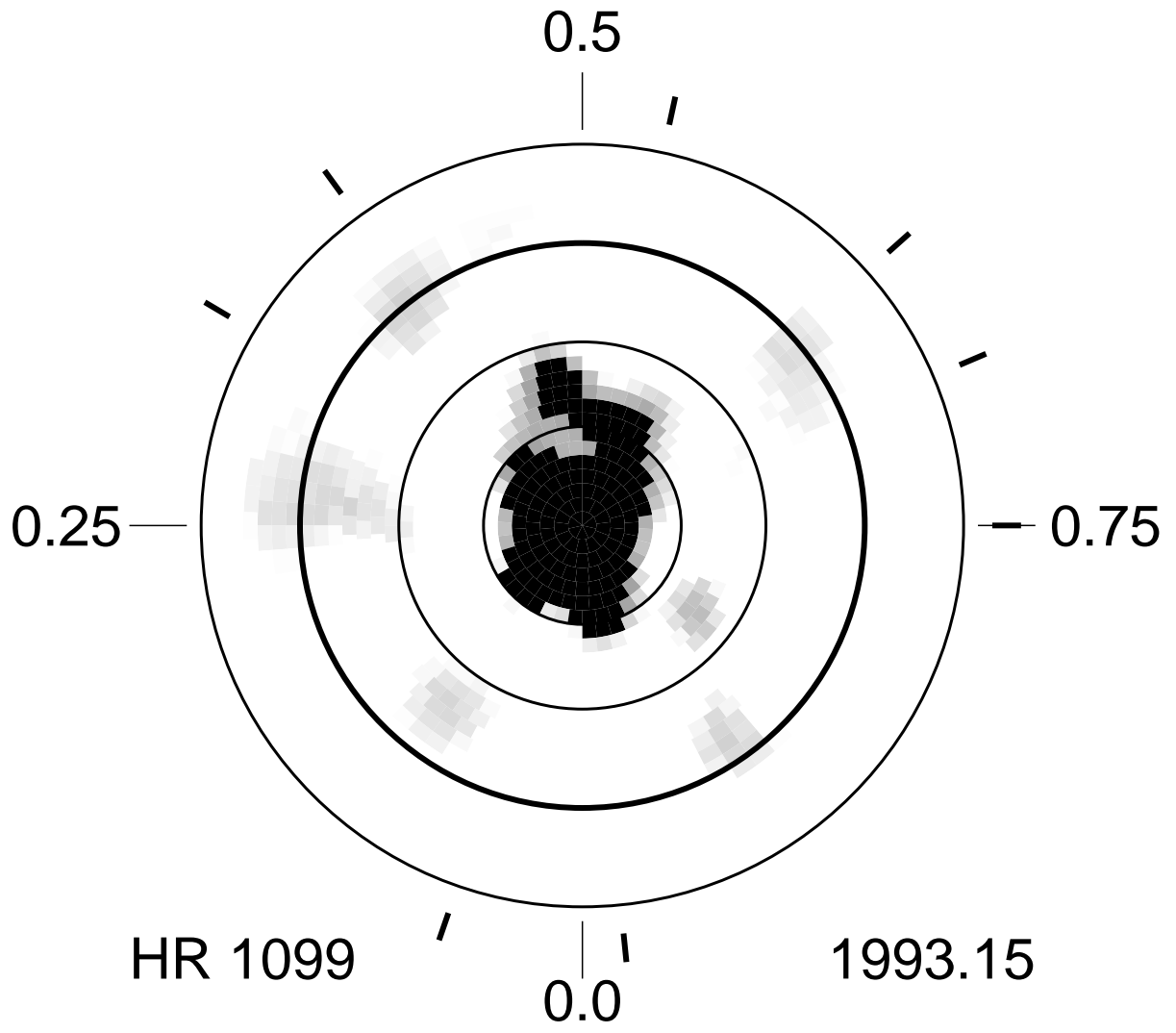


Fig. 82.— HR 1099 raw (unthresholded) Doppler image for 1993.15

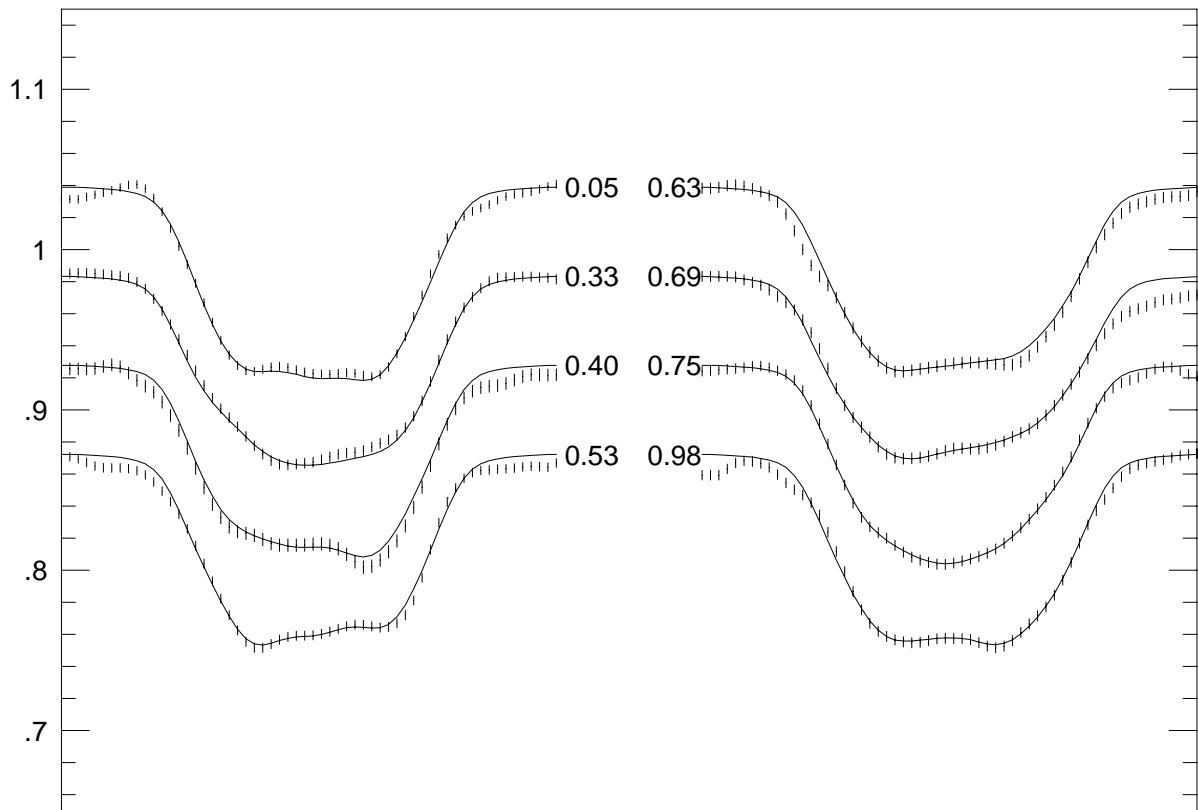


Fig. 83.— Spectral line profiles and fits for 1993.15

The unthresholded image for 1992.68 is shown in Figure 72, with the corresponding spectral line profiles and fits in Figure 73. The unthresholded image for 1992.80 is shown in Figure 74, with its corresponding spectral line profiles and fits in Figure 75. The predicted photometric variation for 1992.80 is shown as the dotted line in Figure 76 along with the b-band photometry (points) of Drake et. al. (1994). The final 1992.80 image, as thresholded by the 1992.83 light curve is shown in Figure 77. The unthresholded image for 1992.95 is shown in Figure 78, with its corresponding spectral line profiles and fits in Figure 79. The predicted light curve for the raw 1992.95 image is shown as the dotted line in Figure 80 along with the 1992.91 photometry (points) of Zhang et al. (1993). The final 1992.95 image, as thresholded by the 1992.91 light curve is shown in Figure 81, and its corresponding light curve is the solid line in Figure 80. Finally, the unthresholded 1993.15 image is shown in Figure 82, with its corresponding spectral line profiles and fits in Figure 83.

The 1992.83 and 1992.95 thresholded images (Figure 77 and Figure 81) both provide much better fits to the photometry than do the raw images. The thresholded images are generally consistent with the raw images except for the low-latitude spot at phase 0.125 in 1992.95 which did not survive the added constraints imposed by the light curve data. This serves as a warning and a reminder that one must be wary of the reality of low-latitude features in our raw Doppler images in cases where good light curves have not been incorporated into the solution.

The spot distribution this season changed significantly from the 1992.04 image taken 8 months earlier, though there are some similarities. The strong protuberance on the polar spot in the 1992.68 image at phase 0.12-0.14 and a similar but apparently detached spot in the 1992.80 image looks at first to be associated with the persistent Feature H from the previous year’s images. However, this feature was also present in the raw image of 1992.95 and unfortunately did not survive the light curve thresholding process, and thus may be

spurious. There was also a large isolated spot (hereafter referred to as Feature I) which appeared prominently near the equator at phase 0.93 in both the 1992.68 and 1992.83 images. There was no corresponding feature in either the raw or thresholded 1992.95 image, so we cannot say whether it would have thresholded away in similar fashion. It was, however, a rather large feature and appeared at very nearly the same latitude and longitude in the two entirely independent data sets, suggesting that, unlike the previous feature whose appearance and position changed randomly, it may well have been real.

Feature I appeared to shrink fast enough to have completely disappeared by the 1992.95 image. If so, it would be an example of a spot well-observed in the act of shrinking, and shows that a major spot can disappear on this star in less than 5-6 months. Feature I also showed no significant evidence of either longitude or latitude movement while disappearing. Note that its fixed longitude is not inconsistent with the $123^\circ \text{ yr}^{-1}$ longitudinal migration rate derived from Feature E. Over the 0.12 years between the 1992.68 and 1992.80 images, it would have drifted only 15° (3 pixels) in longitude, and its longitudinal position probably cannot be determined to that precision due to phase ghosting. It is worthwhile to mention though that Feature I appeared at essentially the same location as both Features D and E, as though this were some stable preferred region of spot formation on HR 1099.

There were also two mid-latitude isolated spots near $30^\circ - 36^\circ$ latitude and at phases 0.63 and 0.87 in the 1992.68 raw image. They were absent in the 1992.80 raw image, though the phase 0.87 spot did survive the thresholding process to re-appear in the final 1992.95 thresholded image. Unfortunately, without accurate light curves with which to threshold all the images, these ephemeral features are simply too near the limits of the present dataset to further quantify.

Finally, there is actually a fairly high similarity between the shapes of the polar spot among this season's raw images. In all cases, there is a distinct tendency for a protuberance

near phase 0.5. This protuberance appears to be well-fixed in longitude. The polar spot also looks very similar in shape and fixed in phase between the 1992.95 and 1993.15 images, once again implying that the polar spot, or at least its high-latitude edge is closely synchronized to the orbital frame.

The EUV light curve of Drake et. al. (1994) showed a maximum at about orbital phase 0.0, and minimum near phase 0.5. On our corresponding 1992.80 Doppler image, phase 0.0 coincides with the time of maximum visibility of both low-latitude spots and phase 0.5 corresponds to the time when both are completely hidden from view. If the EUV emission is at all related to the starpot distribution, this phase correspondence may indicate that the EUV emission is strongly spatially associated with the two low and mid-latitude spots in the 1992.80 image. This is not unexpected, since, following the solar coronal hole analogy, low-latitude spots like Feature I are probably associated with newly emerged mixed-polarity magnetic flux which has only recently become organized enough to form a substantial UMR, and is probably still surrounded with the litter of residual, hot, mixed-polarity emitting regions. Drake et. al. (1994) pointed out that the minimum of their Stromgren b light curve appeared to lead the maximum in EUV emission by about 90° , but they found no other obvious relationship between the two light curves. Their light curve is well-fit by our Doppler image solution and provided a good check on our Doppler image solution, but yields no obvious further insight into the relationship between spots and EUV emission.

4. Discussion

4.1. The omnipresent polar spot

Clearly the most prominent feature of our images of HR 1099, and a recurring theme in other’s images of rapidly-rotating spotted stars, is the ever-present large cool polar spot.

Since the reality of large cool polar spots is still not universally accepted by the cool-star community (for example see Byrne, 1996), a few words in their defense seem in order here. Perhaps the best argument for their reality is that we do *not* see them on some more moderately-rotating RS CVn stars, for example σ Gem (Hatzes 1993), nor do we ever see them on other types of stars we have imaged (Ap stars). In some other cool-star cases, like ZAMS (zero-age main sequence) Pleiades stars (Stout-Batalha and Vogt (1996)), they are at high latitudes, but are *not* symmetrically placed on the pole as would be expected if they were an artifact of our inability to model line profiles properly. We also recently completed a study (Hatzes, Vogt, Ramseyer, and Misch (1996)) in which we showed that the inclination dependence of line core flattening in a sample of stars could not be explained by gravity darkening, by differential rotation, or by a bright equatorial band, but was quite consistent with the inclination aspect-dependence produced by a polar dark spot. Other researchers have also found these polar spots both in intensity images and in Stokes parameter imagery. Finally, phase-independent TiO features in the spectra of some low-inclination spotted stars strongly support the presence of large cool polar spots. So the reality of these polar spots now seems reasonably well-established, and the large cool polar spot on HR 1099 has persisted for the 11-year span of this study.

4.2. Comparison of the images with ‘few-circular-spot’ solutions

Most spotted stars rotate too slowly to be amenable to Doppler imaging. In these cases, one must resort to fitting light curves with simple models involving 2 or 3 circular spots. However, these simple spot models are known to be quite non-unique since a light curve alone offers little constraint for the large set of possible image solutions. It was therefore of particular interest to check the results of such ‘few-circular-spot’ models against the more detailed Doppler imagery of HR 1099. This comparison would reveal how well these

simple models actually did, and thereby help us to better assess their effectiveness for more slowly-rotating spotted stars. We showed such comparisons of few-circular-spot solutions against Doppler images for epochs 1981.70, 1982.74, and 1989.83. In all cases, our Doppler images and others’ ‘few-circular-spot’ solutions *both* adequately fit the broadband light curves. The Doppler images, however, *also* fit a set of line flux profiles and are thus much more highly constrained. Unfortunately, the agreement between these ‘few-circular-spot’ solutions and the Doppler images was not very encouraging, nor was the agreement between the circular-spot solutions of different researchers for the same epoch. Clearly, the light curves alone just do not contain enough information to adequately constrain the spot solutions. So, while some instances of correspondence can be found, these circular-spot solutions do not seem to yield much useful information on the spot distribution. In fact, for all the comparison cases presented in this paper, these solutions were quite misleading.

Conversely, agreement of Doppler images of HR 1099 among different researchers, for example our 1988.80 and 1991.02 images with the Doppler images of Donati et al. (1992), is generally quite excellent. Here, most of the subtle details of the shape of the polar spot are faithfully reproduced between the two research groups, though these images were derived from completely independent data sets, with different imaging software.

4.3. Where do the spots first emerge?

It is probable that small spots can emerge almost anywhere on the star, showing up as changes in the outlines and appendages of existing spots, or as short-lived isolated spots. With only one, or at most several images per year (100-200 rotations for HR 1099), it is not possible to conclude much about the emergence of such small-scale features from our image set. However, one fundamental result revealed by the image set is that major spots do frequently ‘emerge’ (i.e. first appear) at quite low latitudes. Features D, E and I are

three examples of this, having first appeared on or near the equator. Other equatorial and low-latitude spot emergences were also seen.

This well-determined observational result contradicts the theoretical explanation of polar spots put forth by Schüssler and Solanki (1992). In their model, coriolis forces cause buoyant magnetic flux generated deep within the star to rise along paths parallel to the star’s rotation axis rather than along radial paths. Their model then predicts that flux should erupt only at high latitudes, thereby perhaps explaining the ubiquitous polar spots on these stars. However, the common-place emergence of low-latitude spots on the very rapid rotator HR 1099 is in direct contradiction to this prediction, and may be a problem for the Schüssler and Solanki model. Their idea was further developed by Schüssler et al. (1996) who found that there is usually a range of latitudes over which magnetic flux can emerge, with the mean latitude shifting toward the poles for increasing rotation. This model is now in good basic agreement with the polar and mid-latitude distribution of spots on young rapid rotators, but still does not explain the frequent emergence of major flux at low-latitudes in our HR 1099 Doppler images. While their theoretical model looks quite promising, it must be further explored to see if it can also explain this observed low-latitude spot emergence.

4.4. Tracking the movements of individual spots

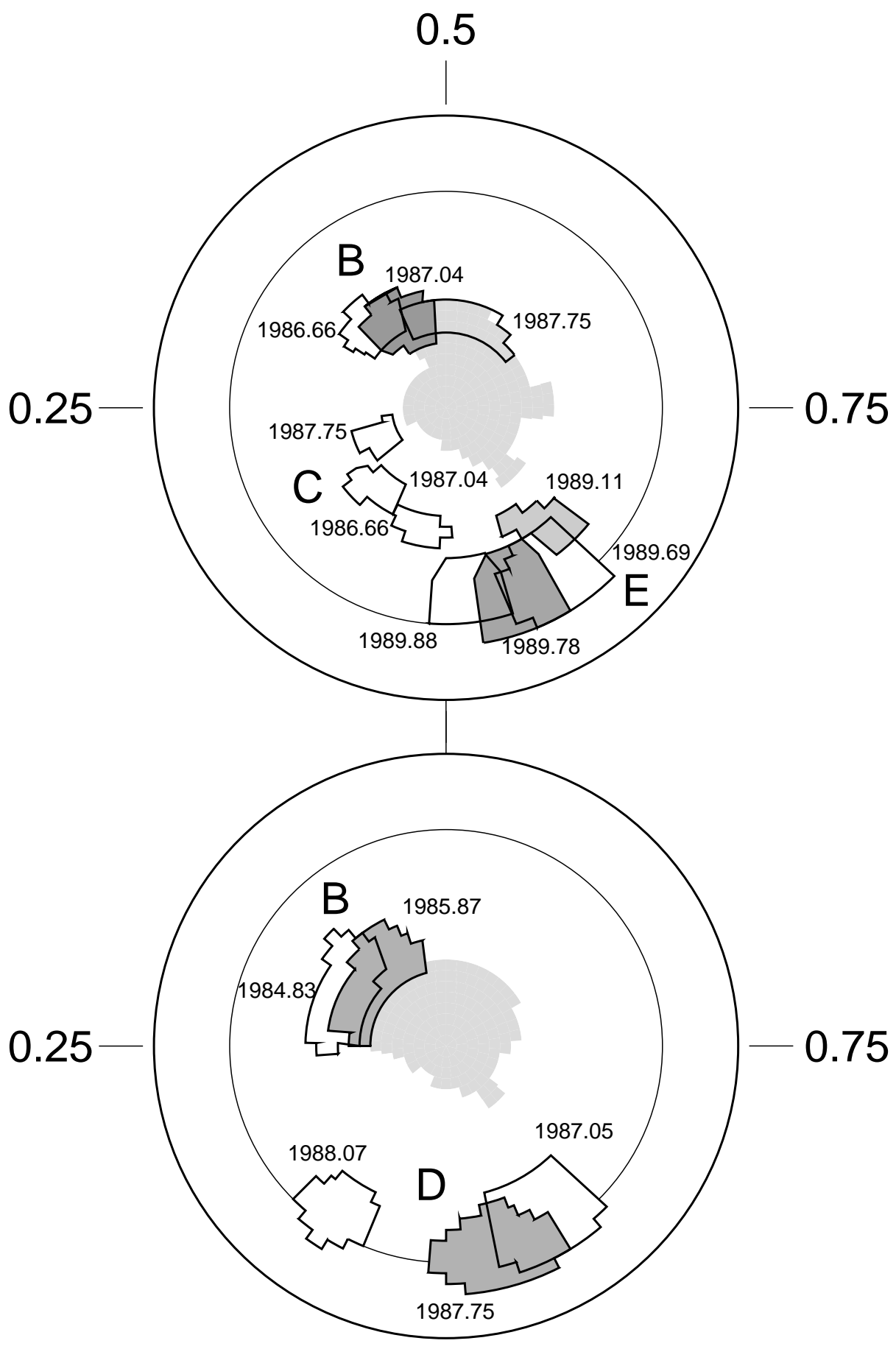
It has often been assumed that the ‘migrating photometric waves’ in the light curves of RS CVn stars are attributable to longitudinal migration of spots on a differentially-rotating star. The phase drift of spotted star light curves is certainly an easily and accurately measured quantity, and attempts have thus been made to derive the differential rotation of spotted stars from such light curve phase drifts. In the presence of latitudinal shear, spots at different latitudes would have different rotation periods, migrating in longitude with

respect to the orbit, causing the light curve to migrate in phase accordingly. In this simple picture, spots appearing above or below some intermediate co-rotation latitude (i.e. like the solar butterfly diagram for sunspots) could cause the photometric light curve minimum to migrate in either direction.

Our imagery reveals that, at least for HR 1099, the situation is far more complex. The phase of the photometric minimum is affected strongly by the appearance and disappearance of a number of relatively-fixed large spots, as well as by the movements of some of these spots, and also by changes in their shapes and areas. It is clearly not valid to invert these phase drifts through so simple a parameterization as longitude migration of one or two spots. *The phase of the migrating wave by itself reveals essentially nothing about the details of the differential rotation pattern on HR 1099.*

Most spots come and go too quickly to track reliably with, on-the-average, one image per year. However, there were a number of isolated, long-lived spots which we were able to track from year-to-year. Figure 84 shows the tracks of Features B, C, D, and E in the frame of reference of the orbit. Thus all migrations are shown here as occurring with respect to the orbital frame, with the secondary (hotter) star fixed at phase 0.5. (The position of spot D in 1988.07 was inferred from the photometry. A spot was required at that position for the predicted photometry from our 1987.75 Doppler image to fit the 1988.07-epoch photometry of Mohin and Raveendran (1993)).

Feature B, at high latitude, lasted for almost 3 years and was seen migrating clockwise and poleward very slowly with respect to the orbital frame. It apparently merged with the polar spot by 1987.75. Feature C, at intermediate latitude, also migrated clockwise, its angular velocity still slower than the orbit but faster relative to the orbit than Feature B. It also followed a poleward-drifting clockwise spiral path finally merging with the polar spot. Features D and E also drifted clockwise, but even faster relative to the orbit than B or C.



The tracks of both Features B and C suggest that some spots which emerge at low or intermediate latitude do migrate poleward, and then apparently merge with the polar spot. Since the dark spots presumably trace magnetic flux, this must mean that some of the magnetic flux which emerges at lower latitudes on HR 1099 then spirals pole-ward in a clockwise manner (slower than the orbit), and eventually merges with the polar spot. It is not yet clear whether this flux is of the same or opposite polarity to the polar spot, and thus whether these poleward-migrating low-latitude spots reinforce or cancel the polar spot field.

Feature B also appeared to get somewhat *stretched* in longitude as it approached the polar spot, and its overall track is quite reminiscent of the annulus of toroidal field found by Donati et al. (1992b) encircling the polar spot of HR 1099 in 1990.9. Perhaps spots such as Feature B become sheared in longitude as they approach the pole, and thereby contribute to an annular ring of strong field around the polar spot. Feature B may thus be showing us directly how field lines get wrapped around the pole into the toroidal structure seen by Donati et al. (1992). Perhaps then, the ‘polar spot’ is simply that region where the field lines get wrapped sufficiently tightly around the pole, like spaghetti around a fork, to create fields strong enough to suppress convection in the photosphere, and thus create the cool polar spots.

4.5. The differential rotation of HR 1099 and other RS CVn stars

The migration rates of these long-lived features were then used to derive the ‘differential rotation’ or rotation period of the star as a function of latitude. Figure 85 shows the measured period vs. several simple parameterizations of latitude (ℓ).

The Sun’s rotation period depends nearly linearly on $\sin^2\ell$, and we have thus used that

as one of the simple latitude parameterizations chosen for Figure 85. As can be seen, the rotation period correlates well with all the chosen parameterizations. Unfortunately, the rather small number of data points and the scatter in the data precludes deriving a more precise functional form from this data set.

Using the standard solar parameterization for differential rotation, one expects angular velocity to vary linearly with $\sin^2 \ell$ where ℓ is the latitude. A formal linear least squares fit of this functional form to our 5 points, including the differing error bars in both dimensions, gives:

$$\Omega(^{\circ}/day) = 126.52 (\pm 0.003) + 0.47 (\pm 0.06) \sin^2 \ell \quad (1)$$

The amount of differential rotation is then generally parameterized by α , the ratio of the difference between polar and equatorial velocities to the equatorial velocity:

$$\alpha = \frac{\Omega_{equator} - \Omega_{pole}}{\Omega_{equator}} \quad (2)$$

Solid body rotation results in $\alpha = 0$, whereas equatorial acceleration has $\alpha > 0$ and polar acceleration results in $\alpha < 0$. Using the above $\sin^2 \ell$ fit gives $\alpha_{HR1099} = -0.004 (\pm 0.0004)$ whereas $\alpha_{Sun} = +0.197$. Thus the differential rotation implied by starspot motions on HR 1099 is of opposite sign to the Sun: the poles rotate faster than the equator, with about a 50 times smaller differential. The same result (poles rotating faster than the equator) was also found for the spotted star UX Ari by Vogt and Hatzes (1991), though in that case, the amount of differential rotation was only about 10 times less than solar, the equator was synchronized to the orbit, and the pole actually rotated faster than the orbit.

Interestingly, the rotation period of HR 1099 also correlates quite well (bottom panel of Figure 85) with $(1 + 3\sin^2 \ell)^{1/2}$, an abscissa proportional to the surface strength of a

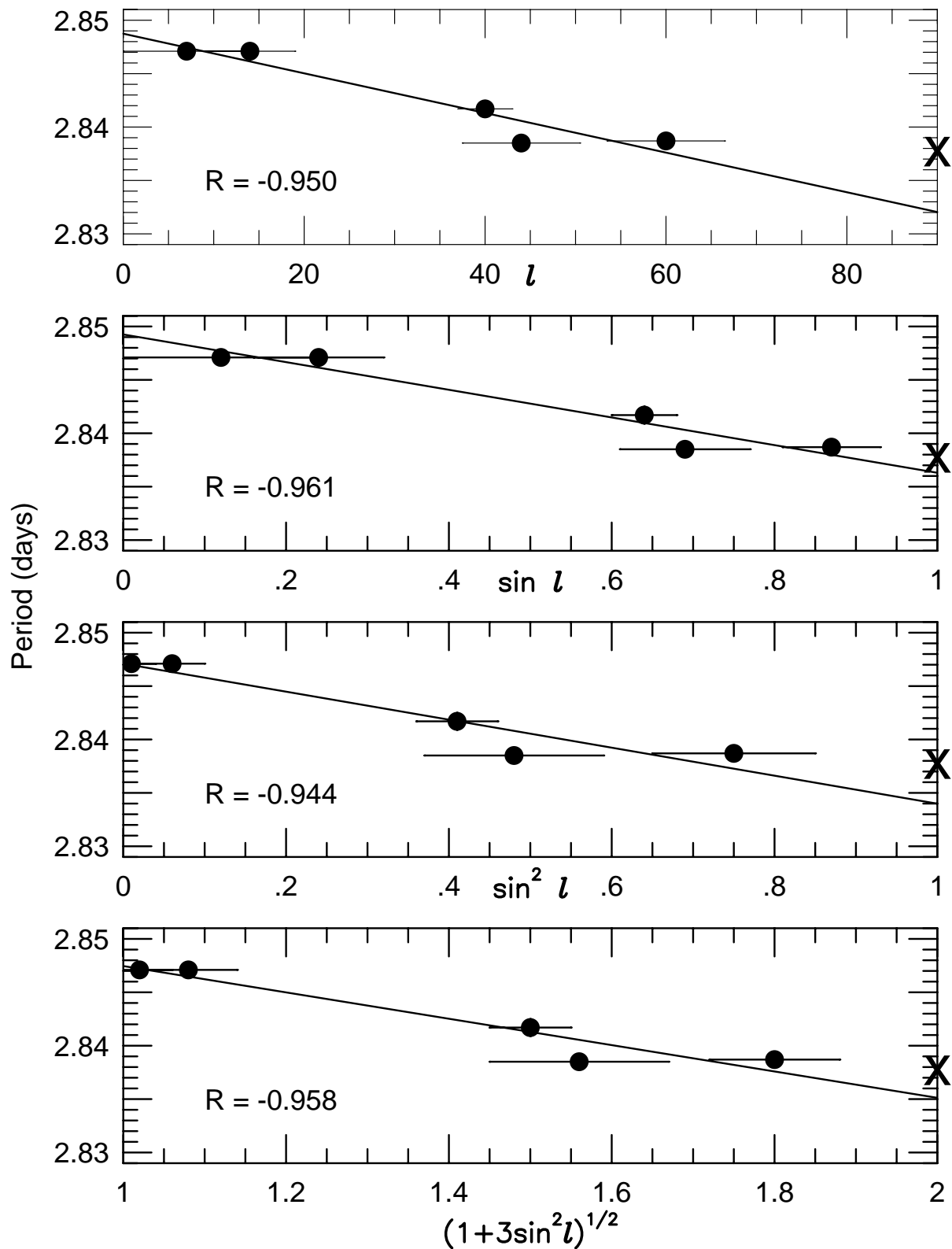


Fig. 85.— The rotation period of individual spot features as a function of various parameterizations of latitude. The location of a synchronously-rotating pole is shown by the cross at the right edge of each plot

centered, axisymmetric magnetic dipole field. Given also that an extrapolation of the observed rotation periods suggests near-synchronous rotation at the pole, these observations may well be indicating that spot migration motions are dominated by a large, aligned, magnetic dipole within HR 1099 which is co-rotating with the orbital frame. The relatively high surface field strengths near the pole would then enforce near-corotation of high-latitude spot features, while the decreasing field strength with decreasing latitude would allow progressively faster ‘slip’ or clockwise longitude migration of spots, just as observed.

Is the pole truly synchronized with the orbit, or actually going slightly faster? The extrapolations of all the fits in Figure 85 do hit slightly below the location of the synchronously-rotating pole (marked by the cross at the right edge of each plot). If, for argument’s sake, the pole rotates faster than the orbit, this would indicate that it is the intermediate-high latitudes (50° to 60°) which are synchronized to the orbit, with the pole then rotating faster than the orbit. This brings to mind the work of Scharlemann (1982) who calculated the effects of tidal coupling in RS CVn binaries. He predicted that, when the tidal coupling torque vanishes (maximum degree of synchronism achieved), part of the star should be rotating faster than the orbit, and part more slowly. Co-rotation with the orbit should occur at some intermediate latitude (the co-rotation latitude). If our simple linear least squares fits and extrapolations do indicate that the pole rotates faster than the orbit, then the implied differential rotation pattern may indeed fit the predictions of Scharlemann (1982). The corresponding implication also is that HR 1099 is at or near a state of maximum degree of tidal coupling.

On the other hand, given the sizes of the error bars, and the scatter of the few data points, the fits are quite consistent with synchronous polar rotation. We certainly did not find any evidence of trackable features at the pole which were rotating faster than the orbit. All indications from the images are that features migrated progressively more slowly with

respect to the orbit as latitude increased, becoming indistinguishable from stationary at the highest discernable latitudes.

There is also no *a priori* reason to expect that differential rotation should vary linearly with $\sin^2\ell$ as it does for the Sun, and thus we should not artificially force such a fit upon the data and then expect it to give a valid result upon extrapolation to the pole. Indeed, the $\sin\ell$ parameterization does extrapolate quite closely to synchronous polar rotation. One problem is that the latitude range of Features B1 and B2 are quite large, and difficult to determine precisely, having extended at various times from at least 40° to 70° latitude. More likely, all we can probably say at the moment is that, if Features B1 and B2 are high enough in latitude to be representative of the polar zones, then the polar zones are nearly synchronized with the orbit.

One simple explanation for polar synchronization is that the star conserved angular momentum as it expanded upon leaving the main sequence. The star may have been tidally locked to the orbit at all latitudes before its ascent up the subgiant branch. As it expanded in radius, conservation of angular momentum would have slowed its outer layers and perhaps also preferentially slowed its equatorial latitudes, causing them to rotate more slowly than the higher latitudes. This would leave the polar regions still closely synchronized to the orbital angular velocity and perhaps only slightly slower, whereas the equatorial regions would be rotating more slowly.

A completely different explanation is that perhaps the large polar spot is the footprint of a strong dipole magnetic field which is firmly anchored to the highly-synchronized core of the main sequence progenitor of this expanding subgiant, at a field strength of several kilogauss. The magnetic energy density of this dipole could be stronger than the kinetic energy density of the differential shearing motions of the gas. This emergent dipole field would then dominate the gas motions at high latitudes, producing apparent synchronization

of the very high-latitude spot features with the orbit.

Whatever the precise form of the rotation period’s latitude dependence, the basic picture which emerges is one of high latitude spots on HR 1099 rotating in near or perfect synchronism with the orbit, and of a rotation period increasing with decreasing latitude. The equator is thus rotating more slowly than the poles, opposite to the solar case. And while the Sun shows a 20% difference between polar and equatorial angular velocity in the photosphere as determined from sunspots, starspots show only about a 0.4% difference on HR 1099. While this is much less than photospheric sunspot motions, *it is quite similar to the small differential rotation values observed in solar coronal holes.*

Navarro-Peralta and Sanchez-Ibarra (1994) measured the solar rotation rate using solar coronal holes. They found that solar coronal holes show an average rotation rate which is almost constant with latitude, for latitudes above 30° and, at lower latitudes, increases to become quite similar to that determined from sunspots. For latitudes above 20° the differential rotation rate determined by the average rotation rate of coronal holes is in the same sense (poles rotate slower than equator) but about a factor of 10 less than that determined from sunspot groups. However, dividing the data set up into two distinct groups, isolated holes and polar hole extensions, they see a more complicated behavior. Polar hole extensions show slowest rotation at intermediate latitudes, with rotation speeding up both toward the equator and toward the pole. Isolated coronal holes, on the other hand, show slowest rotation at the highest latitudes, a flat plateau of constant rotation rate at intermediate latitudes, and then rotation rate increasing steadily to values in excess of that from sunspots at the lowest latitudes. So if the solar case is any lesson here, the true situation is probably much more complex than simple monotonic variation of rotation rate with latitude.

Given that starspots also bear a striking morphological resemblance to solar coronal

holes, this similarly low degree of differential rotation of starspots and solar coronal holes is perhaps not altogether surprising. It is consistent with the basic picture suggested by Vogt and Penrod (1983) that starspots are essentially just coronal hole-like structures (footprints of the unipolar magnetic regions of a current-free global coronal magnetic field), but where the global field is multi-kgauss-strength rather than the few-gauss-strength global fields of the Sun.

Of course one should not attempt to draw too many inferences from the differential rotation of a single complex binary system such as HR 1099. But it can perhaps help to interpret the indirect differential rotation signatures derived from light curve stability measurements for a large number of RS CVn and other active late-type stars. Our results of very small differential rotation for HR 1099 (present work) and for UX Ari (Vogt and Hatzes (1991)) are in excellent accord with the results of Hall (1991) who found that differential rotation signatures (from light curve stability) of a large sample of spotted late-type stars *decrease* rapidly as angular velocity increases. Rapidly-rotating spotted stars such as HR 1099 thus appear to approach solid-body rotation (at least as far as spot movements are concerned).

If there is a strong (multi-kgauss) axisymmetric magnetic dipole within HR 1099 (which is causing the large cool polar spots), it may well be expected to globally dominate the movements of these starspots, just as the current-free coronal field of the Sun does in the case of coronal hole structures (Wang and Sheeley 1993). A 5-10 kG dipole field strength at the pole would still be 2.5-5 kG strength at the equator, and thus strong enough to compete seriously with the shearing forces of photospheric differential rotation. Newly emerging magnetic flux would not emerge into a field-free environment, but rather would be obliged to immediately connect with this powerful external global dipole field, and any tendency for shearing due to differential rotation would be strongly resisted by the current-free global

potential field. This picture might provide a simple explanation for the observed trend toward solid-body rotation of starspots with increasing stellar rotation velocity. More rapid rotation gives rise to a stronger current-free global dipole field which, in turn, enforces increasingly solid-body rotation of the spots (the unipolar magnetic footprints of this field) as the rotational angular velocity increases.

4.6. Spot/Activity cycles

There have been many claims of activity cycles on spotted RS CVn stars over the years, as people search for the analog of the well-known 11-year sunspot cycle. On the Sun, the area of the polar coronal hole varies dramatically and periodically, in anti-phase with the sunspot cycle (Bravo and Otaola (1989), Waldmeier (1981), Simon (1979)). If starspots are indeed stellar analogs of solar coronal hole structures, then probably the best hope of detecting a dynamo cycle is to look for periodicity in the *area* of the polar spot. Properly-thresholded Doppler images do give a good unambiguous map of the polar spot, and variations in its area are easy to measure from Doppler images providing the thresholding process has been done very consistently from one season to the next. We have taken great care to establish a uniform threshold for all our images, and have cross-checked our thresholding process with fits to both the line profiles and the broadband light curves.

The top panel of Figure 86 shows polar, low-latitude, and total spot areas (percent of visible hemisphere as a function of time. There is an overall decrease in the polar spot area of about 11% from 1982–1993 (the solid line represents a linear regression). The lower panel shows the mean brightness level and light amplitude for HR 1099 from Mohin and Raveendran (1993). The line for the mean light data represents a linear regression using the full span (1975-1991) of those data and yields an overall brightness increase of 0.045 mag over the 12-year span of the Doppler images. This observed increase agrees well with

a predicted increase of 0.042 magnitudes (calculated from the Doppler images) and would seem to indicate that *the mean light level here is, to first order, a good proxy of (polar) spot area.*

A Scargle-type periodogram analysis of the de-trended polar spot area is presented in Figure 87. The upper panel is for the detrended polar spot area, while the lower panel is for the total low-latitude spot area. The analysis showed maximum power at a period of 3.0 ± 0.2 yr for the polar spot area, with a false-alarm probability (FAP) of the maximum peak of 0.08. For the low-latitude total spot area, the analysis yielded a period of 2.6 ± 0.2 yr with a FAP of 0.16. Unfortunately, the quantity and quality of the data are probably not sufficient to determine if the variations of the polar spot and low-latitude spots indeed have different periods.

Figure 88 shows the best phase diagrams of the polar and low-latitude spot areas as provided by their respective best periods from the periodograms. The upper panel is for the polar spot area, phased at 3.0 year period, and the lower panel is for the total low-latitude spot area, phased at 2.6 year period.

While there is a hint of periodicity near 3.0 years for the polar spot, with a false-alarm probability of 8%, it cannot yet be regarded as compelling evidence of a cycle. At this point, we can only conclude that both the polar feature and low-latitude spots *may* show marginal evidence for an approximately 3-year periodicity in the variations of their total areas. Of course, we should not expect the solar analogy to be perfect. It may be that the strong dipole fields inside these RS CVn stars do not vary or periodically reverse in a manner similar to the solar cycle, and that perhaps the polar spot also does not show significant periodic area variation.

Baliunas et al. (1996) attempted to derive a dynamo interpretation of stellar activity cycles based on 25 years of records of Ca II H and K observations of single lower main

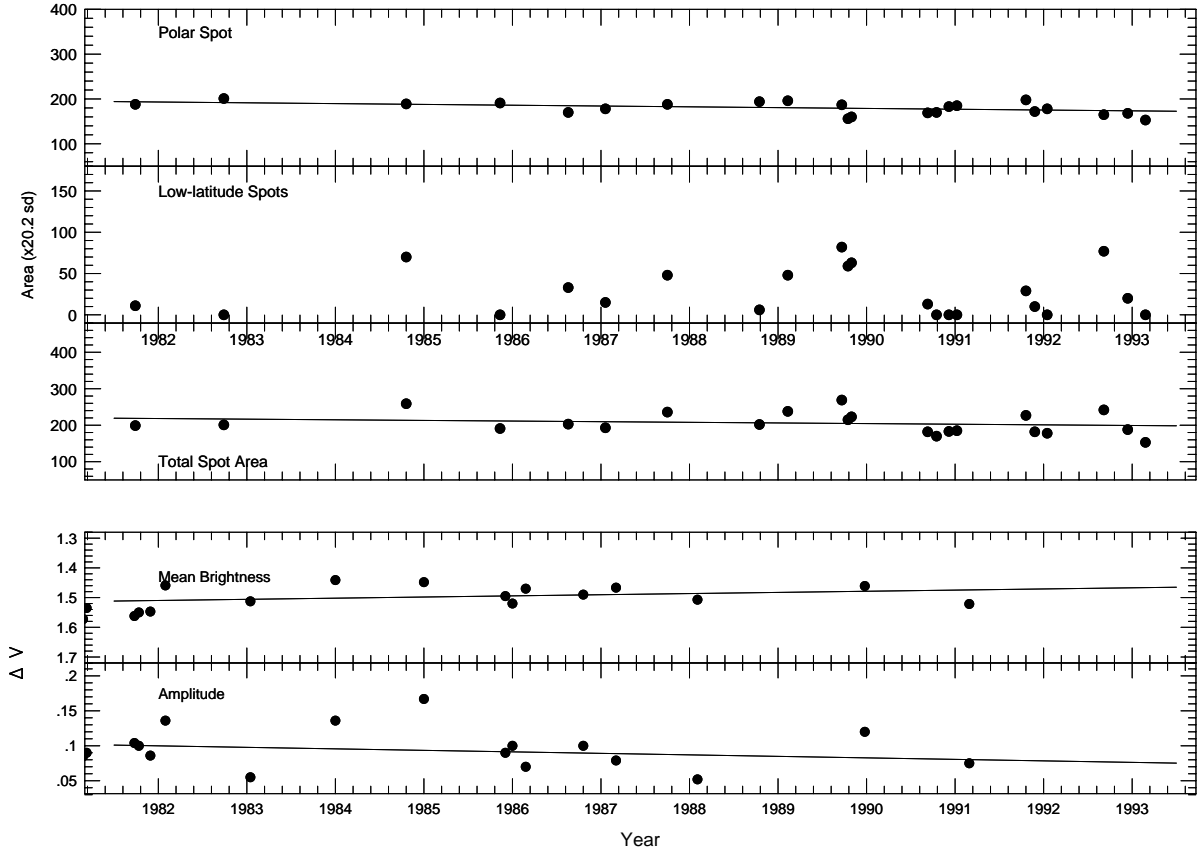


Fig. 86.— Plots of the polar, low-latitude, and total spot area vs. time (upper panel), and mean light and light amplitude vs. time (lower panel).

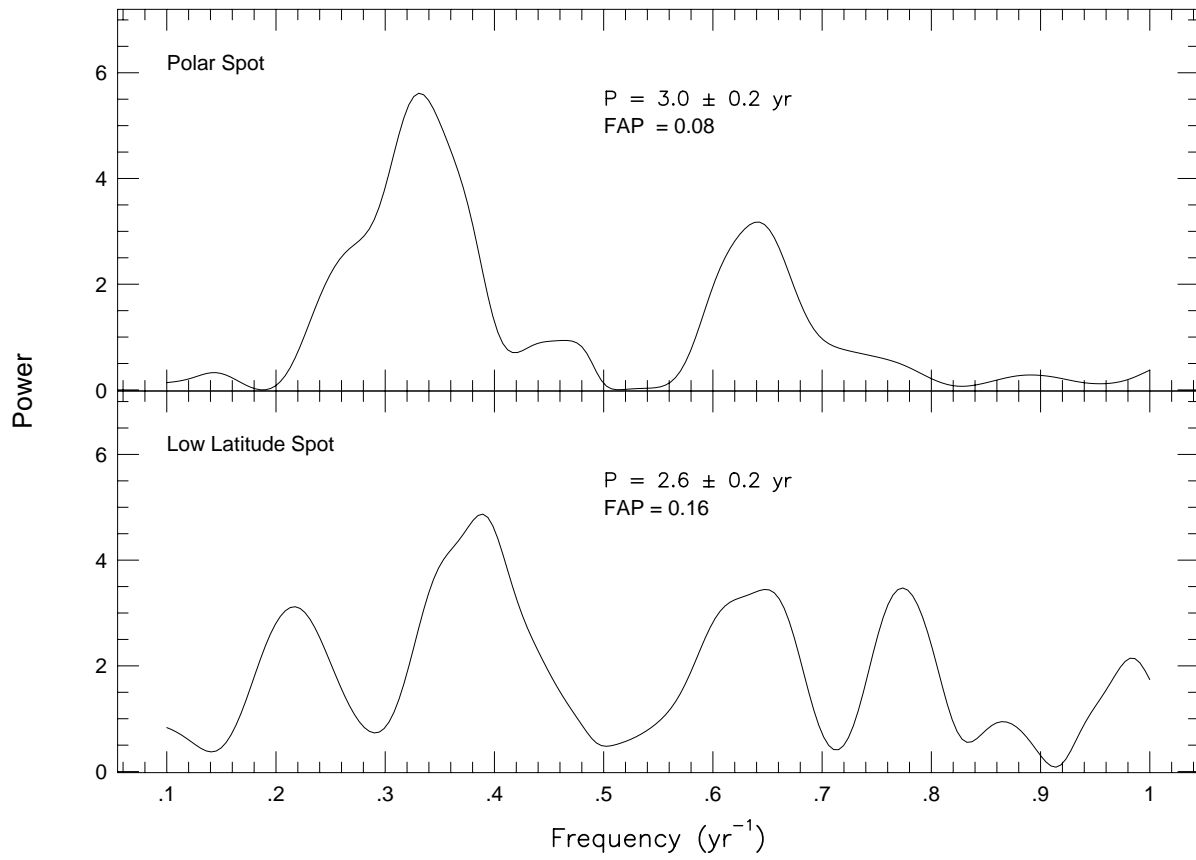


Fig. 87.— Periodogram analysis of polar and low-latitude spot areas

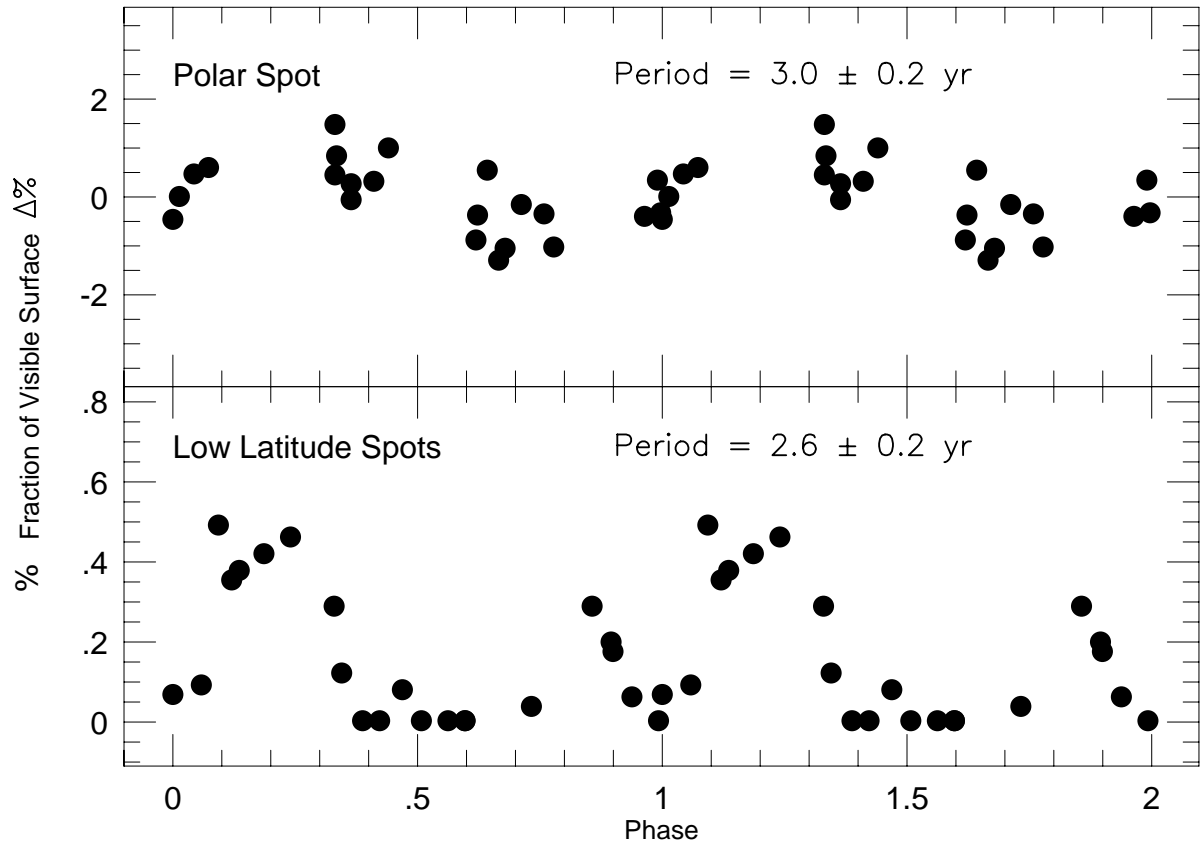


Fig. 88.— Phase diagrams for polar and low-latitude spot areas

sequence stars, 100 of which showed cycles. They showed that ratio of magnetic cycle P_{cyc} to rotation period P_{rot} is expected theoretically to be the observed equivalent of the stellar dynamo number D . They argue that P_{cyc}/P_{rot} should scale as D to some power, where the power is a positive constant greater than $1/3$. Thus a plot of $\log(P_{cyc}/P_{rot})$ vs. $\log(D)$ should be a straight line with slope which gives that exponent. HR 1099, with a 3-year cycle comes in well-below the linear extrapolation of their relation, which predicts a cycle period of about 5.2 years, but there is a lot of scatter in their observed relation. Given their scatter, a cycle period for HR 1099 anywhere between about 4-8 years would still be consistent with their relation.

4.7. Starspots as Analogues of Solar Coronal Holes

The detection by Donati et al. (1992b) of strong (≥ 300 G) largely monopolar surface magnetic fields associated with the edges of the polar spot in 1990.9, and 700 G monopolar fields associated with the low-latitude region near phase 0.27, are further support for the idea (Vogt 1987b, Vogt and Penrod (1983)) that the large, essentially permanent polar spot on HR 1099 and other rapidly rotating RS CVn stars may be closely analogous to coronal hole structures seen in x-ray images of the Sun. Solar coronal holes are well-known to be the footprints of large unipolar magnetic regions. The overall appearance, basic morphology, approximately solid-body rotation, and temporal evolution of solar coronal holes are indeed strikingly similar to the spots on HR 1099 and other RS CVn stars. In particular, the Sun shows a large, roughly circular polar coronal hole (typical diameter of 40°) with frequent attached ‘protuberances’ (these are called *polar hole extensions* in the jargon of solar astronomers) which descend to lower latitudes (for a recent reference see Navarro-Peralta and Sanchez-Ibarra (1994)). Also present are occasional ‘isolated’ coronal holes at lower latitudes, strikingly similar in size and evolution to the low and intermediate

spots on HR 1099. The Sun’s polar coronal hole area varies cyclically in anti-phase with the 11-year sunspot cycle and is intimately connected with the spot cycle as part of a more complex extended cycle (Bravo and Otaola (1989), Waldmeier (1981), Simon (1979)).

Wang and Sheeley 1993 showed that, on the Sun, polar hole extensions form when the superposition of the axisymmetric polar field and non-axisymmetric emergent flux at low latitudes distorts the global coronal field configuration, and thus the polar hole boundaries. The global field configuration is thus a complex, time-variable average over opposite polarity flux which is both merging and decaying. The ‘corridors of open field lines’ formed in the merging of such flux patterns give rise then to large unipolar magnetic regions (UMR’s) within which form the coronal holes. We suspect a similar complex process is at work shaping the polar starspot and other spots on HR 1099.

We thus believe that solar coronal holes are a close analog to the spots we see on the RS CVn stars, the main difference being only the magnetic field strength. On the Sun, magnetic surface field strengths inside coronal holes are only 10-20 G. This is not strong enough to significantly affect convective energy transport in the photosphere, but does affect plasma motions in the low-density corona, creating regions of lower density and temperature in the plasma wind outflow above the spot (hole), and giving rise to prominently visible structures in x-ray images of the corona. However, on the RS CVn stars, magnetic flux densities are several orders of magnitude larger, leading to umbral-strength fields with high filling factor inside the spot. These fields dominate the convective motions which transport heat to the surface, thereby lowering the effective surface temperature within the spot by 1000 K to 1500 K.

4.8. Is HR 1099 hiding a multi-kG aligned global dipole field?

Solar polar coronal holes are well-known to be the direct manifestations of the axisymmetric component of the Sun’s global magnetic field, a 1-2 G periodically reversing dipolar field aligned with the Sun’s rotation axis. The large coronal hole at each pole is a consequence of the unipolar fields at the rotation poles. The polar fields are of opposite polarity, and periodically reverse polarity at sunspot maximum. According to the basic Babcock solar dynamo model, some fraction of this dipole field is transformed, by differential rotation and convection, into a toroidal field which then gives rise to the buoyant magnetic flux ropes whose emergence at low-intermediate latitudes forms sunspot groups. If the solar analogy of coronal holes holds true for starspots, we might then expect, as also suggested by Donati et al. (1992b), that the large, permanent polar spot on HR 1099 is also a direct manifestation of a global dipolar magnetic field closely-aligned with the star’s rotation axis. Since coronal holes, and by analogy starspots, are regions of predominantly unipolar or ‘open’ field, the field lines of the observable polar spot must reconnect (out beyond the star’s Alfvén radius) with an opposite polarity region somewhere else on the star, most probably a spot at the other pole.

Since essentially every rapidly rotating RS CVn star shows a polar spot, and since it is highly unlikely that we are seeing the same pole in all these cases, the ubiquitous presence of polar spots indicates that these stars probably have similar large polar spots at *both* poles. Thus the prominent polar spots seen on HR 1099 and all other rapidly rotating RS CVn stars are probably mirrored by a corresponding opposite polarity spot at the other pole (as in the solar case). These large, essentially permanent polar spots are thus probably the direct manifestation of these stars’ global dipole fields. But whereas the Sun’s poloidal field is only 1-2 G, HR 1099’s dipole field, based on the magnetic measurements of Donati et al. (1992b), would be at least 300 G (and probably more like several kG in strength

following our analogy).

Dipoles of several kG strength are of course well-known for the magnetic Ap stars, but are generally highly tilted (oblique) with respect to the star’s rotation axis, whereas the dipoles we suspect for the RS CVn stars, based on the symmetry of the polar spots, would be highly aligned. Two obvious origins come to mind for these dipoles, fossil fields left over from the frozen-in field of the proto-stellar cloud which have somehow survived the collapse phase, or dynamo-generated fields arising from the mechanical energy of convection and rotation in these deeply convective and rapidly-rotating stars. That more slowly rotating RS CVn stars apparently do not show strong aligned magnetic dipoles leads us to believe that they are not fossil fields, but rather are a product of the deep convective zones and tidally-enforced rapid rotation of the RS CVn stars.

5. Summary discussion: dipoles and dynamo modes

The cool polar spots on HR 1099 and many other rapidly rotating active late-type stars must, if we’ve learned anything from the magnetic fields of sunspots, be telling us that there are multi-kgauss-strength fields filling these polar spots and suppressing convection in the photosphere to a degree that the surface is cooled sufficiently to produce visible spots, just as occurs in sunspot umbrae. However, from the standpoint of locations, areas, shapes, and differential rotation, starspots look much more like solar coronal holes than giant sunspots. In fact, the resemblance between the polar spot of HR 1099 with its variable ‘protuberances’ and the solar polar coronal hole with its ‘polar hole extensions’ is quite striking. Both straddle the pole and have similar areas and shapes.

Starspots also show surprisingly little differential rotation, quite unlike sunspots, but again very similar to solar coronal holes. On the Sun, coronal holes are the footprints of

the unipolar magnetic regions (UMR’s) of the global dipolar coronal field, and their shapes are maintained rigidly (in the face of considerable photospheric shear) by a few-gauss current-free global dipole coronal field as described by Wang and Sheeley 1993, the same dipole field which produces the polar coronal holes. The differential rotation of solar coronal holes is governed by the stability of the globally-averaged current-free coronal field rather than by the latitudinal shear of the solar photosphere. If the solar coronal hole analogy holds true for starspots, then *the differential rotation derived from starspots on RS CVn stars may actually be revealing very little about the latitudinal shear of the photosphere, but rather may be more a consequence of the stability of a powerful, current-free global dipole field.* This global field is probably of multi-kgauss-strength at the pole (and only half as strong at the equator if dipolar), orders of magnitude stronger than the few-gauss global fields of the Sun. Presumably, both the strength and stability of this global field increases with stellar angular rotation velocity (i.e. dynamo strength) thereby offering a simple explanation for why the observed ‘differential rotation’ signature from starspot light curves decreases as angular velocity increases among active stars.

That large polar spots are a quite common feature of rapidly rotating spotted stars, suggests to us that there is a large polar spot at *both* poles of the star. If so, it is reasonable to assume that these UMR polar spots are of opposite polarity and that their field lines connect out beyond the Alfvén radius. These polar spots thus probably bear witness to a strong dipole or low-order multi-pole magnetic field within the star, co-axial with the star’s rotation axis. Whether this axisymmetric field is produced solely by an axisymmetric dynamo or is the result of accumulation of flux from non-axisymmetric dynamos is not clear. Probably both contribute. Indeed, the track of Feature B may be showing us this winding up of field lines around the pole into the toroidal magnetic structure seen by Donati et al. (1992).

We thus conclude from our Doppler imaging studies that the starspots on HR 1099 and many other rapidly-rotating late-type stars are essentially powerful stellar analogs of solar coronal hole structures (UMR's), but formed by multi-kgauss strength global magnetic fields rather than the few-gauss global coronal fields of the Sun. The persistent cool polar spots and increasing stability of spot features with increasing rotation velocity leads us also to conclude that *rapidly rotating and highly convective stars with prominent polar spots are probably all hiding multi-kgauss axisymmetric dipole fields.*

But could such strong axisymmetric dipolar fields on spotted RS CVn stars have escaped previous direct detection? Actually, they probably have already been detected on the most active dMe flare stars (see below), but are harder to detect on rapidly rotating RS CVn stars like HR 1099 for several reasons. First, any purely axisymmetric field component would show no rotational modulation. Second, these very active stars are also quite rapid rotators, and their rotational line broadening makes traditional Zeeman-splitting detections difficult. Finally, most of the magnetic flux would be quite effectively hidden from detection in the optical region of the spectrum by being concentrated in the very cool (and hence optically dark) polar spots. Some of this flux has now indeed been detected directly (at least from areas adjacent to the dark regions) via Zeeman Doppler images of these ubiquitous polar spots. But the bulk of the flux probably remains hidden from optical observers in the very low optical surface brightness spot regions.

Zeeman measurements in the infrared, where spot-to-photosphere contrast is much less, and/or using spectral features such as TiO which are strongly enhanced in the dark spots, may soon be able to routinely measure these hypothesized axisymmetric dipole fields. Saar and Linksy (1985) used the KPNO FTS at 2.2 microns and detected 3.8 kG fields covering 73% of the surface of the dM3.5e flare star AD Leo. Furthermore, these fields were from active regions outside of dark spots. Fields in the dark spots are probably much stronger.

Further recent infrared Zeeman measurements at 2.2 microns with CSHELL on the IRTF by Saar (1996) indicate 3 kG fields covering 60% of the visible surface of the heavily spotted RS CVn star II Peg , and 2.8 kG fields covering 50% of the visible surface of the nearly pole-on K5Ve star Gl 171.2A. The bulk of this magnetic flux is apparently from the dark spots themselves, which dominate the TiO features in the infrared. Similarly, Saar (1996) reports 4 kG fields covering 60-70% of the visible surfaces of the active flare stars AD Leo and YZ CMi, and 3.5 kG fields covering 70% of the visible surface of the heavily spotted star LQ Hya. Johns-Krull and Valenti (1996) also report a recent detection of 2.6-3.8 kG fields covering about 50% of the surface of the M4.5Ve flare stars Gliese 729 and EV Lac. Thanks to the new generation of IR echelles, we now seem to be crossing the threshold to routine direct detection of these hypothesized global dipole fields in rapidly rotating RS CVn stars. Such multi-kgauss global dipole fields are, of course, well-known and quite common among the Ap stars, though in most of those cases, the field axis is highly inclined to the rotation axis, as though the field were some fossil remnant frozen into the star. Here, the precise alignment of the field to the rotation axis probably indicates a dynamo-induced process for its creation. Indeed the axisymmetric dipole is a strongly-preferred dynamo mode.

Our 11-year HR 1099 Doppler image set also revealed that at least some of the magnetic flux which emerges at lower latitudes migrates poleward to join with the polar spot. A polar starspot is thus probably the equivalent of the solar polar coronal hole, complete with variable ‘protuberances’ (polar hole extensions) but filled with multi-kgauss-strength magnetic fields similar to those found in sunspot umbrae. The stability (lack of differential rotation) of spots is probably maintained by this powerful current-free global dipole field and, in HR 1099, this dipole field is apparently also tightly synchronized to the orbit. Given that this dipole probably penetrates through to the core of the star, this is not altogether surprising. The dipole is probably rooted to the rotation rate of a core which was long ago

synchronized to the orbit, and remains so today, even after the outer layers of the star expanded (and slowed) as the star left the main sequence.

We thus propose the following context and simple two-pronged analogy by which to understand starspots in terms of solar activity. Starspots are much like sunspot umbrae by virtue of their large (multi-kgauss) field strengths, which are strong enough to inhibit convection and cause a large enough temperature drop in the photosphere to be easily visible in the optical. However, as regards their global properties (sizes, shapes, locations, differential rotation, and migration), they are a direct analog of solar coronal holes (UMR’s), with their structure and evolution heavily influenced by a strong axisymmetric multi-kgauss global dipole field which has been built up within the star by powerful dynamo action.

While HR 1099 reveals evidence for spots emerging at low latitude and migrating poleward (at a latitude migration rate of 6-30 m/s) to eventually merge with the polar spot, we don’t yet know whether these spots *reinforce* the polar spot with like-polarity flux, or instead *destroy* it in some sort of feedback process which may ultimately produce a periodic polarity-reversal of the polar spot. Whichever the case, magnetic flux which emerges at lower latitudes probably separates out into unipolar magnetic regions, and then migrates poleward to merge, either constructively or destructively, with the spots at each pole. The axisymmetric dipole field within HR 1099, if related to polar spot area, *may* show marginal evidence for ≈ 3 -year periodicity (i.e. a dynamo cycle), but probably varies only weakly, if at all, in total strength.

As shown theoretically by Moss et. al. (1995) from mean field dynamo models, these stars probably excite both axisymmetric and non-axisymmetric dynamo fields. The models show that, at moderate values of the Taylor number, stable non-axisymmetric fields (perpendicular-dipole topology) can be excited in deep convective shells, and this flux rises to the surface, emerging at intermediate-latitudes to form spots. These theoretical studies

apparently have some difficulty producing flux emergence at low latitudes, but should be pursued to see if they can be made to do so at these and even *lower* latitudes, since HR 1099 does indeed frequently form spots at or near the equator. At large Taylor numbers (large differential rotation), only axisymmetric dynamo solutions are stable, and one would therefore expect the axisymmetric field (i.e. polar spots) to become more prominent with increasing angular velocity. There is now some observational support for this. The more slowly-rotating RS CVn stars (Hatzes 1993) exhibit only intermediate-latitude spots, presumably created from such non-axisymmetric dynamos, and do *not* exhibit the permanent polar spot signature of an axisymmetric dynamo mode.

The large polar starspots and low-latitude spots on HR 1099 and other rapidly rotating stars probably indicate that both types of dynamos are excited within these stars, and furthermore that the flux contribution from the axisymmetric component increases with angular rotation velocity, resulting in more prominent and long-lived polar spots. Some of the flux which emerges at low and intermediate latitudes from the less stable non-axisymmetric dynamo modes clearly makes its way to the poles on HR 1099 and may either simply accumulate there to *reinforce* the axisymmetric dipole field, or may *erode* it if of opposite polarity, perhaps as part of a long-term polarity-reversing periodic process, as occurs on the Sun. Further Zeeman Doppler imagery, particularly in the infrared, of stars with polar spots could be very helpful in sorting out this important question.

Based on the Solar coronal field analogy, and on the efficiency of the axisymmetric dynamo mode, we suspect that, close to the pole, the globally-averaged field assumes the topology of an axisymmetric dipole. But perhaps the field topology at lower latitudes within the polar spot is simply a continuation of the toroidal pattern detected around the polar spot periphery by Donati et al. (1992). If so, as perhaps also suggested by the track of Feature B on HR 1099, magnetic flux is literally ‘winding up’ around the pole. The field

strength would thus increase with latitude, and one would be able to detect such toroidal fields only up to a latitude where their strength was sufficient to suppress convection (i.e. the edge of the spot). This would produce a strong bias for field detection precisely at the boundary of the polar spot, just as observed. The latitude of the polar spot edge is exactly where the fields would be the strongest before becoming *invisible* within the spot. At lower latitudes, the fields would be too weak to detect. Above that latitude, the photosphere would then turn dark, forming the polar spot, and the tightly-coiled fields within the polar spot would be effectively hidden from view.

Clearly the axisymmetric and non-axisymmetric dynamo modes need to be further explored through realistic and self-consistent dynamo modeling. The relative contributions of each should be predicted as a function of rotation period, and can then be directly checked through Doppler images of stars over a range of rotation periods. HR 1099 suggests that both modes are probably active in the rapidly rotating RS CVn stars, that magnetic flux which emerges at low latitudes does migrate poleward, and furthermore that there may be a pronounced winding of low-latitude emergent flux into toroidally-wrapped flux near or even in the polar spot. Does this winding of flux continue right up to the polar singularity, or is this toroidal flux being wound tightly around an axisymmetric dipole field? In either case, such complex non-potential field configurations might well be expected to give rise to persistent high temperature/energetic phenomena within or above the polar spot, as detected by Dupree (1996) in EUVE coronal emission from stars with polar spots. These details of the *interaction* between axisymmetric and non-axisymmetric dynamo modes must be quantified, with the aim of understanding how these modes interact over the long term, to see if they can indeed build up sizeable polar fields, and if this field is stable in strength and/or polarity, or if it varies periodically. It is an area of theoretical inquiry now ripe for exploration, and should produce predictions that can be sensibly tested on spotted stars through Doppler imagery.

Finally, the large cool polar spot on HR 1099 is presumably a direct look at the ‘magnetic brake’ which is ultimately responsible for slowing the rotation of many rapidly-rotating single late-type stars. The tidally-locked spotted subgiant star in the HR 1099 binary system is thus probably “standing on the brakes”, but alas in vain in the face of tidal locking to the large angular momentum reservoir of the orbit.

We are very grateful to the Lick and McDonald Observatory TAC’s who made this long-term project possible through major amounts of observing time over the past decade. We are also very grateful for support from the NSF under grants AST-9115376 to SSV and AST-9116478 and AST-9315115 to APH. We also gratefully acknowledge the efforts of G. Donald Penrod in helping to develop the Doppler imaging method.

Table 1. HR 1099: Observations for 1981.70 Image

Phase	JD 2440000+	Exp. (min)	S/N	Station
0.254	4863.892	48	150	Lick
0.297	4864.014	64	170	Lick
0.300	4866.855	96	220	Lick
0.349	4866.997	64	210	Lick
0.575	4896.016	48	230	Lick
0.643	4864.996	48	190	Lick
0.877	4896.874	32	150	Lick
0.943	4897.060	32	180	Lick

Table 2. HR 1099: Observations for 1982.74 Image

Phase	JD 2440000+	Exp. (min)	S/N	Station
0.091	5240.847	96	360	Lick
0.149	5241.012	48	300	Lick
0.337	5250.847	48	300	Lick
0.460	5241.895	96	140	Lick
0.645	5216.880	96	280	Lick
0.677	5253.860	48	250	Lick
0.693	5217.017	48	150	Lick
0.723	5253.993	48	275	Lick
0.985	5251.899	48	200	Lick

Table 3. HR 1099: Observations for 1983.74 Image

Phase	JD 2440000+	Exp. (min)	S/N	Station
0.050	6046.649	30	310	Lick
0.122	6046.853	30	190	Lick
0.204	5981.818	30	600	Lick
0.253	5981.956	30	550	Lick
0.282	5982.041	30	580	Lick
0.546	5979.952	30	500	Lick
0.566	5980.009	20	450	Lick
0.581	5980.052	13	200	Lick
0.638	6042.642	20	410	Lick
0.682	6042.768	20	500	Lick
0.856	5980.832	20	430	Lick
0.928	5981.034	30	540	Lick

Table 4. HR 1099: Observations for 1985.87 Image

Phase	JD 2440000+	Exp. (min)	S/N	Station
0.050	6372.980	30	560	Lick
0.125	6395.903	20	420	Lick
0.266	6370.764	30	370	Lick
0.349	6371.000	30	325	Lick
0.374	6427.826	30	370	Lick
0.564	6368.774	20	400	Lick
0.643	6368.996	20	500	Lick
0.701	6372.000	30	350	Lick
0.843	6400.778	60	250	Lick
0.918	6369.776	20	330	Lick
0.973	6372.770	20	445	Lick

Table 5. Observations for 1986.66 Image

Phase	JD 2440000+	Exp. (min)	S/N	Station
0.180	6659.969	30	450	Lick
0.259	6663.003	25	350	Lick
0.352	6720.051	25	300	Lick
0.525	6660.950	20	430	Lick
0.845	6659.020	30	450	Lick
0.892	6661.991	25	470	Lick

Table 6. Observations for 1987.04 Image

Phase	JD 2440000+	Exp. (min)	S/N	Station
0.210	6807.615	30	450	Lick 80"
0.268	6807.781	30	460	Lick 80"
0.340	6810.830	60	160	Lick 80"
0.384	6813.788	30	280	Lick 80"
0.620	6811.623	60	330	Lick 80"
0.670	6814.619	20	375	Lick 80"
0.690	6811.819	30	230	Lick 80"
0.756	6814.842	40	310	Lick 80"
0.913	6809.612	40	325	Lick 80"
0.977	6809.794	60	350	Lick 80"

Table 7. Observations for 1987.73 Image

Phase	JD 2440000+	Exp. (min)	S/N	Station
0.069	7076.802	30	450	Lick 80"
0.151	7077.035	20	430	Lick 80"
0.312	7051.952	30	460	Lick 80"
0.420	7077.801	30	540	Lick 80"
0.590	7049.912	30	450	Lick 80"
0.627	7050.009	20	400	Lick 80"
0.726	7075.831	30	570	Lick 80"
0.796	7076.028	30	580	Lick 80"
0.945	7050.911	25		Lick 80"
0.974	7050.992	20	390	Lick 80"

Table 8. Observations for 1988.80 Image

Phase	JD 2440000+	Exp. (min)	S/N	Station
0.083	7462.775	60	500	Lick 80"
0.155	7465.817	36	400	McDonald coudé
0.190	7465.917	15	400	McDonald coudé
0.444	7463.801	50	230	McDonald coudé
0.555	7432.901	60	600	Lick 80"
0.589	7432.997	60	500	Lick 80"
0.781	7464.756	50	580	Lick 80"
0.834	7464.907	30	200	McDonald coudé
0.854	7464.964	24	280	McDonald coudé
0.876	7465.025	45	350	Lick 80"
0.925	7433.949	40	620	Lick 80"

Table 9. Observations for 1989.11 Image

Phase	JD 2440000+	Exp. (min)	S/N	Station
0.049	7570.513	14	260	ESO
0.182	7559.539	26	285	ESO
0.232	7562.519	14	350	ESO
0.342	7568.506	14	265	ESO
0.488	7571.758	50	500	Lick coudé
0.533	7574.724	60	250	Lick coudé
0.696	7569.510	14	370	ESO
0.886	7561.536	14	300	ESO

Table 10. Observations for 1989.69 Image

Phase	JD 2440000+	Exp. (min)	S/N	Station
0.000	7788.870	35	500	Lick coudé
0.032	7788.972	50	550	Lick coudé
0.104	7757.961	50	380	Lick coudé
0.350	7789.862	30	350	Lick coudé
0.380	7789.966	35	449	Lick coudé
0.445	7758.935	50	300	Lick coudé

Table 11. Observations for 1989.78 Image

Phase	JD 2440000+	Exp. (min)	S/N	Station
0.060	7811.751	40	600	Lick 80"
0.125	7814.774	60	300	McDonald coudé
0.128	7814.774	40	350	Lick 80"
0.168	7814.898	45	300	McDonald coudé
0.475	7815.768	45	280	McDonald coudé
0.554	7815.991	45	250	McDonald coudé
0.710	7810.763	40	600	Lick 80"
0.770	7810.917	35	600	Lick 80"
0.804	7813.862	40	260	McDonald coudé
0.807	7811.035	35	650	Lick 80"
0.812	7813.886	25	220	McDonald coudé
0.900	7816.974	45	250	McDonald coudé

Table 12. Observations for 1989.88 Image

Phase	JD 2440000+	Exp. (min)	S/N	Station
0.068	7845.827	45	210	McDonald coudé
0.320	7843.717	40	400	Lick 80"
0.380	7846.712	90	270	McDonald coudé
0.400	7843.935	40	420	Lick 80"
0.435	7846.870	60	300	McDonald coudé
0.680	7844.733	40	370	Lick 80"
0.701	7844.788	50	330	McDonald coudé
0.738	7844.890	35	330	Lick 80"
0.764	7844.965	45	360	McDonald coudé
0.963	7876.744	40	450	Lick 80"

Table 13. HR 1099: Observations for 1990.69 Image

Phase	JD 2440000+	Exp. (min)	S/N	Station
0.116	8143.927	21	220	ESO
0.180	8149.786	28	300	ESO
0.248	8152.813	28	430	ESO
0.302	8135.942	35	170	McDonald coudé
0.390	8141.869	21	150	ESO
0.434	8144.828	21	440	ESO
0.636	8136.890	40	200	McDonald coudé
0.710	8142.774	28	320	ESO
0.744	8142.870	28	280	ESO
0.928	8134.879	45	300	McDonald coudé

Table 14. Observations for 1990.80 Image

Phase	JD 2440000+	Exp. (min)	S/N	Station
0.040	8174.927	60	260	McDonald coudé
0.070	8175.010	60	220	McDonald coudé
0.367	8175.849	60	270	McDonald coudé
0.418	8176.000	40	270	McDonald coudé
0.484	8201.726	40	330	McDonald coudé
0.557	8201.932	45	250	McDonald coudé
0.586	8167.963	40	250	McDonald coudé
0.606	8204.910	45	260	McDonald coudé
0.626	8204.966	45	230	McDonald coudé
0.863	8165.912	20	500	Lick HS

Table 15. Observations for 1990.93 Image

Phase	JD 2440000+	Exp. (min)	S/N	Station
0.044	8231.691	60	180	McDonald coudé
0.124	8231.919	30	380	Lick
0.301	8229.583	60	240	McDonald coudé
0.360	8229.756	60	330	McDonald coudé
0.415	8229.906	50	240	McDonald coudé
0.660	8230.612	60	170	McDonald coudé
0.718	8230.768	55	400	McDonald coudé
0.745	8230.845	33	320	Lick HS
0.771	8230.918	60	430	McDonald coudé

Table 16. HR 1099: Observations for 1991.02 Image

Phase	JD 2440000+	Exp. (min)	S/N	Station
0.216	8260.558	60	400	McDonald coudé
0.278	8260.735	60	200	McDonald coudé
0.280	8263.580	28	275	ESO
0.328	8263.714	45	370	McDonald coudé
0.340	8266.585	21	200	ESO
0.572	8261.590	21	230	ESO
0.636	8264.587	21	200	ESO
0.644	8264.772	50	450	McDonald coudé
0.691	8267.581	21	340	ESO
0.861	8259.551	40	360	McDonald coudé
0.918	8259.712	60	400	McDonald coudé
0.923	8262.559	21	400	ESO
0.960	8259.832	60	360	McDonald coudé

Table 17. Observations for 1991.80 Image

Phase	JD 2440000+	Exp. (min)	S/N	Station
0.115	8549.721	50	280	McDonald coudé
0.177	8549.895	50	300	McDonald coudé
0.370	8558.952	30	260	McDonald coudé
0.421	8547.703	45	370	McDonald coudé
0.472	8547.895	30	330	McDonald coudé
0.762	8548.720	75	350	McDonald coudé
0.833	8548.926	70	240	McDonald coudé

Table 18. Observations for 1991.88 Image

Phase	JD 2440000+	Exp. (min)	S/N	Station
0.058	8580.775	45	230	McDonald Coudé
0.107	8580.913	50	300	McDonald Coudé
0.140	8586.800	28	380	ESO
0.342	8581.580	28	450	ESO
0.383	8581.695	45	230	McDonald Coudé
0.420	8584.638	35	240	ESO
0.438	8581.852	50	380	McDonald Coudé
0.460	8587.590	49	240	ESO
0.659	8579.641	45	320	McDonald Coudé
0.665	8579.657	28	450	ESO
0.693	8582.575	28	400	ESO
0.707	8579.776	45	300	McDonald Coudé
0.740	8585.553	42	340	ESO
0.750	8579.899	50	480	McDonald Coudé
0.800	8588.550	28	320	ESO

Table 19. Observations for 1992.06 Image

Phase	JD 2440000+	Exp. (min)	S/N	Station
0.364	8635.558	40	260	McDonald Coudé
0.428	8635.742	45	315	McDonald Coudé
0.555	8641.777	10	320	Lick HS
0.626	8613.601	40	260	McDonald Coudé
0.726	8636.588	40	500	McDonald Coudé
0.792	8636.774	50	340	McDonald Coudé
0.841	8676.642	8	250	Lick HS
0.956	8631.564	47	120	McDonald Coudé

Table 20. Observations for 1992.69 Image

Phase	JD 2440000+	Exp. (min)	S/N	Station
0.035	8872.994	13	300	McDonald SE
0.105	8878.870	10	290	Lick HS
0.307	8870.931	13	230	McDonald SE
0.443	8876.990	20	320	Lick HS
0.681	8871.992	9	280	McDonald SE
0.770	8877.920	15	250	Lick HS
0.953	8869.926	11	230	McDonald SE

Table 21. Observations for 1992.82 Image

Phase	JD 2440000+	Exp. (min)	S/N	Station
0.125	8912.980	15	240	Lick HS
0.407	8913.780	10	200	Lick HS
0.425	8913.830	10	270	Lick HS
0.568	8936.940	20	170	Lick HS
0.748	8911.91	20	150	Lick HS
0.770	8914.810	10	140	Lick HS
0.920	8937.945	15	320	Lick HS

Table 22. Observations for 1992.95 Image

Phase	JD 2440000+	Exp. (min)	S/N	Station
0.092	8969.641	25	260	McDonald SE
0.148	8969.798	15	150	McDonald SE
0.392	8967.653	30	240	McDonald SE
0.464	8967.858	40	250	McDonald SE
0.734	8968.624	15	330	McDonald SE
0.782	8968.775	18	340	McDonald SE
0.954	8957.900	15	280	McDonald SE

Table 23. Observations for 1993.14 Image

Phase	JD 2440000+	Exp. (min)	S/N	Station
0.053	9020.611	15	320	McDonald SE
0.335	9052.625	20	270	Lick HS
0.400	9021.594	30	210	McDonald SE
0.534	9044.676	14	290	McDonald SE
0.634	9050.636	20	240	Lick HS
0.686	9053.619	15	250	Lick HS
0.750	9022.585	30	260	McDonald SE
0.984	9051.629	20	260	Lick SE

REFERENCES

- Andrews, A.D., Rodono, M., Linsky, J.L., Brown, A., Butler, C.J., Catalano, S., Scaltriti, F., Busso, M., Nha, I., Oh, J.Y., Henry, M.C.D., Hopkins, J.L., Landis, H.J., and Engelbrektson, S. 1988, *A&A*, 204, 177.
- Antonopoulou, E., and Williams, P.M. 1980, *Ap&SS*, 67, 469.
- Ayres, T.R., and Linsky, J.L. 1982, *ApJ*, 254, 168.
- Baliunas, S.L., Nesme-Ribes, E., Sokoloff, D., and Soon, W.H. 1996, *ApJ*, 460, 848.
- Bartolini, C., Guarnieri, A., Piccioni, A., Catalano, S., Rodono, M., Brooke, A.F., Landis, H.J., Sarne, M.B.K., Olson, E.C., and Hall, D.S. 1978, *AJ*, 83, 1510.
- Bartolini, C., Blanco, C., Catalano, S., Cerruti-Sola, M., Eaton, J.A., Guarnieri, A., Hall, D.S., Henry, G.W., Hopkins, J.L., Landis, H.J., Louth, H., Marilli, E., Piccioni, A., Renner, T.R., Rodono, M., and Scaltriti, F. 1983, *A&A*, 117, 149.
- Bell, R.A., Eriksson, K., Gustafsson, B., and Nordlund, A. 1976 *A&AS*, 23, 37.
- Bopp, B.W., and Fekel, F.C. 1976, *AJ*, 81, 771.
- Bravo, S., and Otaola, J.A. 1989, *Solar Phys.*, **122**, 355.
- Buzasi, D.L., Huenemoerder, D.P., and Ramsey, L.W. 1991, *PASP*, 103, 1077.
- Byrne, P.B. 1996 in *Stellar Surface Structure*, IAU Symposium No. 176, K.G. Strassmeier and J.L. Linsky, eds, p. 299.
- Byrne, P.B., Doyle, J.G., Brown, A., Linsky, J.L., and Rodono, M. 1987 *A&A*, 180, 172.
- Cutispoto, G. 1992, *A&AS*, 95, 397.
- Cutispoto, G. 1990, *A&AS*, 84, 397.

- Dempsey, R.C., Bopp, B.W., Strassmeier, K.G., Granados, A.F., Henry, G.W., and Hall, D.S. 1992, *ApJ*, 392, 187.
- Donati, J.-F., Semel, M., Rees, D.E., Taylor, K., and Robinson, R.D. 1990, *A&A*, 232, L1.
- Donati, J.-F., Semel, M., and Rees, D.E. 1992, *A&A*, 265, 669.
- Donati, J.-F., Brown, S.F., Semel, M., Rees, D.E., Dempsey, R.C., Matthews, J.M., Henry, G.W., and Hall, D.S. 1992, *A&A*, 265, 682.
- Dorren, J.D., Guinan, E.F., and Wacker, S.W. 1986, in *New Insights in Astrophysics*, ed. E.J. Rolfe (Paris: ESA), 201.
- Dorren, J.D., and Guinan, E.F. 1990, *ApJ*, 348, 703.
- Dorren, J.D., Siah, M.J., Guinan, E.F., and McCook, G.P. 1981, *AJ*, 86, 572.
- Dorren, J.D., and Guinan, E.F. 1982, *ApJ*, 252, 296.
- Drake, J.J., Brown, A., Patterer, R.J., Vedder, P.W., Bowyer, S., and Guinan, E.F. 1994 *ApJ*, 421, L43.
- Dupree, A.K. 1996, in *Cool Stars, Stellar Systems, and the Sun*, 9th Cambridge Workshop (Florence, Italy), eds. R. Pallavicini and A.K. Dupree.
- Feldman, P.A., Taylor, A.R., Gregory, P.C., Seaquist, E.R., Balonek, T.J., and Cohen, N.L. 1978 *AJ*, 83, 1471.
- Fekel, F.C. 1983, *ApJ*, 268, 274.
- Foing, B.H. et al. 1994, *A&A*, 292, 543.
- Foukal, P., and Lean, J. 1986, *ApJ*, 302, 826.
- Gondoin, P. 1986, *A&A*, 160, 73.

- Hall, D.S. 1991, in *The Sun and Cool Stars: Activity, Magnetism, and Dynamos*, I. Tuominen, D. Moss, and G. Rudiger, eds. (Berlin: Springer-Verlag), 353.
- Hall, D.S. 1978, *AJ*, 83, 1469.
- Hatzes, A.P. 1993, *ApJ*, 410, 777.
- Hatzes, A.P., Vogt, S.S., Ramseyer, T., and Misch, A. 1996, *ApJ*, 469, 808.
- Henry, G.W. and Hall, D.S. 1991, *ApJ*, 373, L9.
- Huenemoerder, D.P. 1987, in *Cool Stars, Stellar Systems, and the Sun*, ed. J.L. Linsky and R.E. Stencel, (Berlin:Springer-Verlag), p. 512.
- Johns-Krull, C.M., and Valenti, J.A. 1996, *ApJ*, 459, L95.
- Jones, K.L., Stewart, R.T., Nelson, G.J., and Duncan, A.R. 1994, *MNRAS*, 269, 1145.
- Kang, Y.W., and Wilson, R.E. 1989, *AJ*, 97, 848.
- Lestrade, J.-F., Mutel, R.L., Phillips, R.B., Webber, J.C., Niell, A.E., and Preston, R.A. 1984, *ApJ*, 282, L23.
- Linsky, J.L., Neff, J.E., Brown, A., Gross, B.D., Simon, T., Andrews, A.D., Rodono, M., and Feldman, P.A. 1989, *A&A*, 211, 173.
- Lodenquai, J., and McTavish, J. 1988, *AJ*, 96, 741.
- McCarthy, J.K., Sandiford, B.A., Boyd, D., and Booth, J. 1993, *PASP*, 105, 881.
- Mekkaden, M.V. 1987, *I.B.V.S.*, 3042.
- Mohin, S., and Raveendran, A.V. 1993, *A&AS*, 100, 331.
- Moss, D., Barker, D.M., Brandenburg, A., and Tuominen, I. 1995, *A&A*, 294, 155.

- Nations, H.L., and Ramsey, L.W. 1986, *AJ*, 92, 1403.
- Navarro-Peralta, P., and Sanchez-Ibarra, A. 1994, *Solar Phys.*, 153, 169.
- Neff, J.E., Simon, T., Pagano, I., Rodono, M., and Foing, B. 1993, *BAAS*, 25, 874.
- Olah, K., Hall, D.S., and Henry, G.W. 1991, *A&A*, 251, 531.
- Parthasarathy, M., Raveendran, A.V., and Mekkaden, M.V. 1981, *Ap&SS*, 74, 87.
- Ramsey, L.W., and Nations, H.L. 1980, *ApJ*, 239, L121.
- Robinson, R.D., Maran, S.P., Carpenter, K.G., Brandt, J.C., and Linsky, J.L. 1994, *BAAS*, 26, 865.
- Rodono, M., Cutispoto, G., Pazzani, S., Catalano, S., Byrne, P.B., Doyle, J.G., Butler, C.J., Andrews, A.D., Blanco, C., Marilli, E., Linsky, J.L., Scaltriti, F., Busso, M., Cellino, A., Hopkins, J.L., Okazaki, A., Hayashi, S.S., Zeilik, M., Helston, R., Henson, G., Smith, P., and Simon, T. 1986, *A&A*, 165, 135.
- Rodono, M., Byrne, P.B., Neff, J.E., Linsky, J.L., Simon, T., Butler, C.J., Catalano, S., Cutispoto, G., Doyle, J.G., Andrews, A.D., and Gibson, D.M. 1987 *A&A*, 176, 267.
- Rodono, M., and Cutispoto, G. 1992, *A&AS*, 95, 55.
- Rucinski, S.M. 1983, *IBVS* No. 2277.
- Saar, S.H. 1996, *IAU Colloquium No. 153, Magnetodynamic Phenomena in the Solar Atmosphere - Prototypes of Stellar Magnetic Activity*, ed. Y. Uchida, T. Kosugi, and H.S. Hudson, Kluwer, in press.
- Saar, S.H., and Linsky, J.L. 1985 *ApJ*, 299, L47.
- Scharlemann, E. 1982, *ApJ*, 253, 298.

- Schüssler, M., Caligari, P., Ferriz-Mas, A., Solanki, S.K., and Stix, M. 1996 A&A, in press.
- Schüssler, M. and Solanki, S.K. 1992, A&A, 264, L13.
- Simon, P.A. 1979, *Solar Phys.*, **63**, 399.
- Stout-Batalha, N.M., and Vogt, S.S. 1996 in *IAU Symposium 176, Stellar Surface Structure*, K.G. Strassmeier ed., p. 337.
- Strassmeier, K.G., Hall, D.S., Boyd, L.J., and Genet, R.M. 1989, A&AS, 69, 141.
- Timothy, A.F., Krieger, A.S., and Vaiana, G.S. 1975, *Solar Phys.*, 42, 135.
- Vogt, S.S. 1983, in *Activity in Red-Dwarf Stars*, eds. M. Rodono and P. Byrne, (Dordrecht: Reidel), 379.
- Vogt, S.S., and Penrod G.D. 1983, PASP, 95, 565.
- Vogt, S.S. 1987a, in *Observational Astrophysics with High Precision Data - 27th Liege International Astrophysical Colloquium*, Liege:Universite de Liege, 317.
- Vogt, S.S. 1987b, in *The Impact of Very High S/N Spectroscopy on Stellar Physics*, G. Cayrel de Strobel and M. Spite, (Dordrecht: Kluwer), 253.
- Vogt, S.S. 1987c, PASP, 99, 1214.
- Vogt, S.S., Penrod, G.D., and Hatzes, A.P. 1987, ApJ, 321, 496.
- Vogt, S.S. and Hatzes, A.P. 1991, in *The Sun and Cool Stars: Activity, Magnetism, and Dynamos*, I. Tuominen, D. Moss, and G. Rudiger, eds. (Berlin:Springer-Verlag), 297.
- Waldmeier, M. 1981, *Solar Phys.*, 70, 251.
- Wang, Y.-M., and Sheeley, N.R. Jr. 1993, ApJ, 414, 916.

- Weiler, E.J., Owen, F.N., Bopp, B.W., Schmitz, M., Hall, D.S., Fraquelli, D.A., Pirola, V., Ryle, M., and Gibson, D. 1978, *ApJ*, 225, 919.
- Zhai, D.S., Foing, B.H., Cutispoto, G., Zhang, R.X., Catala, C., Char, S., Zhang, X.B., and Jankov, S. 1994, *A&A*, 282, 168.
- Zhang, R., Zhai, D., Zhang, X., Zhang, J., and Li, Q. 1990, *I.B.V.S.*, 3456.
- Zhang, R.-X., Zhang, J.-T., Zhang, X.-B., Zhai, D.-S. 1993, *I.B.V.S.*, 3930.